



DESIGN AV ELECTRISK MOTOR FOR FORMULA STUDENT

Andre Alexander Laleng

Master i produktutvikling og produksjon

Innlevert: august 2016

Hovedveileder: Terje Rølvåg, IPM

Norges teknisk-naturvitenskapelige universitet
Institutt for produktutvikling og materialer

Design of Electric Motor for Formula Student

Master Thesis



Department of Engineering Design and Materials

André Alexander Laleng

03.08.2016

NTNU - NORWEGIAN UNIVERSITY
OF SCIENCE AND TECHNOLOGY
DEPARTMENT OF ENGINEERING DESIGN
AND MATERIALS

**MASTER THESIS SPRING 2016
FOR
STUD. TECHN. ANDRÉ ALEXANDER LALENG**

DESIGN OF ELECTRIC MOTOR FOR FORMULA STUDENT

Design of Electric Motor for Formula Student

Revolve NTNU is a student organization that each year design and build a formula race car to participate in the engineering student competition Formula Student. Since its birth in 2010, Revolve NTNU has developed rapidly both organizationally and technologically. After achieving titles as best newcomer (FSUK 2012) and best Nordic team (FSUK 2013) with conventional combustion engines, the team took a big technological leap in 2014 and switched to an electric powertrain. The same year Revolve NTNU finished as the best rear-wheel driven electric vehicle (FSUK 2014). In 2015 the 2014 concept was refined and finished as 4th overall (FSA 2015).

To keep up the progress in the future and bring the battle to the decade-long experienced top running teams, Revolve NTNU has decided to change the powertrain layout to a four-wheel driven system with hub-mounted electric motors. This opens new possibilities for regenerative braking, torque vectoring control and overall increased acceleration. Due to very limited availability of suitable motors on the commercial market, the organization has initiated a research & development project. The goal is to develop an electric motor prototype tailored for use in Formula Student within a limited budget.

This master's project work will concentrate on design, analysis, optimization and production. The following tasks shall be focused:

1. Discuss general motor construction, production aspects, engineering materials, load scenarios and product specifications.
2. Develop a preliminary motor design and analyze its performance.
3. Optimize the initial design with respect to performance and production
4. Prepare the final design for production
5. As time and resources allow it, construct a prototype and conduct benchmark tests.

Formal requirements:

Three weeks after start of the thesis work, an A3 sheet illustrating the work is to be handed in. A template for this presentation is available on the IPM's web site under the menu

“Masteroppgave” (<https://www.ntnu.edu/web/ipm/master-thesis>). This sheet should be updated one week before the master’s thesis is submitted.


Risk assessment of experimental activities shall always be performed. Experimental work defined in the problem description shall be planned and risk assessed up-front and within 3 weeks after receiving the problem text. Any specific experimental activities which are not properly covered by the general risk assessment shall be particularly assessed before performing the experimental work. Risk assessments should be signed by the supervisor and copies shall be included in the appendix of the thesis.

The thesis should include the signed problem text, and be written as a research report with summary both in English and Norwegian, conclusion, literature references, table of contents, etc. During preparation of the text, the candidate should make efforts to create a well arranged and well written report. To ease the evaluation of the thesis, it is important to cross-reference text, tables and figures. For evaluation of the work a thorough discussion of results is appreciated.

The thesis shall be submitted electronically via DAIM, NTNU's system for Digital Archiving and Submission of Master's theses.


Torgeir Welø
Head of Division


Terje Rølvåg
Professor/Supervisor

 NTNU
Norges teknisk-
naturvitenskapelige universitet
Institutt for produktutvikling
og materialer

Acknowledgements

I would like to express my deepest gratitude to Revolve NTNU, the Department of Engineering Design and Materials and my supervisor Terje Rølvåg for making it possible for me to work on a subject that is close to my heart. Development of an electric motor for a high performance application like Formula Student has really been a dream come true.

Also I want to thank Sami Ruoho from Normag for giving me tips and feedback on modelling and use of permanent magnets in motor design. Furthermore I wish to thank Dr. Duane Hanselman for writing an excellent book on the design of permanent magnet motors.

Finally I wish to direct a thanks to all the sponsors of the projects, and especially EDR Medeso for providing the simulation tools needed for assessment and optimization of motor prototype.

Summary

Formula Student is an engineering student competition where students from universities all over the world design, build, test and compete with a formula style race-car. Revolve NTNU is competing in the electric segment of this competition and each year builds a new car to surpass the previous. For 2016 the team has decided to go over to a four wheel drive system with integrated electric motors in each wheel. This gives the car a huge potential in acceleration capabilities, yaw rate control through torque vectoring and efficient kinetic energy recovery by using the front wheel motors as generators during hard braking. However, moving from a one-motor rear wheel drive system from the 2015 season, a lot of new and innovative changes is required within powertrain and suspension design. This thesis focuses on the development of an electric motor tailored for use in Revolve's four wheel drive system.

Arriving at the final solution involved building a good understanding of the general product, as well as system requirements and external limitations. A modular motor concept in conjunction with a planetary gearbox proved to be the most promising way to pack enough torque and power density into the powertrain, utilizing the available space within the rim and suspension linkages to the fullest. Extensive use of computer aided design and simulation tools allowed for a very compact motor design with high performance. High focus on production and manufacturing constraints throughout the design process should yield a realizable concept. The final solution features a $\text{\O}100\text{mm} \times 110\text{mm}$, 3.7kg traction motor that should be able to deliver almost 500Nm peak torque output at the wheel. Furthermore, all required technical drawings and assembly manuals for production is also included. This should give the team a good starting point for physical prototyping and validation of the simulation results through physical testing and benchmarking.

Sammendrag

Formula Student er en ingeniørkonkurranse for studenter hvor lag fra universiteter fra hele verden designer, bygger, tester og konkurrerer med en formula racerbil. Revolve NTNU konkurrerer i det elektriske segmentet av konkurransen og bygger en ny bil hvert år for å overkomme den forrige. For 2016 sesongen har laget bestemt å gå over til et firehjulsdrevet system med integrerte elektriske motorer i hvert hjul. Dette gir bilen stort potensial i akselerasjon, svingkontroll gjennom pådragsallokering og et effektivt energi-gjenvinningssystem gjennom bruk av motorene som generatorer under hard brems. Det å gå fra en bakhjulsdreven bil med én elektrisk motor fra 2015 sesongen krever store forandringer innen hjuloppheng og drivverk. Denne oppgaven fokuserer på utvikling av en elektrisk motor, skreddersydd for Revolve sitt nye drivverk.

Veien til den endelige løsningen involverte god forståelse for elektriske motorer, så vel som systemkrav og eksterne begrensninger. Et modulbasert motorkonsept sammen med et planetgir viste seg å være den mest lovende måten å pakke nok dreiemoment og effekt i drivverket, ved å bruke den tilgjengelige plassen i felg og mellom hjulopphengs-stagene til det ytterste. Omfattende bruk av dataprogrammer til design og simulering gjorde det mulig å utvikle et veldig kompakt motordesign med høy ytelse. Et sterkt fokus på produksjon og sammenstilling gjennom hele design-prosessen burde også sørge for et realiserbart konsept. Den endelige løsningen innebærer en $\text{\O}100\text{mm} \times 110\text{mm}$, 3.7 kg trekkmotor som burde være kapabel til å levere nesten 500Nm dreiemoment på hjulet. I tillegg er alle maskintegninger og sammenstillingsillustrasjoner inkludert. Dette burde gi laget et godt utgangspunkt for prototypeproduksjon og validering av simuleringsresultater gjennom fysisk testing.

Abbreviations

AC Alternating Current. 22, 47–49, 52, 61, 133, 236

CAD Computer Aided Design. 66, 95, 110, 151

CTE Coefficient of Thermal Expansion. 153, 155, 156, 166, 167

DC Direct Current. 22, 52, 59, 61, 63, 65, 170

EMF Electromotive-Force. 28, 43, 44, 53, 59, 62–65, 173, 197, 198, 201

FSA Formula Student Austria. 60

FSAE Formula SAE. 58

FSG Formula Student Germany. 12

FSUK Formula Student United Kingdom. 74

IM Induction Motor. 34–36

IP Ingress Protection. 68, 90

PMM Permanent Magnet Motor. 34–36

PWM Pulse Width Modulation. 63, 64, 202, 203, 237

SAE Society of Automotive Engineers. 11

SRM Synchronous Reluctance Motor. 35

Contents

1	Introduction	11
1.1	Formula Student	11
1.2	Revolve NTNU	13
1.3	The Challenge	16
2	Methodology	18
2.1	Introduction	18
2.2	Strategy	18
3	Research	22
3.1	Modern Brushless Motors	22
3.2	Fundamentals	24
3.3	Loss Mechanisms	31
3.4	Brushless Motor Types	34
3.5	PM Motor Fundamentals	36
4	Initial Assessment	57
4.1	Requirements	57
4.2	Performance	68
5	Concept	81

5.1	General Sizing	81
5.2	Concept Development	84
5.3	Concept Considerations	89
5.4	Product Specification Form	93
6	Design	94
6.1	Introduction	94
6.2	Initial Considerations	95
6.3	System Integration	100
6.4	Boundary Conditions	100
6.5	Motor Housing Design	108
6.6	Bearing System	112
6.7	Magnetic System	125
6.8	Material Selection	152
6.9	Interference Fits	157
7	Simulation	168
7.1	Magnetic Analysis	168
7.2	Modal Analysis	203
8	Production	222
8.1	Technical Drawings	222
8.2	Manufacturing Procedure	222
9	Conclusion	225
A	Data Sheets	245
A.1	Heidenhain ECI1100	246
A.2	Micro-Epsilon CT-CF02-C3	248
A.3	AMK DD5	249
A.4	N35EH	252

A.5 36CrNiMo6	253
A.6 42CrMo4	254
A.7 Alumec 89	255
A.8 SS304	256
B Technical Drawings	258
C Assembly Manual	272
D SKF Bearing Stiffness Calculation	320

Chapter 1

Introduction

1.1 Formula Student

Formula Student or Formula SAE is an engineering competition for students. Team members are challenged to construct a single seat formula race-car and compete against other teams from all over the world. The concept was developed by the Society of Automotive Engineers (SAE) to give students an opportunity to experience teamwork, design, manufacture and cost aspects of automotive engineering along with time and project management. Rules and regulations are constantly under revision to encourage the students to be creative in the design and use of alternative fuels. In Formula Student electric vehicles race head to head with combustion vehicles. [1]



Figure 1.1: Endurance event at FSG 2014

Since its origin in 1978, the competition has been a huge success and spread across the globe. Today the event is held annually in many different countries including UK, Germany, Brazil, Japan and several states in the US to mention a few.[2] The rules and regulations are standardized to allow teams to compete in several events. In August 2015 at Formula Student Germany (FSG) a total of 115 teams with over 3000 students from 34 different countries was signed up for the event.



Figure 1.2: Formula Student Germany 2013

The competition is divided into three static and five dynamic disciplines. Static disciplines address the engineering design and documentation, the manufacture and assembly cost of the vehicle and a fictitious business case for the project. Dynamic disciplines test acceleration and turning capabilities, overall performance, reliability and efficiency. Teams are scored according to their result at each discipline. A maximum score of 1000 points is possible. [3]

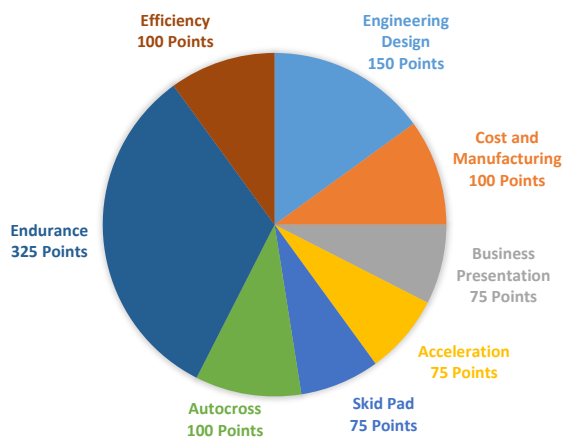


Figure 1.3: Discipline scoring distribution in FSG

1.2 Revolve NTNU

Revolve NTNU was initiated in 2010 by four students at the department of Engineering Design and Materials at NTNU who wanted to work on something practical as an extracurricular activity. The goal was to build a foundation for the new born organization to develop in the future. Simplicity and reliability were the main focus of this first vehicle. Two years later Revolve NTNU had 23 members from 6 different engineering departments and stood ready with their first car - KA Borealis R, on the starting line at Formula Student UK.

The car featured a four cylinder motorcycle engine and a steel tubular space frame, and weighed in at 260kg. This marked Revolve NTNU and Norway's first contribution to Formula Student. The same year Revolve NTNU won an award for best newcomer and finished overall as 17th among 102 competitors.



Figure 1.4: 2012 car KA Borealis R [Sofie Brovold]

The 2013 team expanded to 46 members, and decided to further develop the 2012 concept with petrol engine and steel tubular space frame. The second car was named KA Aquilo R, and featured a full aerodynamic package, adaptive suspension and a continuous variable air intake, weighing in at 249kg. With a new launch control algorithm the car was able to accelerate from 0 to 100km/h in 3.6 seconds. The car competed in Formula Student UK and Formula Student Germany and was awarded National Instruments Measurement and Control award as well as best nordic car, finishing 16th overall.



Figure 1.5: 2013 car KA Aquilo R [Sofie Brovold]

During two successful seasons running a petrol engine with a steel frame, the organization had built up enough confidence, knowledge and skilled people to take a big technological leap. The goals for the 2014 season were to construct Norway's first electric race car, extend the use of carbon reinforced plastic in structural design and deploy as large aerodynamic package as possible. The result was KOG Arctos, featuring a fully electric rear wheel drive powertrain and a carbon fiber monocoque. Through extensive focus on weight in all steps, the car ended up at 185kg, a weight loss of 65kg compared to the 2013 car. The car finished 9th overall in Formula Student Germany.



Figure 1.6: 2014 car KOG Arctos R [Torbjørn Buvarp]

After a huge leap in the 2014 season, the 2015 team decided to refine on the

2014 concept. Reliability and producibility were the main areas of focus, while further reducing weight where possible. New projects this year were an in-house developed inverter and inertial measurement unit. Due to new rules and regulations the entire aerodynamic package had to be reworked. This resulted in Vilje, the fourth car in the ranks. Vilje featured a fully electric powertrain and a carbon fiber monocoque, weighing in at 175kg. Due to its reliability, Vilje was driven each day in the two month long testing period. This resulted in a 4th overall placement in Formula Student Austria.

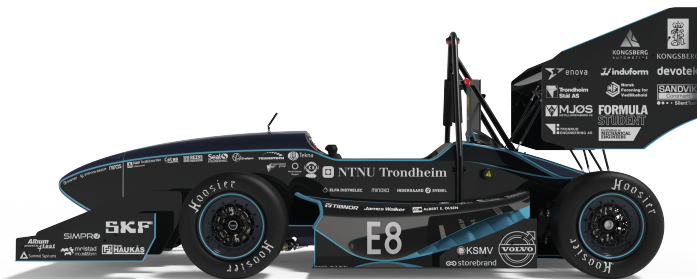


Figure 1.7: 2015 car Vilje [Martin Eie]

1.3 The Challenge

The main goal for the 2016 season is to change the powertrain layout from a rear wheel driven system to a four wheel driven system with hub mounted electric motors, while keeping a carbon fiber monocoque and 10inch rims. This includes re-thinking many of the concepts and designs of earlier cars. One of the challenges is to have a suitable motor, as there are many special and functional requirements posed on the motor when hub mounting is mated with 10-inch rims.

Since the motor is a very important link in the new powertrain, Revolve NTNU has initiated a motor development project. The goal is to develop a motor prototype tailored for the application and comparing it against commercial available solutions. This master thesis focuses on the development process for Revolve's first electric motor prototype.

Chapter 2

Methodology

2.1 Introduction

The development of a specially tailored high performance electric motor is not a trivial task. First of all, fundamental motor theory needs to be properly understood. Furthermore, specific requirements posed by interfacing systems, rules and operating conditions must be established early in the development process to ensure all criteria are met. Practical aspects need to be addressed during the concept and design phase to make sure the chosen concept is realizable.

2.2 Strategy

In order to ensure project integrity, the different stages in the development process were identified and ordered in a logical sequence. Within each stage, clear goals and objectives were established to make sure the progression could be monitored and evaluated.

1. Research

Goal: Understand the key concepts of the underlying theory and basic construction of electrical machines. Also get familiar with the available materials and production methods for motor construction.

Objectives:

- Review fundamental theory.
- Choose a motor technology.
- Investigate the key relations and aspects for the chosen technology.

2. Initial Assessment

Goal: Establish an overview of the powertrain, identifying requirements and limitations of interfacing systems, competition rules and working environment. Analyze traction limitations and establish drive cycles to determine desired torque and speed characteristics.

Objectives:

- Get a system overview.
- Identify requirements and limitations posed on the motor.
- Analyze tire grip characteristics.
- Propose a tire model and determine coefficients.
- Establish drive cycles through lap time simulations.

3. Concept Development

Goal: Develop and consider different motor concepts. Do some initial considerations regarding the chosen concept.

Objectives:

- Systematically develop and evaluate different motor concepts.
- Determine a general concept for further development.
- Do some initial concept considerations regarding compatibility with other systems.
- Create a product specification form.

4. Engineering Design

Goal: Come down to a working prototype concept, satisfying all requirements from the product specification form.

Objectives:

- Identify boundaries and interfaces with other systems.
- Build a geometrical model that includes all motor sub-systems.
- Design all sub-systems.

5. Simulation

Goal: Use simulation tools to analyse and optimize motor design.

Objectives:

- Analyse the initial motor design.
- Do optimization of the magnetic system.
- Decide on a final design.

6. Production Planning

Goal: Prepare the final design for production.

Objectives:

- Create technical drawings.
- Make an assembly manual for the motor.

Chapter 3

Research

3.1 Modern Brushless Motors

Since the first electric motors came in mid 1800's, many different types and constructions have been developed for different purposes. In the first century of electric motors, there were mainly two different types available. The first type were brushed DC motors powered by batteries, which had the advantage of speed control by employing a variable resistance on the electrical circuit. The second type were brushless AC motors, running at a constant speed from a 50-60Hz power grid, but yielding superior robustness and efficiency compared to their DC counterparts.

In the mid 1900's, there was a revolution in power electronics when the first PWM inverter drive was developed. The inverter uses a DC voltage source to modulate AC current sine waves of variable frequencies and amplitude. This made it possible to use the more efficient and robust brushless motors in speed variable applications, and led to the modern brushless electric motors of today. Only this type of motor will be considered in this thesis.

3.1.1 General Construction and Topologies

The electric motor consists of two main components: a rotor and a stator, both cylindrical in shape and concentrically aligned. As the names suggest, the stator is the stationary part of the motor, it contains copper coils and is connected to the inverter. The rotor is connected to the rotating output shaft. These two parts are physically separated from each other and only connected through bearings, allowing for relative movement. The distance separating the stator from the rotor is typically referred to as the air gap.

Different motor topologies are possible, depending on the shape and relative position of the rotor and stator. The most common topology is called a radial in-runner motor. In this topology, the rotor is located inside the stator, which provides a natural protection of the rotating components. The radial out-runner motor is a similar layout, but the rotor and stator have switched places. This topology provides natural retention of the rotor components against centrifugal forces. A third alternative is called an axial motor. Instead of separating the rotor and stator radially, they are separated axially. This typically makes the motor diametrically large and axially short. The actual choice of topology is largely dependent on the available space for the motor. Illustrations of the two types are given in figure (3.1), where the stator and rotor are shown in different colors.

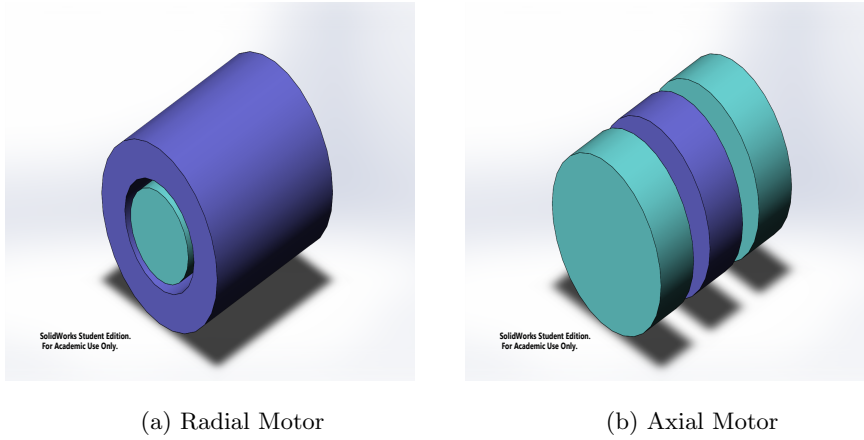


Figure 3.1: Main Motor Topologies

3.2 Fundamentals

The electric motor converts electrical energy to mechanical energy and vice versa through the interaction of the magnetic fields between the rotor and stator. In all cases, the magnetic field of the stator is generated by sending currents through wound coils. The rotor magnetic field can either be generated directly by permanent magnets or indirectly by the stator field.

3.2.1 Magnetic Fields

Magnetism is a field concept, analogous to electrical fields and is described in the same mathematical framework. A magnetic field is the spatial distribution of two field variables called magnetic flux intensity, denoted \vec{H} and magnetic flux density, denoted \vec{B} . The two field variables are related by a constitutive relation. For magnetically isotropic materials commonly used in electric motors its differential form can generally be expressed as

$$d\vec{B} = \mu(\vec{H}, X)d\vec{H} \quad (3.1)$$

The curve described by equation (3.1) is commonly referred to as BH curve. μ is called the permeability of the material and describes how well the material conducts magnetic fields. The parameter X contains the previous history of magnetization and is used to account for hysteresis. Nonmagnetic materials have a linear magnetic behavior, and the value of μ is more or less constant and very close to the vacuum permeability, noted μ_0 . For magnetic materials the BH curve is nonlinear and exhibits hysteresis behavior.

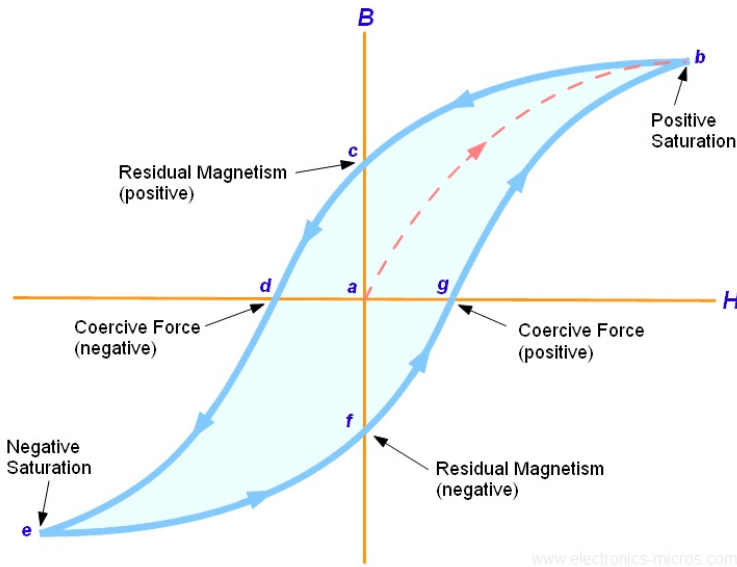


Figure 3.2: A general nonlinear BH curve [4]

Magnetic field lines will always form complete loops. The physical interpretation of this is that a magnetic north pole will always come in pair with a magnetic south pole. In mathematical terms this can be expressed in its differential form as flux continuity.

$$\vec{\nabla} \cdot \vec{B} = 0 \quad (3.2)$$

Typically in practical applications it is desirable to relate field quantities to lumped quantities, describing the field effects as a single scalar quantity. In magnetic fields, the lumped parameter for magnetic field intensity \vec{H} is the magneto-motive force, denoted F . It quantifies the tendency of magnetic field to flow along a curve C , and is analogous to voltage in electrical systems.

$$F = \int_C \vec{H} \cdot d\vec{l} \quad (3.3)$$

The lumped parameter for the magnetic flux density \vec{B} is the magnetic flux, denoted ϕ . It quantifies how much net magnetic flux that penetrates an arbitrary surface defined by a closed boundary line C , and is analogous to current in electrical systems.

$$\phi = \iint_C \vec{B} \cdot d\vec{A} \quad (3.4)$$

Sources of Magnetic Fields

Sending electrical current through a conductor establishes a magnetic field around it. This is described mathematically by Ampere's law. It relates the current enclosed by an arbitrary loop C to the magnetic field intensity along the loop.

$$\oint_C \vec{H} \cdot d\vec{l} = I_{encl} \quad (3.5)$$

Using this principle, a conductor can be wound into a coil, simulating a magnet when current is sent through. The magneto-motive force created through the coil can be found by applying equations (3.5) and (3.3) to a coil arrangement with N number of turns. This yields the following result.

$$F_{coil} = NI \quad (3.6)$$

In other words, the magneto-motive force produced by a current carrying coil is proportional to the product of the current carried and the number of turns. As the coil will work as a magnet when excited with a current, it is also referred to as an electromagnet.

Permanent magnets are the other common source to magnetic fields. These magnets are special metallic alloys that can retain a residual magnetic field after being exposed to a strong magnetic field during production. The main difference to an electromagnet is that no excitation current is needed to generate the magnetic field once the magnet is magnetized.

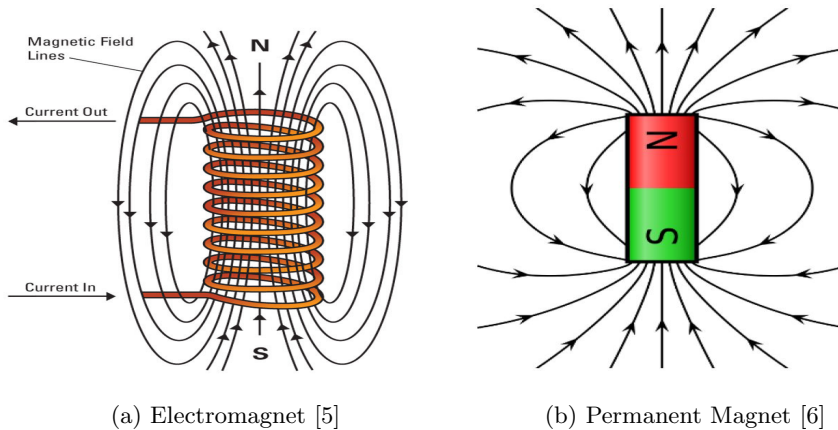


Figure 3.3: Common Magnetic Field Sources

Electromagnetic Induction

Electromagnetic Induction is a phenomenon that couples magnetic fields to electric fields. This is described mathematically by Faraday's Law. It simply

states that a changing magnetic field will induce a circulating electromotive force around it, virtually simulating a voltage source. This induced voltage plays a key role in electric machines and is referred to as back EMF, noted ϵ . In its lumped parameter form, Faraday's law is stated as

$$\epsilon = -\frac{d\lambda}{dt} \quad (3.7)$$

where λ is the magnetic flux ϕ linked to a physical object, e.g. a conductor, and shares its definition. It is important to note that the induced voltage ϵ and the flux linkage λ refer to the same closed curve C defined in equation (3.4). If equation (3.7) is applied to a coil that is linked to a magnetic flux λ , each turn of the coil will experience the induced voltage of ϵ , yielding a terminal voltage proportional to the number of turns.

An essential detail of electromagnetic induction is that if the back EMF is allowed to drive currents in its direction, the induced current will generate its own magnetic field that tends to cancel out the flux change that generates the induced voltage. This is called Lenz' Law, and ensures energy conservation is satisfied.

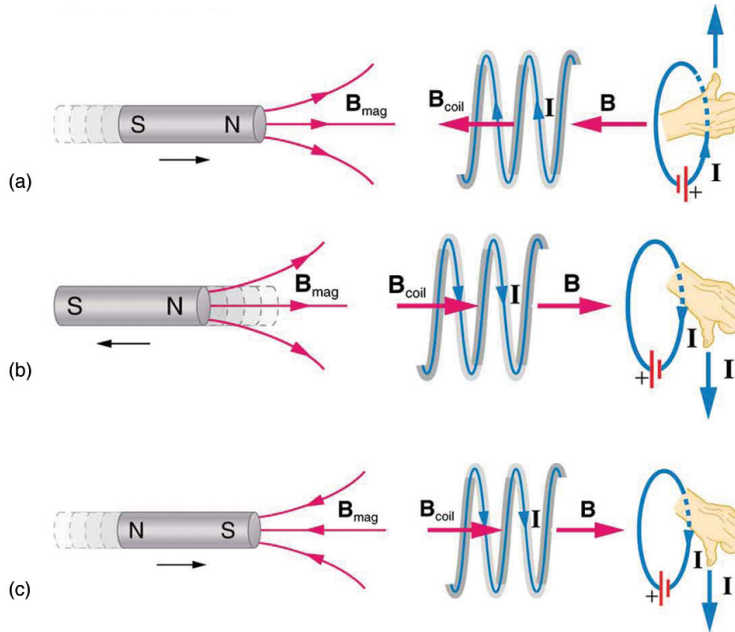


Figure 3.4: Electromagnetic Induction [7]

Another important consequence of Faraday's Law is that if there is a time-varying magnetic field present within any electrical conductive component, circulating currents will occur due to the induced voltages. These induced currents are named eddy currents due to their circulating behavior and are undesirable as they contribute to energy dissipation and heat generation within the motor.

Magnetic Forces

The magnetic force between two physical objects is used to generate all torques in an electrical machine. These forces can either be attractive or repulsive. Two equal magnetic poles will repel each other, two opposite poles attract and ferromagnetic materials will attract to either magnetic polarity. The magnitude of this force is related to the strength of the magnets and the distance between them. If the magnetic field around an object is known, the magnetic force

can be calculated using either the principle of virtual work or Maxwell's stress tensor. The actual in-depth calculation will not be included in this thesis.

3.2.2 Magnetic Materials

There are two main categories of magnetic materials. They are characterized by the shapes of their BH curves. Soft magnetic materials have very thin and tall BH curves. They are excellent for conducting magnetic flux as only a small field intensity is needed to get a resulting high magnetic flux density. These materials are typically used in the stator to carry magnetic flux efficiently around the coils. Iron and cobalt alloys exhibit this behavior. The flux density at the knee region of the BH curve is called the saturation flux of the material. Beyond the saturation flux, the permeability drops rapidly to that of a non-magnetic material, i.e. vacuum, e.g. air.

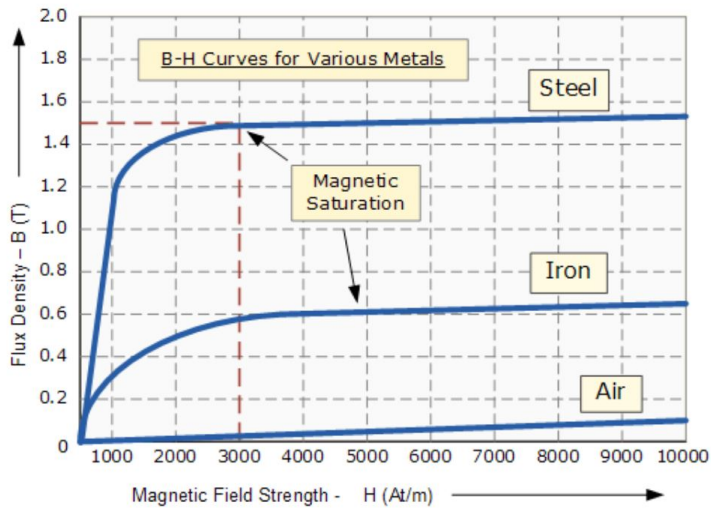


Figure 3.5: Magnetization curves of soft magnetic materials [8]

The second category is called hard magnetic materials, and is characterized by a very wide BH curve. These kind of materials will retain a residual magnetic

field after being exposed to a strong magnetization field because the BH curve will follow a wide hysteresis curve. In other words, this class of materials are permanent magnets. Although the BH curve is nonlinear for permanent magnets, they should only be used in their linear region after first magnetization to avoid permanent demagnetization. Due to this, they are modelled as linear elements in practical analysis.

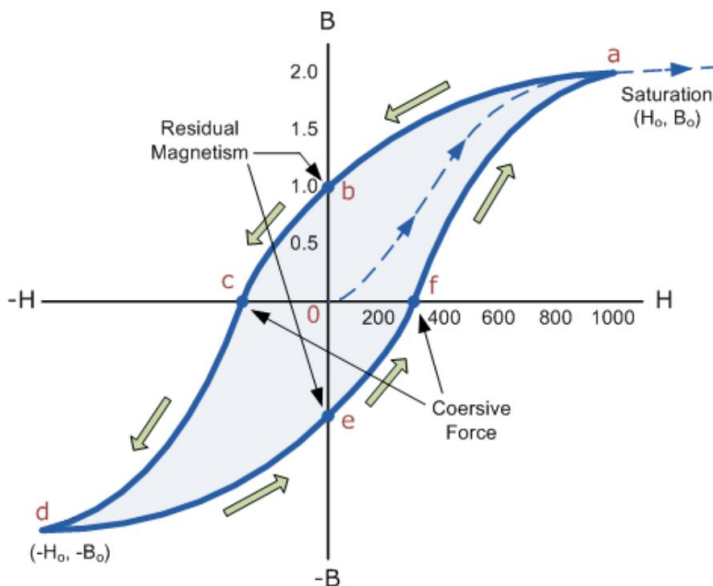


Figure 3.6: Electromagnetic Induction [8]

3.3 Loss Mechanisms

The performance of electrical motors is typically dependent on how efficiently they can produce torque. All motor losses reduce the available torque output, but more importantly they end up as heat in either the rotor or stator. Both the coil insulation and permanent magnets are heat sensitive and deteriorate if operated at high temperatures. To make sure the motor is able to deliver high performance, it is important to know the different loss mechanisms and how

they can be reduced in design.

3.3.1 Ohmic Losses

As all brushless motors use electromagnets to produce torque, the excitation current needed to magnetize the coils will cause heat loss. The loss in a conductor with resistivity R and passing current I is found by combining Ohm's law with the power equation for electrical components.

$$P_{ohmic} = RI^2 \quad (3.8)$$

Although not directly useful for motor design, equation (3.8) shows that if the excitation current is doubled through an electromagnet, the power losses will increase with a factor of four.

3.3.2 Hysteresis Losses

When an alternating magnetic field is applied to a magnetic material, e.g. iron, the magnetic domains of the material will with each cycle align with the applied field. This continuous alternating alignment causes internal losses in the material. As a rule of thumb, the loss increases with the area enclosed by the hysteresis loop, and is typically approximated by ([9], p. 31)

$$P_h = k_h f B_p^n \quad (3.9)$$

where k_h is a material dependent constant, f is the frequency of the applied magnetic field, B_p is the peak flux amplitude within the material and n is a material dependent exponent, usually between 1.5 - 2.5.

3.3.3 Eddy Current Loss

As discussed in section (3.2.1), alternating magnetic fields within a conductive material will induce circulating currents. These eddy currents contribute to motor losses through ohmic dissipation, described by equation (3.8). Although eddy current losses are ohmic, strictly speaking, the category of ohmic losses is reserved to coil excitation currents. Eddy current losses are always undesirable and only contribute to diminish motor performance. For sinusoidal magnetic fields, eddy current losses are commonly approximated by the relationship ([9], p. 31)

$$P_e = k_e h^2 f^2 B_p^2 \quad (3.10)$$

where k_e is a material dependent constant, h is the height of the material perpendicular to the magnetic flux direction, f is the frequency of the applied magnetic field and B_p is the peak flux amplitude within the material.

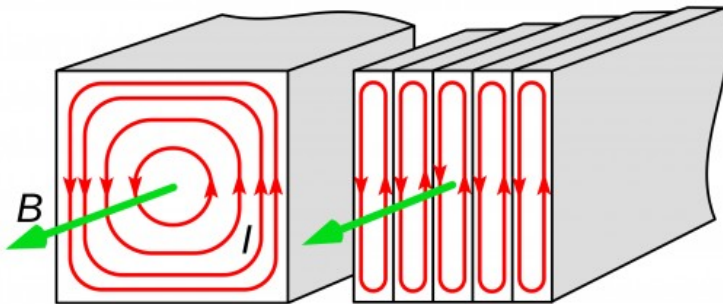


Figure 3.7: Eddy current loss in conductive materials [10]

3.3.4 Friction Losses

When the motor is running, there will be friction losses in the bearings and due to the viscosity of the air between the rotating and stationary components.

These losses are all referred to as frictional losses and are mechanical of nature and more or less independent on electromagnetic design.

3.4 Brushless Motor Types

Modern brushless motors come as three main types, all utilizing the same stator, but they differ in the way that the rotor's magnetic field and torque are produced. This influences both the construction and operation of the motor.

3.4.1 Permanent Magnet Motor (PMM)

The permanent magnet motor utilizes permanent magnets on the rotor in order to establish the rotor's magnetic field. It has the highest torque to weight ratio of the three types. Furthermore, the motor control schemes are relatively simple. Also, the rotor only contains permanent magnets, which simplifies its construction.

On the other hand, high performance permanent magnets are generally expensive. Also, the rotor field is constant regardless of speed, which means the motor must use the stator coils to field weaken the rotor for extended speed operation, which reduces its efficiency. Lastly, the constant magnetic field from the rotor causes hysteresis and eddy current losses in the stator as long as the shaft is rotating, referred to as magnetic drag.

3.4.2 Induction Motor (IM)

Induction motors have embedded coils in the rotor, and induce currents in them using the varying magnetic field from the stator. These induced currents excite the rotor coils, which magnetizes the rotor. The main advantage of induction motors in traction applications is that the rotor's magnetic field can be

indirectly controlled by the stator currents. This allows for coasting at speeds without the magnetic drag of the PMM.

Since electromagnets are used in the rotor, additional ohmic losses will occur here. This reduces efficiency and heats up the rotor, which is much harder to cool efficiently compared to the stator.

3.4.3 Synchronous Reluctance Motor (SRM)

Unlike the PMM or IM that use both repulsion and attraction between rotor and stator magnets in order to produce torque, the SRM uses an oddly shaped ferromagnetic rotor and the attraction of iron to either magnetic polarity to produce torque. As the torque production is only based on attraction it is inherently weaker than the PMM or IM. Magnetic saturation of the rotor core affects the torque characteristics in a nonlinear manner, which is generally undesirable for control.

The advantages of the SRM are the absence of permanent magnets and conductors in the rotor. This makes it very robust against high temperatures. Losses in the rotor are low and it has the advantage of no magnetic drag. Rotor manufacturing could be somewhat difficult due to very thin rotor webs.

3.4.4 Motor Comparison

Based on the qualitative characteristics of the different motor types, a comparison is done to determine the most suited technology for racing applications.

Motor Type	PMM	IM	SRM
Performance	++	+	0
Simplicity	+	0	0
Manufacturability	+	-	0
Controlability	+	-	0
Cost	-	0	+

Table 3.1: Motor Comparison

The permanent magnet motor is chosen based on its superior raw performance and good controlability. The high cost of permanent magnets can be justified by the simplicity and relative ease of manufacture compared to the other types. Only this type of motor will be investigated further in this thesis.

To back up the choice, a paper was written in 2007 on comparison of a PMM and IM for use in a high performance go-kart. Physical tests showed the PMM to yield the highest efficiency and millage in racing applications. [11]

An article written by well known motor expert James R. Hendershot Jr. compares brushless motors for mass production. In this article the PMM has superior performance, but high cost in mass production due to the price of permanent magnets. [12]

3.5 PM Motor Fundamentals

Regardless of motor topology, the general construction and working principles of the PMM are similar. A brief description will be given in this section. The cross section of a typical in-runner PMM is shown in figure (3.8). Magnets are marked in red and blue for north and south pole, respectively. Iron is grey and

coils are marked in green, yellow and orange for the different motor phase coils.

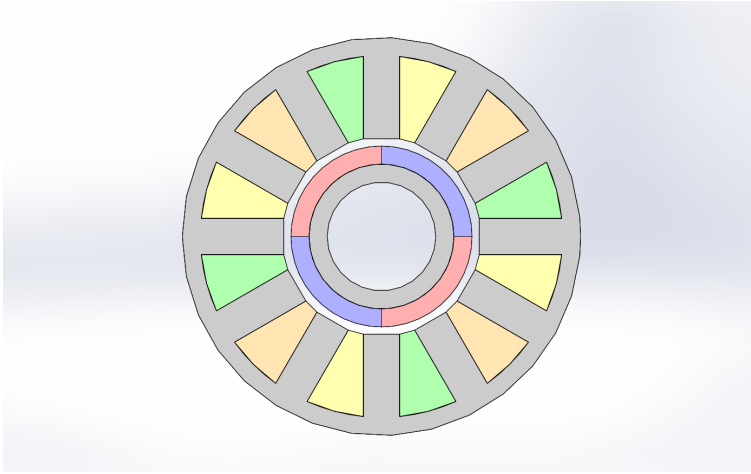


Figure 3.8: Typical PMM in-runner cross section

The active parts of the motor are in essence the magnets on the rotor and the coils on the stator. Torque is produced by magnetic attraction and repulsion between the rotor's permanent magnets and the stator's electromagnets. In order to produce an even torque output, the coils must be excited at the right time with respect to the rotor's position, a process called commutation.

As the magnetic force between two objects increases by the strength of the magnetic field between them, it is desirable to have as high flux as possible between the rotor and stator to maximize torque. Since air has a relatively low permeability, i.e. ability to conduct magnetic flux, a ferromagnetic material is typically used to guide the flux between the magnets and stator coils. There are motors that do not use iron flux carriers, called iron-less, but due to their typically large diameters, they are not considered in this thesis.

3.5.1 General Construction

Several permanent magnets are located on the rotor with an alternating pattern of north and south poles. A motor may be constructed with any even number of magnetic poles. The stator consists of a circular iron core with cut grooves to insert coils. These grooves are called slots, and the radially aligned iron between the slots is called teeth. The circular arc connecting the stator together is called the stator yoke or back iron. (See figure 3.8)

Conducting coils are placed in these slots to make up the electromagnets of the stator. These individual coils may either span one or several stator teeth. The section of the coils that spans from one slot to the next is termed end turns. If each coil spans one tooth, the winding is called concentrated. On the other hand, if each coil spans several teeth and overlaps with other coils, the winding is distributed. The number of slots and the corresponding coil pattern is largely dependent on the number of magnetic poles on the rotor, and is typically determined subsequent to the pole count.

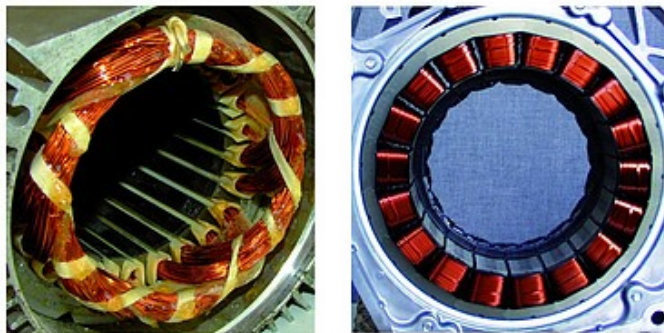


Figure 3.9: Lap and concentrated windings, respectively [13]

Instead of controlling the current into each individual coil of the motor, coils that tend to attract the rotor in a similar direction when energized are connected together to form motor phases. This is done primarily to reduce the number of power electronic devices required to control the winding currents. A motor may be constructed with any number of phases, greater than or equal to one. However, three phase motors dominate all others in industrial and high performance applications as they offer the best compromise between performance and cost.

3.5.2 Magnetic Circuit Analysis

An important concept in the assessment of electric motors is the magnetic circuit. By assuming the direction of the magnetic field is known, the vector field problem is reduced to a scalar problem, which greatly simplifies the mathematics and allows for an analytical solution of the field density within the motor. Although serving as a crude approximation, magnetic circuit analysis yield insight into key performance parameters.

Magnetic Reluctance

Reluctance is a lumped parameter that describes how easily a component conducts magnetic flux, and is analogous to resistance in electrical systems. Its mathematical formulation is given by ([9], eq. 2.7)

$$R = \frac{L}{\mu A} \quad (3.11)$$

where L is the length the flux has to travel, A is the cross sectional area normal to the flux and μ is the permeability of the material. The reluctance relates the magneto-motive force F over the component to the resulting magnetic flux ϕ through it.

$$\frac{F}{\phi} = R \quad (3.12)$$

Permanent Magnet Modelling

As mentioned earlier, permanent magnets should only be used in their linear region to prevent demagnetization. Due to this, the demagnetization characteristic of a permanent magnet is given as ([9], eq. 2.21)

$$B_m = B_r + \mu_m H_m \quad (3.13)$$

where B_m is the delivered flux density in the magnet, B_r is the magnet's remanence and describes the maximum flux density it can deliver by itself, μ_m is its permeability and H_m is the field intensity inside the magnet.

In the magnetic circuit approach, the magnet is assumed rectangular and the field within is considered to be uniform. Using equations (3.3) and (3.4), a lumped circuit element can be derived for a permanent magnet

$$\phi_m = \phi_r + \frac{F_m}{R_m} \quad (3.14)$$

where

$$\phi_r = B_r A_m \quad (3.15)$$

is a fixed source and

$$R_m = \frac{L_m}{\mu_m A_m} \quad (3.16)$$

is the reluctance of the magnet.

Motor Flux Analysis

Air gap flux due to the permanent magnets can be assessed by magnetic circuit analysis, making some simplifications. First, the permeability of the iron core is assumed to be infinite compared to the permeability of air and magnet material. This excludes the nonlinear core material from the analysis. Secondly, all the magnetic flux from the magnet is assumed to cross the air gap, with no leakage flux that short circuits between the magnet poles. Lastly, the permeability of the magnet and air gap is assumed to be equal to the vacuum permeability μ_0 . An illustration of the circuit is shown in figure (3.10).

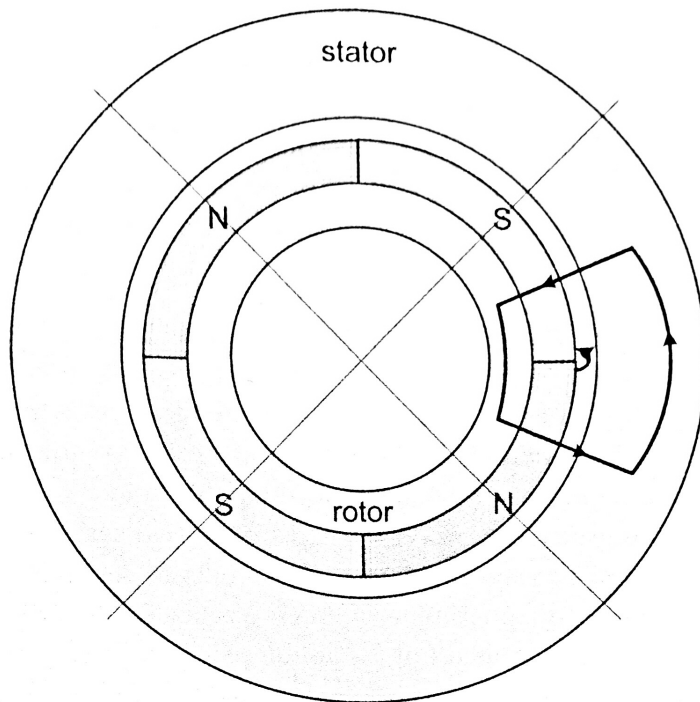


Figure 3.10: Magnetic Circuit in motor ([9], fig. 4-1b)

Since the flux leaving the magnet is equal to the flux crossing the air gap,

the air gap flux density B_g is related to the magnet flux density B_m as ([9], eq. 2.29)

$$B_g = B_m \frac{A_m}{A_g} = B_m C_\phi \quad (3.17)$$

where A_m and A_g are the cross sectional areas of the magnet and air gap, respectively. C_ϕ is the flux concentration factor, and measures how much the magnet flux is concentrated through the air gap. Furthermore, the magnet operating point is given by ([9], eq. 2.33)

$$P_c = \frac{-B_m}{\mu_0 H_m} = \frac{L_m}{L_g} \frac{1}{C_\phi} \quad (3.18)$$

P_c is the permeability coefficient of the magnet and defines its operating point along the magnetization line given by equation (3.13). L_m and L_g are the length of the magnet and air gap, respectively.

This remarkably simple result indicates that the magnetic flux of the air gap, which plays a key role in torque production, can be increased by either increasing the magnet operating point P_c which in turn increases B_m or by increasing the flux concentration factor C_ϕ . However, focusing the magnetic flux by increasing C_ϕ comes at the cost of lowering the operating point P_c .

The permeance coefficient P_c defines the flux density output of the magnet, but more importantly it is directly related to how well the magnet is protected against demagnetization. During high temperature operation under the influence of strong demagnetizing fields from the stator, the magnet may partially demagnetize if the permeance coefficient drops too low. By inspection of equation (3.18), this means the magnet length L_m should be significantly larger than the air gap length L_g , depending on the amount of flux concentration C_ϕ .

3.5.3 Torque Production

In practice, the torque production can either be calculated using a field approach or an energy approach. The field approach requires the use of FE-analysis in order to approximate the actual field distribution in the motor before calculating the torque, typically from the principle of virtual work.

The advantage of an energy based approach is that it provides analytical formulas for torque production by assuming the magnetic field distribution is known, e.g. from magnetic circuit analysis. This approach will be used for the initial assessment of motor performance.

When the rotor is moving relative to the stator, it will generate an alternating magnetic flux that links with the stator coils. According to Faraday's Law (Equation 3.7) a back EMF will be induced. If an external voltage is applied on the circuit to drive the current against the back EMF, the energy absorbed by the magnetic field will go to torque production. By applying the principle of energy conservation, the torque can be calculated by

$$T\omega + \epsilon I = 0 \tag{3.19}$$

Phase Back EMF

Brushless synchronous motors are designed to have sinusoidal back EMF on the phases because it yields better controllability and less torque ripples. Although the actual back EMF wave-shapes always include some higher harmonics, the sinusoidal assumption commonly used to simplify the mathematics.

The number of alternating magnetic poles on the rotor determines the frequency of alternating flux linkage in the motor phases. This is named the

electrical frequency of the motor and relates to the rotational frequency of the shaft according to

$$\omega_e = \frac{N_m}{2}\omega_m \quad (3.20)$$

where ω_e is the electrical frequency, ω_m is the mechanical frequency of the output shaft and N_m is the number of magnetic poles. The frequencies are typically expressed in hertz or radians per second.

The collective flux linkage of a phase winding can in general be approximated by

$$\lambda_{phase}(t) = \phi_g K_s N \sin(\omega_e t) \quad (3.21)$$

where ϕ_g is the average flux crossing the air gap, K_s a constant that accounts for stator geometry and winding pattern, N is the number of turns per coil. Then the phase back EMF is found by applying Faraday's law (Equation: 3.7), yields

$$\epsilon_{phase}(t) = -\omega_e \phi_g K_s N \cos(\omega_e t) \quad (3.22)$$

Mutual Torque

Substituting ω_e for ω_m by equation (3.20) and applying a sinusoidal current phase shifted by 180 degrees to the EMF, given by $I(t) = I \cos(\omega_e t)$, the torque production can then be calculated using equation (3.19), which yields the instantaneous torque per phase

$$T_{phase}(t) = \frac{N_m}{2} \phi_g K_s (NI) (\cos(\omega_e t))^2 \quad (3.23)$$

As the back EMF and currents of each phase winding are separated by 120 electrical degrees, the accumulated torque from all three phases is given by

$$T_m = \frac{3}{4} N_m \phi_g K_s (NI) \quad (3.24)$$

This torque comes from the interaction between the rotor permanent magnets and stator coils and is called mutual torque. Mutual torque is the major torque component in permanent magnet motors and is proportional to the ampere-turns (NI) through the windings. In high performance PM motors, this is the major torque component.

Cogging Torque

When a ferromagnetic material is used in the motor to help link the rotor flux with the stator windings, the permanent magnets will tend to align with the teeth of the stator, which represents the minimum energy state of the field. This aligning torque is called cogging torque and is undesired as it creates torque ripples. These torque ripples come in addition to the mutual torque produced by the coils.

There are essentially two ways of reducing cogging. One is by using a fractional slot to pole motor, i.e. slots per pole is not an integer. This makes the cogging components of each pole/tooth to be out of phase with one another, partially canceling each other out. The alternative way is to skew either the magnet poles or the slots of the stator. This last technique may totally eliminate cogging torque, but it compromises with increasing the complexity of either the rotor or stator.

Reluctance Torque

Some rotor topologies may include another torque component called reluctance torque. This torque mechanism is essentially what reluctance motors, discussed in section (3.4.3), utilize to produce all their torque. It is based on if the

rotor iron has a preferred alignment direction to the imposed stator field. The reluctance torque component is usually small in PM motors.

3.5.4 Motor Losses

All losses that occur in PM motors are related to the loss mechanisms discussed in section (3.3). This section will briefly discuss their appearance and significance in PM motors. Although present, mechanical losses from friction will not be included as there is not a lot that can be done here from a designer's point of view, except choosing low friction bearings.

Copper Losses

Copper losses occur in the windings of the motor whenever current runs through them, and can be described by equation (3.8), where I is substituted by the RMS current I_{rms} . The resistance per slot is given by ([9], eq. 4.42)

$$R_{slot} = \frac{\rho L_{st} N^2}{K_{wb} A_{slot}} \quad (3.25)$$

where ρ is the resistivity of copper, L_{st} is the stack length, i.e. length of the stator iron, N is the number of turns of the coil, K_{wb} is the copper fill factor, i.e. the fraction of bare copper within the slot, and A_{slot} is the slot area. By defining the RMS current density through the coil as

$$J_{rms} = \frac{I_{rms}}{A_{wb}} \quad (3.26)$$

where A_{wb} is the copper diameter of the coil wire, the ohmic loss of the slot can be written as ([9], eq. 4.44)

$$P_{ohmic} = (K_{wb} A_{slot} L_{st}) \rho J_{rms}^2 \quad (3.27)$$

The parenthesis on the right hand side is the volume of the bare copper within the slot. ρJ^2 is the loss density within the copper. ρ typically increases with temperature, and can be approximated linearly by

$$\rho(T) = \rho(T_0)(1 + \alpha_p(T - T_0)) \quad (3.28)$$

For copper, the parameters of this equation are commonly chosen as $\rho(T_0) = 1.72 \cdot 10^{-8} \Omega \cdot m$, $T_0 = 20 \text{degC}$ and $\alpha_p = 4 \cdot 10^{-3}$ ([9], section 4.5). As temperature increases over 100 degC, it will increasingly underestimate the resistivity. With the given α_p value, the resistivity of copper increases with 4% for each 10degC increase of the temperature, i.e. copper at 100 degC has 32% higher resistivity than at 20 degC.

Copper AC Losses

In the previous section the classical ohmic losses were assessed for a copper coil within a slot. When the electric frequency increases, additional AC losses will occur. These frequency dependent losses are due to a phenomenon called skin effect. When the frequency of a sinusoidal current increases through a conductor, current is forced to the skin of the conductor, virtually leaving the middle current free. This reduces the effective area of the conductor, increasing its resistance. The current carrying layer gets thinner with increasing frequency and is characterized by the skin depth

$$\delta = \sqrt{\frac{2\rho}{\mu\omega_e}} \quad (3.29)$$

where ρ is the conductor's resistivity, μ is its permeability and ω_e is the angular frequency of the applied sinusoidal current. The skin depth δ is the depth from the conductor's surface where the current density has dropped to 37%.

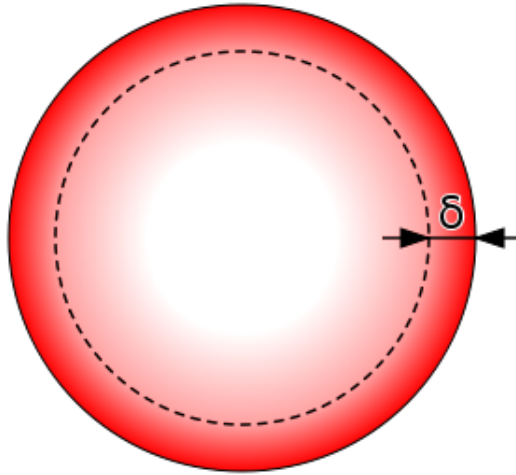


Figure 3.11: Current Distribution in an AC conductor [14]

To mitigate this effect in higher frequency applications, a special wire construction called Litz wire is used. A Litz wire consists of many smaller wire strands, braided together. The braiding pattern is made in such a way that every strand of wire occupies every position over a certain length. This evens out the AC resistance of each strand, which makes sure the current travels through the entire cross section of the Litz wire.

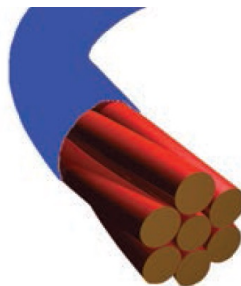


Figure 3.12: Litz Wire Construction [15]

Even though the Litz construction reduces the AC resistance of a wire, there will still be a frequency dependent AC resistance due to skin depth effect. Furthermore, the different wire strands will affect each other through a similar mechanism called proximity effect, which also yields an additional AC resistance to the wire. Despite these effects, a Litz wire has way lower resistance at higher frequencies than a massive conductor.

If a stator slot opening is simplified to a rectangular geometry, an analytical solution of the AC resistance can be found. Also, if the number of conductors deep is large, e.g. $n_d > 5$, and the copper strand diameter is smaller than the skin depth, $d_{wb} \leq \delta$, the analytical solution is closely approximated by ([9], eq. 11.76)

$$\frac{R_{AC}}{R_{DC}} = \left[1 + \frac{1}{9} \left(\frac{d_s}{\delta} \right)^2 \left(\frac{d_{wb}}{\delta} \right)^2 \right] \quad (3.30)$$

where d_s is the depth of the slot, δ is the skin depth and d_{wb} is the diameter of bare copper within a wire strand. It is worth to note that a deeper slot increases the AC losses of the coil.

Iron Losses

The iron used in the stator experiences large periodical magnetic flux variations when the motor is running. This causes both hysteresis loss (Section 3.3.2) and eddy current losses (Section 3.3.3). Since both of these loss mechanisms occur simultaneously and are hard to separate in practice, their sum is referred to as iron loss or core loss.

There is not a great deal that can be done to the hysteresis loss without altering the iron alloy. Eddy current losses on the other hand are reduced by two techniques. One is to add silicon to the iron alloy, increasing its resistance.

Secondly, all the iron in the motor is made up of thin laminated sheets that are insulated from each other. According to equation (3.10), the eddy current losses are proportional to the lamination thickness squared. However, decreasing the lamination thickness typically decreases the stacking factor K_{st} , i.e. the fraction of iron within the lamination, which in turn decreases the amount of magnetic flux that can be carried by the laminated core before saturation.

Estimation of iron losses in an electric motor is typically done by fitting empirical models to match data acquired from physical testing. Several factors make it difficult to yield good predictions for real iron losses in motors. Some of these factors are ([9], section 11.6)

- Material properties can vary as much as 30% from batch to batch
- Mechanical stress and strain have significant influence on iron losses
- Test data is measured from sinusoidal excitation, while the time variation of the magnetic field within a motor is seldom sinusoidal
- If the magnetic field changes direction during a period, additional rotational losses occur. These are typically neglected.

Due to this, iron loss predictions are seldom accurate estimates, but they can be used to predict the right trends. The empirical formula for iron loss used in ANSYS Maxwell is given as ([16])

$$P_v = K_h f(B_p)^2 + K_e (fB_p)^2 + K_a (fB_p)^{1.5} \quad (3.31)$$

where P_v is the specific loss, i.e. per mass or volume. The coefficients that have to be determined by test data are K_h the hysteresis loss coefficient, K_e the eddy current loss coefficient and K_a a coefficient for anomalous losses.

Permanent Magnet Losses

High performance permanent magnets are either made up of NdFeB or SmCo alloys. Both of which have sufficiently low resistivity to allow for significant eddy current losses (Section 3.3.3). Although these losses are typically small compared to the stator losses, they occur on the rotor which has a much longer thermal diffusion path compared to the stator.

To reduce these eddy current losses, the magnets are segmented in both the circumferential and axial direction. Skin depth δ (Equation 3.29) provides a general guideline for the axial and circumferential width of each magnet segment. ([9], section 11.6)

Accurate calculations of eddy current losses within a rotor magnet are not straightforward, and require time consuming 3D finite element analysis. This leaves first hand experience as the primary tool for determining the degree of segmentation.

3.5.5 Performance

Ultimate performance of an electrical motor is strongly related to how efficiently it can produce torque. A more efficient motor can produce more torque for a given loss and temperature increase. High temperatures pose a threat to insulation and permanent magnets, and need to be kept below an acceptable limit.

When the temperature of a magnet is given, it can withstand a certain demagnetizing field before permanently losing some of its own magnetization. Finite element analysis is needed to accurately determine the demagnetization flux for the magnets, because there will be spatial variations of the field within.

Invariance of NI

The fixed area for coil wire within a stator slot poses a constraint on the product (NI), which plays a key role in generation of mutual torque (Equation: 3.24). By noting the relationship between current amplitude and RMS current density $I = A_{wb}\sqrt{2}J_{rms}$, the product of (NI) is equal to ([9], eq. 4.45)

$$NI = (K_{wb}A_{slot}\sqrt{2}) J_{rms} \quad (3.32)$$

Once the slot area A_{slot} and copper fill factor K_{wb} are set by geometry and manufacturing constraints, the only way to increase (NI) is to increase the coil current density J_{rms} , which is directly linked to ohmic losses by (Equation 3.27).

Motor Constant

A very useful parameter for indicating motor performance is the motor constant K_m . Its definition is based on how efficiently a motor is able to produce torque, and reads

$$K_m = \frac{T}{\sqrt{P_{ohmic}}} \quad (3.33)$$

Unlike typical efficiency values, which take into account all the losses within the motor, the motor constant only accounts for copper DC losses. This greatly simplifies its calculation as frequency dependent AC, hysteresis and eddy current losses are eliminated. Although it is a simplification, copper DC loss is typically the largest contributor to motor losses, which means the motor constant serves as a performance indicator of the magnetic design.

By substituting the analytical formulas for torque (Equation: 3.24) and copper DC losses (Equation: 3.27) into the expression for the motor constant, it yields

$$K_m = \frac{\frac{3}{4}\phi_g K_s (NI)}{\sqrt{V_{wb} \rho J_{rms}^2}} \quad (3.34)$$

where V_{wb} is the total bare wire volume within the stator. By further expanding the expression for air gap flux $\phi_g = B_g (\pi D_{ro} L_{st})$, where the parenthesis is the rotor surface area, and applying the (NI) invariance (Equation: 3.32), the expression for K_m simplifies to

$$K_m = \left(\frac{3\sqrt{2}}{4} \right) K_s \frac{B_g D_{ro}}{\sqrt{\rho}} \sqrt{V_{wb}} \quad (3.35)$$

As shown above, the motor constant can generally be increased by increasing the average air gap flux density B_g and decreasing the coil wire resistivity ρ . The actual motor geometry together with the pole count, slot count and winding pattern determines values for K_s , D_{ro} and V_{wb} .

Analytical Motor Model

Due to the complexity involved in magnetic design it makes it impossible to derive an expression for the motor constant for a realistic motor. However, an analytical result can be derived by considering an ideal, simplified case ([9], section 11.1). The following assumptions are made

- Magnetic flux density crossing the air gap B_g is constant over the rotor's circumference, consisting of N_m magnetic poles.
- The stator has a full pitch winding, i.e. the angular pitch of the coils matches the angular pitch of the magnetic poles. There is one slot per pole per phase, i.e. $N_s = 3N_m$, where N_s is the number of slots.
- Phase back EMF is given as a direct consequence of the two previous assumptions, and has a square-wave shape. Square-wave current is applied to produce maximum, constant torque.

- The flux density within the teeth and yoke of the stator iron is given by B_s .
- Length of the coil end turns is approximated by half circles, i.e. $L_{end} = \frac{\pi D_{so}}{N_m}$, where D_{so} is the stator outer diameter.
- Rotor outer diameter is given by D_{ro} .

By applying these assumptions and approximations, the motor constant of this ideal motor can be derived. To simplify the final expression, the following non-dimensional parameters are introduced

$$\delta_L = \frac{L_{st}}{D_{so}}, \quad \delta_R = \frac{D_{ro}}{D_{so}}, \quad \delta_B = \frac{B_s}{B_g}$$

where δ_L is the stack length to diameter ratio, δ_R is the radius ratio and δ_B is the stator flux ratio. Now the expression for the motor constant K_m is given as ([9], eq. 11.18)

$$K_m = \left(\frac{D_{so}}{2}\right)^2 \sqrt{\frac{K_{wb} \pi}{\rho}} \left(\delta_L \sqrt{\frac{D_{so}}{\delta_L + \pi^2/(2N_m)}} \right) \cdot \left[B_g \delta_R \sqrt{\left(1 - \frac{\pi \delta_R}{N_m \delta_B}\right)^2 - \delta_R^2} - \frac{2 \delta_R}{\delta_B} \left(1 - \frac{\pi \delta_R}{N_m \delta_B} - \delta_R\right) \right]$$

For the ideal motor considered here, its motor constant has several notable features. If the outer diameter is fixed, the most significant way of increasing K_m is to increase the average air gap flux density B_g . Furthermore, the second term in parenthesis isolates the influence of the stator length through δ_L , and the final term in the square brackets isolates the effects of the air gap flux density B_g , stator flux density through δ_B , and radius ratio δ_R . Since the last term is not a function of D_{so} , δ_L , K_{wb} or ρ , the optimum radius ratio is not a function of these parameters.

By calling the last term in parenthesis, the normalized motor constant k_m , and assuming values for $B_g = 1$ and $\delta_B = 1.5$, the performance of a cross sectional slice of the motor can be assessed as a function of the radius ratio δ_R and magnetic pole count N_m .

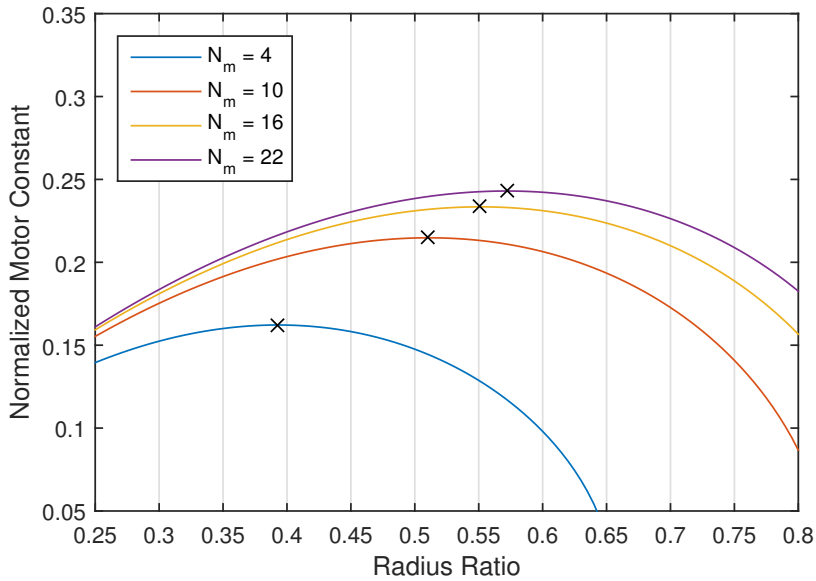


Figure 3.13: Normalized Motor Constant vs Radius Ratio

In figure (3.13), it can be seen that the optimum radius ratio has a positive correlation to the magnetic pole count. Also, the radius ratio has a small influence on the motor constant around its optimum value.

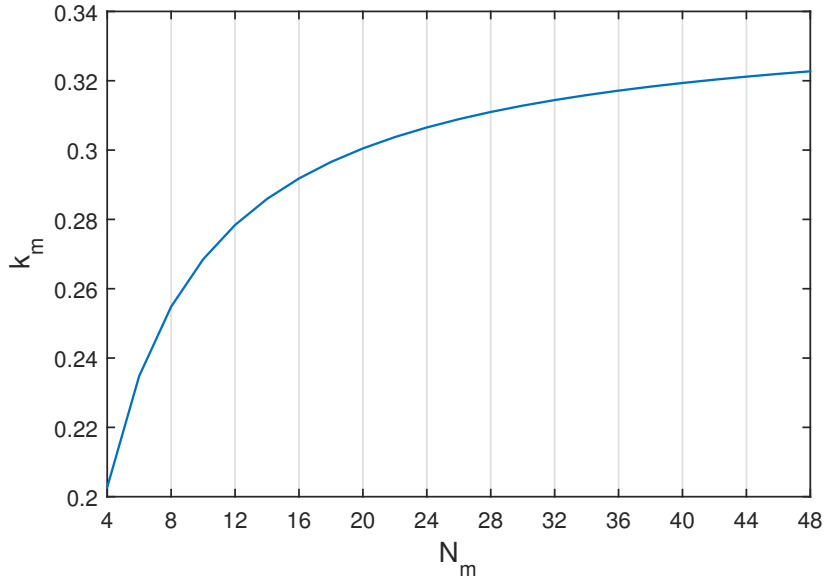


Figure 3.14: Optimized Normalized Motor Constant vs Pole Count

As shown in figure (3.14), the motor constant generally increases with increasing magnetic pole count. This is because the magnetic flux has to travel less distance from one pole to the next, decreasing the required stator yoke thickness to carry the flux, leaving more space for windings.

Chapter 4

Initial Assessment

4.1 Requirements

An electric powertrain consists of an accumulator, inverter and a motor. These components have to be compatible with each other in order to ensure a functioning powertrain. Furthermore, the implementation of an electric powertrain in a high performance formula race car poses additional constraints on the motor. This chapter will be used to identify and discuss these constraints, both qualitatively and quantitatively. Figure (4.1) illustrates the main systems that influence motor requirements in a formula student race car.

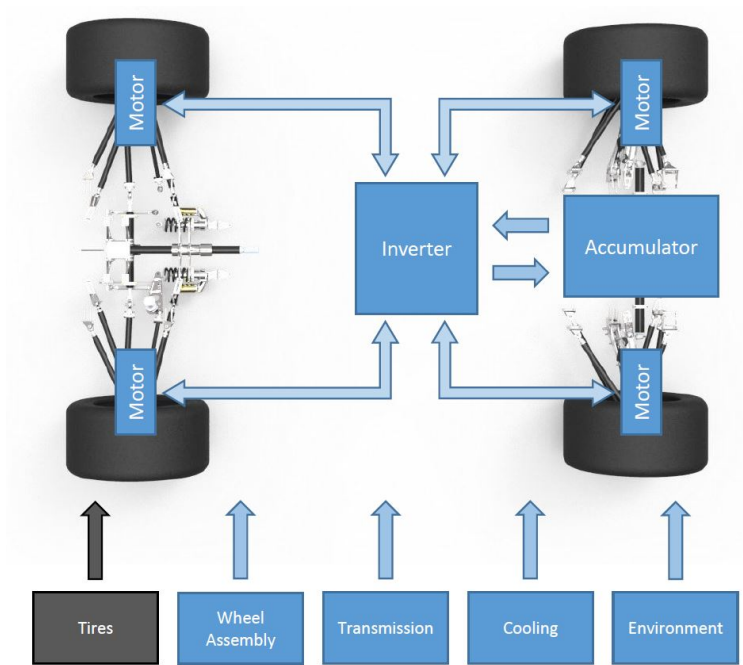


Figure 4.1: Electric Powertrain Overview [17]

4.1.1 Overall Requirements

Overall requirements for the prototype motor are set by the long term goals of the team and restricted by the official FSAE rules and regulations [18]. These requirements can be listed as

- Must support four wheel drive
- Hub mounting within a 10-inch rim
- Compatibility with all interfacing systems
- Should utilize all available traction
- EV 2.1.2 ([18], p. 100) - The rotating part of the motor must be contained

within a structural casing where the thickness is at least 3mm for Al6061-T6 or 2mm for steel.

- EV 2.1.3 ([18], p. 100) - If the motor casing rotates around the stator or the motor casing is perforated, a scatter shield must be included around the motor. The scatter shield must be at least 1mm and be made from Al6061-T6 or steel.

4.1.2 Accumulator Analysis

The accumulator stores energy in chemical form using a lithium polymer chemistry, and has a maximum terminal voltage of 600V. In order to push the current against the back EMF induced in the motor coils (Section: 3.5.3), the available voltage range during operation has to be known.

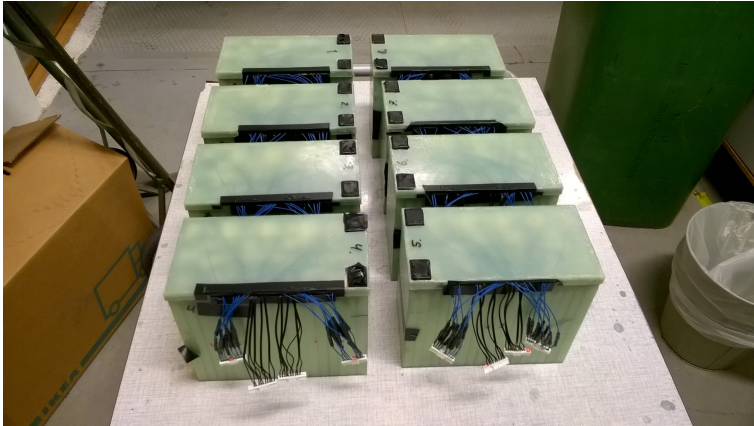


Figure 4.2: Revolve Accumulator 2015

There are two main mechanisms that reduce the available voltage at the accumulator terminals, referred to as DC link voltage. The first is related to internal resistance of the battery cells used, i.e. the voltage drops when current is drawn. Secondly the cell voltage drops as the remaining energy decreases. In order to quantify these two effects, logged data from the endurance and

acceleration event in FSA 2015 is used.

Filtering out wild points, the two effects show a linear correlation to available terminal voltage. The relations are approximated by a linear least squares fit. Internal resistance accounts for a voltage drop of $0.33V$ per ampere drawn (Figure: 4.3). Furthermore, the terminal voltage drops $9.9V$ per kWh used (Figure: 4.4).

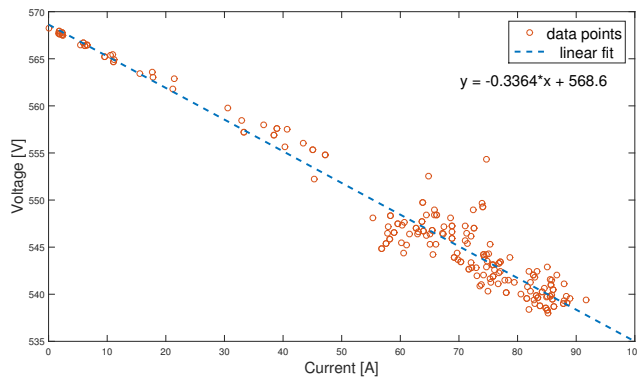


Figure 4.3: Internal Resistance Relation [17]

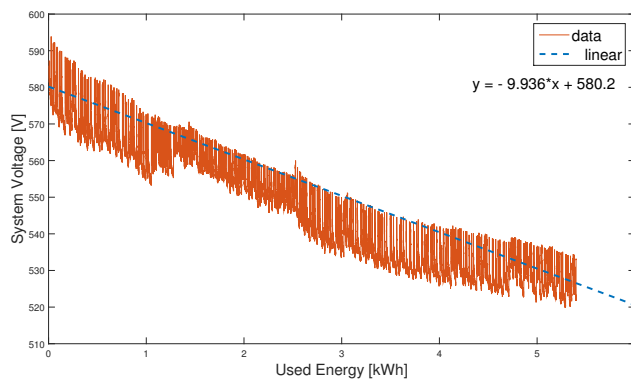


Figure 4.4: Accumulator Voltage vs Energy Used [17]

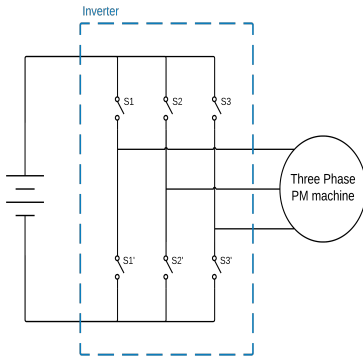
The accumulator can store up to $7.1kWh$ energy. If a maximum of $80kW$ is drawn from when there is no remaining energy, the terminal voltage can in theory drop as low as $473V$. This gives a conservative operating window between $473V$ and $600V$ for the DC link voltage. Furthermore, the inverter is only capable of utilizing 70.7% of the DC link voltage, which leaves an operating voltage between $334V$ and $424V$ at the motor terminals. It should be noted that if a new cell technology is implemented in the future, this accumulator assessment must be revised.

4.1.3 Inverter Analysis

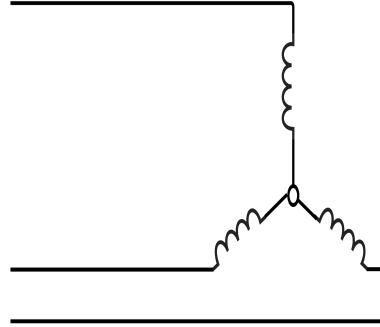
In order to transform the DC currents delivered from the battery into AC currents needed for motor operation, an inverter is present as an interface between the motor and accumulator. It is built up of semiconductor switches in a special arrangement to allow for two way current flow. Additionally, the inverter is responsible for controlling the requested speed and torque of the motor.

Switch Arrangement

There are different ways of arranging the semiconductor switches in order to allow for two-way current flow into all three motor phases. However, a very compact and economical topology called Y-Connection will be used in the car. This yields a good compromise between performance, number of wires and semiconductor switches. The layout is shown in figures (4.5a) and (4.5b).



(a) Inverter Topology [17]

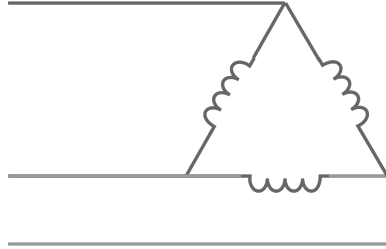


(b) Y-connection [17]

Figure 4.5: Inverter and Motor Phase Connections

This arrangement requires the motor windings to be balanced, i.e. back EMF of each motor phase must be identical in shape and amplitude, and 120 degrees shifted from the two other. Additionally, the output lead of all three motor phases must be connected together in a central node within the motor (Figure: 4.5b).

There is an alternative to the Y-connection that does not affect the inverter topology. It is called Δ -connection, and differs in how the motor phases are interconnected (Figure: 4.6). The Δ -connection may yield easier manufacturability as only two and two phases are joined together in a node instead of three. However, it allows for circulating currents within the motor that causes extra copper losses. Because of the relative high power level of traction motors, this topology is not suited and will not be considered further.

Figure 4.6: Δ -connection [17]

Pulse Width Modulation (PWM)

A technique abbreviated PWM is commonly used to modulate AC currents from a DC voltage supply. Phase windings within a motor can be modelled as an elementary circuit with a resistance R , an inductance L and two external voltages, back EMF ϵ and applied voltage V_i . The differential equation of the resulting circuit reads

$$L \frac{dI}{dt} = -RI + \epsilon + V_i \quad (4.1)$$

By using the semiconductor switches to apply short voltage pulses of different durations, a sinusoidal current can be modulated by the use of the PWM technique. The actual theory behind this technique is outside the scope of this task, but it is important to assess how the maximum switching frequency of the semiconductor switches relates to how well a sinusoidal current can be modulated. This will limit the maximum allowable electrical frequency of the motor.

To investigate this relationship, the m-ratio is introduced as

$$m = \frac{f_{pwm}}{f_e} \quad (4.2)$$

where f_{pwm} is the maximum switching frequency and f_e is the frequency of the modulated sine current. The electric circuit was simplified by leaving out the back EMF and resistance, and a PWM signal generator added to the input.

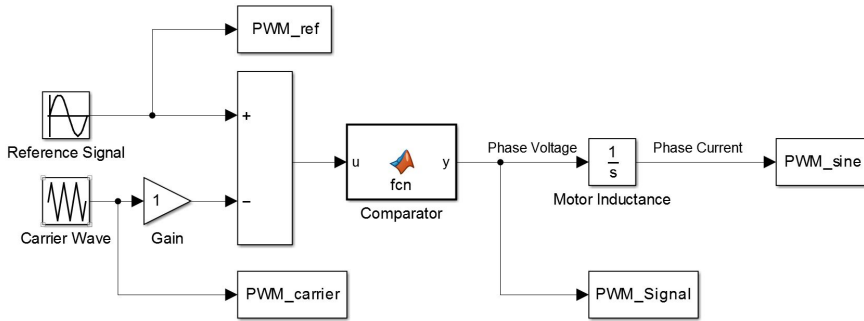


Figure 4.7: Simulink PWM Generator [17]

A Fourier transform was done on the output current of the circuit, and the quality of the modulated sine was assessed by comparing the fundamental harmonic component to the total harmonic content of the signal.

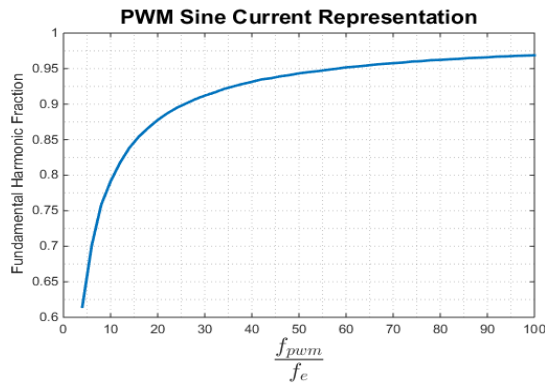


Figure 4.8: Fundamental Harmonic Fraction vs M-ratio [17]

As seen in figure (4.8), a m-ratio between 20 and 30 brings the harmonic ratio just above the knee region of the graph, yielding a desirable operating point for higher motor speeds.

Vector Oriented Control

Modern control schemes for brushless motors rely on a technique called vector oriented control, or VOC for short. By acknowledging that the angular phase of the sinusoidal back EMF and corresponding desired phase currents are dependent on the rotor position, a coordinate system rotating with the rotor can be defined to transform the sinusoidal currents into DC values. The control loops can then be set to follow a DC value instead of chasing a constantly changing sinusoidal signal. A block diagram for a typical real time control system is shown below.

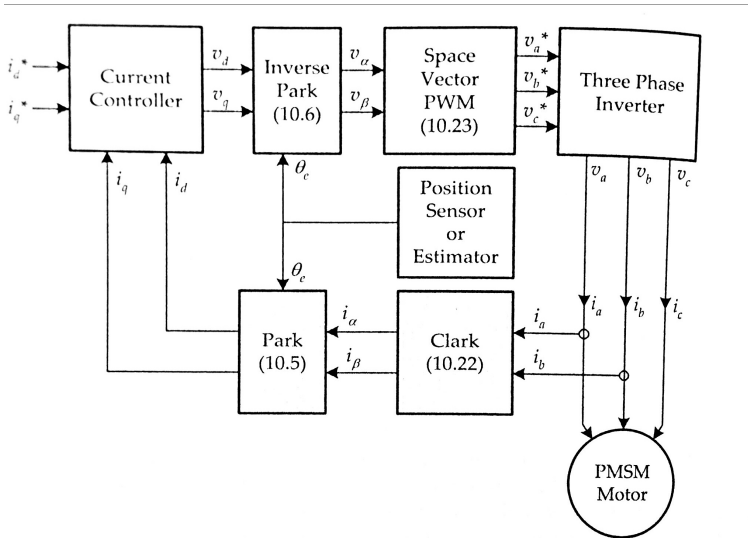


Figure 4.9: Vector Control Block Diagram ([9], fig. 10-8)

Using this transformation requires information regarding rotor position. This can either be measured directly by a sensor or estimated on-line. However,

on-line estimators need a certain minimum motor speed to work properly, so for use in a race car a rotor position sensor is required.

4.1.4 Wheel Integration

The motor will be integrated into the wheel of the car. This poses spatial constraint on the design space. Revolve has decided to continue using rims with 10 inch outer diameter, which greatly limits the available space within. In addition to the motor, the wheel assembly contains a hub, upright, suspension linkages and possibly a gearbox. Furthermore, the connections for power and cooling need to be taken into consideration.

In order to assess the space available for the motor, a preliminary CAD model of the rims and suspension linkages was created. This was done in collaboration with the suspension and rim designers of team 2016. The available space is shown below.

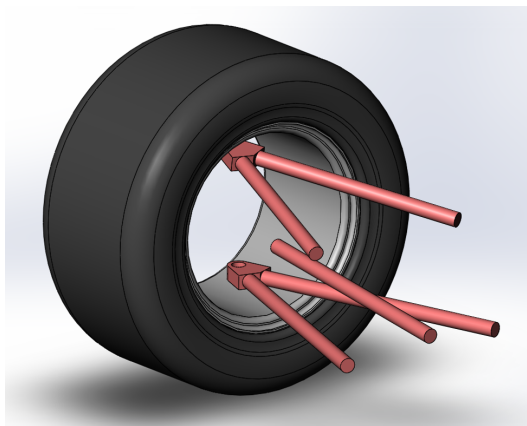


Figure 4.10: Suspension and Rim Model [17]

As team 2016 uses a commercial servomotor to drive the car, a two-stage planetary gearbox design is already developed and available in the team. It features a very compact solution with a gearing ratio of 15.4:1. Furthermore, if the prototype motor is designed to be interchangeable with the commercial motor from AMK, it reduces risk during implementation as AMK can serve as a backup.

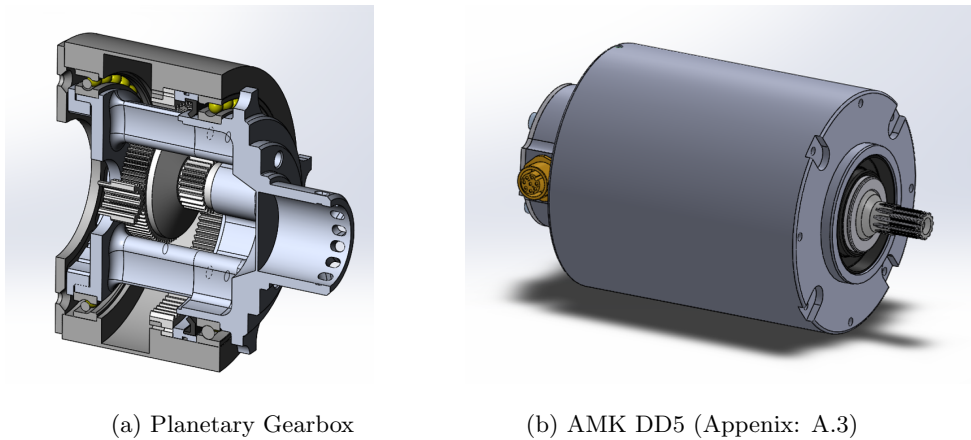


Figure 4.11: Transmission and Motor

4.1.5 Other Considerations

Temperature and Cooling

The coil wire insulation and permanent magnets are temperature sensitive and must be kept within a certain limit during operation. In order to monitor these critical parameters during operation, both rotor and stator temperature probes should be employed in the design.

A liquid cooling system has superior heat transfer to an air cooled system due to the large increase of surface area in the radiator. Secondly there is already a liquid cooling system present in the car for the inverters. Furthermore, the external aerodynamics of the car are optimized to yield good air flow to the radiator, but use most on the incoming air to produce down force. Due to these reasons, the prototype motor will be designed to use liquid cooling.

Environmental Protection

The car will be racing in dry and wet conditions. Since the motor is situated within the rim, it will be exposed to water and dirt during racing. In order to protect the internal components from corrosion and foreign object damage, the internal components must be protected. Based on recommendations from the electronics group, an IP65 rating is set as an requirement to the casing.

Vibration

Unless the motor is a structural part of the wheel, the external forces acting on it should be quite low. But due to periodical magnetic forces and rotating components within the motor, the structural resonant frequencies should be assessed. Furthermore, the rotor should contain measures to allow for balancing of the assembly. A highly unbalanced rotor will cause vibrations in the structure.

4.2 Performance

Except for aerodynamic forces, all forces working on the car are transmitted through the four contact patches between the tire and the road. Additionally, there are predefined tracks that define the drive cycles of the vehicle. These factors should be incorporated into the desired torque and power requirements

at the wheel.

4.2.1 Tire Analysis

Revolve NTNU is a part of the formula student tire consortium. This gives access to experimental tire data from the Calspan tire testing facility in the US. The data includes force and moment measurements for different slip angles and slip ratios for the tire. Using this data, tire characteristics can be analysed. However, the actual magnitudes of the generated forces are not reliable as the tire testing machine uses coarse grit sand paper instead of tarmac.

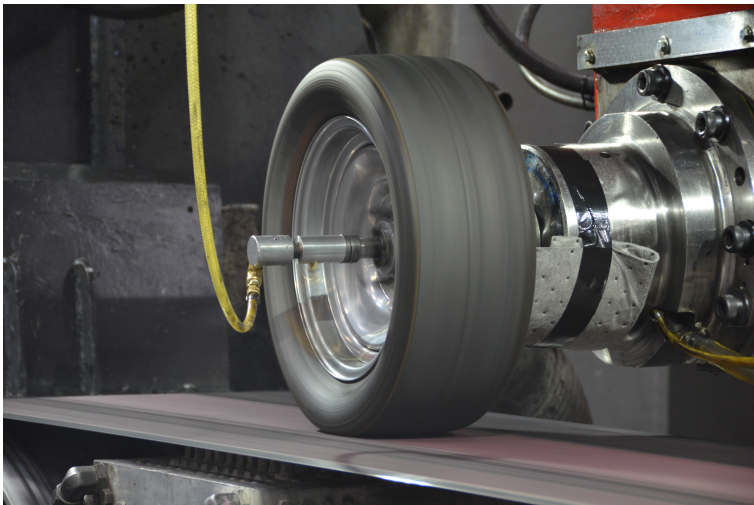


Figure 4.12: Tire Testing at Calspan [Calspan]

In simplified vehicle analysis, the tire component is reduced to a constant friction coefficient. The validity of this assumption will be assessed by looking at the load sensitivity characteristics of a real tire, i.e. how the friction coefficient depends on the normal load carried by the tire.

To filter out measurement noise, an empirical tire formula is fitted to the data using a least square method. The chosen formula is a simplified version of the Magic Formula, proposed by Hans J. Pacejka ([19], eq. 4.49)

$$F = D \sin \left[C \arctan \left(B s - E [B s - \arctan B s] \right) \right] \quad (4.3)$$

where F is the generated force and s is the slip of the tire. Lateral slip, i.e. slip angle SA , is related to lateral force F_y , while longitudinal slip, i.e. slip ratio SR , is related to longitudinal force F_x . By fitting lateral and longitudinal curves for different tire loads at nominal inflation pressure and camber angle, the load sensitivity could be assessed.

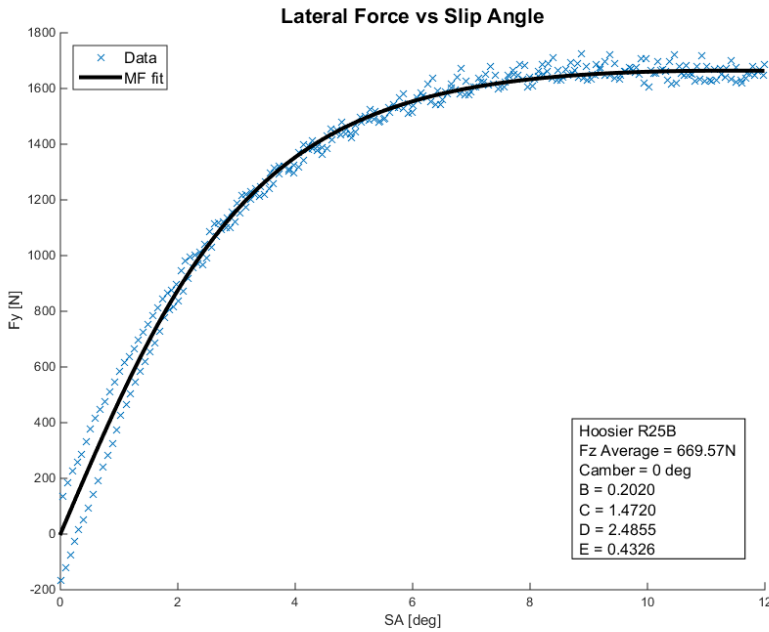
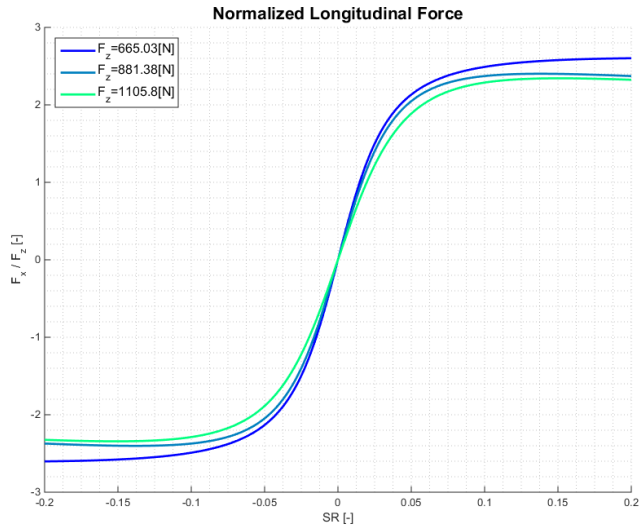
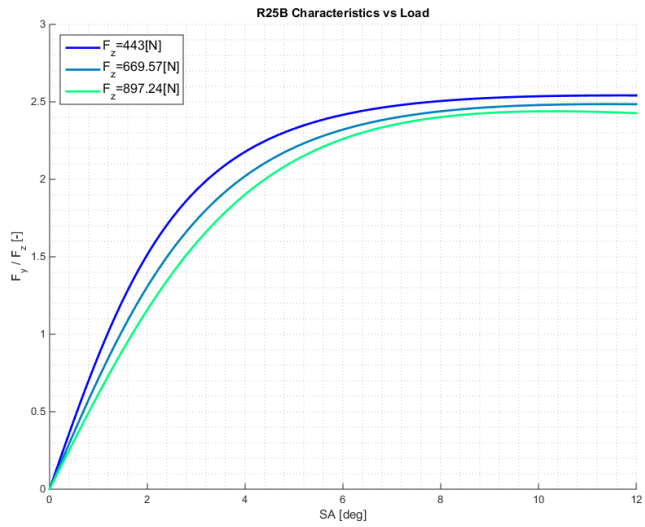


Figure 4.13: Least Square Fit of Tire Data

Figure 4.14: Fitted Normalized Curves for F_x [17]Figure 4.15: Fitted Normalized Curves for F_y [17]

As seen in figure (4.14) and (4.14), the longitudinal and lateral friction

coefficients experience some reduction over the load range, but this is considered small enough to be neglected for further analysis. A proposed tire performance envelope is given by

$$F_x = \mu_x F_z \quad (4.4)$$

$$F_y = \mu_y F_z \quad (4.5)$$

where μ_x and μ_y are the constant friction coefficients for the longitudinal and lateral direction. F_z is the normal load carried by the tire. A huge advantage of the constant friction assumption is that load transfer is eliminated from vehicle analysis, and the car can be reduced to a point mass.

4.2.2 Grip Analysis

Now that a tire performance envelope is determined, the friction coefficients can be determined by using data from competition results. Lumped vehicle parameters were collected from the winning car in each event. These parameters consist of

- Vehicle Mass
- Power Limitation
- Powertrain Efficiency
- Drag Coefficient
- Lift Coefficient
- Top speed

Lateral Friction

The lateral capacity of the car is found by measuring the time it takes to drive clockwise and anticlockwise around a pre-defined circle. This is the skid pad event at the competition and its track is shown in figure (4.16)

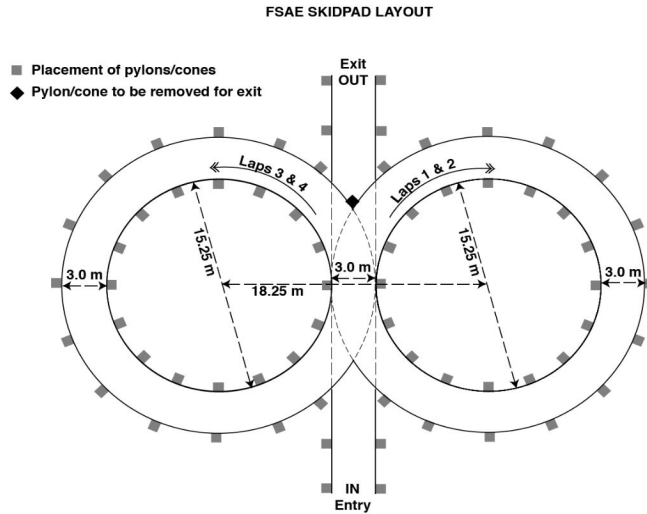


Figure 4.16: Skid Pad Layout ([18], p. 160)

Modelling the car as a point mass, and using analytical formulas for centripetal acceleration and aerodynamic downforce, an analytical equation is made from Newton's second law in a steady state turn.

$$m \frac{\bar{v}^2}{r} = \mu_y \left(mg - L_{nom} \left(\frac{\bar{v}}{v_{nom}} \right)^2 \right) \quad (4.6)$$

$$\bar{v} = \frac{2\pi r}{Skid\ pad\ time} \quad (4.7)$$

where m is the vehicle mass, \bar{v} is the average skid pad speed, r the skid pad radius, L_{nom} the nominal lift force at the nominal speed v_{nom} . The left hand side is derived from centripetal acceleration and the right hand side is the total friction force from the tires.

By inserting gathered parameters for the fastest vehicle at skid-pad FSUK [20], together with their result time, the lateral friction coefficient μ_y is estimated to 1.466.

Longitudinal Friction

To estimate the longitudinal friction coefficient of the tires, results from the acceleration event is used [21]. The acceleration event measures the time it takes for each car to cover a distance of 75m. Tire friction, drivetrain, aerodynamics and a point mass car are assumed to capture the main physics of the event. A low fidelity model is made in Matlab Simulink.

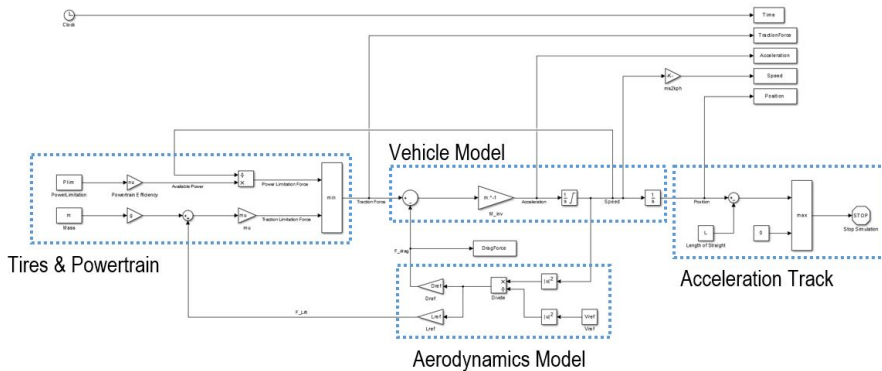


Figure 4.17: Simulink Acceleration Model [17]

Vehicle mass, aerodynamic parameters and power limitations are assumed to match the specification sheet given by the winning team. A parameter sweep was run to investigate how the longitudinal friction coefficient and powertrain efficiency affect the finishing time.

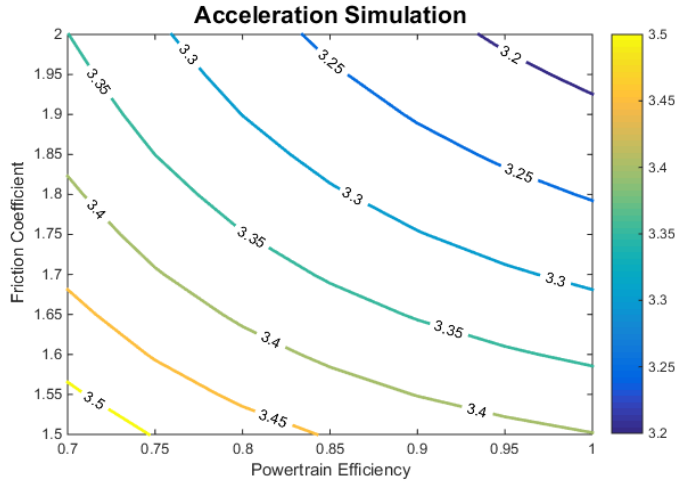


Figure 4.18: Finishing Time vs Grip and Efficiency [17]

Actual powertrain efficiency of the winner car is not known, but assumed to be between 0.8 and 0.875. Based on the parameter sweep results, the longitudinal friction coefficient μ_x is estimated to be between 1.8 and 1.9. The relatively large difference between the lateral and longitudinal friction coefficients can be explained by the fact that it is easier to control the slip ratio than slip angle of every wheel. This means the tires can work optimally in the longitudinal direction, yielding a higher value for the friction coefficient.

4.2.3 Desired Peak Performance

Now that the tire friction coefficients are estimated, desired vehicle performance can be assessed. Peak performance is given by the acceleration event, as all available grip should be used. Changing the car's parameters to match the planned values for the next Revolve car, an acceleration event simulation was done by using the model in figure (4.17).

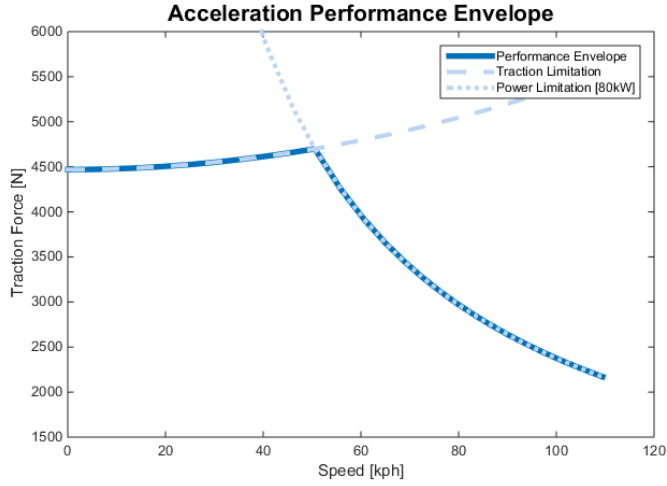


Figure 4.19: Vehicle Acceleration Envelope [17]

By extracting the car’s instantaneous acceleration, the steady state load transfer to the rear wheels could be determined. Available grip at each wheel is then found by (Equation: 4.4)

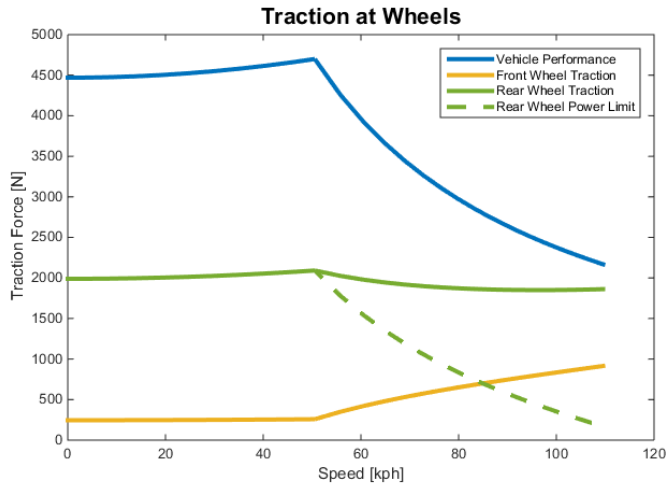


Figure 4.20: Wheel Traction [17]

When the vehicle hits the power limitation curve, the vehicle is no longer restricted by tire friction. The surplus grip available can transfer torque request from the rear wheels to the front wheels, lowering the needed performance at the back. Based on this, a peak performance curve is shown below.

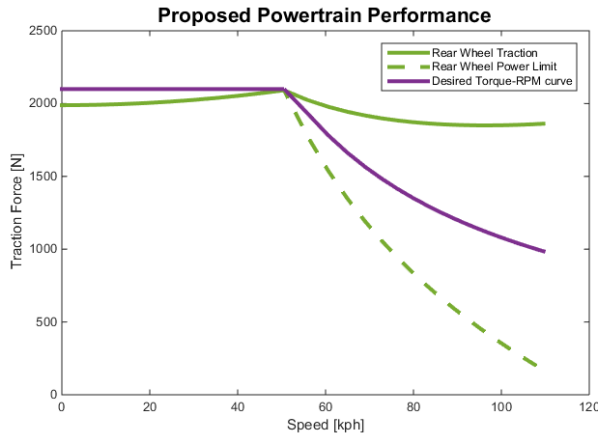


Figure 4.21: Proposed Motor Performance [17]

Or expressed as a torque-power curve

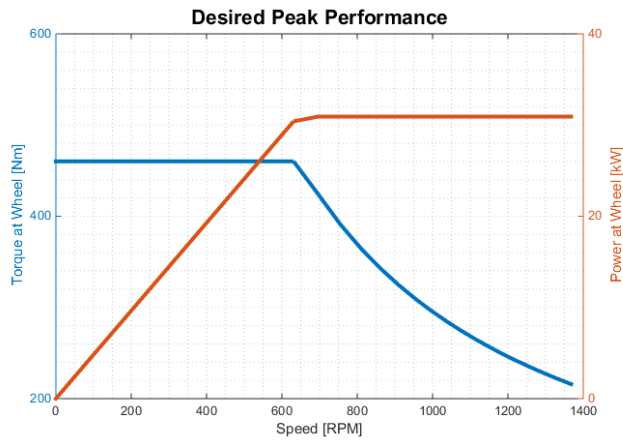
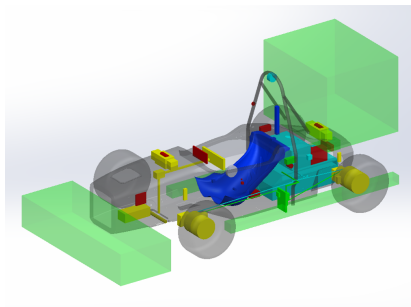


Figure 4.22: Desired Torque-Power Curve [17]

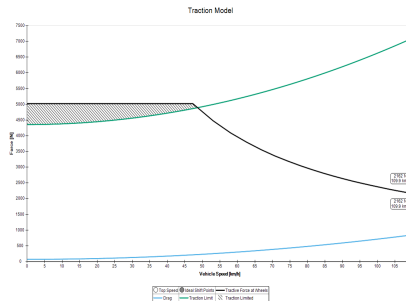
The motor should ideally be able to deliver 460.2 Nm peak torque up to a speed of 631 RPM at the wheel.

4.2.4 Desired Continuous Performance

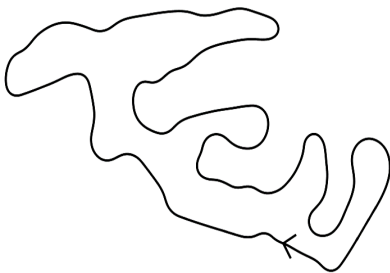
Continuous performance is given by the autocross and endurance events, which run on the same track. Due to the complexity of the autocross track compared to straight line acceleration, a commercial software will be used to analyse torque. Optimum Lap is based on a point mass vehicle and requires only essential inputs already estimated. Also due to its low fidelity it is relatively quick to set up and run.



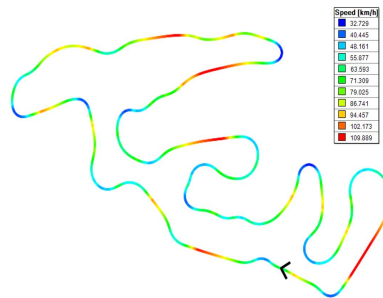
(a) Vehicle Mass and Aerodynamics



(b) Powertrain Performance



(c) FSG Track 2012



(d) Lap Speed Plot

Figure 4.23: Optimum Lap [17]

Optimum lap only outputs speed, acceleration and torque requests for a

point mass vehicle. These values need to be post-processed in order to yield single-wheel performance. The torque vectoring system assigns torque request to each individual wheel proportional to the relative weight carried by that wheel, i.e.

$$\frac{TR_{wheel}}{TR_{total}} = \frac{N_{wheel}}{N_{total}} \quad (4.8)$$

where TR_{total} is the total vehicle torque request, TR_{wheel} is the allocated wheel torque, N_{wheel} is the wheel load and N_{total} is the total load on all four wheels. From acceleration curves, the torque request from a single wheel can be deduced by considering load transfer in longitudinal and lateral direction. The simulated torque request on the rear left wheel is shown in figure (4.22).

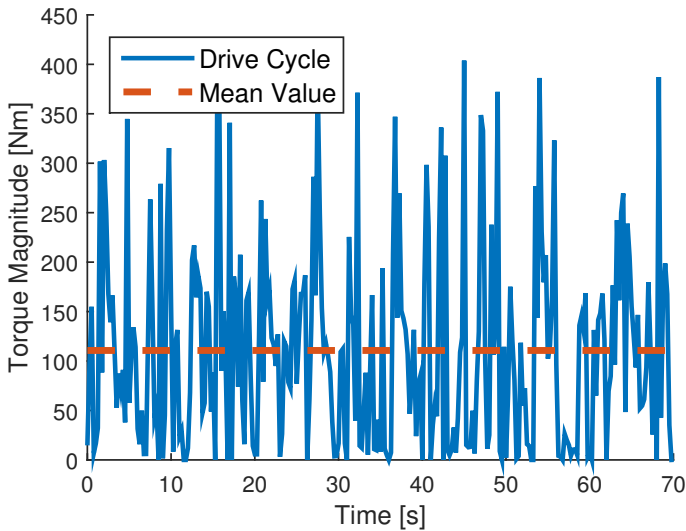


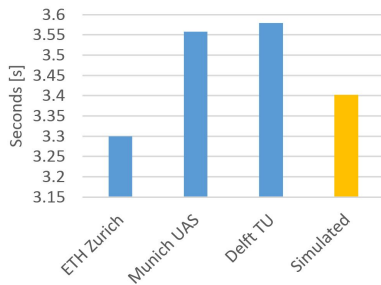
Figure 4.24: Torque at Rear Wheel [17]

As seen in figure (4.24), the car is not able to use peak torque during an autocross or endurance race. The mean torque request is only 24% of the desired peak torque, which corresponds to 110.7 Nm at each wheel. However,

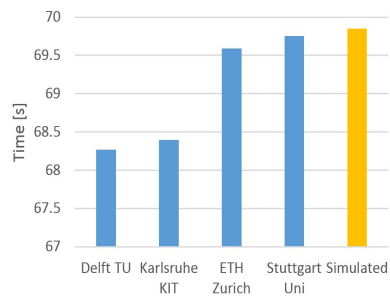
this is a low fidelity model, assuming a perfect driver. Higher torque spikes is assumed in reality due to driver imperfection.

4.2.5 Simulation Verification

In order to verify the validity of the acceleration and autocross simulations, the resulting finishing times of the simulated Revolve vehicle were compared against result times from the competition [21]. Comparison graphs are shown in figure (4.25a) and (4.25b).



(a) Acceleration Verification



(b) Autocross Verification

Figure 4.25: Simulation Verifications [17]

Chapter 5

Concept

5.1 General Sizing

In order to assess different concepts based on their performance, a general sizing relation should be established to estimate output torque. As discussed in section (3.5.5), the real relationship is very complex and dependent upon motor construction and materials. However, a general guideline is typically given as ([9], eq. 1.10)

$$T = k D^2 L \quad (5.1)$$

where T is output torque, k is torque density, D the motor diameter and L the motor length. A handful of high performance PM motors, typically used in Formula Student, were selected to investigate the value of k and the motor weight based on motor volume. This included the already used AMK motor (Appendix: A.3), as well as a the Emrax motor family from the Slovenian company Enstroj [22].



Figure 5.1: The Emrax Motor Family [22]

Motor	Volume	Weight	Peak Torque	Cont. Torque
AMK DD5	1.045 [dm^3]	3.55 [kg]	21 [Nm]	9.8 [Nm]
Emrax 207 [22]	2.861 [dm^3]	9.4 [kg]	140 [Nm]	65 [Nm]
Emrax 228 [22]	3.511 [dm^3]	12.3 [kg]	240 [Nm]	120 [Nm]
Emrax 268 [22]	5.133 [dm^3]	20.3 [kg]	500 [Nm]	250 [Nm]

Table 5.1: Sample Motor Parameters

Peak and continuous torque density, along with mass can be correlated to motor volume using the values from table (5.1). The correlation plots are shown in figures (5.2) to (5.4).

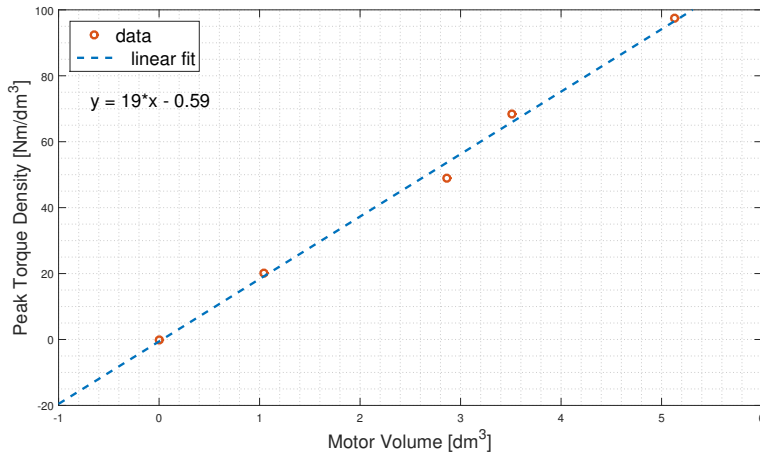


Figure 5.2: Peak Torque Density Relation [17]

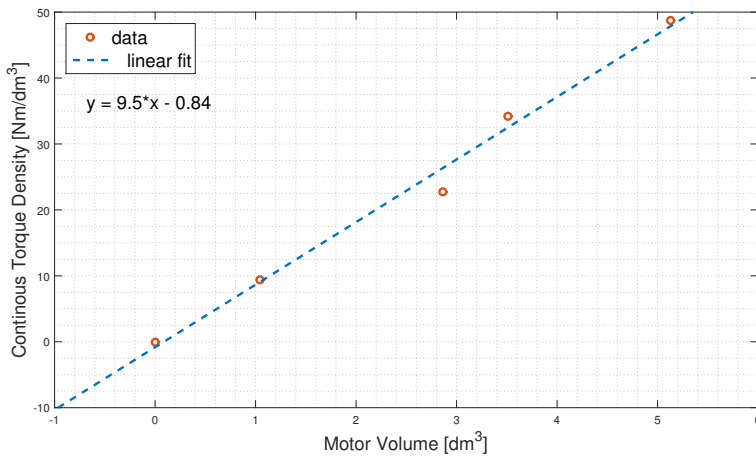


Figure 5.3: Continuous Torque Density Relation [17]

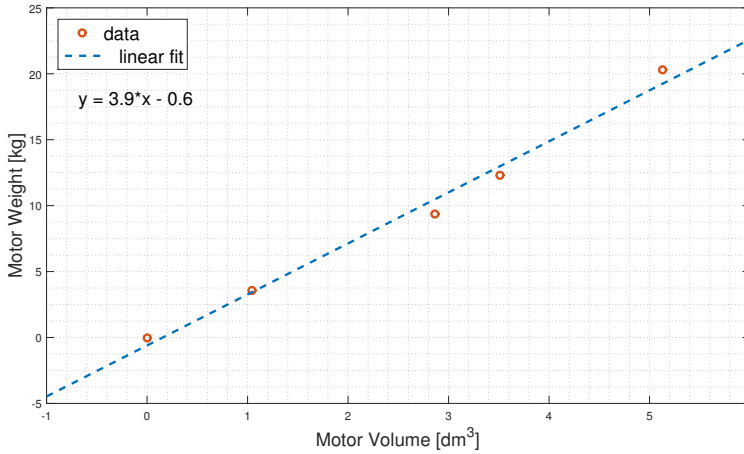


Figure 5.4: Motor Weight Relation [17]

Observing the plotted data points, there is a linear correlation between both torque density and mass to motor volume. A linear fit was done using least squares, including the trivial solution at (0.0), to determine formulas for k and m , yielding

$$k_{peak} \approx 19V \quad k_{cont} \approx 9.5V \quad m \approx 3.9V$$

where V is the motor volume in [dm^3], k is torque density in [Nm/dm^3] and m is mass in [kg].

5.2 Concept Development

The main challenge of developing an in-wheel motor for Revolve is to get enough torque out of a motor within a very limited design space. Four distinctively different motor concepts were developed for further assessment. To distinguish between the different components, a color code was added. Rim and tire are black, upright is cyan, motor yellow and transmission/shaft purple.

5.2.1 Concept 1

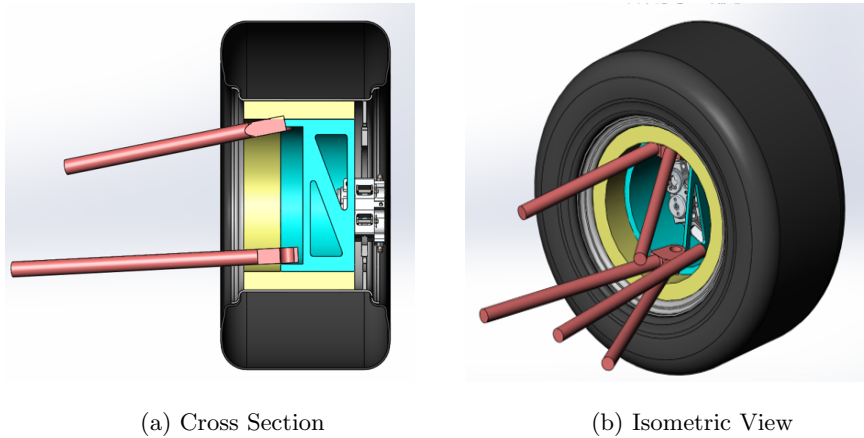


Figure 5.5: Rim Integrated Motor [17]

A relatively simple concept with the rim and motor as one unit (Figure: 5.5). This eliminates the need for a wheel hub and gearbox, since everything is integrated into the motor. However, suspension interference is quite severe and very large, low profile bearings are needed. Furthermore, the low modularity restricts the ability of quick swap of rain tires or back in case of weather change during a race.

5.2.2 Concept 2

The second concept is integrating the motor as a part of the upright (Figure: 5.6). In order to get enough volume on the motor, it is placed inside the suspension linkages. This allows for quick change of tires, and eliminates transmission. The major disadvantages are related to safe integration of high voltage wires and cooling hoses to the motor, in addition to relatively large overhang of the hub shaft and very limited space for the brake rotor and rim center.

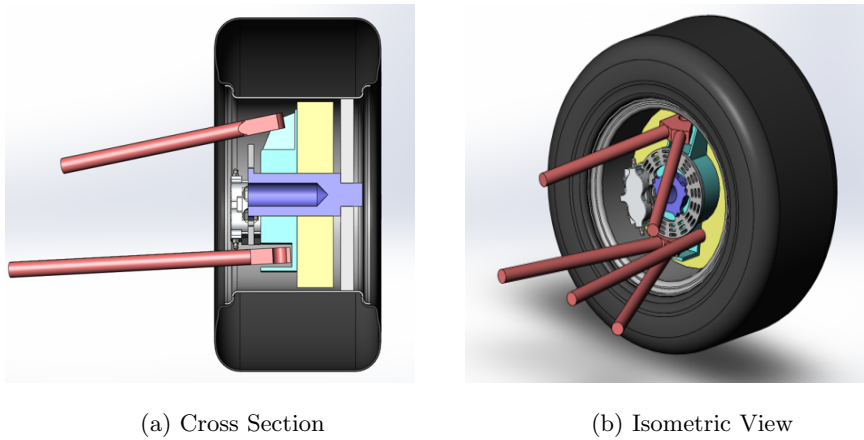


Figure 5.6: Upright Integrated Motor [17]

5.2.3 Concept 3

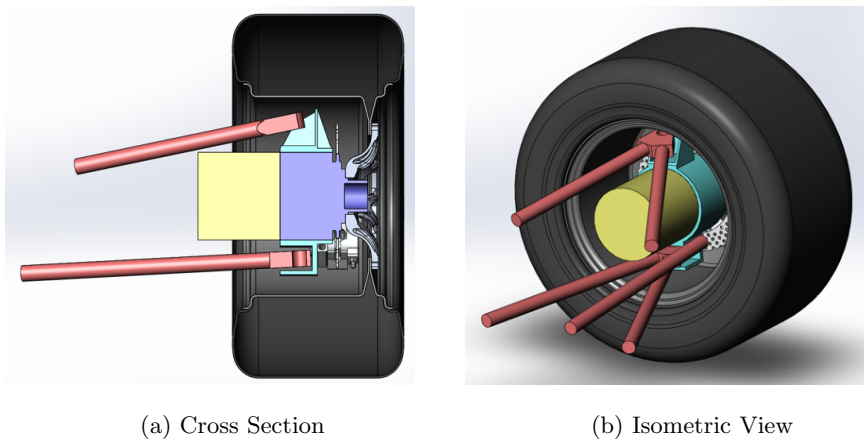


Figure 5.7: Modular Concentric Motor [17]

By mounting the motor to the upright and employing the available planetary transmission within the hub, a very space efficient design can be implemented (Figure: 5.7). Due to the high modularity of the system, maintenance and component replacement are made simpler. Additionally, this concept is

compatible with the commercial AMK motors.

5.2.4 Concept 4

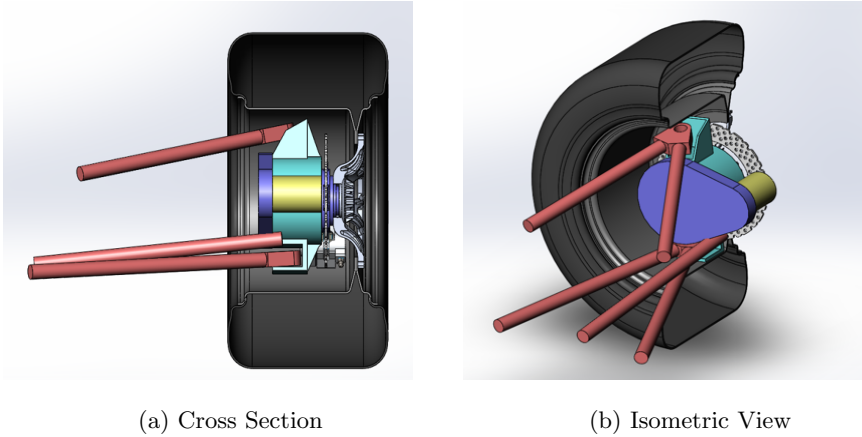


Figure 5.8: Modular Parallel Motor [17]

An extension of the concentric motor concept. In this case the motor is placed parallel to the hub and connected through an extra gear stage (Figure: 5.8). This concept features no interference with suspension, but requires a very complicated gearbox.

5.2.5 Concept Evaluation

All four concepts are compared qualitatively and quantitatively. The qualitative comparison assesses the concept with regards to in-wheel packaging and interference. Sizing relations from section (5.1) are used to estimate torque output and weight of each concept. These numbers are then compared to the desired performance found in section (4.2.3) and (4.2.4). The weight of motor, transmission and rim center are estimated from earlier Revolve designs, and calculated peak torque density is added as a figure of merit.

	C1	C2	C3	C4
Cross Section	1.045	3.55	21	9.8
Motor Volume [dm^3]	2.533	2.297	1.045	0.166
Gear Ratio	1:1	1:1	15.4:1	28.2:1
Max Speed [rpm]	1373	1373	21144	38719
Desired Peak Torque [Nm]	460.2	460.2	30.8	17
Estimated Peak Torque [Nm]	121.9	100.2	20.76	0.526
Mean Autocross Torque [Nm]	110.7	110.7	7.41	4.09
Estimated Cont. Torque [Nm]	60.95	50.1	10.38	0.263
Estimated System Weight [kg]	9.28	8.86	6.28	3.37
Peak Torque Density [Nm/kg]	13.14	11.31	49.38	4.22
Suspension Interference	-2	0	0	0
Rim Center Interference	0	-1	0	0
Brake System Interference	0	-1	0	0
Transmission Complexity	+1	+1	-1	-2
AMK Compatibility	0	0	+1	0
Qualitative Score	-1	-1	0	-2

Table 5.2: Concept Evaluation

From a performance perspective, concept three is the only viable option, as none of the other concepts are close to deliver the desired torque output. On the qualitative side, concept three yields the best use of available space and offers minor interference with other systems within the rim. Due to these clear results, concept three is chosen for further design.

5.3 Concept Considerations

5.3.1 Motor Topology

As discussed briefly in section (3.1.1), there are three typical topologies available for PM motors: axial motors that typically have a small length to diameter ratio, radial out-runners that typically have a higher torque density and radial in-runners that are inherently safer and easy to mount.

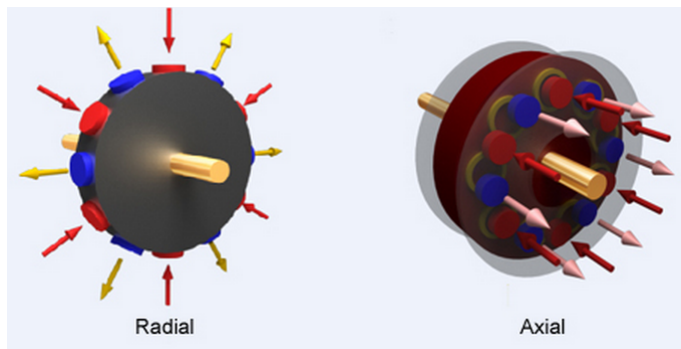


Figure 5.9: Radial vs Axial Motor [23]

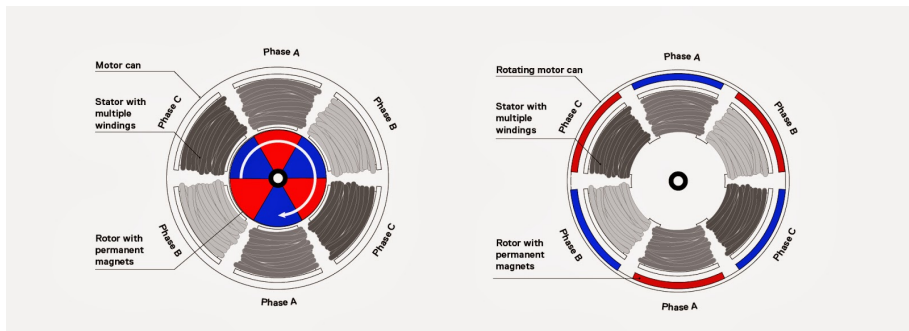


Figure 5.10: Radial in-runner vs out-runner [24]

Based on the available design space of the chosen concept, an axial topology is not favorable as the diameter is close to the length. Furthermore, the mounting and mechanical output shaft have to be on the same side, which means a

out-runner topology is problematic. Because of this, an in-runner topology is chosen.

5.3.2 Cooling Concept

The main heat loss in a PM motor occurs in the stator, both due to the copper loss and iron loss. In order to deliver continuous performance, this heat loss has to be removed. Given a radial in-runner topology with liquid cooling, there are two fundamentally different places to put the cooling pipes: either on the outside of the stator (Figure: 5.11a) or among the coil windings (Figure: 5.11b).

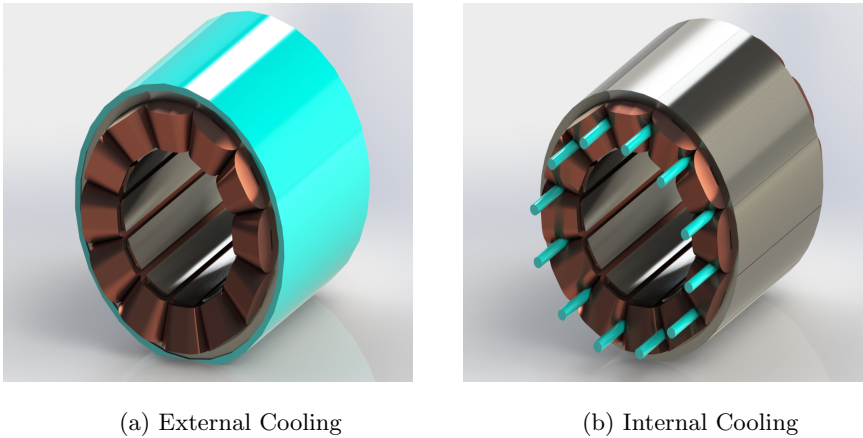


Figure 5.11: Cooling Concepts

Placing the cooling on the outside of the stator yields a simpler modular construction. Since the available dimensions are small, this makes manufacturing easier. Additionally, the whole cooling system is outside the motor, so the IP65 requirement is easier to uphold due to less cables entering the motor housing.

Performance-wise the integrated cooling circuit is better, as most of the heat is generated within the coils, so the thermal diffusion path is shorter. However, extra care has to be taken in order to ensure proper insulation between the cooling and electrical system. Furthermore, deeper slots tend to increase AC copper losses (Equation: 3.30).

Due to its simplicity, a modular cooling system on the outside of the stator is chosen. It enables modification of the flow channels after the motor is produced to optimize performance from actual test conditions. To allow for a cooling system on the outer diameter of the rotor, the diameter of the motor design space is reduced from 110mm to 100mm. A conceptual modular cooling sleeve is shown in figure (5.12)

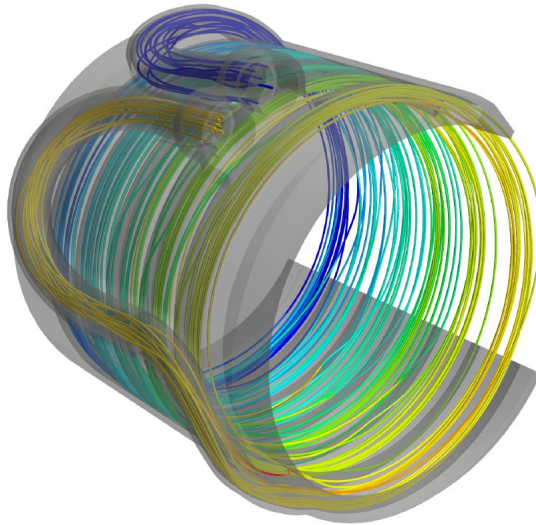


Figure 5.12: Flow Lines through External Cooling System

5.3.3 Cost

A high performance electric motor is a fairly complicated piece of machinery, and its final performance is largely dependent on the build quality. The motor prototype developed in this thesis is the first in Revolve's history, and there is fairly little competence of practical production of such a product within the team. In order to ensure an economically viable approach to the development of custom motors, the engineering materials chosen for this first prototype must have a good balance between performance and cost. Once Revolve has produced a few well working prototypes, more expensive, high end materials can be considered to push performance limits.

Another important aspect of cost is utilizing sponsored components to make up the prototype. Revolve NTNU is a non-profit organisation and is dependent on funding through external sponsors. Component sponsorship is typically a lot easier to get than capital sponsorship. For this reason, the choice of external components for the motor is dependent on current sponsorships.

5.4 Product Specification Form

#	Description	Value
1	Overall	
1.1	Dimensions (Diameter x Length)	100mm x 110mm
1.2	Hub Compatible	Must
1.3	Motor Topology	Radial In-runner
2	Mechanical	
2.1	Peak Torque	30.5 Nm
2.2	Maximum Speed	20 kRPM
3	Electrical	
3.1	Phase Connection	Y
3.2	Operating Voltage	334V to 424V
3.3	Three Phase Cable Diameter	10.1mm ± 0.5mm
4	Sensor Feedback	
4.1	Rotor Position	Must
4.2	Stator Temperature	Must
4.3	Rotor Temperature	Should
5	Cooling	
5.1	Coolant	Liquid
5.2	Cooling Element	External Sleeve
6	Environmental	
6.1	IP Protection	IP65
7	AMK Compatibility	
7.1	Rotary Encoder	ECI1100 (Appendix: A.1)
7.2	Output Spline	DIN 5480 (Appendix: A.3)

Table 5.3: Product Specification Form

Chapter 6

Design

6.1 Introduction

Engineering design and optimization of a high performance electric motor is no streamlined work-flow. There are several systems within, and the design must ensure compatibility both internally and externally. Furthermore, everything has to be efficiently packed due to the limited space available. Because the different systems within the motor affect each other, the work-flow is iterative, going back and forth while doing adjustments until a satisfying solution is reached.

It is difficult and unnecessary to capture all the small design iterations in a written report. Nevertheless, the system integration of all components was a major part of the design work and the author feels it should be reflected in the report. The logical approach used will be presented with its main findings and results.

6.2 Initial Considerations

Before the actual design work can start, all components must be defined in order to make sure nothing is left out in the final design. Furthermore, manufacturing and assembly constraints must be assessed to make sure the design turns out realizable.

6.2.1 External Components

A typical restriction in any product development project is the form factor of standardized components. Some components like bearings and seals are available in several dimensions, while others are more restrictive. The more restrictive components will be addressed here.

Heidenhain Rotary Encoder

In order to comply with requirement 7.1 (Table: 5.3), the Heidenhain ECI1100 rotary encoder must be used in the design. It connects to one end of the shaft and has a pre-defined mounting geometry. To integrate this into the design, a simplified model was created in the CAD environment. The data sheet is added in appendix (A.1).

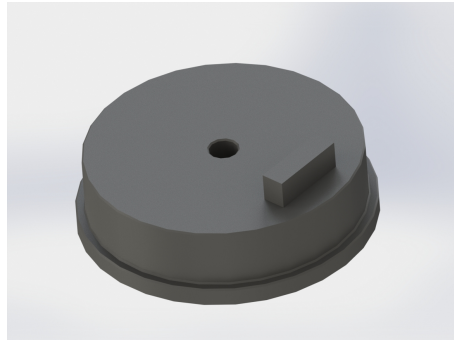


Figure 6.1: Heidenhain ECI1100 Mock-up

Temperature Sensors

Requirements 4.2 and 4.3 (Table: 5.3) demand temperature readouts from stator and preferably rotor. Temperature measurement in the stator coils is relatively simply done using a thermistor wire, i.e. a temperature dependent electrical resistance, which does not impose any spatial constraints. However, since it has to be placed inside the stator coils, cable holes in the motor housing have to be planned.

Temperature measurement of the rotor is harder, as it is constantly moving. To overcome this problem, the CT-CF02-C3 lightweight optical IR sensor is proposed. Due to its considerable size, it is imported into the CAD environment. With the close focus optics, CF02, the sensor should be mounted at a distance between 5mm to 40mm from the measured object, ideally at 25mm. The data sheet is added in appendix A.1.

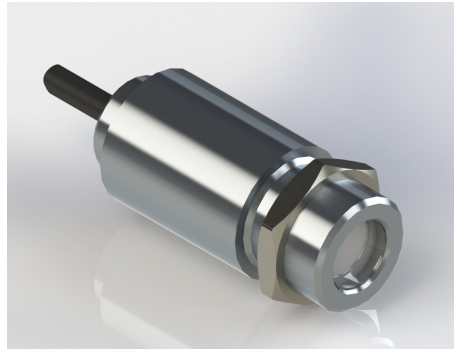


Figure 6.2: The CT-CF02-C3 infrared sensor

6.2.2 Environmental Protection

The motor is exposed to water and dust during racing, which is reflected in requirement 6.1 (Table: 5.3). In order to seal off the internal motor compartment from the outer environment, O-rings will be used in all external housing joints where space allows it. They offer good reliability and ease of disassembly. Where electrical cords penetrate the housing, cable glands and connectors with an IP65 rating must be used. As the estimated inverter power cable has a maximum outer diameter of 10.5mm (Table: 5.3, point 6.3), a suitable cable gland from Hylec is proposed.

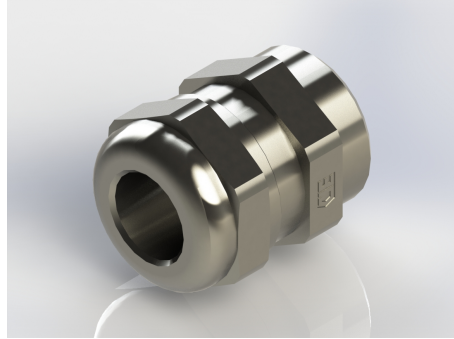


Figure 6.3: Hylec Cable Gland

In addition to environmental protection of the motor compartment, the Heidenhain encoder needs protection as well. This means it has to be enclosed in a sealed housing. A low current connector must be integrated to get sensor signals out. As there are no cable glands small enough for the thermistors, the free holes for these cables can be integrated with the encoder compartment and run through the encoder connector. A total of 8 pins is needed for the thermistor and encoder signal, which makes the already available 9-pins connector from Deutsch Connectors ideal for the purpose.

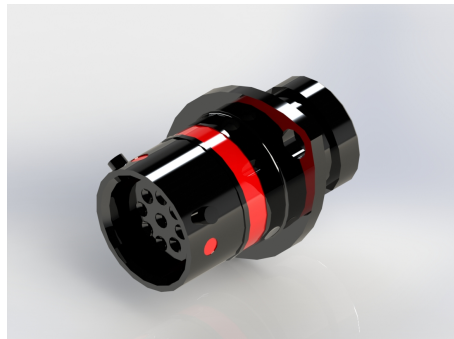


Figure 6.4: Deutsch ASDD006-09SKT-HE3

6.2.3 Manufacturing and Assembly

General manufacturing of housing and shaft will be done by a combination of turning and milling in order to achieve the required tolerances for rotor-stator concentricity and run-out tolerances for bearing seats. If possible, all components should be designed in such a way that 5-axis milling is unnecessary in order to reduce manufacturing costs. This puts restrictions on oblique holes and complex surface geometries. Circular symmetry and straight edges are favored shapes. Manufacturing of magnetic assemblies, i.e. rotor and stator, will be considered later.



Figure 6.5: 5-Axis Milling [25]

Assembly and disassembly of the motor must be taken into consideration during the design. Although enclosed brushless motors tend to be more or less maintenance free, the first prototype will be thoroughly tested and inspected to assess its reliability. An easy assembly and disassembly will both save time during the testing phase, reduce maintenance intervals and decrease the chance of assembly faults.

6.3 System Integration

All boundary conditions of the motor surfaces are given from the chosen concept, and they must be met in the final design. Due to this, an outside-in approach is used for integration of all the components. By building inwards, the remaining available space will be used for magnetic design.

6.4 Boundary Conditions

The cylindrical motor volume consists of three surfaces: two plane ends and one cylindrical body. This entire shell is the motor housing. If the end caps are individual components, they are referred to as end bells. The cylindrical body around the stator is referred to as the stator housing.

From the chosen concept, one end is mounted against the hub and features the output shaft (Figure: 5.7). In order to get maximum continuous performance out of the motor, as large cooling area as possible should be used for the cooling sleeve (Figure: 5.12). From this, the whole circular area is allocated for cooling. This leaves the last end available for electrical connections and sensors. Each of these interfaces will be discussed in further detail.

6.4.1 Mechanical Interface

The mechanical interface is primarily governed by requirements 1.2 and 7.2 (Table: 5.3). In order to offer compatibility with several motors, the hub mounting is designed to use an external adapter plate. The adapter plate bolts on to the motor and hub, and uses carefully machined cylindrical faces to ensure proper alignment between the motor's output spline in relation to the transmission input.

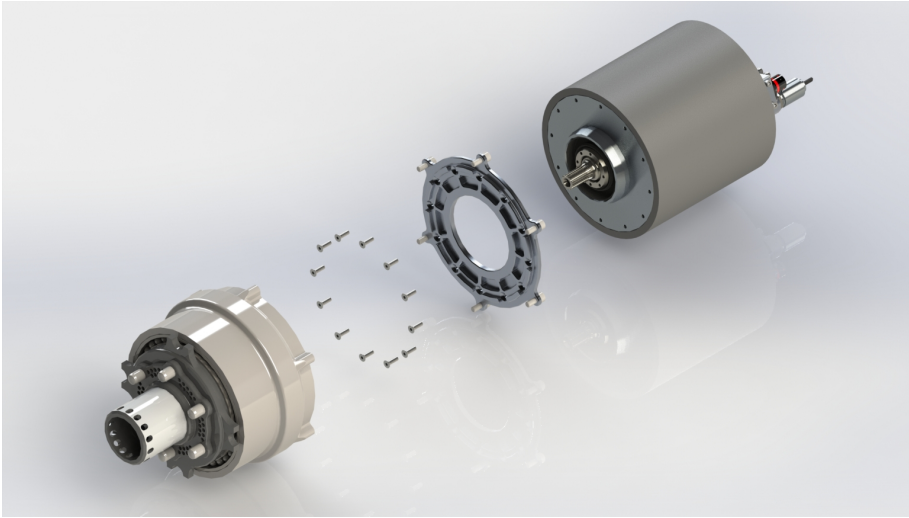


Figure 6.6: Mechanical Connection

The pitch circle diameter of the bolt circle used to fasten the motor to the adapter plate should be pushed as large as possible to be able to use the corners of the motor casing for bolt holes. Furthermore, a large bolt circle diameter decreases the forces at each fastener due to a larger second moment of area $I_{xy}^{circle} \propto D^3$ [26]. However, the cylindrical alignment face against the hub is set as the outer diameter of the hub bearings, i.e. 100mm, and no part of the fastener can protrude this circle.

Due to very limited space within the hub, countersunk bolts are used to prevent interference with the rotating hub. Smaller bolt diameter allows for less required material around each hole and a larger pitch circle diameter due to smaller bolt head. Because of this, M3 bolts were chosen, which yielded a maximum pitch circle diameter of 92mm. This also coincided well with the corner of the motor housing. The number of fasteners were set to 12 in order to yield

approximately the same accumulated bolt area as 8 x M4 bolts, used in the commercial AMK motor (Appendix: A.3).

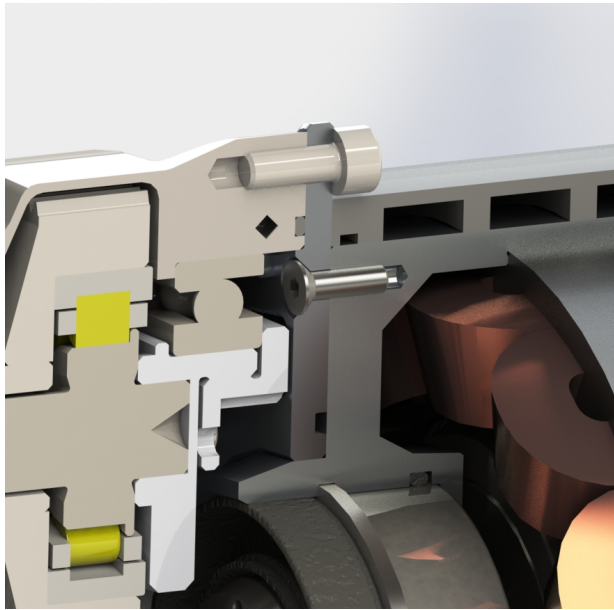


Figure 6.7: Adapter Plate Connection

Alignment of the motor to the adapter plate is done by a centering cylinder in the motor casing and a hole in the adapter plate. Further alignment with the hub is done by a circular extrusion in the adapter plate that is post milled to make room for motor fasteners. Lastly, the distance from the mounting surface to the output spline was adjusted to ensure good meshing of the sun gear to the first stage of the planetary gears.

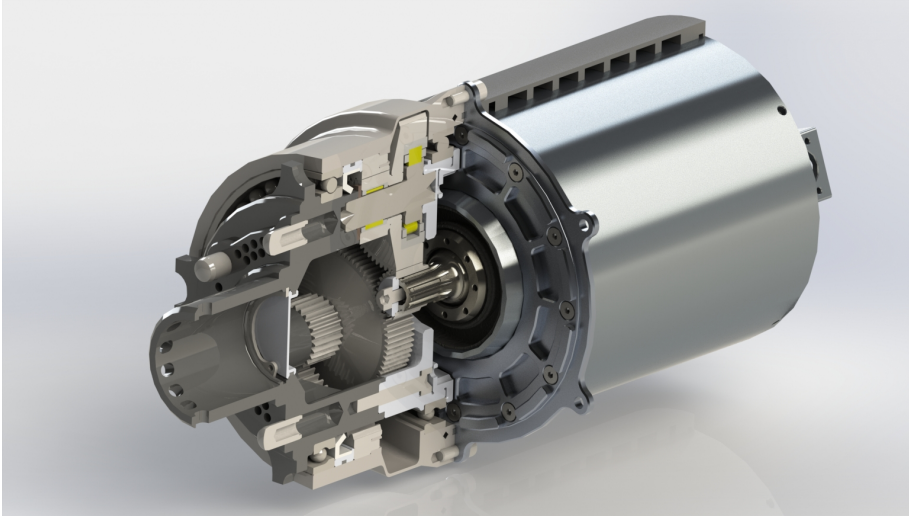


Figure 6.8: Hub and Transmission Interface

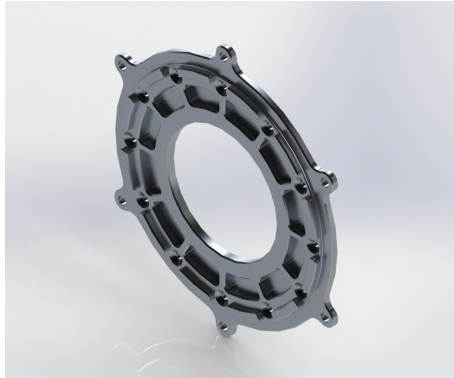


Figure 6.9: Adapter Plate

6.4.2 Cooling System Interface

The whole outer cylindrical area of the motor housing is allocated for cooling interface. This restricts the placement of radial bolt holes as coolant may seep through. If radial holes are present, measures must be employed to prevent coolant from entering the motor compartment.

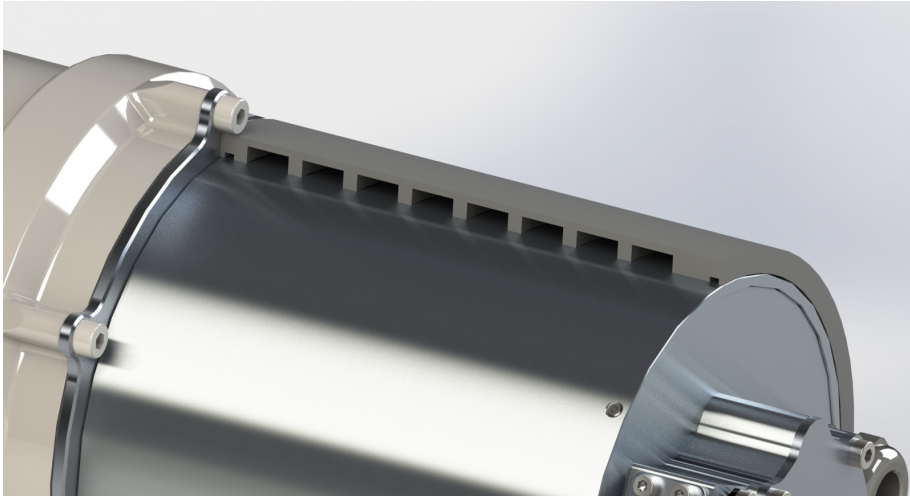


Figure 6.10: Cooling Sleeve

A conceptual cooling solution is shown in figure (6.10), illustrating the use of the cylindrical surface.

6.4.3 Electrical Interface

Several connectors and sensors are included in the electrical interface. All of these must be integrated into the end of the motor. During manufacturing, the stator coils have to be soldered together after being inserted into the stator housing. To provide access to the stator coils, the electrical end must be removable from the stator housing. Furthermore, there must be a grounding connection from the motor housing to the inside of the three phase cable.

The Heidenhain Rotary Encoder (Figure 6.1) must be placed concentrically to the motor shaft, and is the first component placed onto the end bell with

the corresponding mounting geometry (Appendix: A.1). A thin walled compartment is made around it.



Figure 6.11: Encoder Integration

Next, the optical IR sensor is integrated as close to the center as possible. As the sensor is mounted in a M12 hole, while the lens diameter is 7mm, it is mounted in the encoder compartment lid to get it closer to the shaft center. A sensor hole separated from the encoder compartment is made to ensure that the sensor cables cannot interfere with the IR sensor's line of sight and shield the sensor cables from electromagnetic noise created by the motor coils. The IR hole is made parallel to the end bell surface for ease of manufacturing, but this requires the rotor to have an outer diameter of at least 58mm. If the rotor has a smaller diameter, the hole needs to be angled.

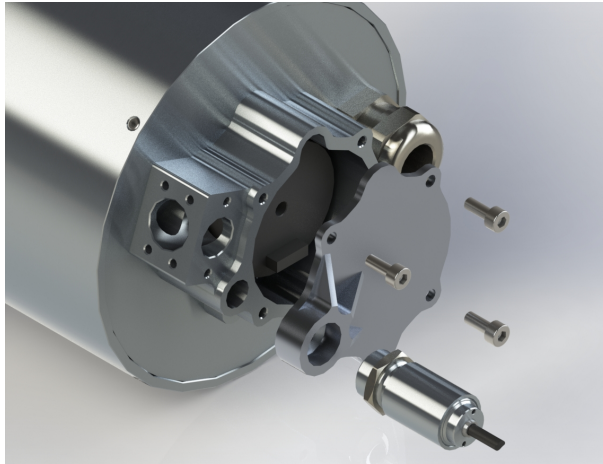


Figure 6.12: IR Sensor Mounting

As suggested in section (6.2.2), the stator thermistor cables can use the same connector as the Heidenhain encoder to ensure environmental protection through the motor housing in addition to eliminating an extra connector. It is desirable to mount the sensor connector externally to the encoder compartment lid, as all sensor cables can be mounted securely and controlled before the lid is closed independently. An extension of the encoder compartment is made to mount the Deutsch connector and has through-holes for the thermistors.

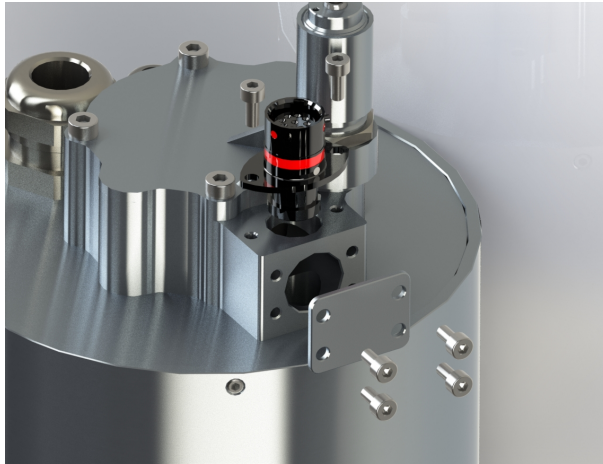


Figure 6.13: Extended Sensor Compartment

Lastly the cable gland (Figure: 6.3) for the three phase inverter cable is placed onto the end bell. In addition to the three phase connections to the coils, the motor casing has to be connected to electrical ground for safety. The grounding cable must connect any part of the housing to the shielding sleeve of the three phase cable, furthermore the grounding connection should be bolted on to ensure good electrical contact. As no threaded holes can be made in the cylindrical part of the motor housing, the connection must be in the end bell. Due to ease of assembly, the grounding connection is put on the outside of the end bell and an additional cable gland is used to connect it to the inside of the three phase cable.

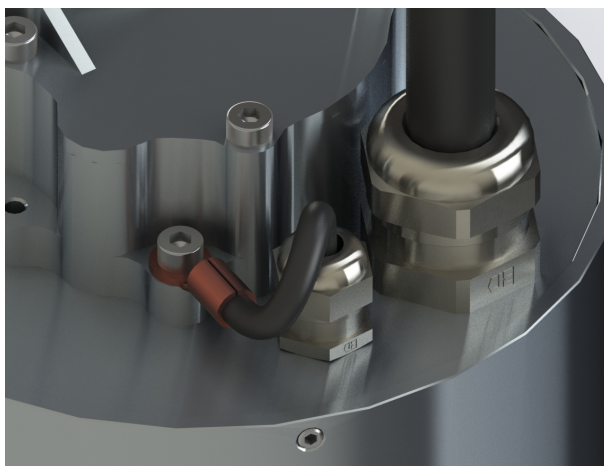


Figure 6.14: Ground Cable Connection

6.5 Motor Housing Design

The stator housing basically consists of a tube for fitting the rotor core and cooling jacket, and two end bells for bearings and external connections. As the sensor end bell must be removable to access the coil terminals during manufacture, there are basically two design variations for the motor housing. Either it is manufactured in two pieces: one removable end bell and one stator housing (Figure: 6.15), or in three pieces: two removable end bells and one stator housing (Figure: 6.16).

Two fundamentally different ways of joining the end bells by fasteners to the stator housing are considered. One is to use an axial flange with a cylindrical aligning surface between the parts, with fasteners oriented axially. An axial flange is mechanically strong, but requires a lot of radial space. The second alternative is to employ a radial flange with threaded studs locking the two

parts together. A low strength glue can be used on the studs to improve axial compliance. A radial flange is mechanically more compliant than an axial flange, but is much more compact. Furthermore, in order to satisfy requirement 6.1 (Table: 5.3), an o-ring is used in each joint. Because of strict spatial requirements, only cylindrical fitted o-rings will be considered.

Two Piece Design

The two piece design is focused on space efficiency. Since the stator housing includes one end bell, its outer shell may be machined very thin. In addition to save weight, this is favorable in case of a press fit between the stator core and stator housing due to more flexibility in the housing. To compliment the thin housing shell, a radial flange is used for the demountable end bell.

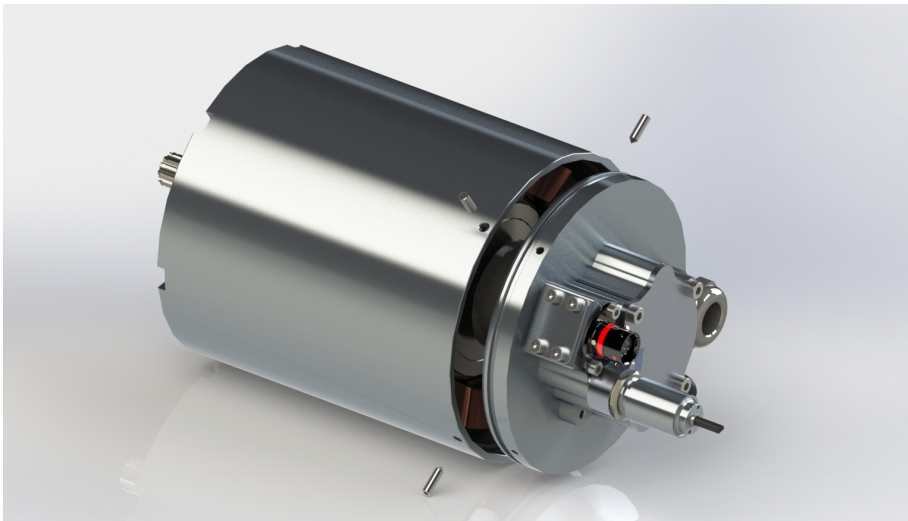


Figure 6.15: Two Piece Design

Three Piece Design

In a three piece design, mechanical integrity of all the joints becomes even more important as an additional flexible joint is introduced. Because of this,

an axial flange is proposed for both the end bells. As additional material has to be added at the flange points, there is no way to slide an external cooling sleeve over the outer circumference of the motor. To accommodate this, the cooling channels are integrated into the motor housing.

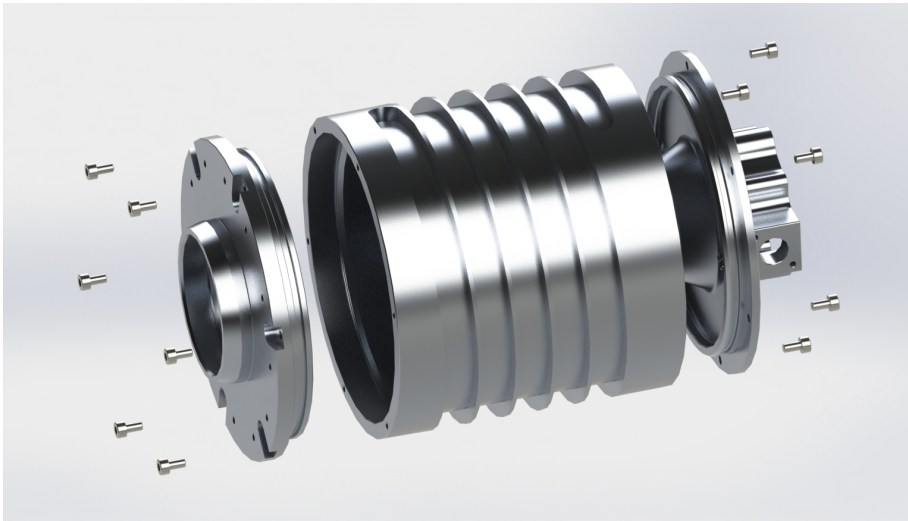


Figure 6.16: Three Piece Design

Design Comparison

By modelling the two design variations in the CAD environment, a qualitative comparison is made between them (Table: 6.1).

	Two Piece	Three Piece
Compactness	Very Compact	Bulky Design
Mechanical Robustness	Good	Very Good
Handling Robustness	Good	Exposed Cooling Channels
Machinability	Simple	Complicated
O-ring Seals	Single	Double

Table 6.1: Housing Design Comparison

The two piece design surpasses the three piece design in all considered categories except its mechanical robustness in axial direction for the end bell. However, axial forces in the end bell can be reduced to a minimum in the design of the bearing system. Because of this, the two piece concept is the clear winner of this comparison.

Design for Manufacturing

To facilitate machining of the stator housing, a two piece design is proposed. By using an interference fit to join the two parts together, they will function as one. The parts will also be glued together for extra safety. However, it is only a proposal and it may be produced as one single component if it is considered easier to machine.

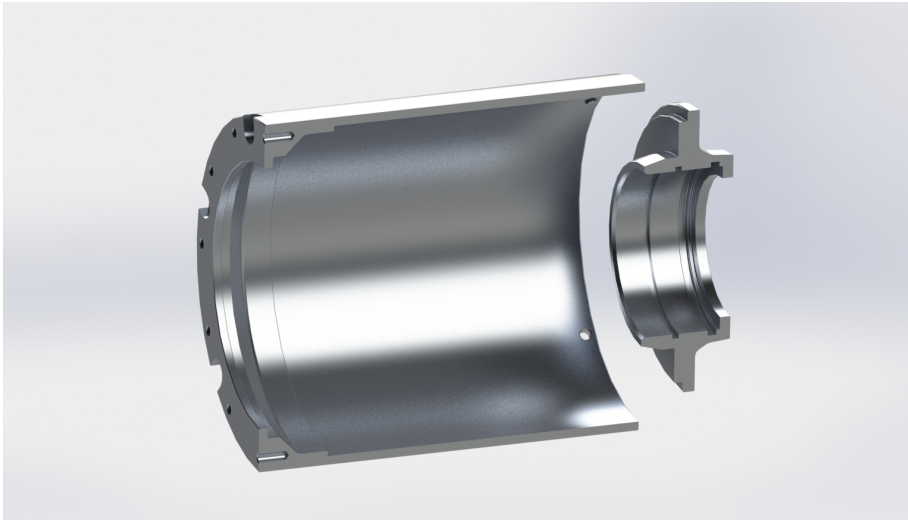


Figure 6.17: Split Housing

6.6 Bearing System

6.6.1 Considerations

Operational Loads and Speeds

An important aspect of bearing selection are the load and speed conditions during operation. The loads typically determine the size of the bearings, while the speed mainly restricts the diameter of the inner raceway.

Typical bearing loads in an electrical motor are related to bending moments on the output spline, either from misalignment or parallel gears / pulleys mounted directly on the rotor shaft. This load is primarily concentrated on the drive-side bearing, i.e. the bearing closest to the mechanical output. Other loads include gravity, inertia or unbalanced magnetic forces. In this scenario the output spline is connected to the sun gear of a planetary gearbox, which ideally

only transfers torque. There might be some radial bending loads due to slight misalignment of the meshing teeth, but this is considered to be minor. Furthermore, rotor mass and magnetic area are relatively low, so gravity, inertia and magnetic loads are also considered to be minor.

However, even though the load magnitude on the motor bearings is considered to be neglectable with regards to the limiting loads, the nature of the load may influence bearing performance. The dominating loads in PM motors with low mass rotors tend to be either inertial or magnetic, as gravitational loads are relatively small. All of the dominating loads tend to have an indeterminate radial direction. This must be taken into consideration when determining bearing fits with shaft and housing.

Inertial loads may come from unbalanced mass or vibration of the rotor. Magnetic unbalanced loads are typically divided into two categories: unbalanced radial forces and unbalanced dynamical forces. As the permanent magnets are attracted to the stator iron core, an unbalanced radial force may result from either an odd number of stator slots or an inconsistent air gap length. Additionally, the attraction and repulsion between the permanent magnets and energized coils may yield dynamically unbalanced forces if the winding does not include an even number of symmetries.

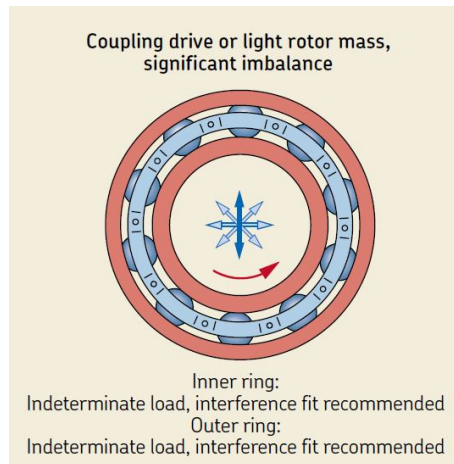


Figure 6.18: Indeterminate Load Direction ([27], p. 67)

The maximum speed of the motor is set to 20 kRPM, based upon the limiting speed of the commercial AMK motors, which the selected bearings have to withstand.

Temperatures and Gradients

During start-up and continuous operation, the motor temperature will increase from ambient to operational, furthermore the stator and rotor have different heat losses and cooling strategies, which results in temperature gradients across the bearing elements.

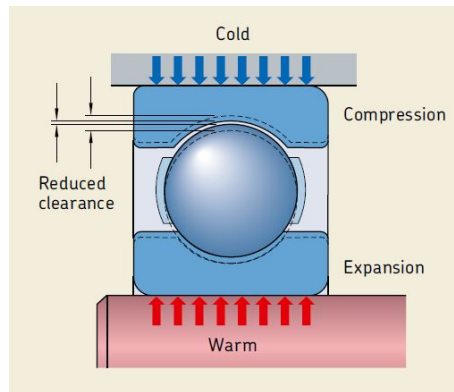


Figure 6.19: Bearing Temperature Gradients ([28], p.167)

Bearing raceways are typically made of steel, which expands when heated up. If the inner raceway of the bearing has a larger temperature than the outer raceway, the internal clearance of the bearing will decrease. If the internal clearance zeroes out, the bearing is said to be preloaded, which greatly increases friction and reduces bearing life (Figure: 6.20). Because of this, SKF recommends the use of greater internal clearance than normal for electric motors, denoted C3 clearance.

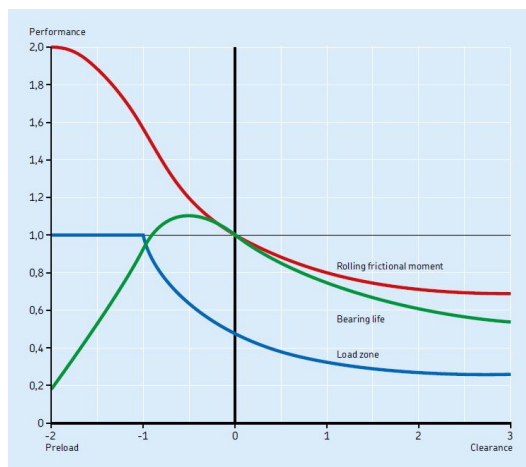


Figure 6.20: Performance vs Preload ([28], p.212)

Shaft Retention

Bearings are responsible for retaining the shaft at its position. For electrical motors, a bearing is located on each end of the shaft. To accommodate thermal expansion of the shaft during operation, only one bearing is fixed to both the shaft and housing, responsible for reacting axial forces. The other bearing is designed to slide freely in the axial direction, typically in the housing. SKF recommends that the fixed bearing is retained by interference fits and secured through mechanical measures, e.g. circlips or seat shoulders. The fixed bearing is often called locating bearing, while the axially free is called non-locating bearing.

Bearing Material

A common bearing failure mode in electric motors that employ inverters to modulate excitation currents is electrical erosion of the raceways. The high frequency switching may induce voltages between rolling elements and raceways. If both components are made of a conductive material, e.g. steel, sparks can occur between them, leaving small pits. These pits degrade bearing performance and may eventually lead to failure.

Hybrid bearings employ ceramic rolling elements made of silicon-nitride within conventional steel raceways. Unlike steel, the silicon-nitride is an excellent insulator and eliminates the risk of electrical erosion. Other advantages of hybrid bearings are the high hardness of the rolling element, which yields lower friction, higher maximum speed and longer bearing life.



Figure 6.21: Hybrid Bearings ([27], p. 28)

6.6.2 Implementation

The bearing system should have good integration with the mechanical and electrical motor boundaries (Section: 6.4). Furthermore, it should be noted that the hub mounted side is exposed to gearbox oil, and must be sealed to prevent gearbox oil from entering the motor compartment. Additionally, assembly and disassembly of the bearing system must be possible without a risk of damaging any of the motor components.

Bearing Type

There are many different types of bearings available. However, the hybrid bearings from SKF are only available as single row deep groove ball bearings and single row cylindrical roller bearings, so only these two will be considered.

Deep groove ball bearings can carry radial, axial and combined loads, making them suitable both for locating and non-locating operation. They are characterized by low friction and low noise. Due to internal clearance, they tend

to be less sensitive to misalignment compared to cylindrical roller bearings. Cylindrical roller bearings are typically used to carry heavy radial loads, and they cannot accommodate axial forces. Their friction is generally higher than deep groove ball bearings and they have a lower maximum speed limit.

As the expected bearing loads are small and low friction is favorable to prevent heat buildup in the rotor, the deep groove ball bearings are the natural choice. Also, this type offers the largest assortment and lowest cost of the two types.

Bearing Arrangement

The chosen two piece stator housing design (Section: 6.5) has reduced stiffness and axial capacity of the end bell. Because of this, the locating bearing will be positioned on the drive side of the motor, and the non-locating bearing in the end bell.

Non-locating bearing

The dimensions of the non-locating bearing should integrate well with the rotary encoder mounting points. An outer diameter of 35mm enables the mounting points for the rotary encoder to integrate well into the bearing seat. To be compatible with the shaft connection for the Heidenhain encoder (Appendix: A.1), the inner diameter must be larger than 9.3mm. For an outer diameter of 37mm and an inner diameter larger than 9.3mm, the following deep groove ball bearings are available from SKF.

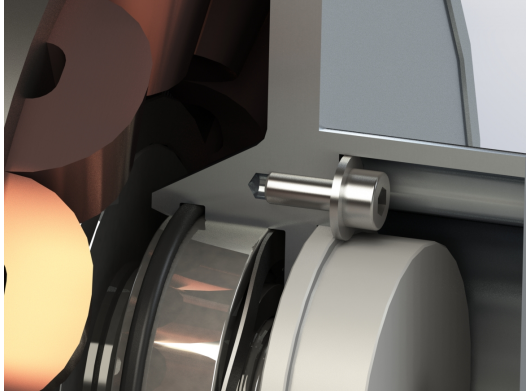


Figure 6.22: Encoder Mounting Integration

Designation	ID	OD	B	C	Ref. Speed	Lim. Speed	Weight
E2.6300-2Z	10	35	11	8.32	55 000	29 000	53
E2.6202-2Z	15	35	11	7.8	47 000	25 000	45
E2.6003-2Z	17	35	10	5.85	49 000	25 000	39

Table 6.2: Non-locating bearing selection

where ID is inner diameter, OD is outer diameter, B is width and C is load rating in [kN]. The reference speed yields a quick assessment on the thermal speed capabilities of the bearing, while limiting speed is the mechanical limiting speed, both given in [RPM]. Weight is given in gram.

Hybrid bearings are not standard components, so their specifications are not listed explicitly in any catalogue. In order to do an assessment on bearing dimensions, the energy efficient class (E2) is enlisted instead to get an indication on how different geometries affect performance parameters.

With regards to speed and load capabilities, the 6300 comes out as the best.

However, the 6003 bearing is significantly lighter and more compact than the 6300. Additionally, a larger shaft diameter is favorable as it increases the stiffness of the rotor. As the load and speed rating of the 6003 bearing satisfy the requirements (Table: 5.3, point 2.2), it is chosen for its compactness and lightweight. After consulting with SKF, the hybrid version of 6003 with a C3 internal clearance is denoted: 6003 2RSLTN9/HC5C3WT, and has a limiting speed of 32 000 rpm.

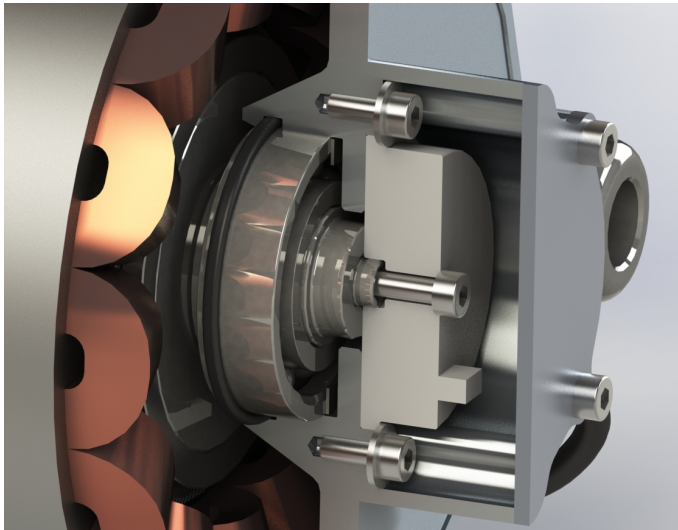


Figure 6.23: Bearing Integration

Locating Bearing

The locating bearing must be mechanically retained from movement to either side on both inner and outer raceway. It must allow for easy assembly and disassembly of the bearing system. Also, the form factor must integrate well with the fixed output spline (Table: 5.3, point 7.2), and a shaft seal must seal it from the gearbox.

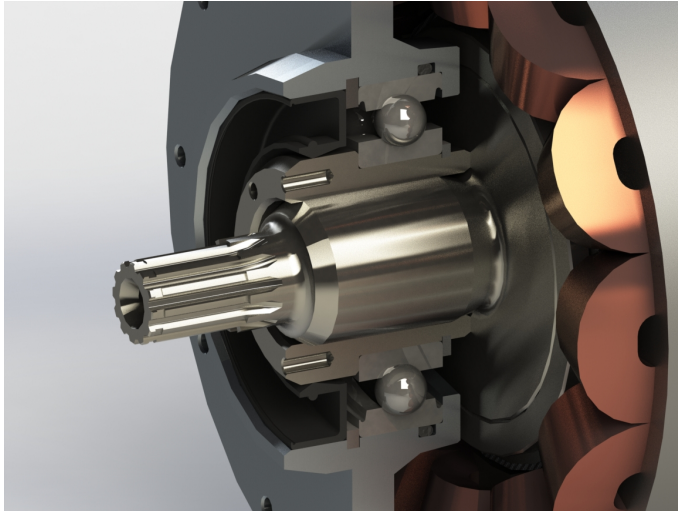


Figure 6.24: Drive Side Bearing Assembly

In order to facilitate disassembly of the bearing, a sleeve is added between the shaft and bearing. The bearing will be mounted to the sleeve, and the sleeve shrink fitted on to the motor shaft. By fixing the sleeve with the disassembly holes, the shaft can be pressed out of the sleeve again, e.g. using a hydraulic press.

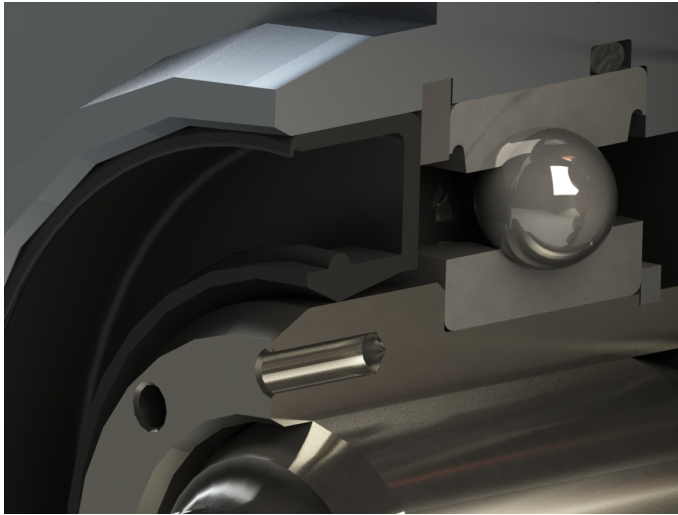


Figure 6.25: Seal Integration and Bearing Retainment

Another advantage of a bearing sleeve is that a shoulder can be added to both support the bearing axially and serve as a sealing surface for a shaft seal. Additionally, an external circlip groove can be cut into the sleeve without having to worry about stress concentration and potential crack initiation in the shaft.

Due to the form factor of the spline and minimum thickness of the bearing sleeve, the inner diameter of the locating bearing should be at least 25mm. Furthermore, a shaft seal has to be available with outer diameter equal to the bearing and an inner diameter equal to the shoulder section of the bearing. The available bearings with an inner diameter of 25mm and an available seal dimension are listed below.

Designation	ID	OD	B	C	Ref. Speed	Lim. Speed	Weight
61905	25	42	9	7.02	36 000	22 000	45
16005	25	47	8	8.06	32 000	20 000	60
6005	25	47	12	11.9	32 000	20 000	78

Table 6.3: Locating bearing selection

All the bearings satisfy the speed constraint of the motor. 61905 is the most compact and lightest alternative. However, weight saved in bearing mass is partially added to the motor housing due to the centering cylinder for the motor adapter plate. During the assembly and disassembly of the rotor to the stator, the bearing might experience some bending moments due to misalignment. Because of this, the more robust 6005 bearing was chosen. The hybrid version of 6003 with C3 internal clearance is denoted: 6005 2RSLTN9/HC5C3WT, and has a limiting speed of 22 000 rpm.

Shaft Seal

In order to prevent gearbox oil from seeping into the bearings or motor compartment, a shaft seal is added. When determining the locating bearing, the availability of compatible shaft seals were checked. The only available shaft seal that fits to the 6005 bearing is 30x47x8.

Due to the high rotational speeds of the rotor, the surface speed of the sealing lip interface may come as high as 31m/s at 20 000 rpm. Fluor rubber is the lowest friction material that SKF has available, but it has a recommended surface speed of 18m/s which is significantly below the worst case scenario. After consulting with SKF, the seal was found to be applicable at higher speeds, but seal wear should be checked periodically. Extra seals were ordered in case replacement was needed. The designation of the used seal is 30x47x8 CRW1

V.

Axial Preload

Deep groove ball bearings used in the design have some axial compliance due to internal clearance. An axial spring can be added to the non-locating bearing to preload the arrangement axially. This will reduce noise and vibration during operation. SKF has a recommended axial preload based on bearing inner diameter, given by

$$F = k d \quad (6.1)$$

where F is the desired preload force in [kN], k is a factor between 0.005 and 0.01 and d is the bearing bore diameter. ([28], p. 224) As the bore diameter of the chosen bearings differ, the preload force should be within the intersection of the two intervals, i.e. $F \in [0.085, 0.170] \cap [0.125, 0.250]$, which yields a preload force between 0.125 and 0.170 [kN]. A waved washer is added on the outer diameter of the bearing raceway, yielding a preload of 0.137 at nominal length.

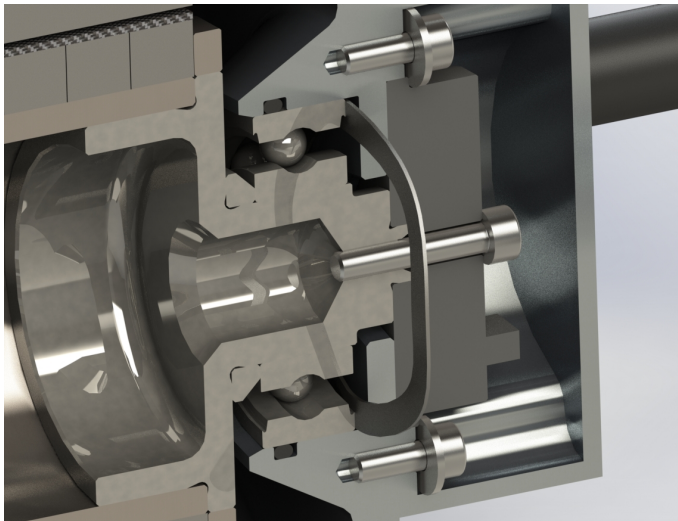


Figure 6.26: Integration of wave washer at non-locating bearing

6.7 Magnetic System

In order to integrate the magnetic system into the motor, an initial design must be determined. As discussed in the section (3.5.1), the magnetic system consists of a rotor with permanent magnets attached to a shaft. For the chosen in-runner topology (Section: 5.3.1), the stator is concentrically aligned and enclosing the rotor. The stator is axially longer than the rotor due to the coil end turns that span from one slot to the next.

6.7.1 Engineering Materials

The design of any electric motor is dependent on the magnetic materials used. A brief discussion is done of the engineering material that goes into the essential components of any PM motor: the permanent magnets, iron flux carriers and coil wire.

Permanent Magnets

Modern high performance permanent magnets are either made up of a Neodymium Iron Boron alloy (NdFeB) or a Samarium Cobalt alloy (SmCo). Both of these magnet types comes in many different grades. A commonly used performance indicator for permanent magnets is the maximum energy product. it is defined as the product between demagnetization flux intensity $-H$ and output flux B along the operating line of the permanent magnet.

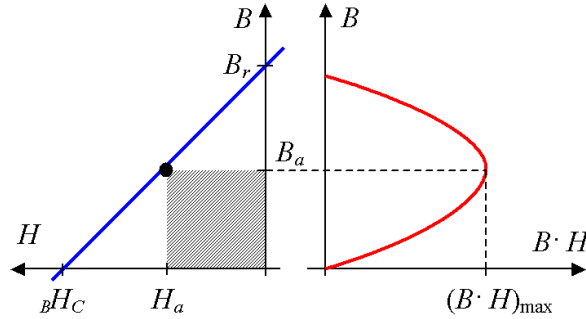


Figure 6.27: Max Energy Product [29]

As seen in figure (6.27), the energy product does not give the actual performance in a motor. However, the slope of the BH curve is approximately the same for all magnets, so a higher energy curve typically yields higher magnetic output. Most importantly, it summarizes the magnetic output to a single scalar parameter.

All permanent magnets show degraded performance at elevated temperatures, which lowers their energy product. Different magnet grades and magnet materials exhibit different temperature characteristics. A performance sweep of different magnets is shown below.

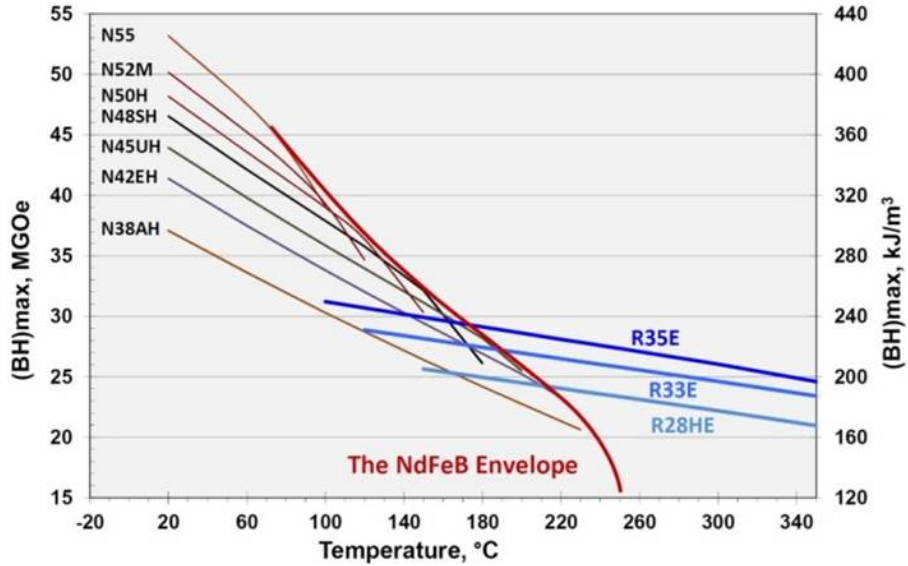


Figure 6.28: Magnet Performance [30]

where the first letter designates the magnet material: N for NdFeB and R for SmCo. The following number is the nominal energy product, and the last letters designate its temperature rating. NdFeB magnets show significantly better performance at temperatures below $100^{\circ}C$, while SmCo is less sensitive to temperature and excels at high temperatures.

However, the energy product only tells half the story of a magnet's performance. Another very important aspect is the protection against demagnetization. Under the influence of strong magnetic fields from the stator, a magnet may permanently demagnetize. SmCo magnets are in general very well protected against demagnetization at elevated temperatures. NdFeB requires the addition of rare dysprosium to perform well at higher temperatures, which adds to the cost and generally lowers the nominal energy product.

A class of neodymium magnets with nominal energy product 35 is assessed for demagnetization temperature when the internal magnet flux is forced to 0 T by an externally applied magnetic field.[31] [32]

Material	N35H	N35SH	N35UH	N35EH	N35AH	R35E	R33E
Temp.	80°C	100°C	150°C	180°C	220°C	250°C	300°C

Table 6.4: Demagnetization Temperatures

With increasing amounts of dysprosium in the NdFeB magnets, they are gradually better protected against demagnetization at elevated temperatures. However, SmCo excels at the top with a demagnetization temperature of above 250°C.

Another aspect of magnet material is mechanical, electrical and thermal characteristics. The magnets have to be retained from centrifugal forces when the rotor is spinning. This favors low mass density. High electrical resistivity is desirable as it reduces eddy current losses and heat buildup (Section: 3.3.3). Thermal conductivity should be high to facilitate heat transfer from the rotor. Table (6.5) shows typical material characteristics for permanent magnets.[31] [32]

Material	Density	Resistivity	Thermal Conductivity
NdFeB	7.5	147	7.5
SmCo	8.3	81	10

Table 6.5: Magnet Material Parameters

where density is given in $[g/cm^3]$, resistivity in $[\Omega \cdot m]$ and thermal conductivity in $[W/m \cdot K]$. From its physical properties, the NdFeB magnet comes out slightly better than SmCo.

NdFeB is significantly cheaper than SmCo. To keep the price tag on the first prototype motor low, a N35-class magnet is chosen. It offers a reasonable compromise between performance and price. Additionally, its magnetic output is close to SmCo at lower temperatures, which means the magnet material can be swapped for the next prototype without large modifications to the motor geometry. Based on a maximum allowable stator temperature of 140°C , a maximum rotor temperature of 150°C is anticipated due to a longer thermal diffusion path. From table (6.4), a thermal class of EH is used to have a safety factor with respect to demagnetization. The designation of the chosen magnet grade is N35EH. Its data sheet is added in appendix (A.4).

Iron Core

Steel with added silicon (SiFe) is commonly used in electric motors due to its availability and low price. Cobalt steel (CoFe) can be used instead to increase performance, but comes at a considerably higher price. SiFe is about 1/3 the cost of CoFe. The magnetization curves for the two materials are shown in figure (6.29). CoFe data is provided by Vacoflux 48 by Vacuumschmelze [33], while SiFe data comes from Arnon 7 by Arnold Magnetics [34].

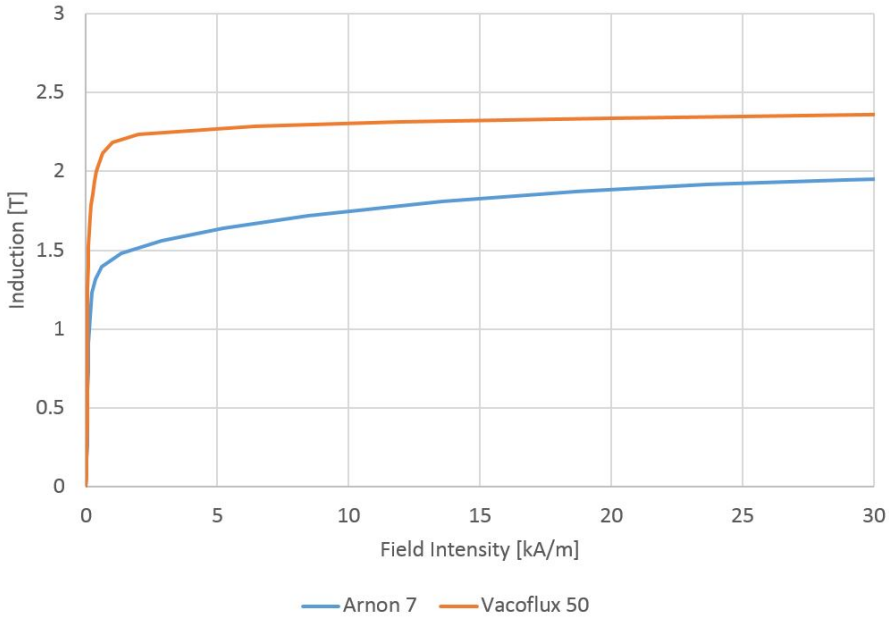


Figure 6.29: Magnetization Curves: SiFe vs CoFe

If comparing magnetic saturation of the two flux carriers, CoFe is considerably better with a saturation flux of around 2.2T compared to 1.4T for SiFe, which means it will be easier to carry stronger magnetic fields. In a practical design this means the flux carriers in the stator can be made thinner, leaving more space for windings. Also, flux concentration can be employed in the rotor to increase air gap flux B_g .

However, the higher flux carrying capacity comes at a price. Due to the higher flux density peaks B_p , higher eddy current losses will occur in the core (Equation: 3.10). Figure (6.30) shows the core loss comparison of CoFe and SiFe at a excitation frequency of 1000 Hz. As the CoFe has a higher flux operating point, the core losses are significantly higher, depending on the actual

design. Due to this, CoFe is generally not recommended in applications where the electrical frequency exceeds 1200 Hz. [34]

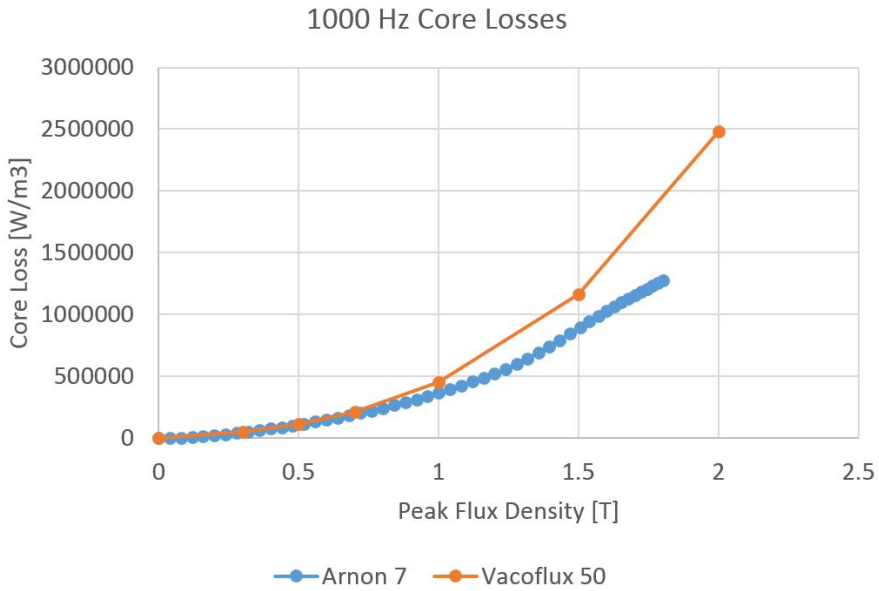


Figure 6.30: Core Losses: SiFe vs CoFe

Due to the very high price of CoFe, SiFe is chosen for this first prototype. Arnold magnetics can deliver SiFe in two different lamination thicknesses: Arnon 5 with 0.005 inch (0.127mm) sheet thickness, while Arnon 7 comes in 0.007 inch (0.178mm) sheet thickness. Arnon 7 yields slightly higher saturation flux due to better fill factor, while Arnon 5 has slightly lower core losses due to thinner laminations (Equation: 3.10). Furthermore, thicker lamination sheets, i.e. Arnon 7, means less time in cutting and lamination during production. Since core losses are not considered to be a problem with laminated SiFe, Arnon 7 is chosen primarily to save cost during manufacture.

Coil Material

The conducting coils in the stator should have as low material resistivity as possible to reduce ohmic losses (3.27). Other important aspects are high thermal conductivity and low weight. Copper is very commonly used as it offers a very low resistivity and high thermal conductivity at a reasonable price. The only metallic material offering slightly lower resistivity is silver, but it cannot compete on price. Another, more cost effective alternative is aluminium.

Material	Density	Resistivity	Thermal Conductivity
Copper	8.9	1.72	386
Aluminium	2.7	2.65	204
Relative Factor	3.3	0.65	1.9

Table 6.6: Coil Material [35] [36] [37]

where density is given in $[g/cm^3]$, resistivity in $[10^8\Omega \cdot m]$ and thermal conductivity at $20^\circ C$ in $[W/m \cdot K]$. Copper is over three times as dense as aluminium, but has almost twice the thermal conductivity and half the resistance. As the design space is very limited, copper conductors are chosen over aluminium due to their superior resistivity and thermal conductivity.

All coil wires come with insulation, and the insulation has a thermal class, i.e. how high operating temperatures it can withstand. Typically for high performance motors, a thermal class of $155^\circ C$ is common, using a polyurethane film on the conductor's surface ([38], p. 44) . To protect the insulation, a maximum operating temperature of the stator coils is set to $140^\circ C$.

6.7.2 Motor Layout

Number of Magnetic Poles

One of the main parameters in PM motors is the number of magnetic poles. This determines the electrical frequency of the motor (Equation: 3.20). As shown in section (3.5.5), a higher pole count generally increases the motor constant due to a thinner stator yoke, which leaves more space for copper. However, an increased electrical frequency increases AC losses (Section: 3.5.4). Furthermore, the inverter switching capabilities must be able to keep up. (Section: 4.1.3)

Considering the inverter, requiring a minimum of 20PWM cycles per electrical period to operate above the knee region in figure (4.8), the 40kHz switching frequency allows for a maximum electrical frequency of 2kHz.

Investigating the recommended litz wire sizes for motor applications, both AWG 28 and AWG 30 are available. AWG 28 is recommended between 60Hz and 1kHz, while the AWG 30 wire is recommended between 1kHz to 10kHz ([38], p. 48). As this is higher than the 2kHz maximum for the inverter, copper AC losses are not a limiting factor.

By regarding the available space for the stator, a core volume is estimated to be around 150cm^3 . Using core loss data from Arnon 7 and assuming a sinusoidal saturation flux of 1.4T, an initial core loss estimate could be done. At an electrical frequency of 2kHz, the initial estimate yields a maximum of 300W core loss. Comparing this to the rated power of the commercial AMK

motors at 12.3kW, it makes up only 2.4%. In other words, core losses are not considered to be a problem at 2kHz.

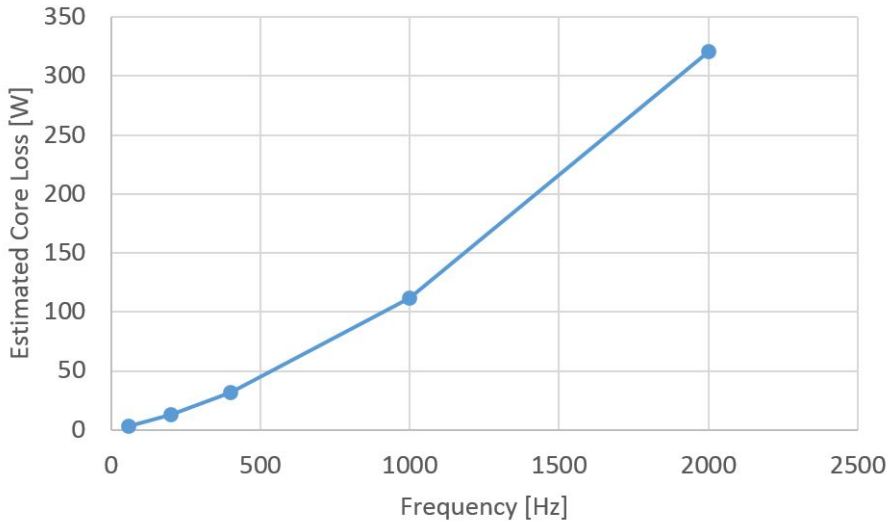


Figure 6.31: Estimated Core Losses at 1.4T Peak Flux

Counting in the maximum mechanical frequency of 333Hz (20 000 RPM), and using the inverter frequency limitation of 2kHz, a maximum pole count of 12 is found by applying equation (3.20).

Slot and Winding Layout

Once the pole count is determined, a matching slot and winding layout can be determined. In order to form a balanced three phase winding, there are only certain allowable patterns that are dependent on the number of magnetic poles. A list of valid pole and slot counts for three phase motors is given ([9], Appendix E). Each combination has several different characteristics, expressed by the following parameters:

- N_s is the number of slots in the stator. A higher slot count means less space for each slot and tooth. Due to the small dimension of the motor, this number should be kept below 18 to ensure a sufficient amount of space for each tooth and coil.
- N_{spp} is the number of slot per pole per phase. An integer number means that all the coil back EMFs are in phase, which yields a phase back EMF with a high harmonic content. A fractional number means that the coil back EMFs are slightly out of phase, yielding a much more sinusoidal back EMF. These two variations are denoted an integer slot motor and a fractional slot motor, respectively. A sinusoidal back EMF is desired from an inverter control perspective.
- N_{wl} is the number of winding layers possible. The number of winding layers designates how many separate coils that share each slot. Phase coils in a double layer winding will have half the cross sectional area compared to a single layer winding, but there will be twice as many coils (see picture x). A double layer winding is favored as it reduces the axial length of the end turns, making it more compact.
- N_{cg} is the number of coil groups. If this number is higher than one, radial forces created by the excitation coils will be balanced by another coil group, leaving the layout dynamically balanced. This reduces noise and vibration.
- N_{rad} is the harmonic index of the first radial force component. If no index is given, the layout is statically balanced, and there will be no net radial forces on the rotor from the attraction of the magnets to the stator teeth. A statically balanced layout reduces vibration and noise.
- N_{cog} is the harmonic index of the first cogging torque component. A

higher index indicates less cogging torque. Cogging torque gives torque ripples and should be reduced.

As the lowest valid slot count for a 12 pole motor is 18, the available space for each tooth and coil becomes too small to be practical. Because of this, 10 pole motor layouts are considered instead.

N_s	N_{spp}	N_{wl}	N_{cg}	N_{rad}	N_{cog}
9	3/10	2	1	1	9
12	2/5	1	2	-	6
12	2/5	2	2	-	6
15	1/2	2	5	-	3

Table 6.7: Valid 10 pole layouts

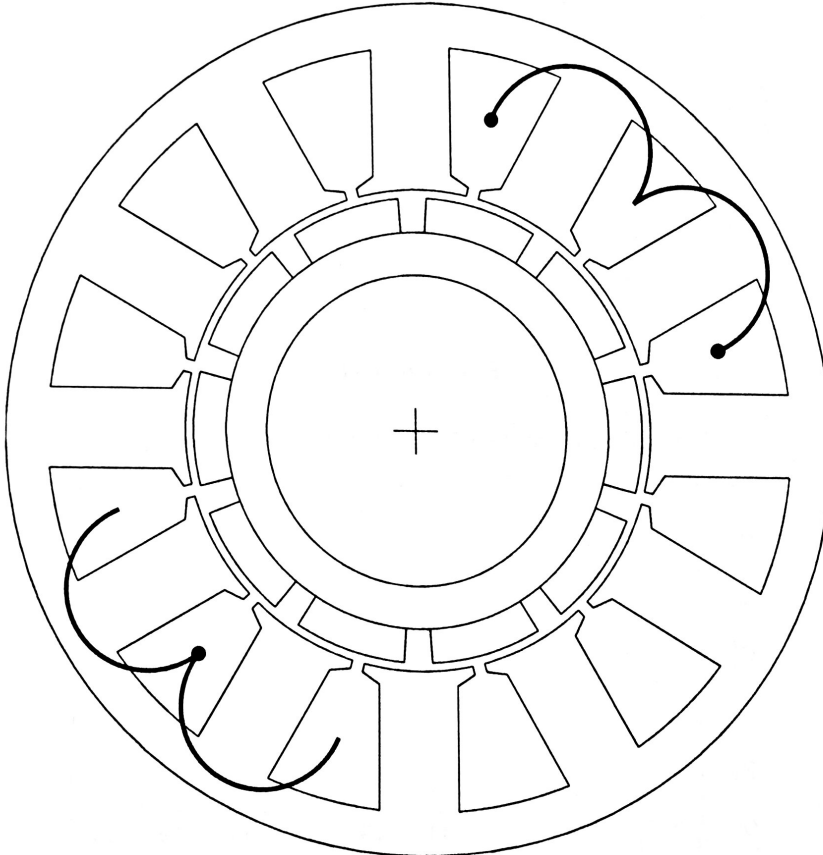
The 12 slot layout is compatible with both single and double layer winding. Due to the axially shorter end turns of the double layer winding, the single layer winding is discarded. Remaining layouts are qualitatively compared.

N_s	Advantages	Disadvantages
9	Lowest Cogging	Statically and Dynamically Unbalanced
12	Balanced	-
15	Balanced	Highest Cogging

Table 6.8: Qualitative Winding Comparison

Comparing the three winding layouts, the 12 slot comes out as the best compromise between a balanced layout and lowest cogging. Furthermore, due to a relatively low number of slots, there is more space for each coil and tooth, leaving the dimension sizes practical to manufacture.

N_m	N_s	N_{spp}	N_{wl}	N_{cg}	N_{rad}	N_{cog}	α_{sk}
10	12	2/5	2	2	-	6	1/5



Coil	Angle	Phase A		Phase B		Phase C	
		In	Out	In	Out	In	Out
1	0	1	2	5	6	9	10
2	-30	3	2	7	6	11	10
3	0	8	7	12	11	4	3
4	-30	8	9	12	1	4	5

Figure 6.32: Chosen slot and winding layout ([9], p. 376)

6.7.3 Rotor Topology

Now that a motor layout has been chosen, the next step is to determine a suitable rotor topology. There are several available topologies possible, but only

the ones containing the maximum amount of magnet material will be discussed here.

Surface Mounted Magnets (SMM)

This topology is the most commonly used for motor construction due to its simplicity and high performance. The permanent magnets have an arced geometry that fits with the circumference of the shaft. Due to high rotational speeds, a retaining sleeve must be placed on the outer circumference of the magnets to prevent them from flying off.

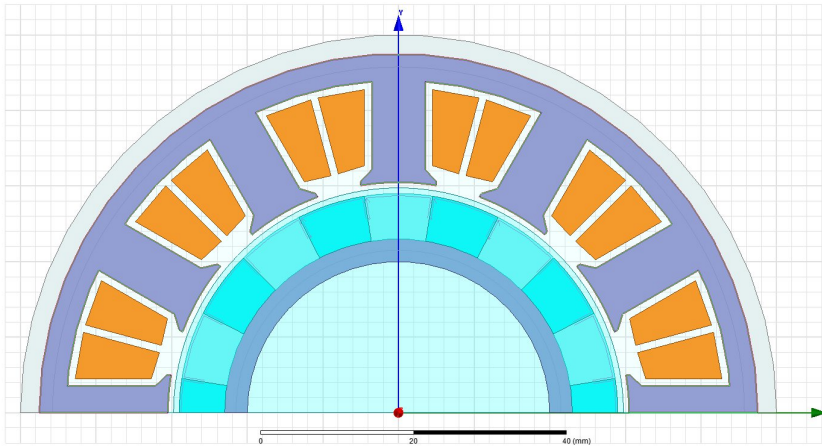


Figure 6.33: Surface Mounted Magnets

Another advantage of the surface mounted topology is that a so called Halbach array can be employed. By magnetizing some of the magnets in the circumferential direction instead of radially, the permanent magnets can partially work as a rotor yoke, focusing the field towards the air gap and weakening it towards the shaft.

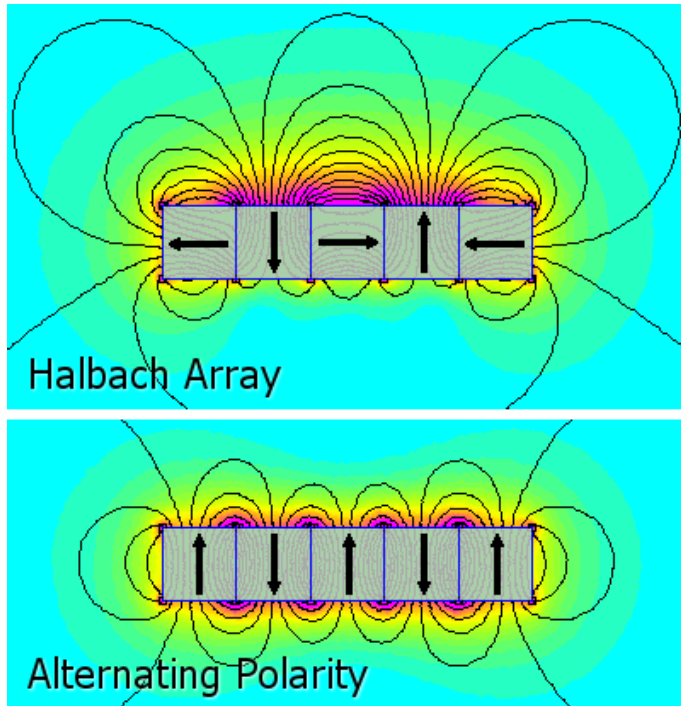


Figure 6.34: Halbach Array [39]

From a constructional point of view, the shaft is simple and can be hollow to save weight. However, the arced magnets are somewhat harder to manufacture than rectangular ones.

Internal Spoke Magnets (ISM)

The spoke topology was originally invented to employ flux concentration (Equation: 3.17). However, the remanence flux of the chosen magnets is around 1.2T, depending on the temperature, while the saturation flux of SiFe is around 1.4T. This means that flux concentration is less powerful, and the core material will limit the amount of flux that can be concentrated. If CoFe was used instead of SiFe, the flux concentration capability could be very advantageous.

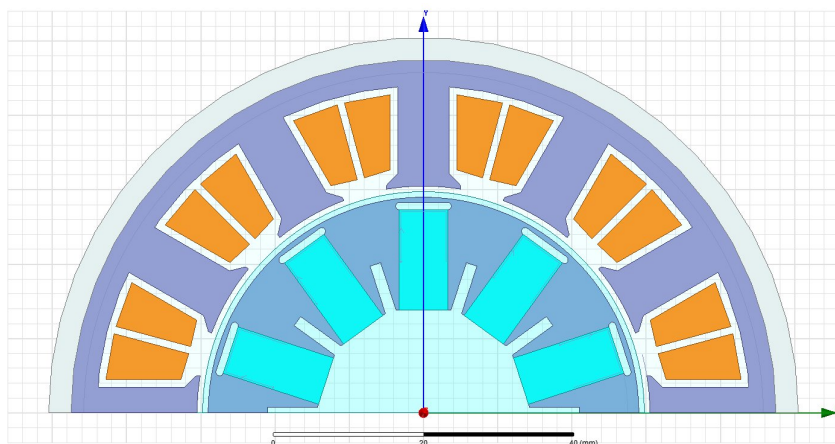


Figure 6.35: Internal Spoke Magnets

From a manufacturing point of view the topology accepts rectangular magnets. However, as the rotor core geometry is somewhat complex and thin walled, it makes assembly procedure difficult considering the strong magnetic forces between the core and permanent magnets.

Buried Magnets (BM)

A topology closely related to the surface mounted magnets. Instead of mounting the magnets directly to the shaft, they are buried within a laminated rotor core. This yields the advantage of accepting rectangular magnets and providing natural magnet retention. However, the flux concentration of this design is negative and magnetic flux will leak through the flux bridges on the rotor, diminishing performance.

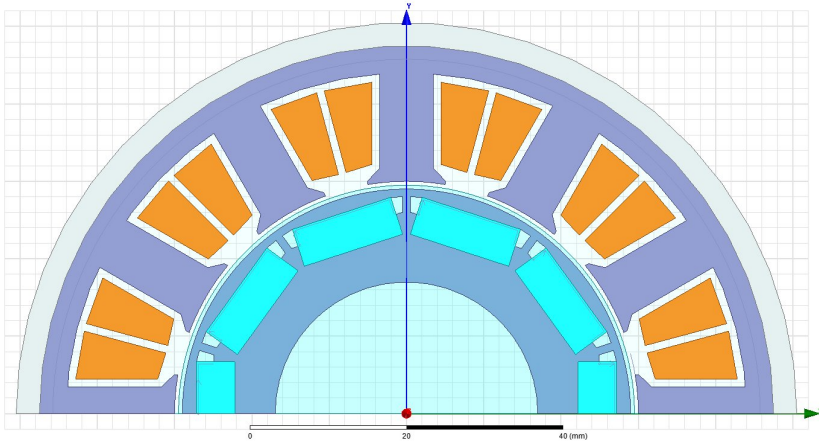


Figure 6.36: Buried Magnets

Manufacturing and assembly of the magnetic rotor with magnets is considered very simple. However, when mating the magnetic assembly to the shaft, an interference fit should be used to ensure concentricity. This may cause preload of the retention webs, leading to stress concentration in the corners.

Comparison

All three proposed topologies were qualitatively compared on simplicity, magnetic output, weight and anticipated manufacturing difficulty. The surface mounted magnet topology seems to yield best results across all categories, making it the natural choice.

	SMM	ISM	BM
Simplicity	+	-	0
Magnetic Output	+	+	-
Weight	+	-	0
Production	0	-	0

Table 6.9: Qualitative Rotor Comparison

6.7.4 Rotor Design

A magnetic rotor consists of a shaft, permanent magnets, a retention sleeve and mechanical balancing measures as shown in figure (6.37). Shaft ends are made to fit with the bearing system and motor boundary conditions, discussed in sections (6.4) and (6.6).

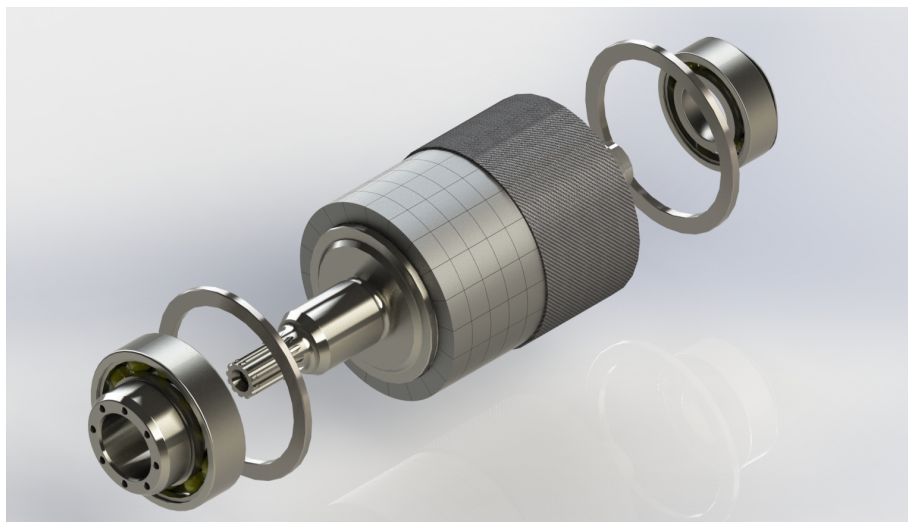


Figure 6.37: Rotor Assembly

Magnet Retention

The chosen rotor topology (section 6.7.3) requires some form of magnet retention. A sleeve will be mounted around the outer circumference of the magnets to keep them in place during high rotational speeds. As the sleeve will be exposed to strong alternating magnetic fields created by the stator, it is paramount that it is made of a non-magnetic material and inhibits a high electrical resistivity to keep eddy current losses low. Furthermore, as the sleeve is non-magnetic, its length adds to the air gap between the magnets and stator teeth. Because of this, it should be made out of a strong material that allows the sleeve to be

as thin as possible.

Stainless steel sleeves are typically used due to their non-magnetic behavior in combination with high resistivity and high strength. Another promising material for the retaining sleeve is carbon fiber reinforced plastic. It too is non-magnetic, but has an even higher strength and resistivity compared to stainless steel.

By curing the carbon fiber sleeve on to the rotor assembly after the magnets are attached, the sleeve will cure in the rotor's expanded state from thermal expansion. If the curing schedule is set higher than the operating temperature, thermal expansion during operation will not cause any loads on the sleeve.

Retention Sleeve Thickness

An analytical formula for the ring in the retention sleeve was derived by applying the following simplifying assumptions to the magnet retention case:

- All sleeve stresses are oriented along the fiber direction, i.e. circumferential. Carbon fiber is much stiffer in the fiber direction compared to other directions, so loads will travel there.
- No bending stresses are present in the sleeve. The sleeve is very thin, so its bending stiffness is negligible.
- All forces come from centrifugal retention of the magnets. The magnet mass is much larger than the sleeve mass.
- No ring stresses are present in the magnets. The magnetic poles are separated in the circumferential direction, so no loads will be carried from magnet to magnet.

- Circumferential angular width of each magnet is small. To reduce eddy current losses, the magnetic poles will be segmented in both the axial and circumferential direction (Equation: 3.10)

By considering a free-body diagram of one magnet segment with a retention sleeve of thickness t , with a centrifugal force added to the permanent magnet (Figure: 6.38), the stresses in the sleeve can be expressed by applying force equilibrium, yielding

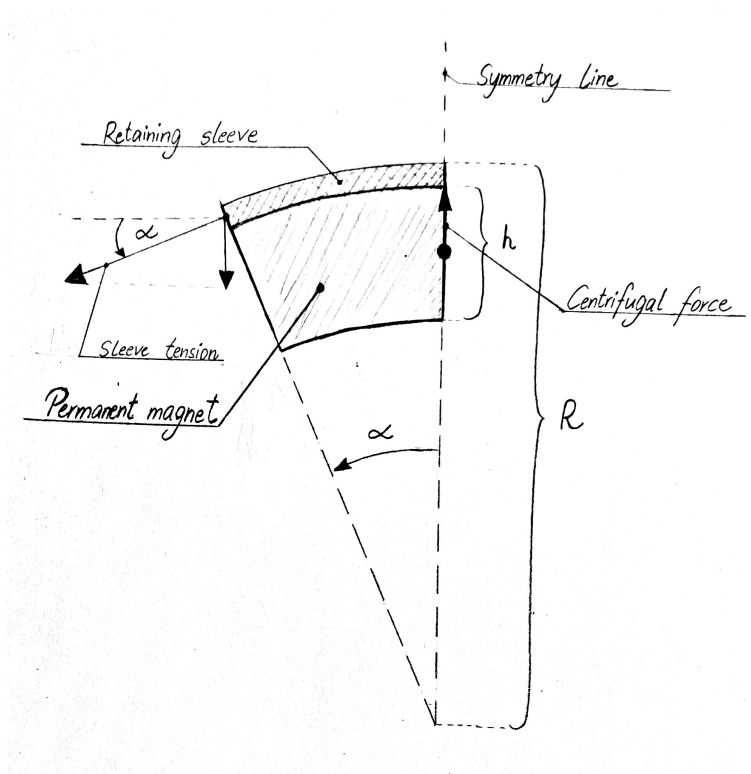


Figure 6.38: Free Body Diagram for One Magnet Segment

$$t \cdot \sigma = \frac{\rho}{2} \omega^2 \left(R - \frac{h}{2} \right) \left(Rh - \frac{h^2}{4} \right) \quad (6.2)$$

where t is the sleeve thickness, σ is the sleeve stress, ρ is the magnet mass

density, ω is the angular velocity, R is the rotor outer radius and h the magnet height. With a rotor diameter of 58mm, a magnet height of 6mm and sleeve stress of 150MPa, the required sleeve thickness is $\approx 0.5\text{mm}$ at maximum rotor speed of 20 000 rpm and NdFeB magnets (Figure: 6.39).

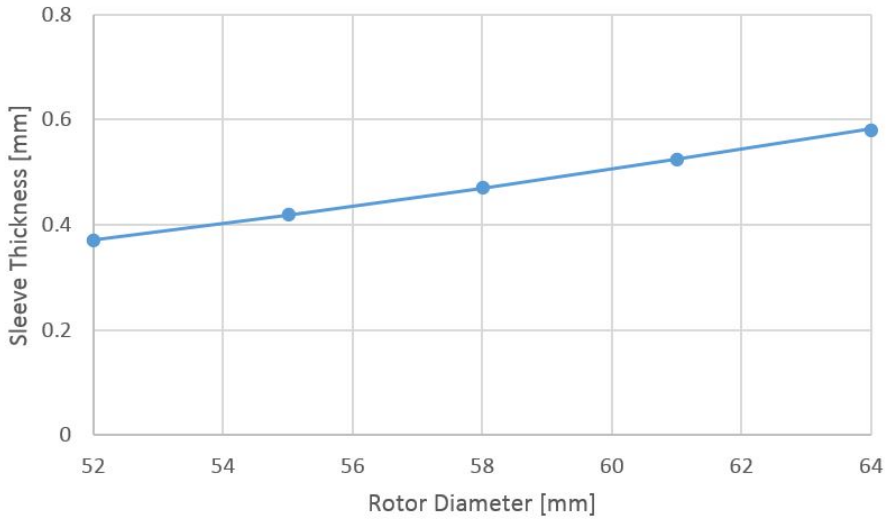


Figure 6.39: Required Sleeve Thickness for a 6mm Magnet Height

Balancing Measures

As the permanent magnets and retaining sleeve are glued on to the shaft, some unbalanced mass is expected. Balancing measures in the form of metal discs will be added to the rotor. Mass can be removed from these to balance the rotor assembly. In order to balance a rigid rotor statically and dynamically, two independent balancing discs must be added ([40], section 3.6.2). One disc will be added to either of the rotor sides. The discs will be assembled by an interference fit to ensure good concentricity.

Shaft

Electromagnetic analysis of the motor indicates that a non-magnetic material should be used for the shaft body to reduce eddy current losses in the rotor (Section: 7.1.4). On the other hand, the bearing seats should be made of similar steel as the raceways to ensure equal thermal expansion. If the thermal expansion of the shaft differs from the raceway, the bearing fit may get too tight or too loose depending on the temperature. Furthermore, the shaft should be hollowed out to save weight.

To satisfy all the above requirements, a three piece rotor is proposed. In order to improve run-out tolerances for the bearing seats, the three parts will be joined together using an interference fit. A shoulder is added for the shaft inserts for improved alignment during assembly.

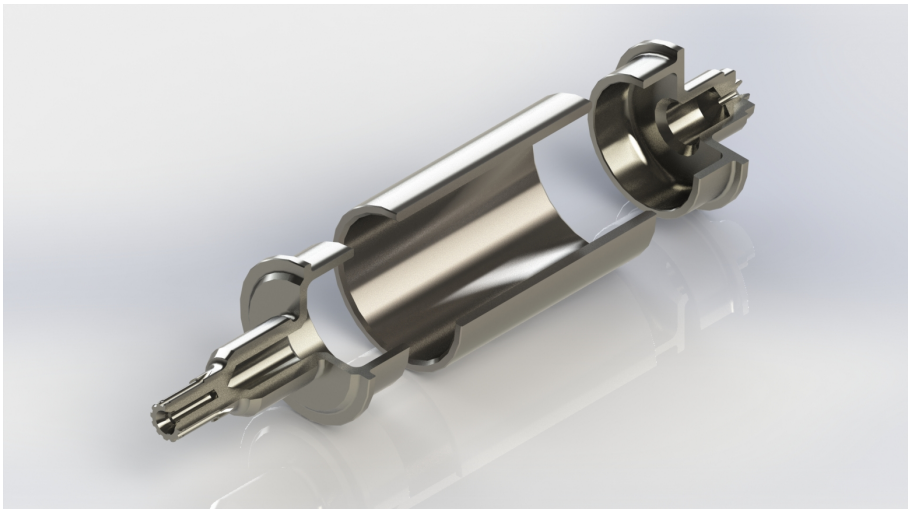


Figure 6.40: Shaft Assembly Cutout

6.7.5 Stator Core Design

It is of high importance to make sure the stator and rotor are concentrically aligned to keep a consistent air gap length. The permanent magnets are attracted to the stator teeth, with the attractive force increasing for decreasing air gap. If large variations in the air gap occur along the rotor's circumference, considerable cogging torque and motor vibration can be the result. The best way of ensuring proper concentricity between the stator core and motor housing is by the use of an interference fit.

Core Segmentation

The stator core can either be produced in one piece or several segments. A one piece design has the advantage of good tolerances on the outer diameter and no gaps within the stator core. However, winding coils within the stator slots is difficult due to poor accessibility. A segmented design will allow for winding of the stator coils individually, yielding a much better access. The performance of a motor is dependent on how high copper fill factor one can achieve in the stator slots, and better access typically yields a higher copper fill factor. A qualitative comparison is made between the two designs.

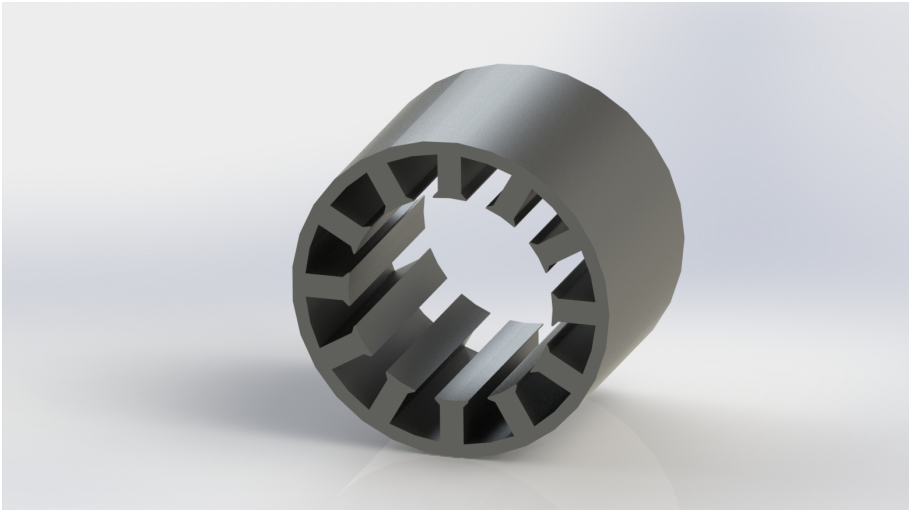


Figure 6.41: Single Piece Core

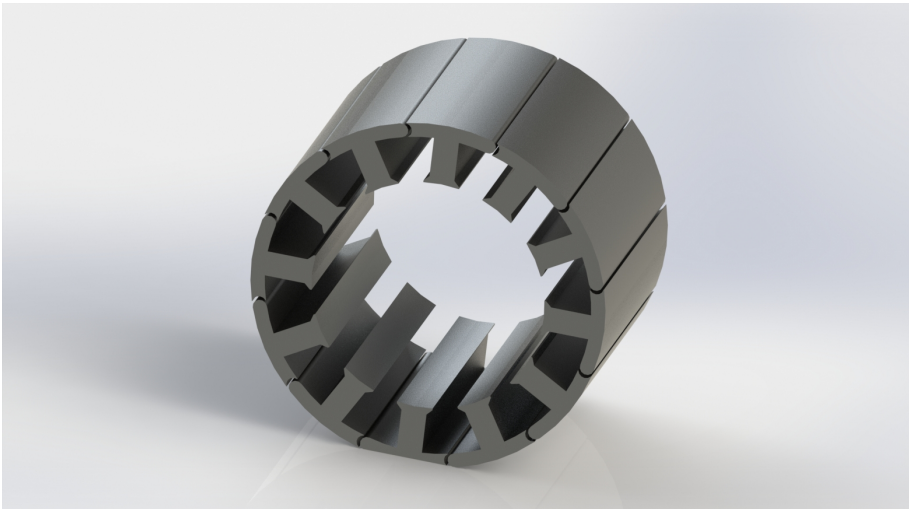


Figure 6.42: Segmented Core

	Single Piece	Segmented
Magnetic Performance	Best	Good
Copper Fill Factor	Decent	Best
Manufacture	Less Cutting	Less Material Waste
Winding Difficulty	Hard	Easy
Outer Diameter Tolerance	Good	Poor

Table 6.10: Stator Core Design Comparison

There are pros and cons with each design, but the cons of a segmented core can be handled by good engineering design. To minimize the gaps between the core segments, the core will be held together by a tight interference fit with the stator housing. This is also favorable with respect to heat transfer from the stator core to the housing. However, the stresses from the interference fit should be limited due to its detrimental effect on core magnetization and core losses. ([9], p. 282)

Core Manufacturing

In order to make the iron core, steel sheets have to be cut and laminated together. Two cutting methods are common for low volume prototypes ([41], section 4.4.1)

- Wire EDM: By laminating the core prior to cutting, the core can be cut in one go with common tolerances of $\pm 5\mu m$ (refer to site). The cutting procedure is done by electrical erosion of the workpiece, and cutting speeds are typically low.
- Laser Cutting: The thin steel sheets can be laser cut to precise tolerances using a CNC controlled machine. Laser cut parts will have an oxidized bur along the cutting edges, improving insulation between the sheets.

However, a laser cutter is limited by the depth of the workpiece, which forces cutting prior to lamination. To maintain good tolerances, a lamination fixture must be made to align the cut profiles during lamination.

	Laser Cutting	Wire EDM
Geometric Tolerances	Good with use of fixtures	Best
Labor Intensive	High with segmented core	Reference
Eddy Current Losses	Somewhat lower due to burs	Reference

Table 6.11: Stator Core Manufacturing

As a segmented core is chosen, Wire EDM is clearly the best choice. Good geometrical tolerances for each segment are needed to keep the accumulated tolerance of the stator core within reasonable limits. Furthermore, laminating the stack together prior to cutting reduces the stacking and lamination labor considerably, as there are 12 segments.

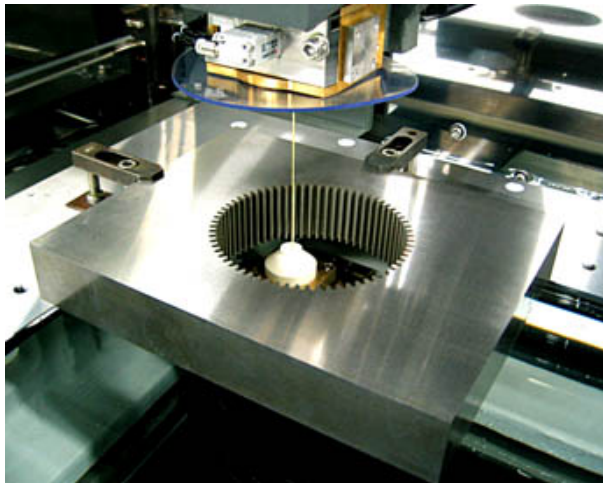


Figure 6.43: Wire EDM Machine [42]

Core Lamination

Three common ways of laminating plane steel sheets together is either using adhesives, welding or by applying fasteners.(ref blue book) Their pros and cons are discussed below:

- Adhesive bonding is very compact and helps insulate the steel sheets from each other. However, the laminated core is relatively weak.
- Welding beads along the axial length of the stack is commonly used in mass produced motors due to its high strength and relatively easy application. However, the welding beads will short circuit the sheets, causing excessive localized eddy current losses if placed in an area of high flux density variations.
- Fixing the lamination stack together using fasteners is also used in mass production due to its simplicity. Unlike welding, the fasteners can be made of a non-magnetic material, reducing eddy current losses. However, holes have to be machined into the core where long threaded rods will be inserted, removing the local flux carrying capacity.

Due to the compact design, there are no low flux density areas where either welding beads or fasteners can be placed. Bonding with adhesives remains shows to be the only viable option, and will be used for the prototype.

6.7.6 Integration

Creating a mock-up of the magnetic system in the CAD environment, compact integration was ensured by estimating the required length of the end turns.

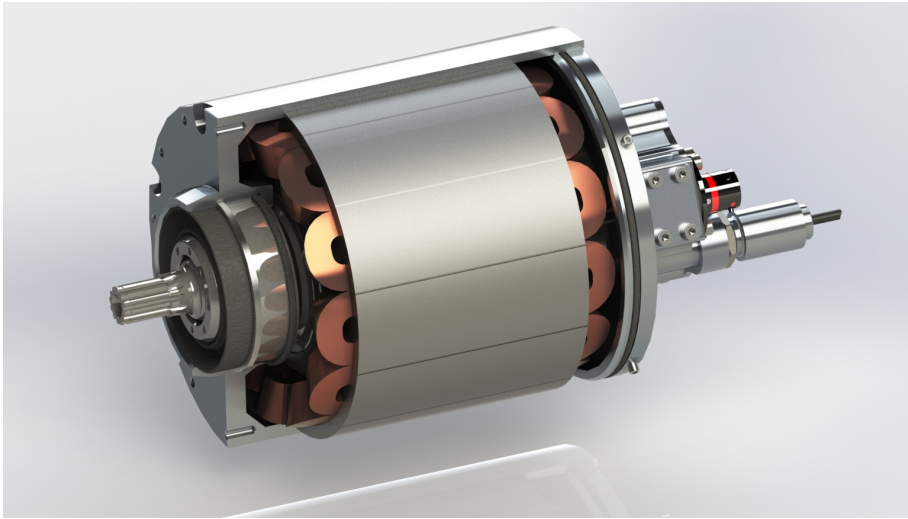


Figure 6.44: Magnetic System Integration

6.8 Material Selection

Now that all the components within the motor have been geometrically and functionally determined, a closer assessment on material selection for each component can be done. A list of common high performance materials are provided below, together with their characteristic properties. They are divided into two categories: ferromagnetic and non-magnetic.

Materials	AISI 1045 [43]	34CrNiMo6 (A.5)	42CrMo4 (A.6)
Density [g/cm^3]	7.85	7.85	7.85
Stiffness [GPa]	205	205	205
Tensile Strength [MPa]	700-850	1200-1400	1100-1300
Yield Strength [MPa]	500	1000	900
CTE [$\mu m/m \cdot K$]	12.1	12.1	12.1
Thermal Conductivity [$W/m \cdot K$]	-	33.7	45.1
Heat Treatability	May warp	Good	Good

Table 6.12: Ferromagnetic Engineering Materials, Quenched and Tempered

Materials	Ti6Al4V [44]	A7075-T6 (A.7)	SS 304 (A.8)
Density [g/cm^3]	4.42	2.83	8.03
Stiffness [GPa]	114	71.5	293
Tensile Strength [MPa]	897	590	621
Yield Strength [MPa]	828	550	290
CTE [$\mu m/m \cdot K$]	8.6	23	16.9
Thermal Conductivity [$W/m \cdot K$]	7.2	165	16.2
Resistivity [$\mu\Omega \cdot cm$]	170	2.82	72

Table 6.13: Non-Magnetic Engineering Materials

Stator Housing and End Bell

Due to its low weight, superior thermal conductivity, corrosion resistance and very good machinability, aluminium is used for the stator housing and end bell. The compromise is its very large value for CTE. This makes interference fits with steel parts loosen when the motor warms up to operational temperature, which mainly affects the bearing and stator core fits.

Thermal loosening of bearing fits are accommodated by placement of o-rings in the bearing seats. They serve as soft springs and apply enough pressure to keep the outer ring from creeping. This is a proven method recommended by SKF for electric motors with aluminium housings ([27], p. 42). O-ring hardness is recommended to be approximately 70° shore A.

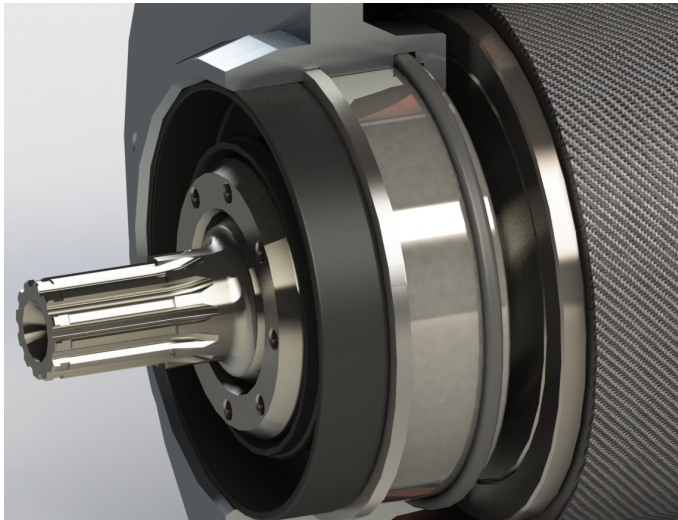


Figure 6.45: O-ring installed in bearing seat

The low stiffness and thickness of the aluminium housing signifies it will be very soft in a press fit, which means a large interference can be applied to accommodate for both thermal expansion and accumulated diameter deviation of the segmented stator core. Furthermore, since both the stator yoke and housing are thin compared to their diameter, modest stresses are expected from the fit.

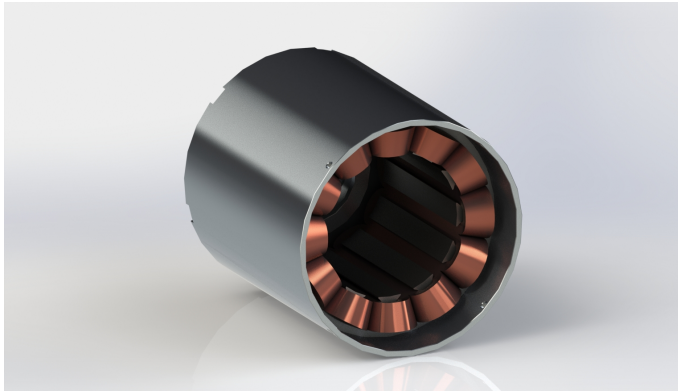


Figure 6.46: Interference Fit Between Core and Housing

Shaft Inserts and Bearing Sleeve

All parts influencing a bearing fit should have a coefficient of thermal expansion (CTE) similar to the raceway. This is to keep the interference fit consistent with temperature changes in the motor. Furthermore, the output shaft end should be heat treated to increase the fatigue strength of the spline connection. To ensure a good alignment of the spline connection, careful measures must be employed to reduce warping during heat treatment.

Both 42CrMo4 and 34CrNiMo6 are suitable materials for these parts due to their CTE and hardenability. 42CrMo4 is chosen over 34CrNiMo6 due to its higher thermal conductivity, which helps transferring heat out of the rotor. The rotor is not considered to be a highly strained part, so the lower mechanical strength of 42CrMo4 is irrelevant.

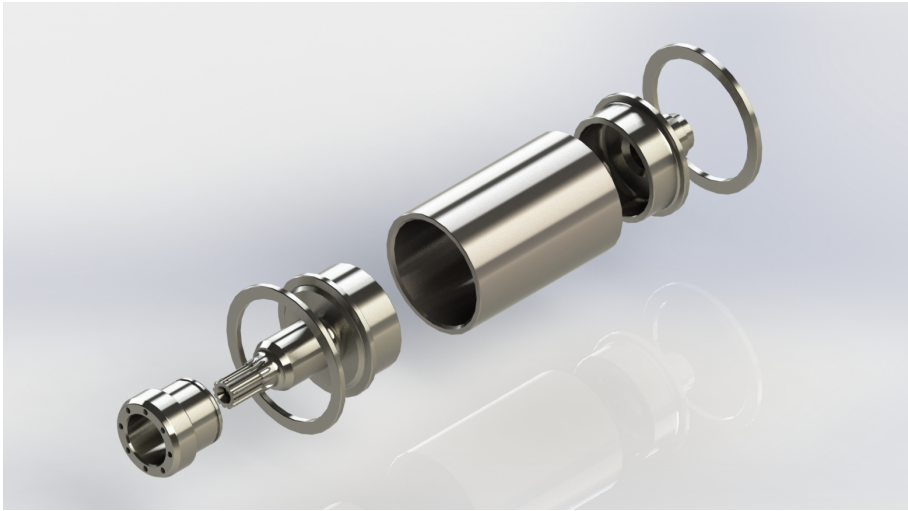


Figure 6.47: Material Selection for Rotor Components

Rotor Sleeve

Magnetic analysis of the motor (Section: 7.1.4) suggests a non-magnetic material with high resistivity should be used on the rotor sleeve to prevent high eddy current losses. The mechanical integrity of the rotor is dependent on the interference fits between the central sleeve and the two shaft inserts. By using a material with lower CTE than the shaft inserts, this fit will tighten when the temperature increases, providing an inherent safety of the joint. Ti6Al4V (Grade 5 titanium) offers a good compromise between desirable CTE, low weight, high resistivity and non-magnetic properties, and is chosen for the rotor sleeve.

Balancing Discs

The discs used for balancing the rotor assembly are in close proximity to the air gap. To keep eddy current losses under control, they must be made up of a non-magnetic material with high resistivity. Furthermore, due to their compact design, a dense material is desired as more mass can be removed in order

to balance the assembly.

SS304 (Stainless Steel) has a good mix between resistivity and density of the considered non-magnetic materials. Thermal conductivity is also good compared to titanium, facilitating heat transfer from the rotor magnets. However, careful considerations has to be done regarding its thermal expansion, as the fit will loosen from the shaft when the motor heats up. Titanium could also function as a good candidate here.

6.9 Interference Fits

Several joining methods within the motor are based on interference fits between a shaft and boring. To make sure the assembly stays together as planned, each fit is assessed, ensuring it fulfils functional and material requirements.

6.9.1 Analytical Formula

Due to the circular symmetry of the loads and geometry in an interference fit, the problem can be simplified to a plane stress/plane strain case. By also assuming a linear material, an analytical solution for the stresses and deformation within the part can be found. ([40], appendix C.1)

$$\sigma_r(r) = -p_i \frac{r_i^2}{r_y^2 - r_i^2} \left(\frac{r_y^2}{r^2} - 1 \right) - p_y \frac{r_y^2}{r_y^2 - r_i^2} \left(1 - \frac{r_i^2}{r^2} \right), \quad (6.3)$$

$$\sigma_\phi(r) = p_i \frac{r_i^2}{r_y^2 - r_i^2} \left(\frac{r_y^2}{r^2} + 1 \right) - p_y \frac{r_y^2}{r_y^2 - r_i^2} \left(1 + \frac{r_i^2}{r^2} \right), \quad (6.4)$$

$$u(r) = \frac{p_i}{E} \frac{r_i^2}{r_y^2 - r_i^2} r \left[1 - \nu + (1 + \nu) \frac{r_y^2}{r^2} \right] - \frac{p_y}{E} \frac{r_y^2}{r_y^2 - r_i^2} r \left[1 - \nu + (1 + \nu) \frac{r_i^2}{r^2} \right] \quad (6.5)$$

where σ_r and σ_ϕ are the in-plane stresses in the radial and circumferential

direction, respectively. u is the radial deformation, E the Young's modulus and ν the Poisson's ratio. r_i and r_y are the inner and outer radius of the geometry, and p_i, p_y the inner and outer pressures on the component, respectively.

By acknowledging that the pressures, p , must be continuous across components in an interference fit, the above formula can be used to determine the contact pressure between two components and the resulting stresses, given the amount of geometrical interference. Due to the linearity of the solution, several solutions can be superimposed to yield answers for concentric fits between three components, e.g. the bearing sleeve.

This 2D approximation typically yields good values for the actual mean contact pressure between two fitted components. The end effects in 3D problems typically introduce an extra stress concentration, but affect the joining function to a small degree ([40], p. 127).

6.9.2 Tolerances and Fits

Interference fits are made by machining the diameter of a shaft slightly larger than the bore of a hub, typically in the order of $10\mu m$. However, due to the accuracy limitation of production processes, all parts will come with an uncertainty in their geometrical dimensions. The degree of uncertainty is categorized into tolerance grades in ISO 286, denoted IT (International Tolerance) and numbered from 1 to 18. A larger number denotes a wider tolerance. Typical tolerances in modern machining centres are IT5 to IT7, depending on the material and geometry of the part.

When joining two parts, the diametrical interference between them is dependent on the tolerances of each component. If the shaft and hub have the same

nominal diameter d_{nom} , but upper and lower tolerance limits of es and ei for the shaft and ES and EI for the hub, the diametrical interference δ lies between

$$\delta_{min} = ei - ES \quad (6.6)$$

$$\delta_{max} = es - EI \quad (6.7)$$

However, as the resulting fit of a component is typically normally distributed around the mean value of the tolerance zone, it is overly conservative to assume that both the shaft will hit its smallest allowable diameter and the hub its largest allowable diameter (or vice versa). Since both diameters can be treated as normally distributed independent stochastic variables, the diametrical interference will also be a normally distributed stochastic variable. Its mean value, probable deviation and limits are given by ([40], section 8.2.4)

$$\delta_m = \frac{1}{2} [(es + ei) - (ES + EI)] \quad (6.8)$$

$$\Delta\delta = \frac{1}{2} \sqrt{(es - ei)^2 + (ES - EI)^2} \quad (6.9)$$

$$\bar{\delta}_{min}^{max} = \delta_m \pm \Delta\delta \quad (6.10)$$

All machined surfaces have a surface roughness. When two components are fitted together, the tops and bottoms of the surface will fill each other, effectively loosening the fit. For machined surfaces, the effective probable interference is given by ([40], section 8.2.5)

$$\bar{\delta}_e = \bar{\delta} - 4(R_a^{shaft} + R_a^{hub}) \quad (6.11)$$

6.9.3 Interference Fit Calculator

Based on equations presented in section (6.9.1) and (6.9.2), an excel based calculator was made to assess all the fits in the motor assembly. It inputs nominal

diameter and tolerance range for the shaft and bore to calculate the probable diametrical interference. Together with geometry and material parameters, it outputs contact pressures, deformations and stresses. It can either calculate a single fit between two components or a double fit between three. The calculator outputs are validated against FE-simulations.

Tolerance Combination			Shaft			Shaft Stresses at Interference			
	Shaft	Hub	Material		Geometry				
Tolerance	34M7	34M7	E [GPa]	72	nID [mm]	47	Radial Stresses	-0.0736475 [MPa/um]	
Nominal ϕ [mm]		81	nu [-]	0.35	nOD [mm]	81	Ring Stresses	-0.1484119 [MPa/um]	
High Limit [um]		48				Ring Factor	2.0151654 [-]	Von Mises Stress	0.1285297 [MPa/um]
Low Limit [um]		13							
Surface Roughness (Ra)		0.8							
Probable Interference	48	24.74873734							
Probable Interference Values			Hub			Hub Stresses at Interference			
Max Interference		83 [um]	Material		Geometry				
Probable Max Interference		72.74873734 [um]	E [GPa]	72	nID [mm]	81	Radial Stresses	-0.0736475 [MPa/um]	
Probable Max Eff. Interference		66.34873734 [um]	nu [-]	0.35	nOD [mm]	89.5	Ring Stresses	0.740477 [MPa/um]	
Min Interference		13 [um]				Ring Factor	-10.054338 [-]	Von Mises Stress	0.7799131 [MPa/um]
Probable Min Interference		23.25126266 [um]							
Probable Min Eff. Interference		16.85126266 [um]							
			Influence Coefficients & Fit Stiffness			Interference due to temperature difference			
			alpha_sy	1.8733111 [um/MPa]		CTE Difference			23 [um/m°C]
			alpha_hi	11.704881 [um/MPa]		delta T			5
			alpha	13.578192 [um/MPa]		delta Interf.			9.315 [um]
			Contact Pressure						
			0.0736475 [MPa/um]						
			Ring Compliances						
			alpha_si	-1.968233 [um/MPa]					
			alpha_hy	11.255046 [um/MPa]					

Figure 6.48: Calculator Input Parameters and Analytical Relations

	Analytical Solution						
	Max	Prob. Max	Prob. Eff. Max	Average Fit	Prob. Min	Prob. Eff. Mir Min	Min
Interference [um]	83.00	72.75	66.35	48.00	23.25	16.85	13.00
Contact Pressure [MPa]	6.11	5.36	4.89	3.54	1.71	1.24	0.96
Shaft Von Mises [MPa]	10.67	9.35	8.53	6.17	2.99	2.17	1.67
Hub Von Mises [MPa]	64.73	56.74	51.75	37.44	18.13	13.14	10.14
Shaft Inner Diameter [um]	-12.03	-10.55	-9.62	-6.96	-3.37	-2.44	-1.88
Hub Outer Diameter [um]	68.80	60.30	55.00	39.79	19.27	13.97	10.78

Figure 6.49: Various Outputs for Single Fits

Superposition Interference Matrix: Contact Pressure at Primary Interference [MPa]							
Primary IF	Max	Prob. Max	Prob. Eff. Max	Average Fit	Prob. Min	Prob. Eff. Min	Min
Secondary IF [um]	24.0	20.9	17.7	13.0	5.1	1.9	2.0
Max	81.0	72.7	64.2	51.7	30.7	22.2	22.4
Prob. Max	77.8	69.6	61.1	48.5	27.5	19.0	19.3
Prob. Eff. Max	75.8	67.5	59.0	46.5	25.5	16.9	17.2
Average Fit	70.1	61.9	53.4	40.9	19.8	11.3	11.6
Prob. Min	62.4	54.2	45.7	33.2	12.2	3.6	3.9
Prob. Eff. Min	60.4	52.2	43.6	31.1	10.1	3.6	3.8
Min	59.3	51.0	42.5	30.0	9.7	3.6	3.8

Figure 6.50: Contact Pressure Matrix for Double Fits

6.9.4 Bearing Fits

Bearing fits are typically more critical than other structural fits. The fits are supposed to keep the raceway from creeping in its seat during operation, but not cause unnecessary preload on the rolling elements (Figure: 6.20). SKF has listed recommended fits for various applications ([27], p. 68 - 69). However, these fits are only valid for solid steel shafts and steel housings, while the motor shaft is hollow and housing is made of aluminium. Because of this difference, a good way of using the SKF values is to match the reduction of internal clearance. A bearing seat roughness of $R_a = 0.4$ is recommended for an IT5 tolerance fit, and is used in the calculations. ([28], p. 204)

SKF 6005 and Bearing Sleeve

The recommended fits for the SKF6005 bearing are k5 and K7 for shaft and housing, respectively. Using the interference fit calculator, the following values were obtained

	Shaft	k5	Hub	K7
	Max $\bar{\delta}_e$	Min $\bar{\delta}_e$	Max $\bar{\delta}_e$	Min $\bar{\delta}_e$
Interference [μm]	16.43	2.97	11.86	0
Contact Pressure [MPa]	23.26	4.21	5.68	0
Internal Clearance Reduction [μm]	13.20	2.39	9.56	0

Table 6.14: Recommended SKF 6005 Fits

By adding together the maximum internal clearances for shaft and hub, the total reduction in internal clearance is between 2.4 and 22.8 micrometers for the recommended fits.

There are two requirements of the double fit with the bearing and bearing sleeve. They can be listed as

- The reduction of internal clearance in the bearing should coincide within the recommended SKF interval.
- There must be an interference fit between the shaft and bearing sleeve, but the total friction force between the two components must be less than 35kN to facilitate disassembly.

By using a n5/H6 tolerance combination on the shaft-bearing sleeve fit, and a j5 fit against the bearing raceway, the following contact pressure matrix for the bearing was calculated

Superposition Interference Matrix: Contact Pressure at Secondary Interference [MPa]									
Secondary IF	Primary IF	Max	Prob. Max	Prob. Eff. Max	Average Fit	Prob. Min	Prob. Eff. Min	Min	
	[μm]	24.0	20.9	17.7	13.0	5.1	1.9	2.0	
Max	15.0	40.7	38.0	35.3	31.2	24.3	21.5	21.6	
Prob. Max	12.2	37.0	34.4	31.6	27.5	20.6	17.9	18.0	
Prob. Eff. Max	10.4	34.7	32.0	29.2	25.1	18.3	15.5	15.6	
Average Fit	5.5	28.1	25.4	22.7	18.6	11.7	8.9	9.0	
Prob. Min	-1.2	19.2	16.5	13.7	9.7	2.8	0.0	0.1	
Prob. Eff. Min	-3.0	16.8	14.1	11.3	7.3	0.4	0.0	0.0	
Min	-4.0	15.5	12.8	10.1	6.0	0.0	0.0	0.0	

Figure 6.51: Bearing-Sleeve Contact Pressure Matrix

A conservative contact pressure interval on the inner bearing raceway lies within ≈ 0 to 29.2 MPa. 29.2 MPa corresponds to a 16.6 μm reduction of internal clearance. To accommodate the possibility of near-zero contact pressure, a bearing locking compound will be added during assembly.

As the thermal expansion of the aluminium housing makes it impossible to retain a soft interference fit with the outer raceway over the operating temperature range of the motor, there is no point in having it for low temperatures either. A H6 tolerance is set for the bearing seat in the housing, and a bearing

locking compound will be used instead. This means there will be no further reduction in internal clearance from the outer raceway.

Superposition Interference Matrix: Contact Pressure at Primary Interference [MPa]								
	Primary IF	Max	Prob. Max	Prob. Eff. Max	Average Fit	Prob. Min	Prob. Eff. Min	Min
Secondary IF	[um]	24.0	20.9	17.7	13.0	5.1	1.9	2.0
Max	15.0	81.0	72.7	64.2	51.7	30.7	22.2	22.4
Prob. Max	12.2	77.8	69.6	61.1	48.5	27.5	19.0	19.3
Prob. Eff. Max	10.4	75.8	67.5	59.0	46.5	25.5	16.9	17.2
Average Fit	5.5	70.1	61.9	53.4	40.9	19.8	11.3	11.6
Prob. Min	-1.2	62.4	54.2	45.7	33.2	12.2	3.6	3.9
Prob. Eff. Min	-3.0	60.4	52.2	43.6	31.1	10.1	3.6	3.8
Min	-4.0	59.3	51.0	42.5	30.0	9.7	3.6	3.8

Figure 6.52: Shaft-Sleeve Contact Pressure Matrix

The contact pressure on the bearing sleeve will lie between 3.6 and 59.0 MPa along 12mm of its axial length (Figure: 6.52), due to the bearing fit. Assuming a friction coefficient of 0.5, the maximum total static friction force of the bearing section is 21kN. By doing the same calculation for the fit and friction under the sealing lip section, which has an axial length of 7.5mm, a maximum friction force of 10kN is found. Adding these together yields a conservative friction capacity of 31kN, which satisfies the 35kN requirement.

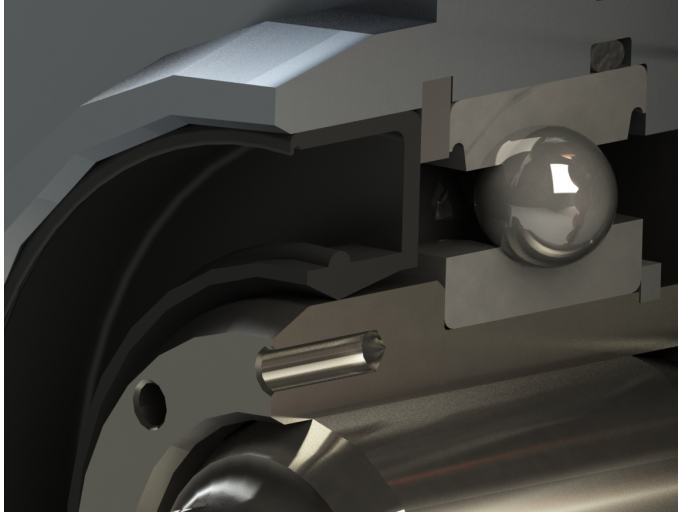


Figure 6.53: The bearing sleeve has different pressure sections

SKF 6003

SKF recommends j5 and K7 fits for shaft and housing, respectively. Again, using the interference fit calculator, the following values were obtained

	Shaft	j5	Hub	K7
	Max $\bar{\delta}_e$	Min $\bar{\delta}_e$	Max $\bar{\delta}_e$	Min $\bar{\delta}_e$
Interference [μm]	8.86	0	11.86	0
Contact Pressure [MPa]	22.46	0	9.44	0
Internal Clearance Reduction [μm]	6.86	0	9.54	0

Table 6.15: Recommended SKF 6003 Fits

By employing a k5 tolerance to the shaft and a H6 tolerance to the housing, the contact pressure range and internal clearance reduction lie within the interval from the recommended fits.

6.9.5 Stator Core Fit

The stator core consists of 12 segments, with surface tolerances set to $\pm 5\mu\text{m}$ for the radial mating surface and $\pm 10\mu\text{m}$ for the circumferential mating surfaces.

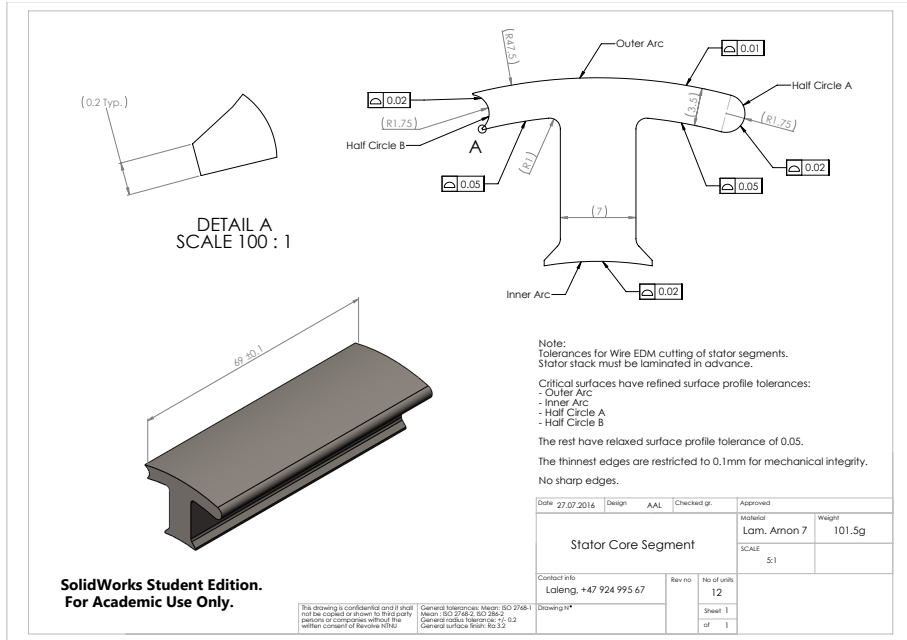


Figure 6.54: Technical Drawing of Stator Segment

Deviations on the segment's sides will add and subtract from their circumference, while the outer arc will add and subtract from the outer diameter. By assuming the tolerances on each side of a segment are normally distributed equally and independent of each other, the probable circular and radial deviation of the whole stator core assembly can be calculated adding the normally distributed stochastic variables as in equation (6.9)

$$\Delta\delta = \frac{1}{2}\sqrt{n \cdot (es - ei)^2} \tag{6.12}$$

where n is the number of independent variables added, $\Delta\delta$ is the probable deviation, e_s and e_i are the maximum and minimum allowable dimensions. Using equation (6.12), the following deviations are computed

	Tolerance	n	$\Delta\delta$	$\Delta\delta_D$
Radial	$\pm 5\mu m$	12	$\pm 17.32[\mu m]$	$\pm 34.64[\mu m]$
Circumferential	$\pm 10\mu m$	24	$\pm 48.99[\mu m]$	$\pm 15.59[\mu m]$
Total Radial	-	-	-	$\pm 37.98[\mu m]$

Table 6.16: Stator Core Tolerances

By recognizing that circumferential length is related to diameter as $C = \pi D$, and radius to diameter by $R = D/2$, the contribution to diametrical deviation is calculated. The total radial deviation is then found by summing the two contributions, using equation (6.12).

A housing bore range of $(95 - 0.200, 95 - 0.222)mm$, which corresponds to an IT6 tolerance grade is proposed. Inserting an equivalent stator core stiffness of 184 MPa, taking account for a 92% stacking factor, and a stator yoke thickness of 3.5mm yields

	Max $\bar{\delta}_e$	Min $\bar{\delta}_e$
Interference $[\mu m]$	247.35	168.25
Contact Pressure [MPa]	7.55	5.14
Core Von Mises [MPa]	95.33	64.84
Housing Von Mises [MPa]	151.3	102.92

Table 6.17: Stator Core Fit

The difference in CTE between the steel and aluminium is $11\mu m/m \cdot K$ yields an interference relief of $125.4\mu m$ if the stator heats up from $20^\circ C$ to

140°C (ref to max stator temp). Furthermore, assuming a surface roughness of $R_a = 0.8$ on the stator segments adds an additional relief of $7.7\mu m$ on the diameter. Subtracting these contributions from the minimum interference yields a reserve fit of $35.15\mu m$. Due to the large surface area between the core and housing, only $2.7\mu m$ is needed to transfer 40 Nm torque, assuming a friction coefficient of 0.5. The proposed fit is acceptable.

6.9.6 Structural Fits

The remaining fits are simple, structural fits between two components, and are less sensitive to preload. A brief discussion and results will be given here. All fits were validated using the interference fit calculator.

Shaft Inserts

Shaft inserts are fitted into the shaft sleeve in order to carry loads and transfer torque to the output spline. A 40N7/n7 fit is chosen to give the shaft a minimum torque carrying capacity of 72Nm, which yields a safety factor of 2.3 to the maximum desired output torque of 31Nm.

Balancing Discs

The balancing discs are made of stainless steel, which has a CTE difference of $4.8\mu m/m\cdot K$ to the shaft steel. This yields an interference relief of $28.7\mu m$ when the rotor heats up from 20°C to 150°C (Table: 6.4 for N35EH). Centrifugal forces cause an additional relief of $6\mu m$ at 20 000 RPM, calculated using an analytical formula for thin discs ([40], appendix C.2). By choosing a 46P6/n7 fit, the probable minimum interference is $37.26\mu m$, which leaves a reserve of $2.56\mu m$.

Chapter 7

Simulation

7.1 Magnetic Analysis

In order to validate and optimize the initial magnetic design, a magnetic finite element analysis tool is used to solve for the actual fields within the motor. This thesis uses ANSYS Maxwell for all magnetic simulations, which employs second order tetrahedral elements to estimate the magnetic field distribution within the motor.

7.1.1 Analysis Types

There are three common analysis types used for electric motors. Most commonly 2D simulations are used because the torque producing section of the motor is plane in geometry and the magnetic field lies within the same plane, yielding a good approximation of the 3D performance. 3D simulations are less common due to their long solving times.

- **2D Magneto-static**

A magneto-static analysis solves the field distribution within the motor

for a particular moment in time. Both torque and demagnetization flux can be obtained from this analysis. As only one time step needs to be solved, it is very quick to solve, and the mesh can be refined to improve accuracy. However, due to its static nature, time dependent effects, i.e. core and eddy current losses, are not taken into account.

- **2D Transient**

A 2D transient solver takes time dependent effects into account by solving for the magnetic field at different rotor positions. The mesh is divided into two domains, the stator and rotor, which are allowed to glide relatively to each other. This solver can output torque and demagnetization fluxes at each rotor position, as well as modelled core losses from empirical data. Due to the three-dimensional nature of eddy currents, a 2D simulation will not yield a good approximation. However, it can give an indication of where eddy current losses will be present by showing the change of magnetic flux at each point within the motor. A magneto-static analysis is essentially solved at each time step, so the relative solving time is proportional to the number of time steps.

- **3D Transient**

To capture the three-dimensional nature of eddy currents, a 3D Transient simulation must be run. In an electric motor, this is typically done to assess the eddy current losses within the permanent magnets. However, as mentioned earlier, the solving times for 3D transient simulations are very long.

Model Considerations

The analysis types are listed in order of increasing fidelity. A higher fidelity model will have longer solving times, and in this case yield more model inputs

and outputs. Due to the very long solving times of three-dimensional analysis, it is not considered to be suitable for practical design and will not be used in this thesis. Eddy current considerations in magnets will be based on rules of thumb instead.

To facilitate practical optimization, the number of input and output parameters should be kept as low as possible. A transient analysis introduces an additional model input and output parameter compared to magneto-static: frequency and core loss, respectively. As discussed in section (3.5.4), core loss estimations are inherently inaccurate, and are therefore not suited as an optimization parameter. Because of this, transient analysis will only be used for initial assessment and validation of a magnetic design.

The magneto-static analysis eliminates frequency dependent effects, outputs torque and demagnetization, and is fast to solve. It can take ohmic DC losses into account, which means the motor constant K_m (Equation: 3.33) can be estimated. This makes the magneto-static solver ideal for practical optimization.

7.1.2 Approach

Due to the relatively simple geometry of an electric motor, a parametric model will be created in order to investigate the effect of geometry on motor performance. Before any simulation is done, a mesh study will be conducted to ensure the model mesh is sufficiently fine to yield good results, but not finer than necessary.

Based on typical parameters, the initial magnetic design will be validated through a 2D transient analysis. General considerations regarding torque production and eddy current losses will be drawn from these results. Using the 2D

transient analysis, a 2D magneto-static simulation will be validated on torque and demagnetization outputs.

The 2D magneto-static analysis will be used for optimization, before the optimised design is compared against the initial for validation. Finally, considerations regarding number of turns and magnet segmentation will be done.

7.1.3 Finite Element Model

A parametric motor geometry was made. Using model symmetries, the rotor and stator can be cut in half. The geometric input parameters are listed below.

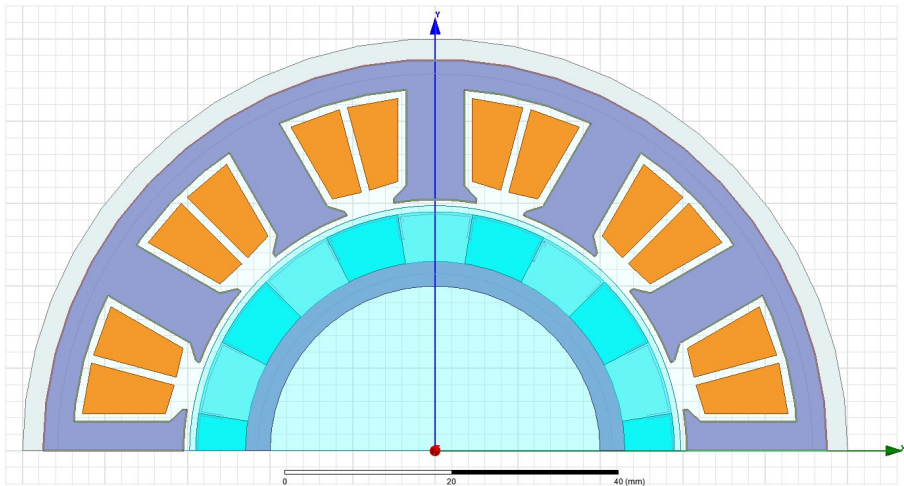


Figure 7.1: Parametric Model

- Quadrature current density: J_{rms} [A_{rms}/mm^2]
- Stator Yoke Thickness: $t_{StatorYoke}$ [mm]
- Rotor Yoke Thickness: $t_{RotorYoke}$ [mm]
- Rotor Outer Diameter: $RotorOD$ [mm]

- Fraction of radially magnetized magnets: $wMagnet$ [-]
- Radial Magnet Height: $hMagnet$ [mm]
- Air Gap Length: $AirGap$ [mm]

The stator tooth width was fixed to twice the yoke thickness to simplify the design. This is done because two yoke segments are connected to each tooth. If the magnetic flux density is assumed to be constant in the tooth and yokes, a tooth will carry twice the flux of the yoke, and needs twice the area.

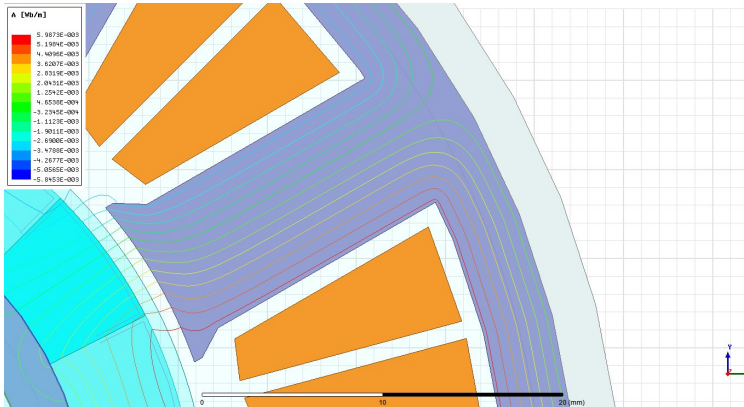


Figure 7.2: Simulation showing tooth field lines split at yoke intersection.

To output the demagnetization flux within each magnet, flux probes are placed along their outer circumference. They probe the magnetic field in the magnetization direction.

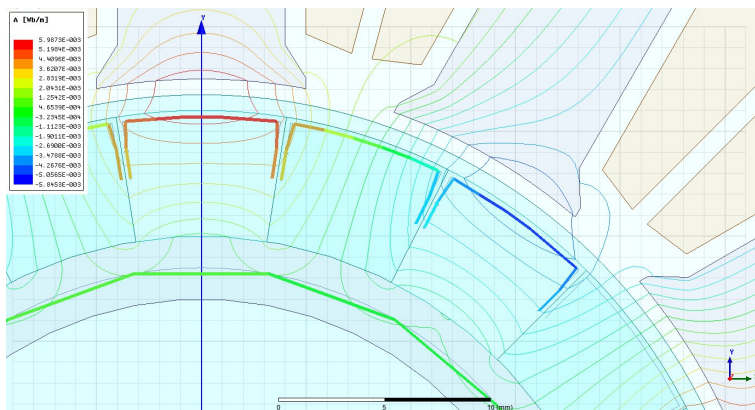


Figure 7.3: Thick lines are directional magnetic field probes

From the parametric inputs, the model calculates slot area and copper volume. The length of end turns is accounted for in the copper volume. Copper loss can then be calculated from equation (3.27), and the coil ampere-turns are calculated from equation (3.32). The excitation current is purely in the quadrature direction, i.e. phase shifted 180 degrees to the back EMF, which maximizes mutual torque produced by the motor (Section: 3.5.3).

Initial Design Parameters

Initial design parameters were based upon general guidelines ([9], section 12.2), backed up by equations from section (3.5).

- The air gap length was set to 1.5 mm to accommodate a 0.5 mm carbon fiber sleeve. Since the magnet height should be significantly larger than the air gap, a radial length of 6 mm is chosen. Fraction of radially magnetized magnets is set to 0.5 as an initial value.
- Copper fill factor K_{wb} is set to 0.6, based on guideline values ([9], p. 314), and the copper temperature is set to 100°C , which corresponds to a resistivity of $2.27 \cdot 10^{-8} \Omega \cdot \text{m}$ (Equation: 3.28).

- The magnetic residual induction is set to $B_r = 1.23T$, and its permeability $\mu = 1.1 \mu_0$ from the data sheet. Note that these values are performance measures at $20^\circ C$.
- Stator yoke thickness is set to 4 mm as it creates a resulting stator flux density of 1.4 T from the permanent magnets alone. This matches the saturation flux for the SiFe in the core.
- Stator outer diameter and stack length are determined on the available space within the motor, and set to 95 mm and 69 mm, respectively.
- Initial rotor outer diameter is based on results from the ideal motor considered in section x. The motor constant peaks at a radius ratio around 0.55, which corresponds to a rotor radius of 52 mm.
- For the particular design, the rotor yoke and shaft are the same component. Due to manufacturing constraints, it has a set thickness of 3 mm.

Mesh Study

A Maxwell magneto-static solver has an automatic mesh refiner, that is based upon calculated energy error of the field at each point in the domain. The user input is the allowable percentage of energy error in the results. A mesh refinement study was done on output torque and by both using the automatic refiner as well as local mesh controls. The shown results are for a current excitation of $J_{rms} = 20 [A_{rms}/mm^2]$.

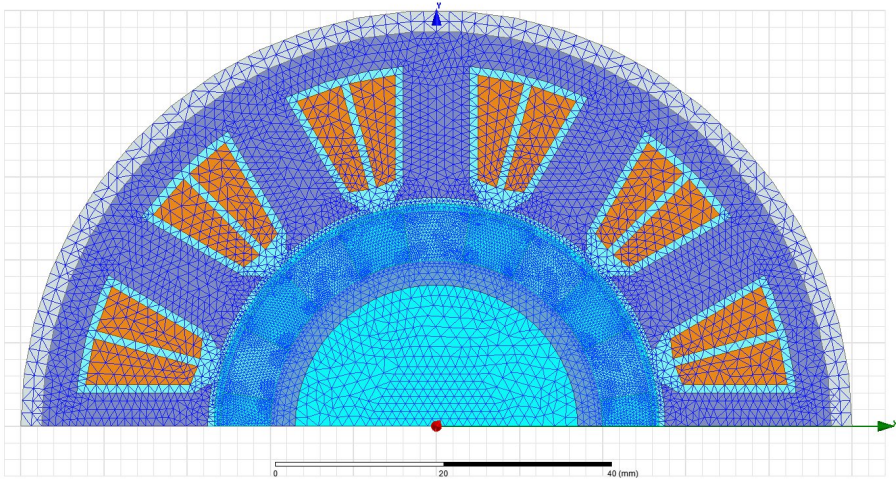


Figure 7.4: Visualization of the FE-mesh

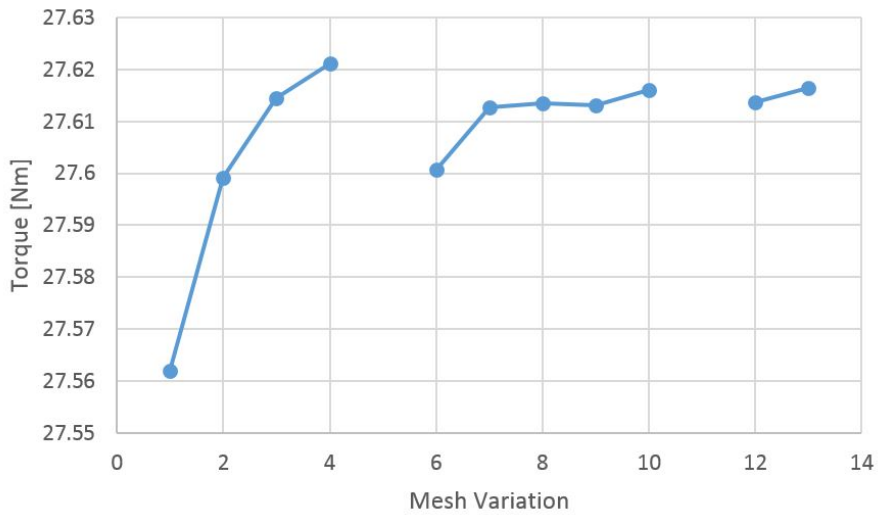


Figure 7.5: Torque vs Mesh Variation

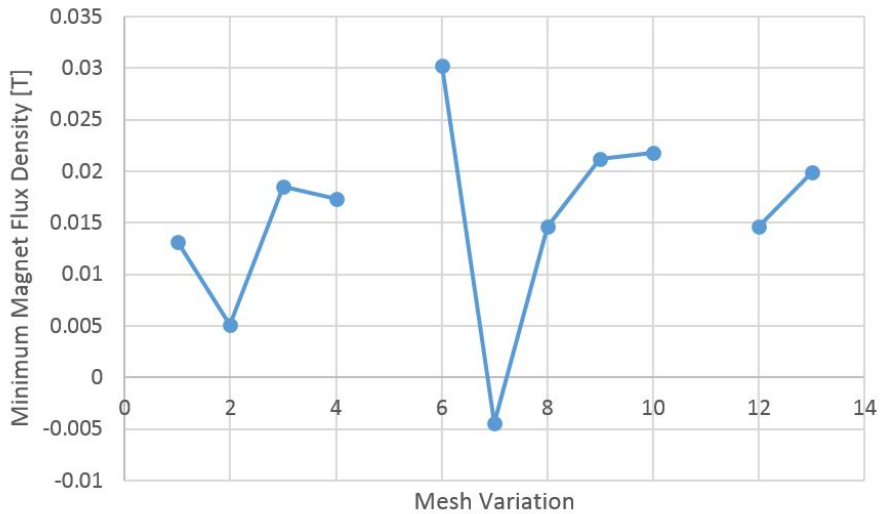


Figure 7.6: Minimum Directional Magnet Flux vs Mesh Variation

Mesh variations 1 to 4 are only based on the automatic mesh refiner. Variations 6 to 10 are based on a combination of local controls and automatic refiner, while 12 and 13 are purely on local mesh controls. The meshes in each variation group are refined towards higher numbers. As only local mesh controls may be employed in transient simulations, mesh variation 12 is used for further analysis.

7.1.4 Initial Design Analysis

To validate the initial design, a 2D transient simulation was run at a rotor speed of 12 500 RPM. The results are shown below.

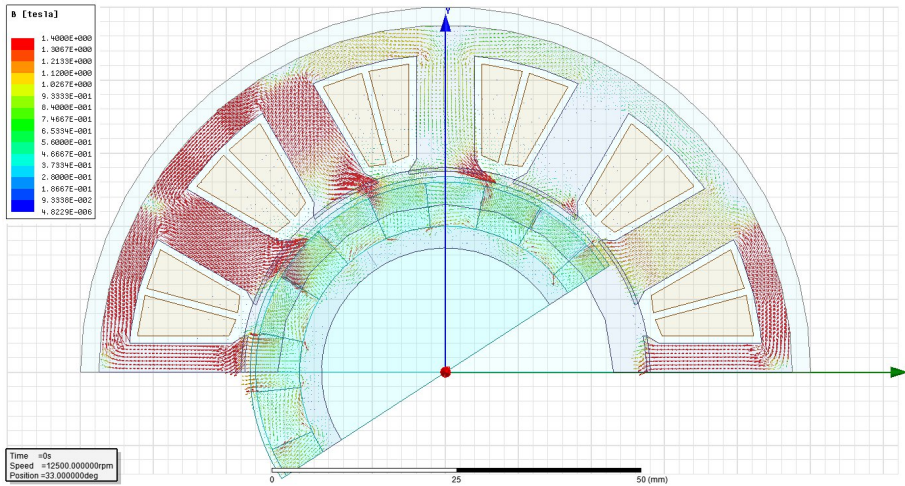


Figure 7.7: Magnetic Field Distribution

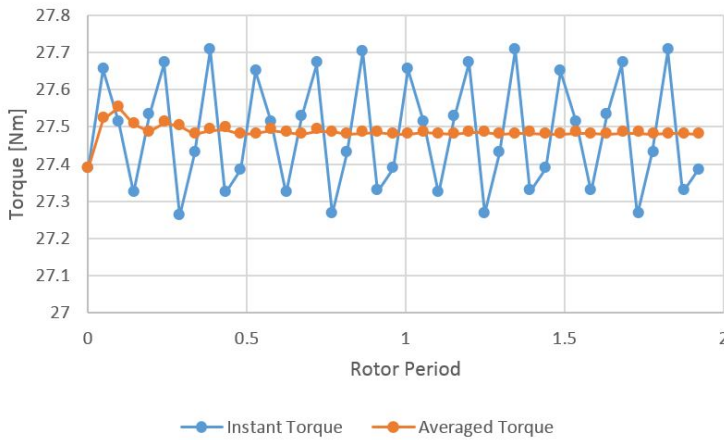


Figure 7.8: Motor Output Torque

The mean torque output seems reasonable, and corresponds well with the predicted torque from the mesh study. Variations occurring are due to the slotting of the stator core, yielding cogging torque contributions at the sixth harmonic of the electrical frequency, as predicted in table (6.7). However, this torque ripple is only 1.4 % of the mutual torque.

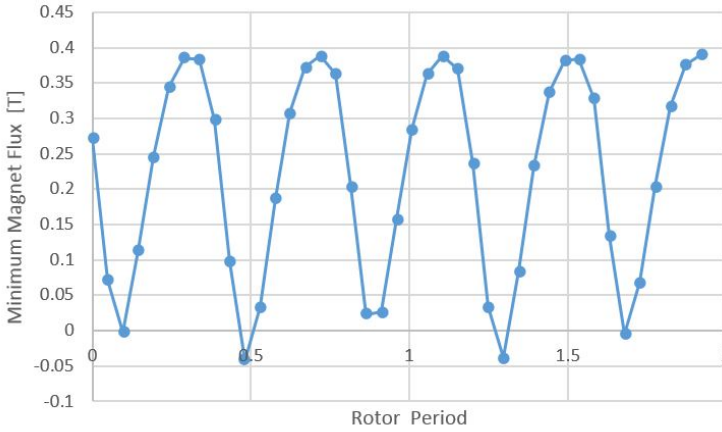


Figure 7.9: Minimum Magnet Flux

Magnetization flux within the magnet is also varying due to the stator slotting. This causes them to be prone to eddy current losses. However, the lowest flux density corresponds well with the results from magneto-static predictions.

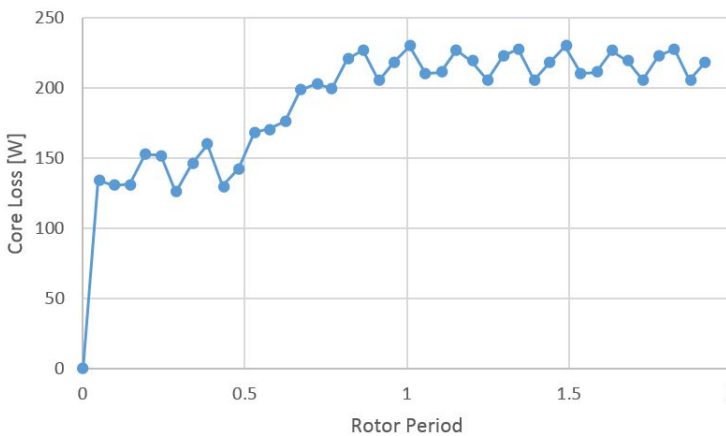


Figure 7.10: Stator Core Losses

Core losses are frequency dependent effects, and for estimation the solver needs to run for a whole electrical period before the core losses converge to a

stable value. The final value is around 220W, which is a fraction of the ohmic DC loss of 939W.

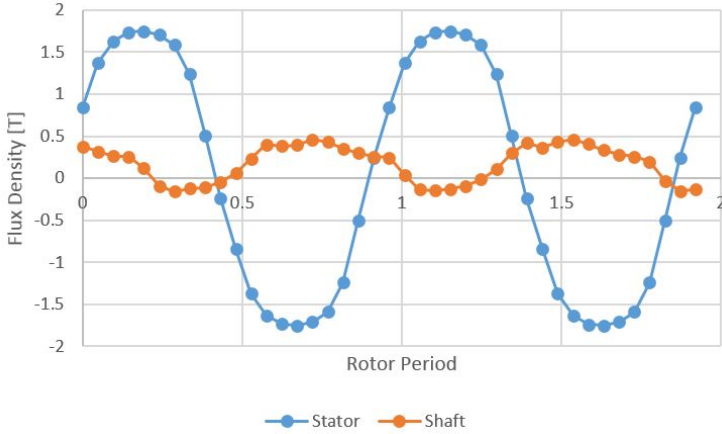


Figure 7.11: Motor Steel Flux Densities

Examining the nominal flux density variations in the shaft and stator core, it is observed that the shaft experiences a significant variation in flux density. As the shaft must be solid to retain its mechanical integrity, significant eddy current losses may occur. Alternative non-magnetic shaft materials should be considered to reduce these potential losses.

7.1.5 Motor Constant Optimization

Optimization of the motor geometry will be based upon qualitative maximization of the motor constant (Equation: 3.33), measuring how efficiently torque is produced. Parametric sweeps of the magneto-static model will be done to evaluate the effect of different geometrical parameters on motor performance. Demagnetization flux will also be considered to make sure no permanent degradation of the magnets occur. As there are many different parameters to be determined, the motor optimization is split into several smaller studies.

The optimization procedure is based on an input/output response mapping of the model. A parameter sweep is run on the input variables, yielding a response point for motor constant and demagnetization flux. Then a response function is created using a linear superposition of second order polynomials for each input parameter. Coefficients of this function are determined by the means of a least square fit to the response points. This function can then be visualized to investigate the relation between input and output parameters.

Halbach Array and Shaft Yoke

This first sweep study will investigate if the shaft can be changed into a non-magnetic material (Section 7.1.4), and how the Halbach array plays a role for the motor performance. From a manufacturing point of view, the geometry of the radially magnetized magnets should be equal to the circumferential magnetized magnets, i.e. $wMagnet = 0.5$. To simulate how the ferromagnetic rotor yoke affects performance it will be swept from 3 mm to 0.5 mm. A non-magnetic shaft would in this case equal a ferromagnetic rotor yoke of 0 mm.

Swept parameters for this study:

- $wMagnet \in [0.5, 0.9]$
- $hMagnet \in [4, 8]$
- $tRotorYoke \in [0.5, 3]$
- $Jrms \in [5, 20]$
- $tStatorYoke = 4$
- $RotorOD = 52$
- $AirGap = 1.5$

By observation of the response points, a fairly linear correlation is observed between magnet height and motor constant K_m (Figure: 7.12). This indicates that the magnet height will only affect the magnitude, but not the shape of the response surface.

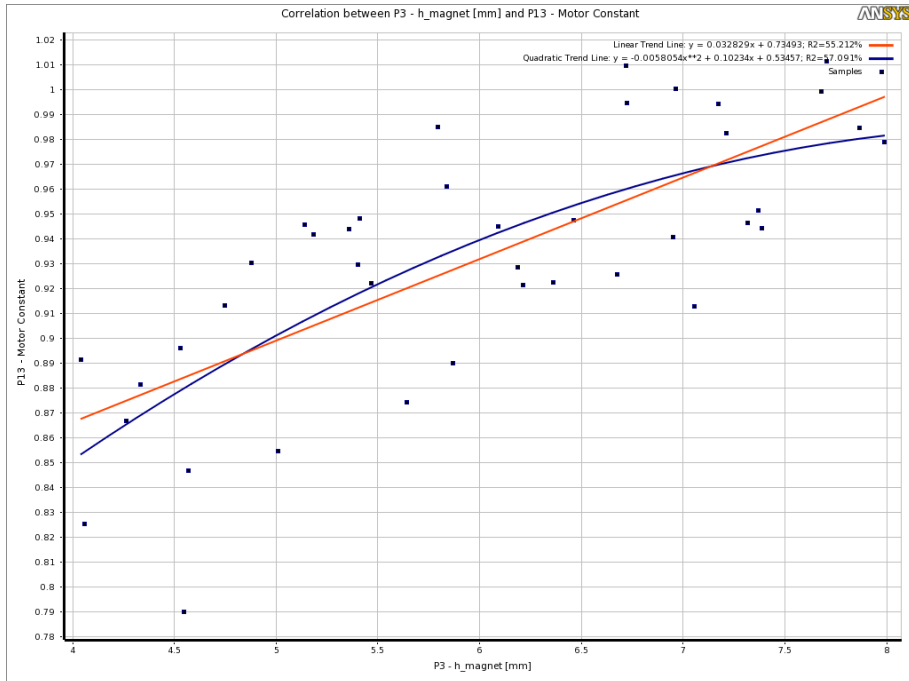


Figure 7.12: Correlation between Magnet Height and Motor Constant

Plotting the response surface for the motor constant as a function of $wMagnet$ and $Jrms$ for a rotor yoke thickness of 0.5 mm (Figure: 7.14) and 3 mm (Figure: 7.15) reveals an interesting result. As expected, an even Halbach array, i.e. $wMagnet = 0.5$, performs better for a thin rotor yoke thickness, while a more radially dominated array, $wMagnet > 0.5$, performs better for thicker rotor yokes.

However, there is no significant difference in the peak motor constant for the two cases. This means a non-magnetic shaft can be used together with a Halbach array without any noticeable decrease in performance. Furthermore, this standardizes the magnet geometry, which lowers the price tag on magnets.

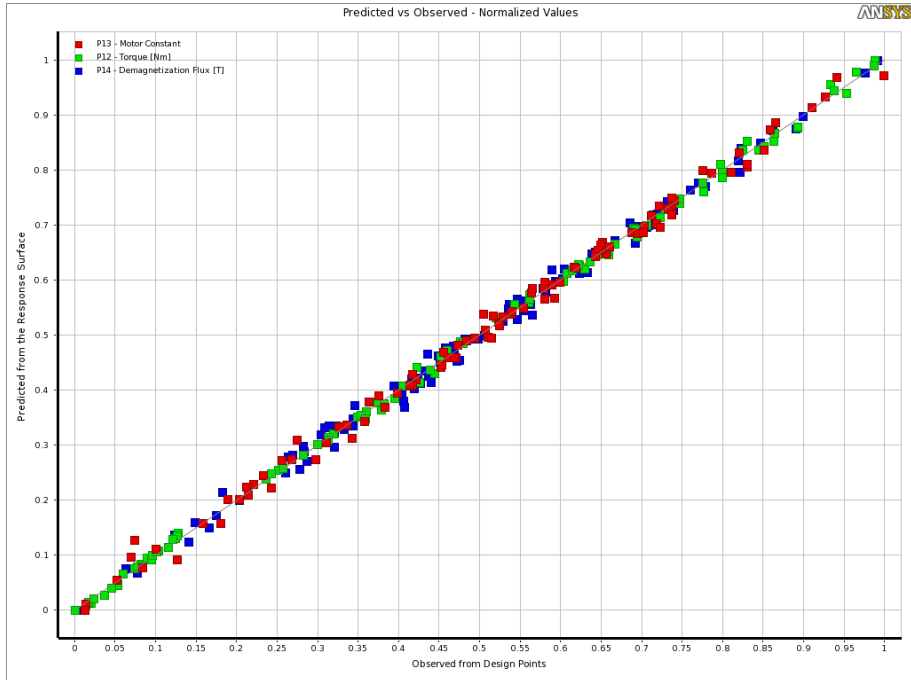


Figure 7.13: Goodness of Response Surface Fit

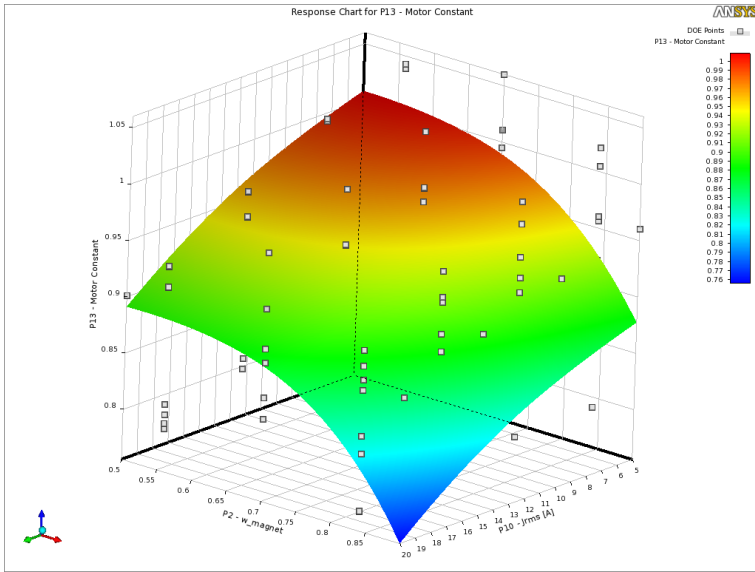


Figure 7.14: Response Surface for 0.5mm Rotor Yoke

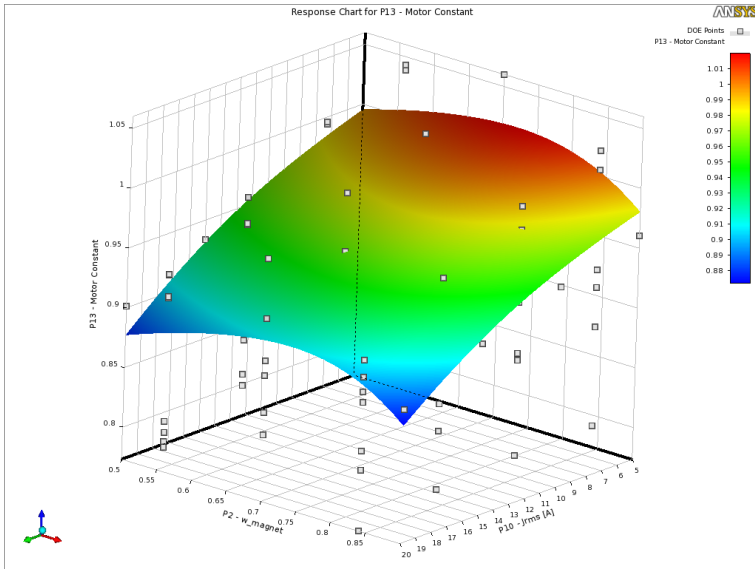


Figure 7.15: Response Surface for 3mm Rotor Yoke

Rotor Outer Diameter

Now that an even Halbach array, $wMagnet = 0.5$, and a non-magnetic shaft are chosen, two input parameters are eliminated from the sweep. The next study will introduce the rotor outer diameter as a variable.

Due to the hollow design of the rotor, a significant amount of motor weight can be removed by employing a larger rotor diameter. Furthermore, stator core losses decrease due to less iron volume, and copper AC losses decrease due to shallower slots (Equation: 3.30). Additionally, if the rotor diameter is 58 mm or larger, the IR temperature sensor can be mounted straight on the end bell, simplifying end bell manufacturing considerably (Section: 6.4.3).

On the other hand, an increase in rotor diameter requires more magnet material due to larger circumference. The retaining sleeve must be thicker to accommodate increased centrifugal forces. Finally a higher rotor inertia is expected. However, due to the small motor volume, the total amount of additional magnet material is negligible. The required sleeve thickness for a 58 mm rotor is calculated to be 0.5 mm, which is already thin from a manufacturing point of view.

The rotor inertia can be estimated by equation (7.1), assuming all of its mass M is concentrated around a cylinder of radius R . Accounting for increased rotor inertia due to the transmission, its equivalent inertia can be compared against a similar estimate for the tire (Table: 7.1). The added inertia for an increased rotor radius turns out to be negligible compared to the tire inertia.

$$I = M R^2 \tag{7.1}$$

Part	Weight	Eqv. Radius	Inertia	Gearing	Eqv. Inertia
Small Rotor	1kg	0.025m	$6.25 \cdot 10^{-4}$	15.4	0.00962
Large Rotor	1kg	0.030m	$9 \cdot 10^{-4}$	15.4	0.01386
Tire	4kg	0.120m	0.0576	1	0.05760

Table 7.1: Rotor Inertia Comparison

The accumulated effect of a larger rotor diameter is considered beneficial for the design. This study will focus on how a larger rotor outer diameter affects the motor constant and demagnetization flux within the permanent magnets. The effect of stator yoke thickness will also be monitored.

Swept parameters for this study:

- $RotorOD \in [52, 64]$
- $tStatorYoke \in [3, 5]$
- $hMagnet \in [4, 8]$
- $Jrms \in [5, 30]$
- $AirGap = 1.5$

Once again, considering the correlation plot for magnet height $hMagnet$, it is quite linear for both the motor constant and demagnetization flux. By further inspection of the response surface, this parameter only scales the height, but not the shape.

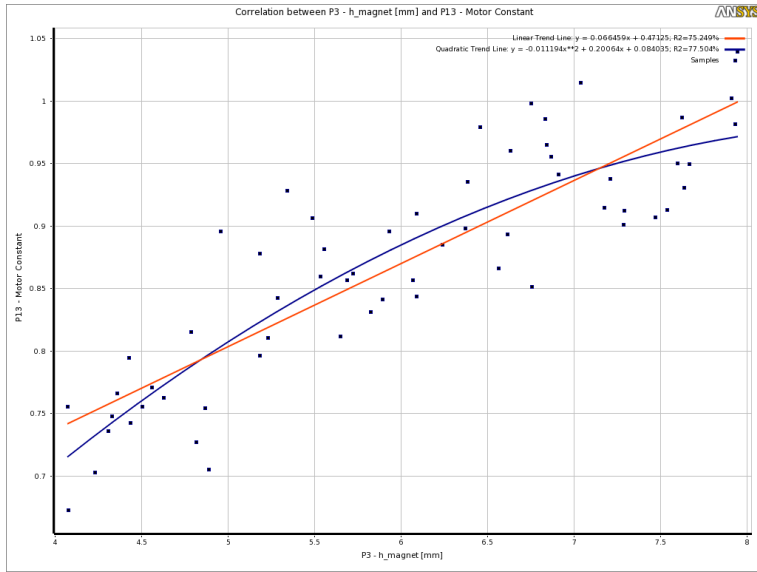


Figure 7.16: Correlation between Magnet Height and Motor Constant

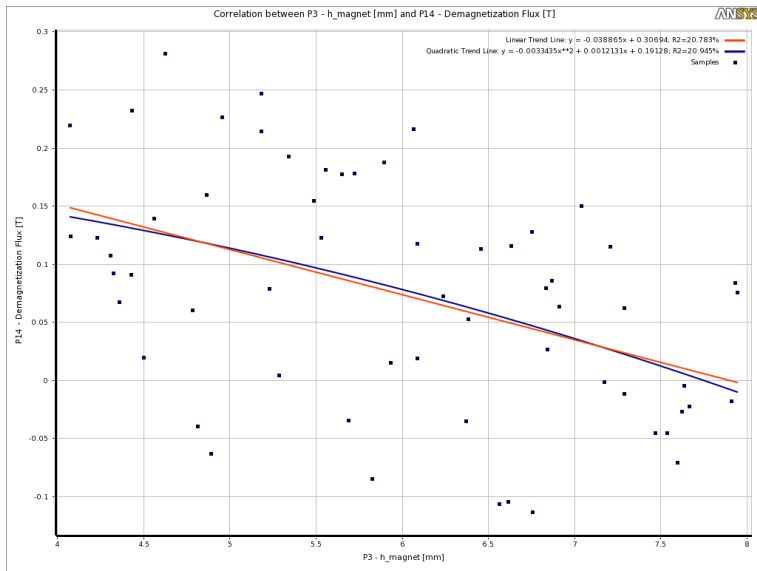


Figure 7.17: Correlation between Magnet Height and Magnet Flux

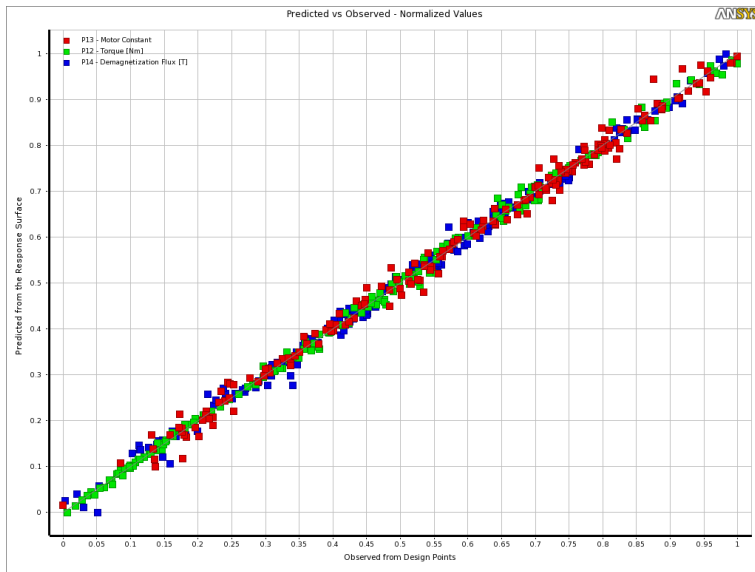


Figure 7.18: Goodness of Response Surface Fit

When considering the motor constant for different values of outer rotor radius, stator yoke thickness and excitation current, a lower rotor radius has a generally better performance for lower excitation currents while a larger radius is beneficial for higher excitation currents.

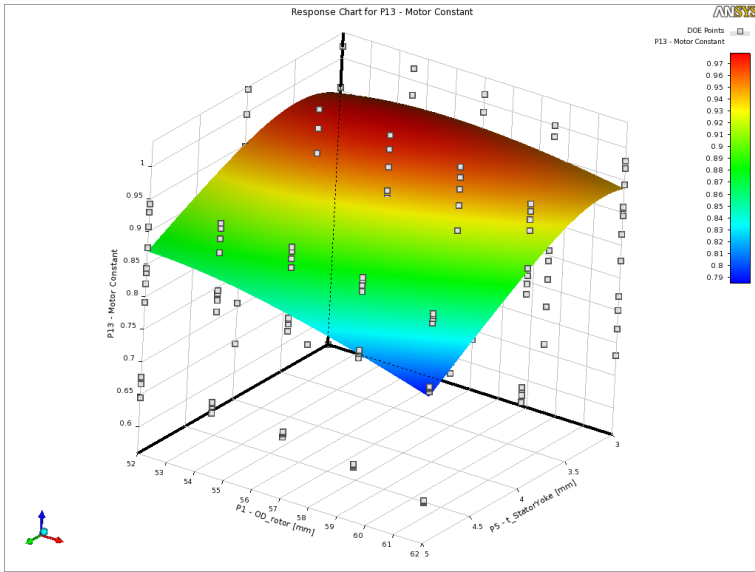


Figure 7.19: Response Surface for $J_{rms} = 5$

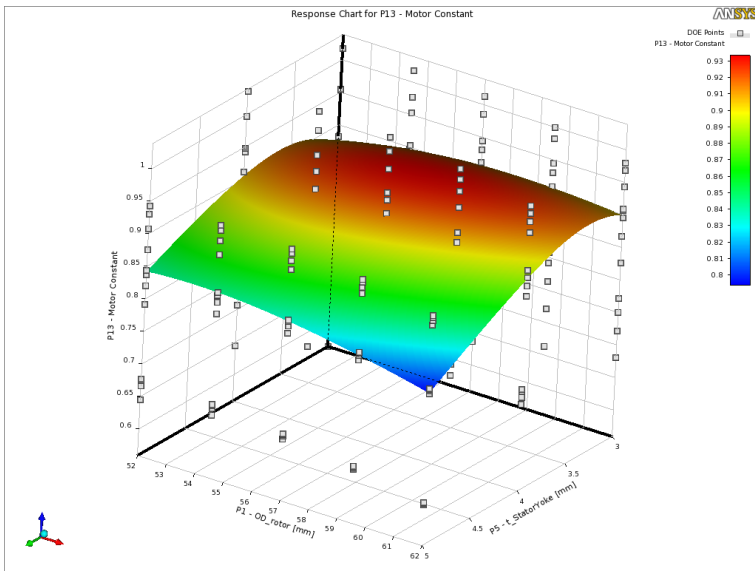


Figure 7.20: Response Surface for $J_{rms} = 15$

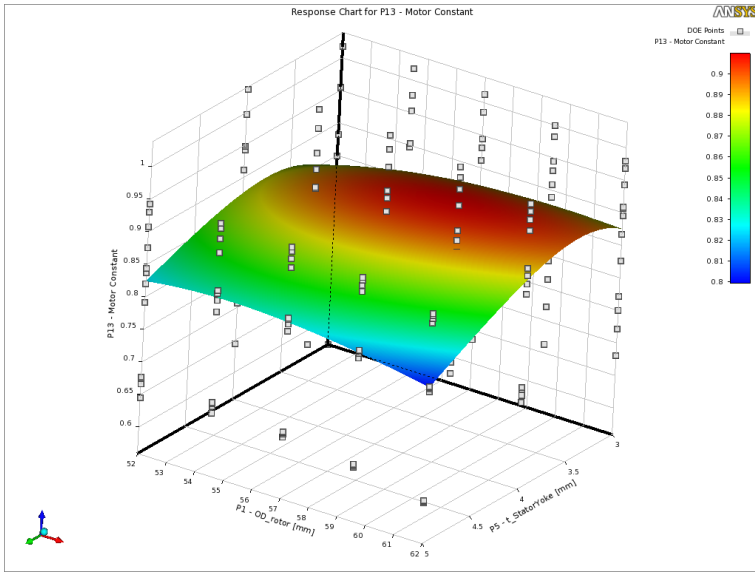


Figure 7.21: Response Surface for $J_{rms} = 20$

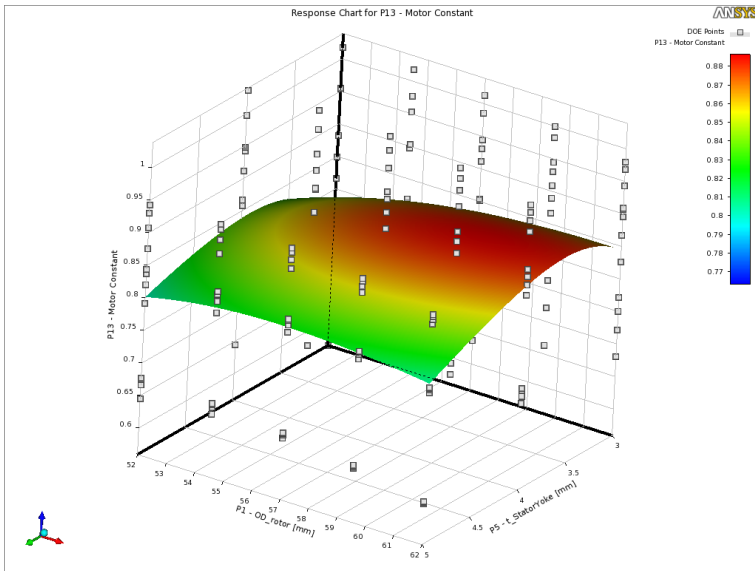


Figure 7.22: Response Surface for $J_{rms} = 25$

By observing the magnet flux for different swept values, smaller rotor radii

cause less demagnetization at low current levels, while larger rotor radii only have a slightly lower demagnetization flux at higher current levels.

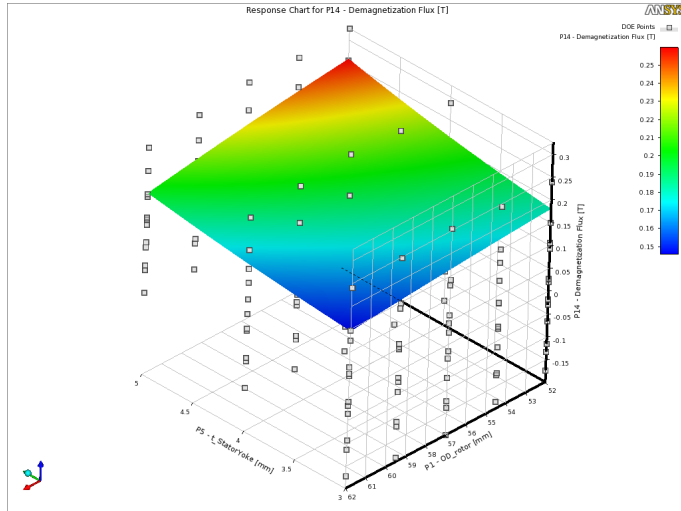


Figure 7.23: Response Surface for $J_{rms} = 5$

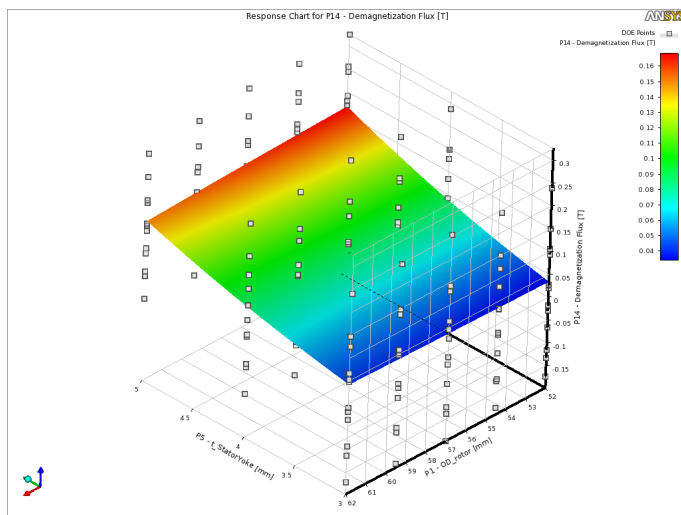
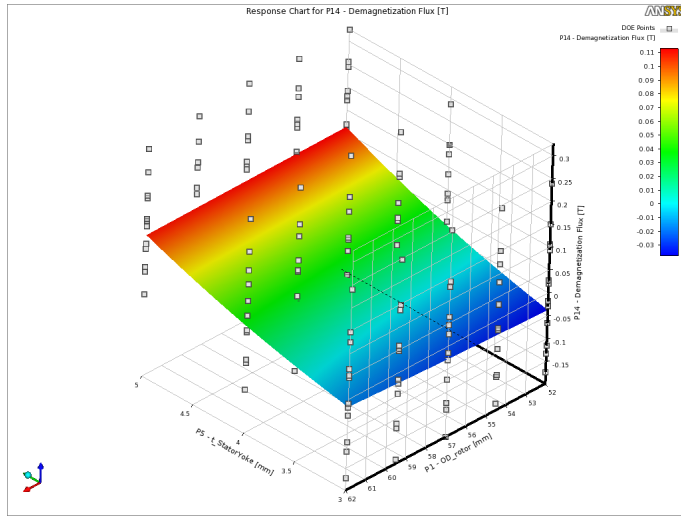
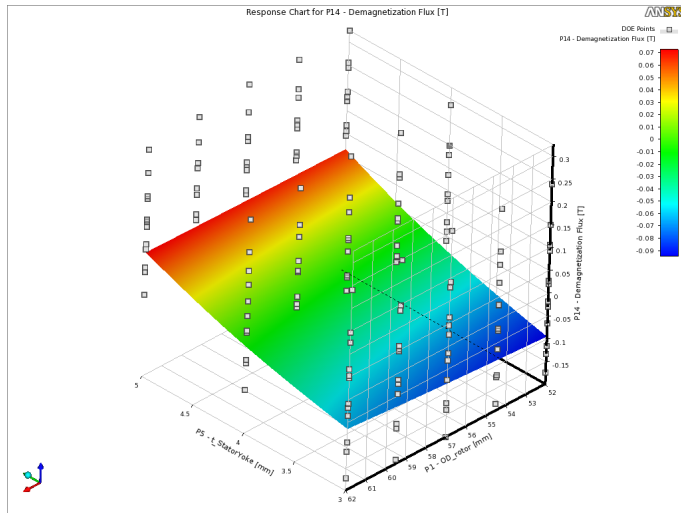


Figure 7.24: Response Surface for $J_{rms} = 15$

Figure 7.25: Response Surface for $J_{rms} = 20$ Figure 7.26: Response Surface for $J_{rms} = 25$

As the outer diameter of the rotor has a smaller influence on demagnetization flux at higher excitation currents, it is optimized with respect to the motor constant. The middle value of 58 mm yields a good compromise between low

current and high current performance. Additionally, this satisfies the IR sensor requirement and reduces the motor mass.

Magnet Height and Stator Yoke

The only two remaining variables for the motor geometry are the stator yoke thickness and magnet height. A last parameter study will be done to determine these two parameters.

Swept variables:

- $t_{StatorYoke} \in [3, 5]$
- $h_{Magnet} \in [4, 8]$
- $J_{rms} \in [5, 30]$
- $AirGap = 1.5$

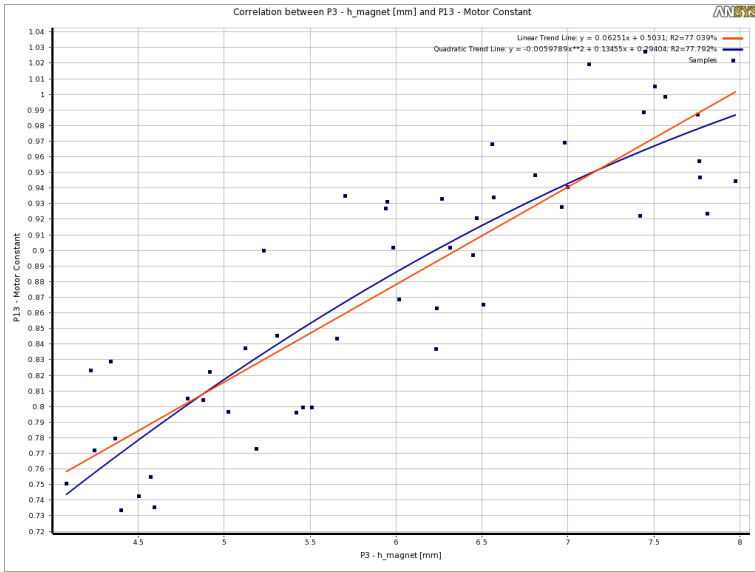


Figure 7.27: Correlation between Magnet Height and Motor Constant

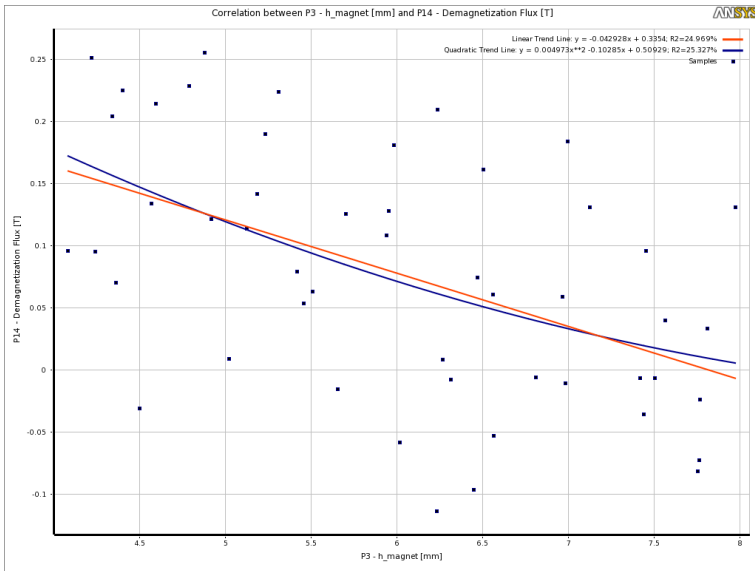


Figure 7.28: Correlation between Magnet Height and Magnet Flux

Once again, the magnet height has virtually no influence on the shape of

the response surface. From the response surfaces, a stator yoke thickness of $\approx 3.5\text{mm}$ optimizes the motor constant for the whole operation range (Figure: 7.29) . However, increasing the thickness yields better protection against demagnetization.

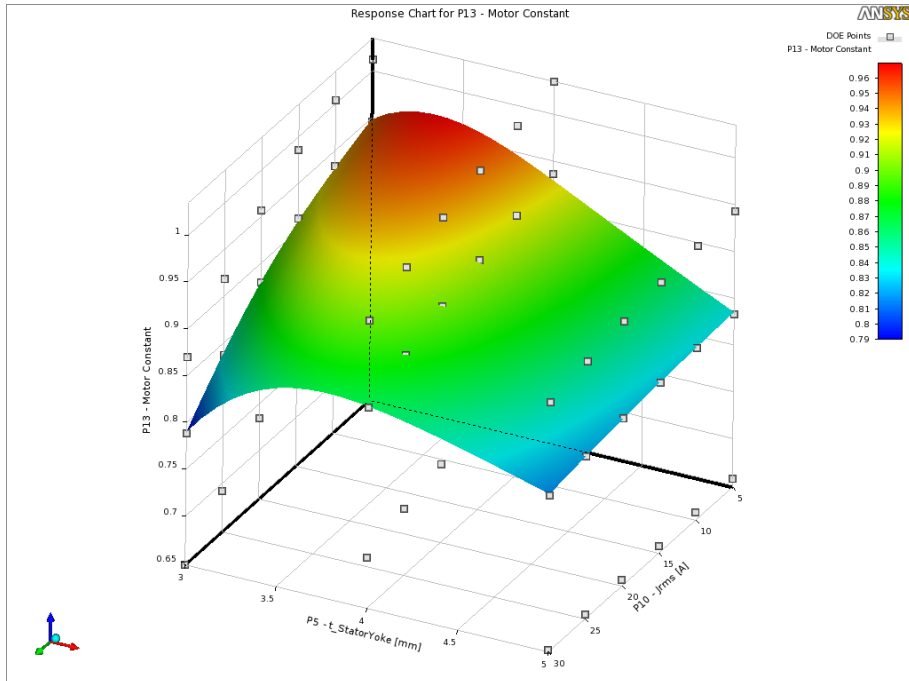


Figure 7.29: Motor Constant Response Surface

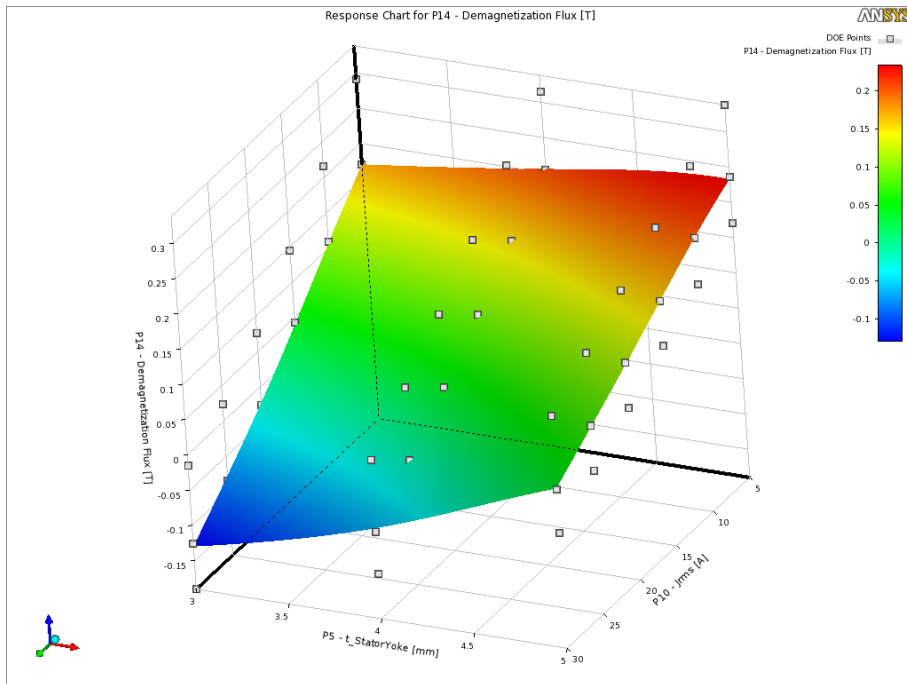


Figure 7.30: Magnet Flux Response Surface

A magnet height of 6 mm is chosen as it yields a good compromise between performance, weight and cost. For a torque output of 30.5 Nm (Table: 5.3, point 2.1), the minimum magnet flux for a yoke thickness of 3.5 mm is only slightly below 0 Tesla. This is considered to yield enough safety for operation at elevated temperatures.

Optimized Design

To validate the magnetic performance of the optimized design, it is compared against the initial. In figure (7.31) and (7.32), the motor constant and minimum magnet flux are shown against generated torque. From a magnetic point of view, the initial design has an overall slight performance advantage to the optimized. However, the optimized design has eliminated the ferromagnetic

shaft and has inherent lower time dependent losses. Furthermore, considering the weight, it saves 236 g on the magnetic components compared to the initial design (Table: 7.2).

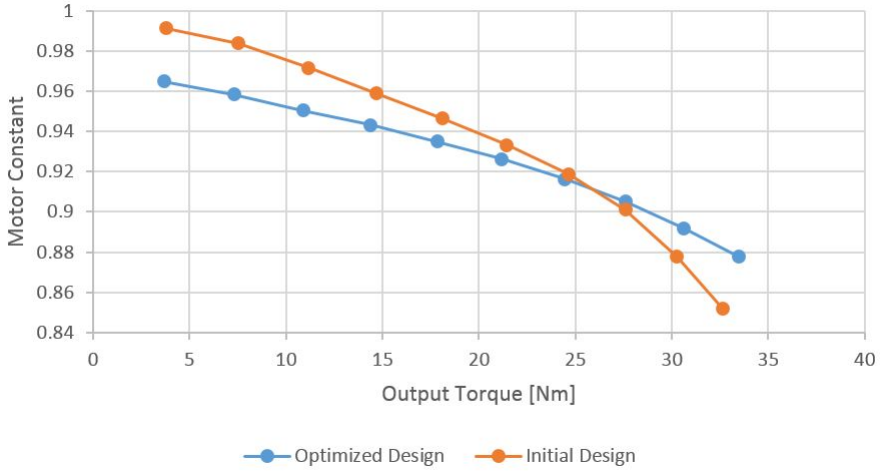


Figure 7.31: Motor Constant Comparison

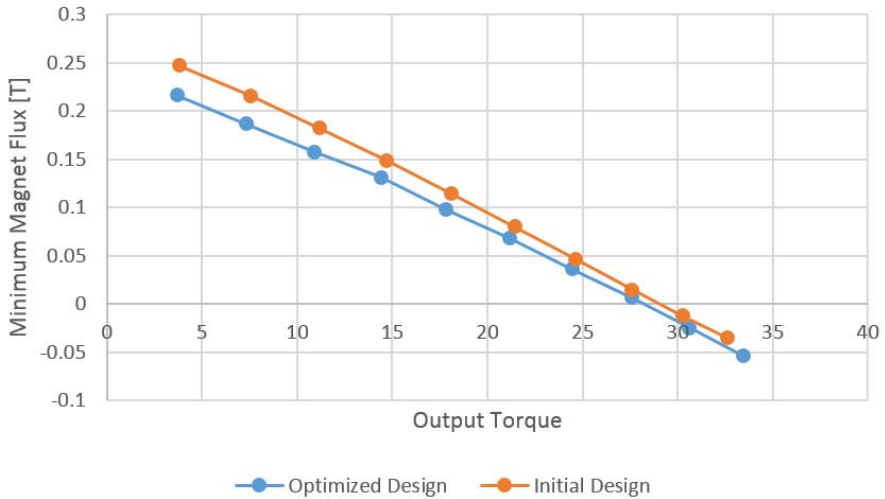


Figure 7.32: Minimum Magnet Flux Comparison

Part	Optimized Design	Initial Design
Coils	985g	1151g
Stator Core	1098g	1225g
Permanent Magnets	486g	430g
Total Weight	2569g	2806g

Table 7.2: Estimated Weight of Magnetic System

When considering the results from this optimization, an interesting observation can be made. Once the stator outer diameter and motor topology are set, the only significant way of increasing the motor performance is by increasing the amount or quality of magnet material. Other geometric parameters like rotor outer diameter and stator yoke thickness have a lesser impact on performance as long as they are kept within reasonable limits.

7.1.6 Other Considerations

Number of Turns

As shown in equation (3.32), the motor constant can not be increased by varying the number of turns. However, the number of turns determines the back EMF constant of the motor and how much current it will draw from the power electronics. A lower EMF constant requires a higher current to produce the same torque.

The induced back EMF at the motor terminals increases linearly with speed, but if it reaches the vicinity of the available inverter voltage, the power electronics are no longer able to push current against the back EMF voltage, and the motor speed stalls. However, extended speed range is achievable using a technique called field weakening. By phase advancing the currents to the back

EMF, the currents can be generated before they are needed to produce torque. The disadvantage with this technique is that it diminishes motor efficiency. Because of this, the back EMF constant should ideally be set so the maximum induced terminal voltage is somewhat lower than the available inverter voltage.

On the other hand, the semiconductor switches in the inverter have current ratings in order to prevent overheating. Thus, the amount of allowable current to the motor is limited by the inverter cooling and semiconductor ratings. This must also be considered when determining the number of turns.

Running a transient simulation of the final design, the phase back EMF is found for two different excitation currents at a rotor speed of 1000 RPM (Figure 7.33 and 7.34). It should be noted that the back EMF will distort when a high excitation current is run through the coils, yielding an effective higher EMF. By subtraction of the phase EMFs, i.e. $\epsilon_T = \epsilon_A - \epsilon_B$, the terminal back EMF amplitude is found for the Y-connected phase windings.

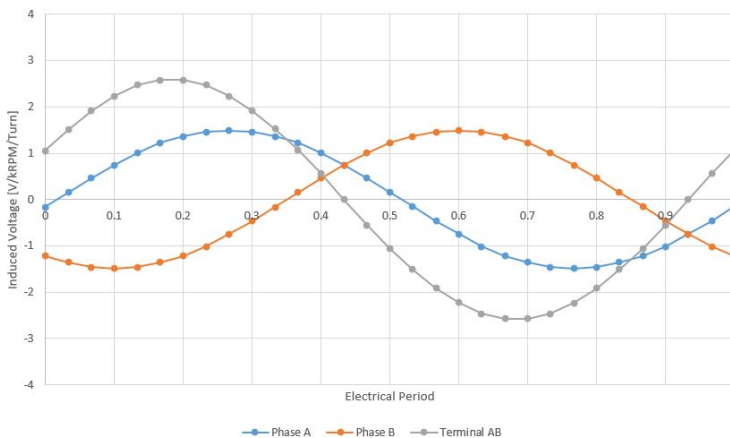
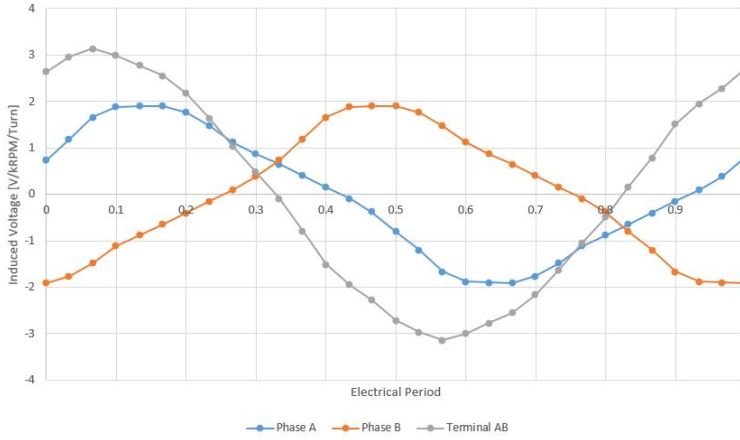


Figure 7.33: Back EMF at $J_{rms} = 0$

Figure 7.34: Back EMF at $J_{rms} = 25$

Excitation Current	Terminal Back EMF Constant
0 Arms/mm^2	2.584V/kRPM/Turn
25 Arms/mm^2	3.14V/kRPM/Turn

Table 7.3: Terminal Back EMF Constants

Figure (7.35) shows how the induced terminal voltage at maximum speeds relates to the number of turns. Available voltage range for the inverter is added to the plot (Table: 5.3).

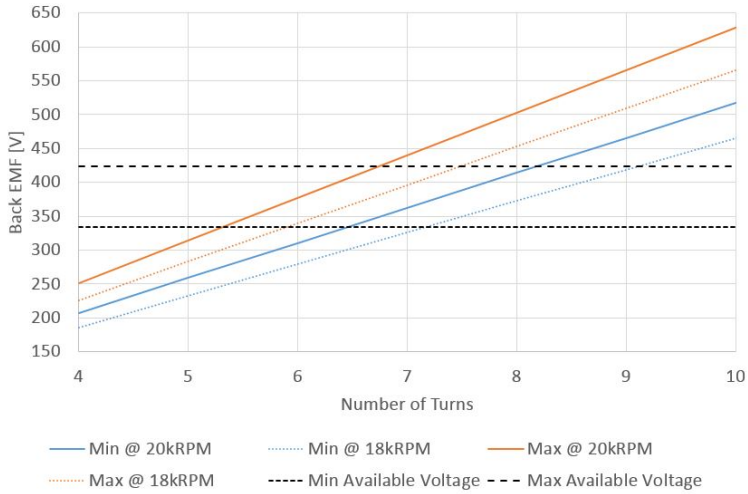


Figure 7.35: Back EMF vs Number of Turns

The coil current density J_{rms} and inverter currents I are related through equation (3.32). The inverter current rating is $90 A_{rms}$ and $180 A_{rms}$ for continuous and peak performance ($\approx 5sec$), respectively. Figure (7.36 shows how the required current varies by number of turns for a given coil current density J_{rms} .

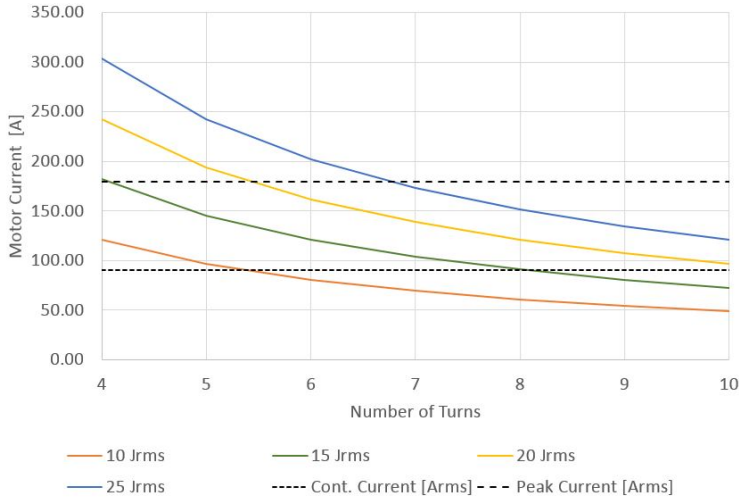


Figure 7.36: Motor Current vs Number of Turns

By comparing figure (7.35) and (7.36), using 7 number of turns per coil yields a good compromise between terminal back EMF and achievable coil current density, as 25 *Jrms* translates to 33.5 Nm torque output.

Furthermore, the winding layout has two coil groups (Figure: 7.37). If the two coil groups are connected in parallel instead of series, the number of turns has to double, i.e. 14 turns. Both can be used, and the one that yields the best copper fill factor should be taken.

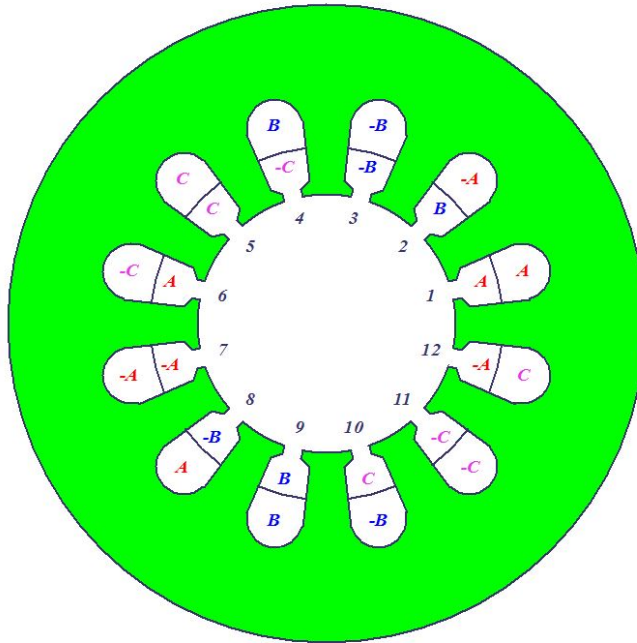


Figure 7.37: Motor Winding Layout

Magnet Segmentation

During motor operation, the permanent magnets are exposed to a changing magnetic field due to stator slotting and current ripples in the coils. The variation due to stator slotting can be seen in figure (7.9). These changing fields cause eddy current losses in the magnets (Section: 3.3.3). To reduce the losses and heat build-up in magnets, they should be segmented in both the axial and circumferential direction.

The degree of segmentation is based upon the frequency of the changing magnetic field. Stator slotting and coil excitation cause variations at the electrical frequency. However, when a PWM technique is used to modulate currents into the phase coils, a current ripple can occur at the PWM frequency. An

approximate guideline to the segmentation length is given by the skin depth (Equation: 3.29). It should be noted that the resistivity of permanent magnets are not isotropic. For NdFeB it is typically lower transverse to the magnetization direction, i.e. the eddy current plane. A 17% decrease in resistivity is used based on results from [45]. Room temperature is also used to get a conservative estimate.

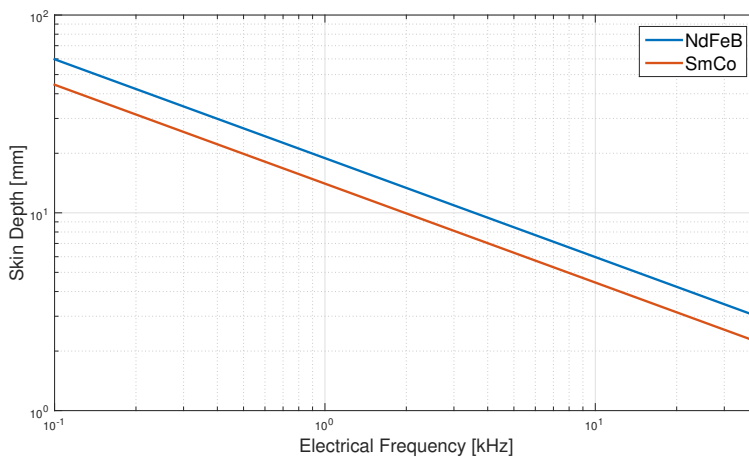


Figure 7.38: Permanent Magnet Skin Depth vs Frequency

The PWM frequency for the used inverter is 40 kHz, which corresponds to a skin depth of 3 mm for NdFeB magnets (Figure: 7.38). Depending on the manufacturing cost, the magnets should be segmented circumferentially and axially with a segment length of at least 3 mm.

7.2 Modal Analysis

The largest magnetic force component within a permanent magnet motor is the radially attractive force between each magnet pole and its corresponding stator tooth. Finite element simulations indicate that the maximum value of

this force is in the vicinity of 900 Newton. Although quite considerable for a magnet, it is relatively small compared to the material strength of the structural parts. Furthermore, the motor is not part of any load carrying structure of the car, and thus external loads are also considered to be small.

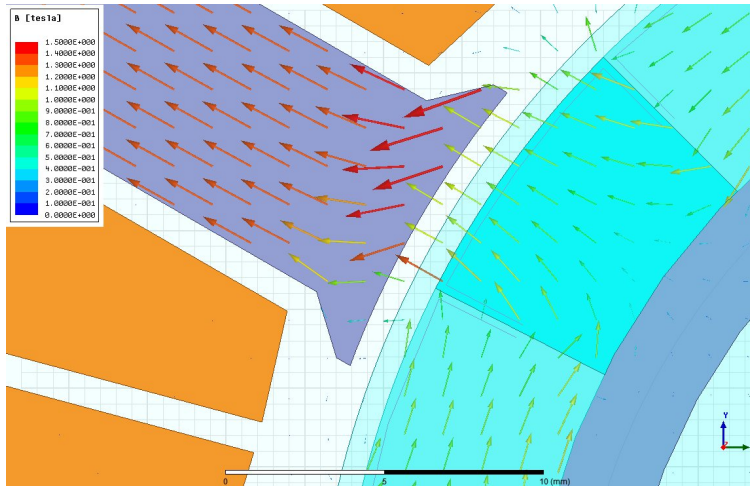


Figure 7.39: Strong Air Gap Flux between Rotor and Stator

In other words, loads on the motor structure are not considered to be a threat to its structural integrity. However, due to the time-varying nature of these loads, vibrational problems may occur if the structure is forced into resonance. Because of this, a modal analysis will be done to assess the structural resonance frequencies and their vicinity to expected excitation force frequencies.

7.2.1 Rotordynamics

Whenever the rotor rotates, gyroscopic effects will be present for lateral vibrations. These effects will tend to move the resonance frequencies of the rotor by

causing swirl, depending on the rotational speed. Analytical models are only available for simplified cases of a Jeffcott rotor on rigid bearings or a rigid shaft on flexible bearings ([46], chapter 2). However, in real applications both rotor and bearing are flexible, and mass is unevenly distributed. Because of this, a finite element approach is used to assess the resonant frequencies of the rotor, and how they are influenced by gyroscopic effects over the speed range.

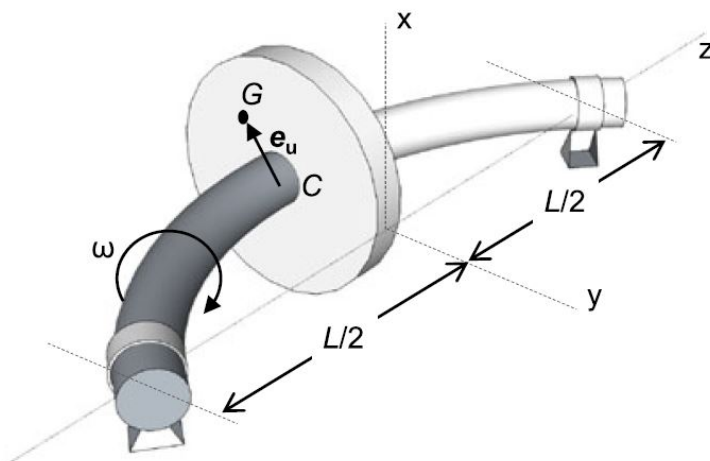


Figure 7.40: Jeffcott Rotor ([46], fig. 2.1a)

Support Stiffness

First step in a rotordynamic analysis is to assess the stiffness of the support points of the shaft. In the particular design in this thesis, the rotor is supported by two bearings on each side. These bearings are then supported by the motor housing, which in turn is supported by the wheel hub. All of these flexible components can be considered as springs connected in series.

Bearing stiffness is in general dependent on several factors, like external load, internal clearance / preload and bearing material to name a few. However,

based on a lightly loaded scenario with no internal preload, bearing stiffness was calculated for the chosen ceramic bearings, carried out and provided by SKF engineering service (Appendix: D).

Bearing	6005 C3	6003 C3
Radial Stiffness [N/mm]	$11.6 \cdot 10^4$	$10.1 \cdot 10^4$

Table 7.4: Radial Bearing Stiffness

To assess the stiffness of the bearing seats, a structural finite element model was created for the stator housing. Geometric features of the stator not contributing to stiffness were removed to facilitate meshing and to reduce simulation times. Due to the irregular geometry of the housing, second order tetrahedral elements were used to capture the geometry and yield reasonable element shapes.

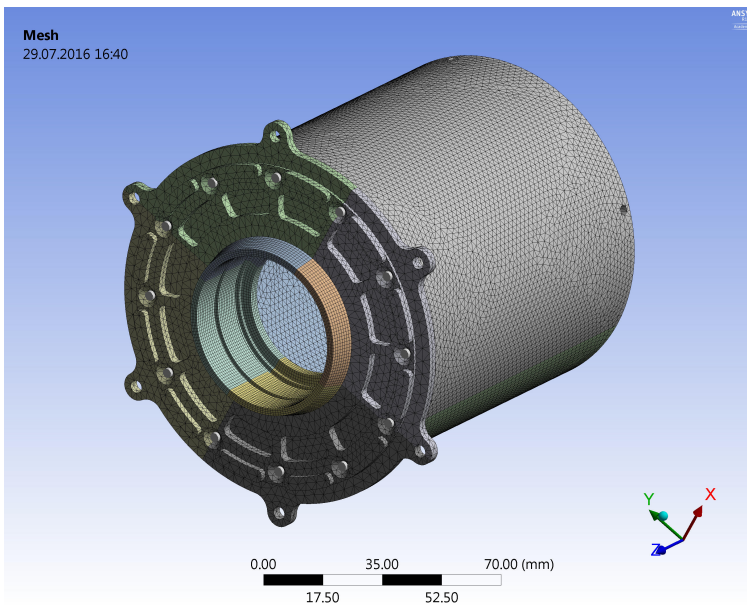


Figure 7.41: Stator Mesh

The hub is manufactured using selective laser sintering metal printing. It has a hollow, thin walled titanium structure with an internal lattice structure to prevent buckling of the shell and to facilitate load distribution around external point loads, i.e. fasteners. Due to the complex nature of its geometry, the hub support stiffness is difficult to determine accurately using classical FEM analysis. However, the hub is optimized to yield high support stiffness to the wheel and the planetary gearbox within. This also gives the motor mounting points an inherent high stiffness, and is considered rigid to facilitate the analysis of bearing support stiffness.

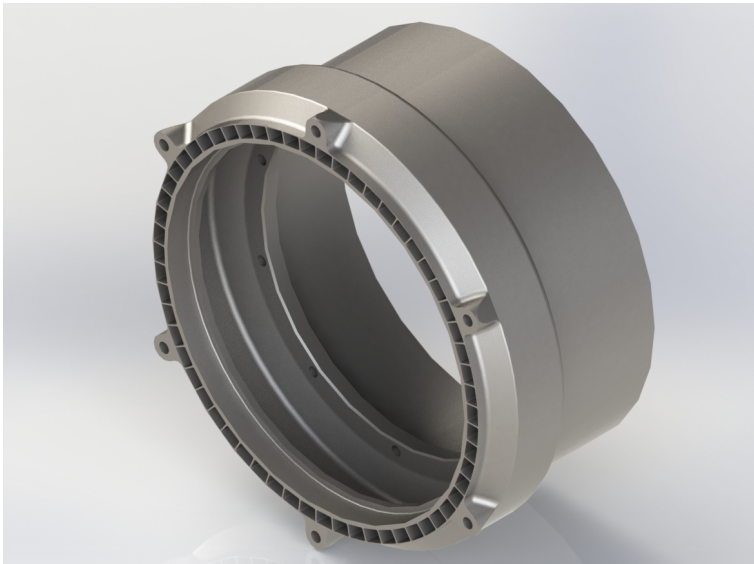


Figure 7.42: Hollow Hub Interface Cross Section

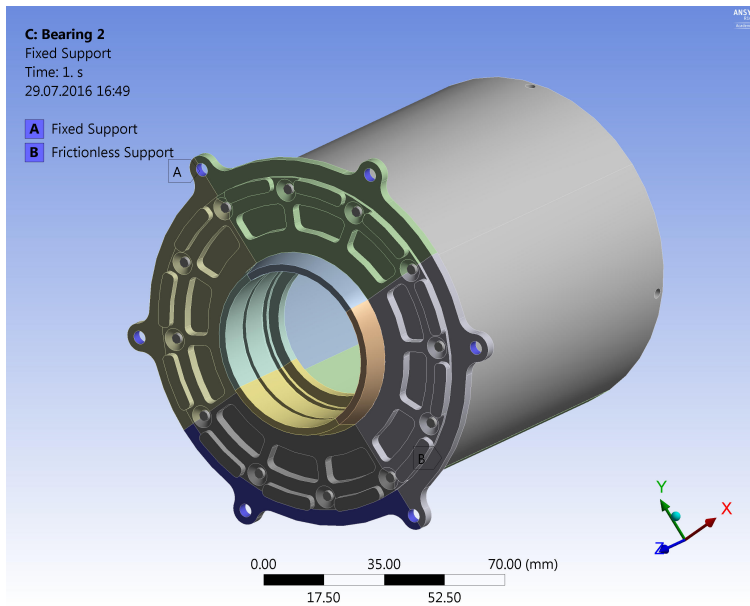


Figure 7.43: Hub Boundary Conditions

In order to model the connection between the motor adapter plate and motor housing, some initial considerations were made. Due to the large bolt circle diameter, all shear and bending loads between the two components can be assumed to be transferred by the bolt connections. To eliminate computationally expensive contact conditions between the adapter plate and motor housing, all fasteners are modelled as flexible beams, attached to the inside of the bolt hole. The beam stiffness is determined by the cylindrical bolt geometry and material. This not only reduces simulation time, but provides a softer connection that yields a conservative approximation for the modal frequencies and partly makes up for the rigid hub assumption.

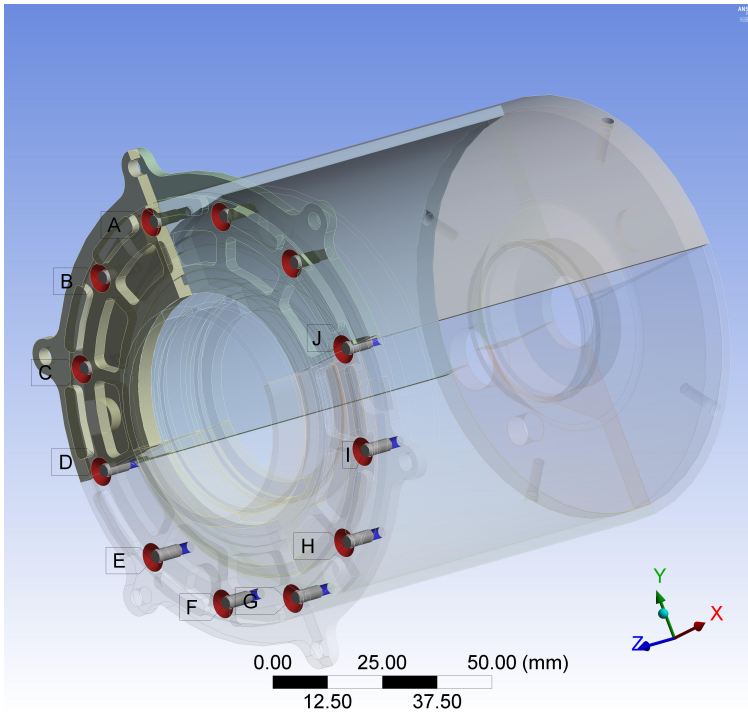


Figure 7.44: Adapter Bolt Connections

Support stiffness is extracted by adding a sinusoidal distributed load of 1000 N to each of the bearing seats in the stator and measuring the corresponding directional deformation. Since the two supports are connected together by the housing, they have some affect on each other. The resulting stiffness matrix of the two bearing seats with respect to the hub is given in table (7.5).

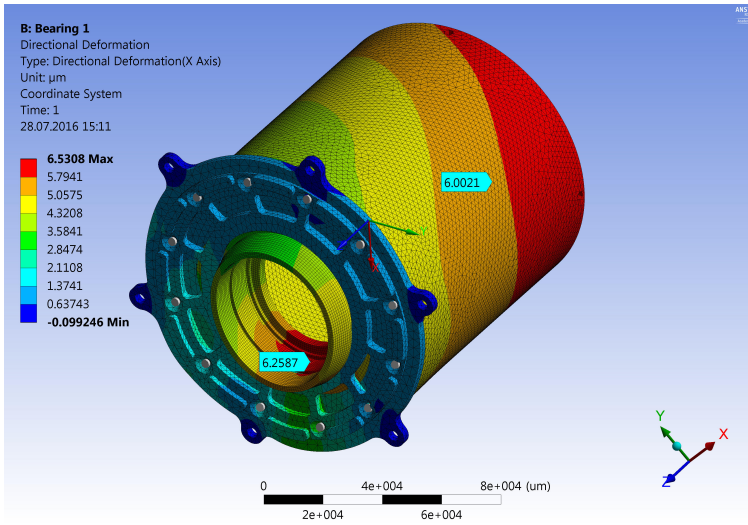


Figure 7.45: Deformations due to Load in Seat 1

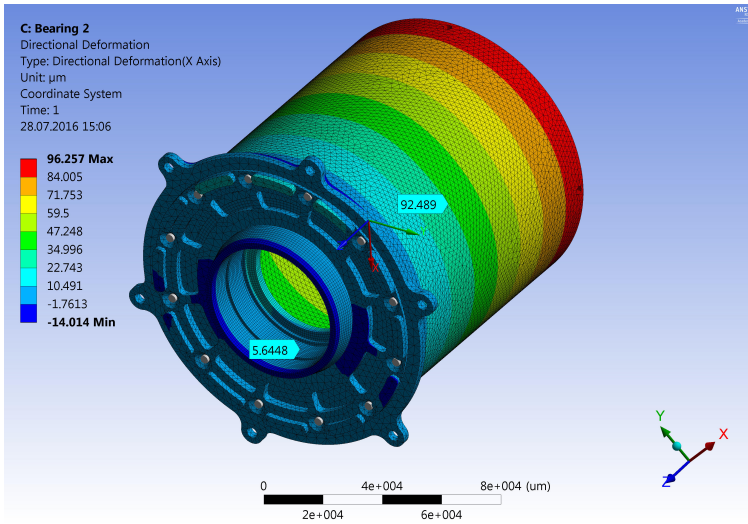


Figure 7.46: Deformations due to Load in Seat 2

Applied Force	Deformation Seat 1	Deformation Seat 2
1 kN in Seat 1	6.23 μm	6.00 μm
1 kN in Seat 2	5.64 μm	92.49 μm

Table 7.5: Bearing Seat Deformations

The overhung geometry of the motor causes loads on the outer bearing to have a far greater influence on housing deformations compared to the inner bearing. Because of the large difference in stiffness, the cross coupling between load in bearing seat 1 and deformations in seat 2 can be neglected. Furthermore, since seat 1 is far stiffer than seat 2, its exact stiffness is assumed to have a lesser influence on rotor modes, and the second cross coupling is neglected to facilitate further analysis.

Neglecting both cross coupling contributions, the total support stiffness can be found by considering the bearing stiffness (Table: 7.4) in series with the seat stiffness, calculated from table (7.5).

[N/mm]	Seat Stiffness	Bearing Stiffness	Total Stiffness
Support 1	16.1 · 10 ⁴	11.6 · 10 ⁴	6.74 · 10 ⁴
Support 2	1.08 · 10 ⁴	10.1 · 10 ⁴	0.976 · 10 ⁴

Table 7.6: Rotor Support Stiffness

Rotor Modes

Now that the support stiffness is determined for both supports, a rotor model can be created. Complicated rotor geometry that does not contribute significantly to mass or stiffness, e.g. output spline, was removed prior to analysis.

Furthermore, since rotor stresses are not of interest, all fillets were removed to facilitate meshing. Due to the simple circular geometry, second order hexahedral elements were used in a partially swept mesh for good accuracy and fast solving.

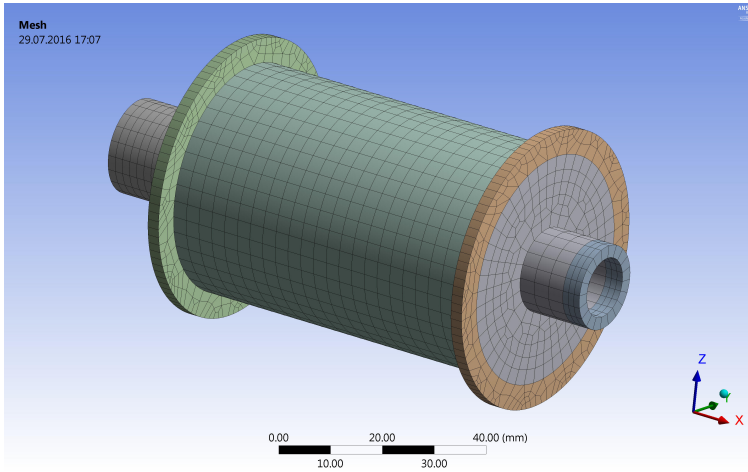


Figure 7.47: Rotor Mesh

As the permanent magnets are segmented, they do not contribute significantly to rotor stiffness. However, their mass contribution is considerable and must be accounted for. In the finite element model, the permanent magnets will be omitted from the geometry, but their mass will be distributed over the shaft surface. Mass is taken from table (ref estimated magnetic system mass), and adjusted for the decreased cylinder radius by equation (7.1) to yield an equivalent moment of inertia. This provides a conservative estimate for the modal frequencies as it overestimates the total mass of the magnets.

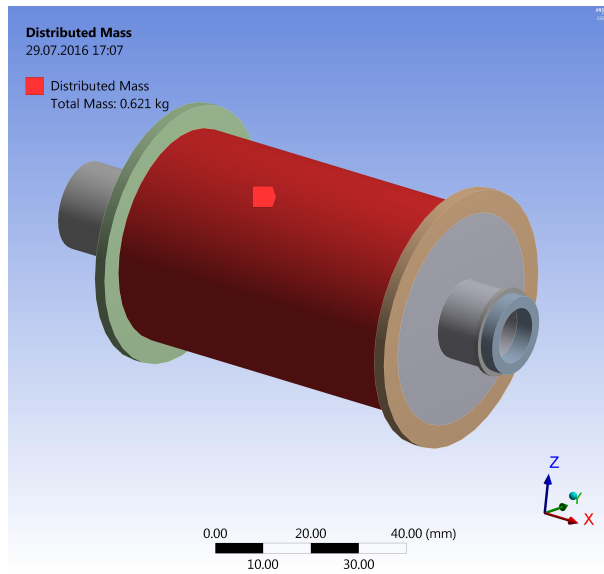


Figure 7.48: Distributed Magnet Mass

Bearing supports are modelled by attaching the centerline of the bearing seat on the shaft to a single node located concentrically to the bearing raceway. Then a combination of two orthogonal directional springs connect the centre node to the ground. The spring stiffness is adjusted to match the support stiffness from table (7.6). Furthermore, bearing node 1 is fixed from axial movement and rotation around the spin axis to eliminate rigid body modes.

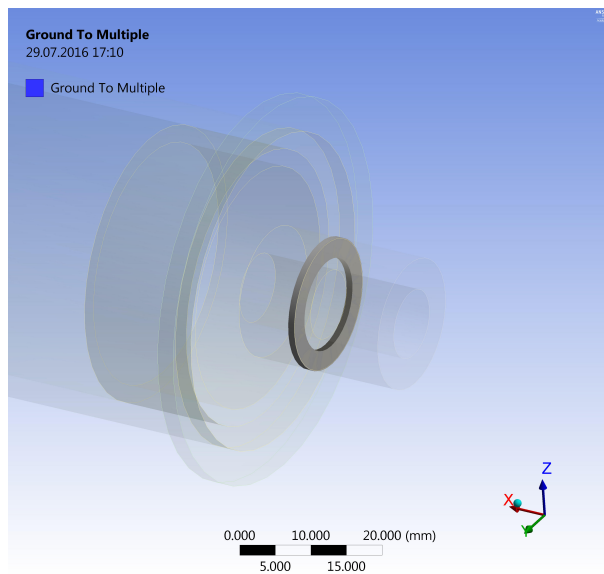


Figure 7.49: Flexible Shaft Support

A modal analysis was run for different shaft speeds between 0 and 20 000 RPM to assess the influence of gyroscopic effects. Only the six lowest frequency modes were calculated. The results are presented in a Campbell diagram (Figure: 7.50).

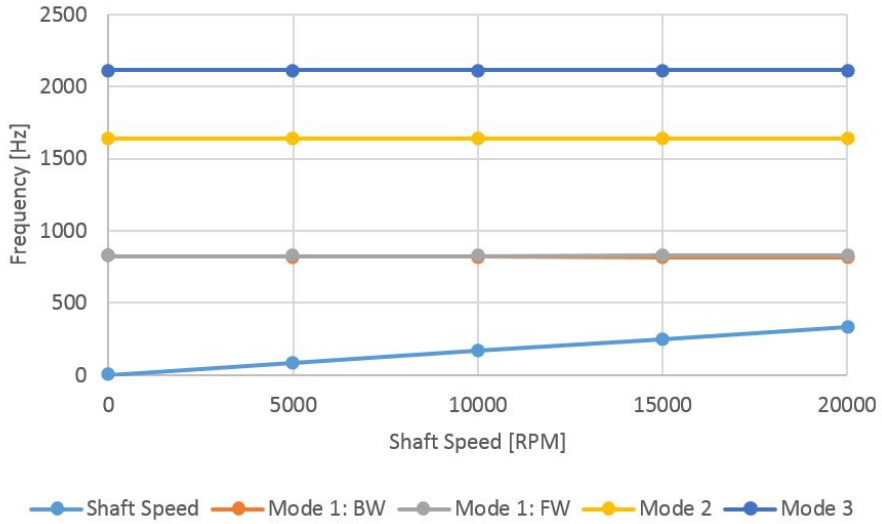


Figure 7.50: Campbell Diagram

By examining figure (7.50), the gyroscopic effects can be neglected within the speed range in question. This can be explained by the high stiffness to weight and inertia ratio on the rotor. The two lowest and highest modes are fundamental and secondary conical modes, while the two middle ones are torsional and axial, respectively.

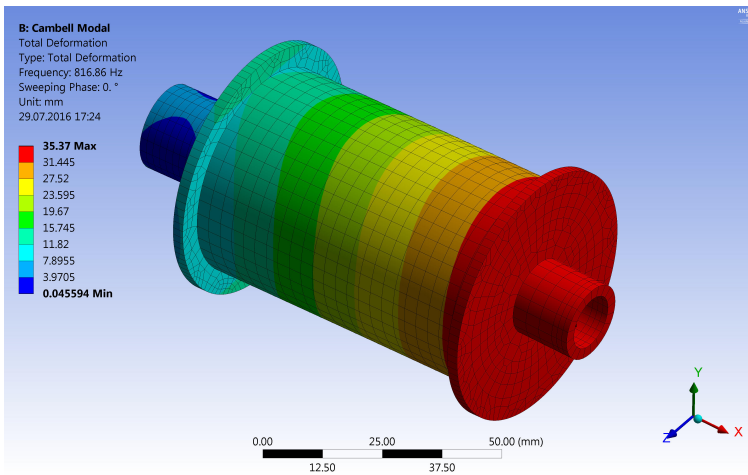


Figure 7.51: Fundamental Conical Mode

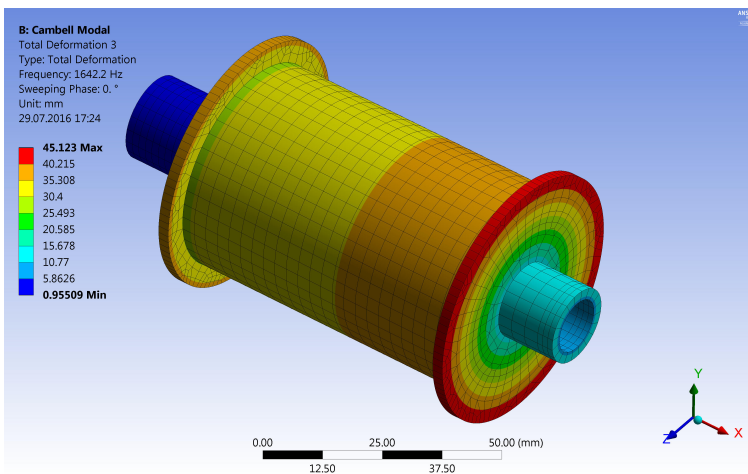


Figure 7.52: Torsional Mode

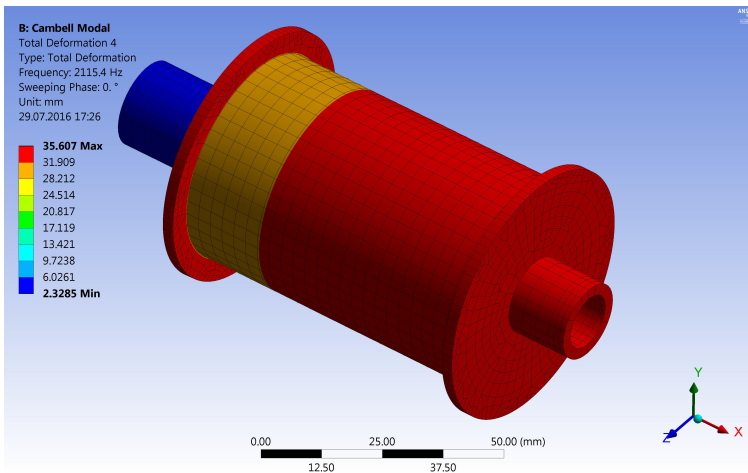


Figure 7.53: Axial Mode

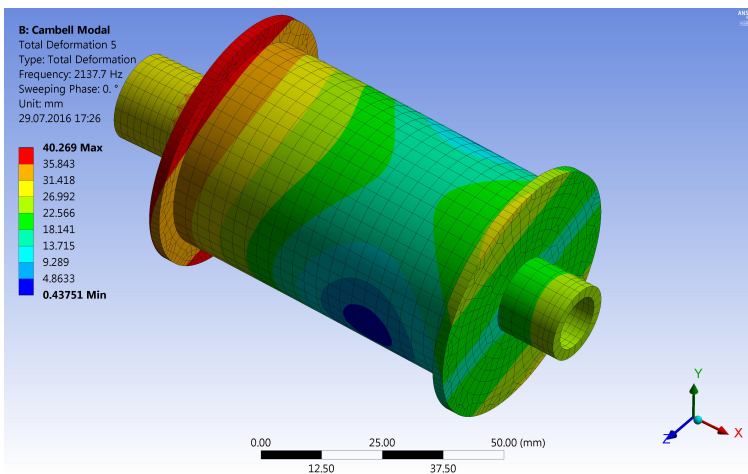


Figure 7.54: Secondary Conical Mode

7.2.2 Stator Modes

The stator modes were assessed by reusing the mechanical model developed in section (7.2.1). In order to support modal analysis, distributed mass is added for the stator core (table magnetic system weight), and the estimated total

rotor mass was divided between the two bearing seats.

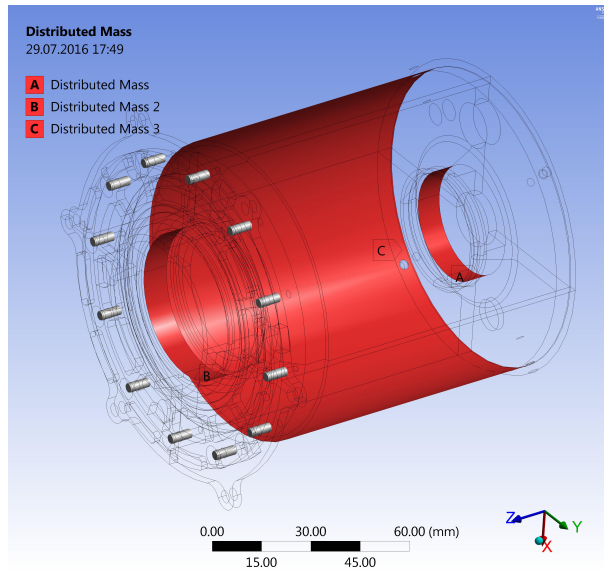


Figure 7.55: Added Model Mass

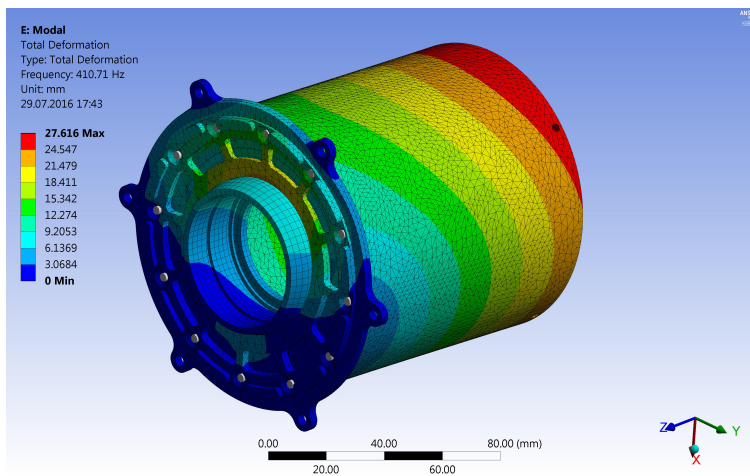


Figure 7.56: Fundamental Cantilever Mode

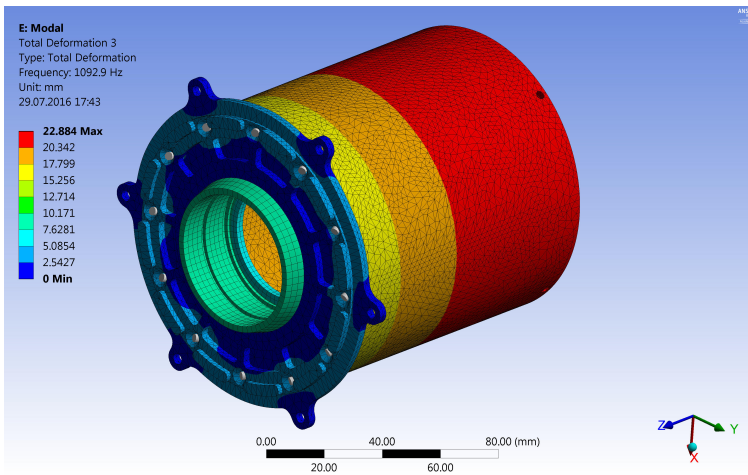


Figure 7.57: Torsional Mode

As expected, the two lowest modes correspond to the fundamental mode shape of a cantilever beam. The next interesting mode has a torsional shape.

7.2.3 Vibrational Assessment

The resulting natural frequencies from sections (7.2.1) and (7.2.2) are listed in increasing order of frequency (Table: 7.7).

Component	Frequency	Mode Shape
Stator	410.71 Hz	Cantilever
Rotor	822.25 Hz	Conical 1st
Stator	1092.9 Hz	Torsional
Rotor	1642.2 Hz	Torsional
Rotor	2115.4 Hz	Axial
Rotor	2158.4 Hz	Conical 2nd

Table 7.7: Motor Natural Frequencies

A common mechanical vibration source comes from an unbalanced rotor. The excitation frequency for this source is the shaft speed. In order to ensure the vibrations stay small, the modal frequencies should be strictly higher than the speed range of the motor. The maximum motor speed of 20 000 RPM corresponds to a frequency of 333.3 Hz, which is significantly below the lowest natural frequency of the motor.

However, if the mass unbalance of the rotor is large enough, vibrations will occur at the mechanical rotor frequency. Balancing discs are added to the rotor assembly for compensating unbalanced mass. Based on guideline values from ISO 1940-1:2003, a balance quality grade of G 2.5 is set as a requirement for the rotor.

Other sources to vibrations can come from the magnetic system. Some obvious ones come from known sources such as cogging torque, unbalanced radial forces or uneven mutual torque. Manufacturing tolerances play a key role here. These tolerances are mainly related to dimensional and material tolerances. If either the rotor is offset from ideal concentric placement or the permanent magnets are unevenly magnetized, variations will occur for cogging torque, mutual torque and radial forces. The frequency of these excitations is at the shaft's rotational frequency and its harmonics. Many also appear at the slot passage frequency, i.e. $f_{slot} = N_s \cdot f_{shaft}$. ([9], section 11.5).

The frequencies of these excitations are typically very high for our application and are less dangerous to cause any problems because motor inertia will

effectively filter them out. However, there is one aspect that requires some discussion. The torsional mode of the rotor is approximated to have a resonance around 1600 Hz (Table 7.7). This lies very close to the maximum electrical frequency of the motor at 1666 Hz (20 000 RPM). Care should be taken to ensure that torque ripples do not occur at this frequency during cruising at maximum speed, as shafts typically have very low damping in torsion, which can lead to fracture of the spline.

Chapter 8

Production

8.1 Technical Drawings

Technical drawings are made for the mechanical components of the design. They can be found in appendix (B). It should be noted that SKF recommends very tight run-out tolerances for bearing seats and abutments (Ref skf handbook). Due to the hollow rotor and housing design it is very hard to meet these requirements. However, the recommended values are meant for a long lifespan of the components. Because of the shorter lifespan of the traction motors in Revolve, these tolerance requirements have been relaxed to yield manufacturable parts. This is reflected in the technical drawings.

8.2 Manufacturing Procedure

To ensure the final design is realizable, the whole manufacturing procedure was assessed once the first initial design was proposed. An assembly manual was created and is given in appendix (C). However, some significant design changes have been carried out for the final design, which are not reflected in the as-

sembly manual. The major differences are rotor topology and integration of IR sensor, but apart from that the manual describes the assembly procedure quite well.

The main steps in manufacturing the parts not covered in appendix (C) are given below:

- **Rotor Assembly**

First the three piece shaft is machined and shrink fitted together to form a complete shaft. Run-out measurements should be done at this stage to verify it is within reasonable values (Dialogue with SKF). Then the segmented magnets are glued on to the shaft, followed by fitting of the balancing discs to either side. Finally, pre-impregnated carbon fibre is laid and cured directly on the finished assembly. Any surface irregularities of the carbon fibre can be ground down in a lathe to form a circular finish on the rotor. Balancing should be done at this stage before the rotor is ready for assembly.

- **Stator Segments**

Thin steel sheets are cut and laminated into a block of stack length 69 mm. The block is cut into stator segments, given in (appendix x), by a wire EDM machine. Each stator segment is wound by hand to produce the different coils of the motor with either 7 or 14 turns depending on the chosen phase connection. Careful measurements should be taken here to ensure the segments will go together without interference.

The rest of the main production steps are covered well by appendix (C). However, it should be noted that all manufacturing steps are general guidelines. If a better solution comes up through experience, the procedure should be

changed accordingly.

Chapter 9

Conclusion

The task at hand was to develop a tailored electric motor prototype for Revolve NTNU, capable of delivering high performance at low weight, as a step to further optimize the individual-wheel motor concept for the future. The motivation behind the development project was to give Revolve a more flexible motor choice for four wheel drive, as there are very few commercial products that can deliver the necessary performance within a 10-inch rim. Furthermore, developing a motor in-house yields technical know-how on an essential part of the electric powertrain, enabling the organization to do incremental changes on the design from year to year to pursue perfection.

Although there was not enough time to produce the prototype, a final design is set and ready for the production phase. It features a $\text{Ø}100\text{mm} \times 110\text{mm}$ motor that weighs in at 3.7kg. Compared to the commercial AMK motor at $\text{Ø}96\text{mm} \times 110\text{mm}$ and 3.55kg, it is slightly larger and heavier but has a lower total density. A larger motor will typically provide better performance as there is space for more copper and magnets. However, as the motor's performance is

very dependent on external cooling and inverter control, a prototype must be built and benchmark tested to validate real performance.

As the task was to specially tailor a motor prototype for Revolve NTNU, careful analysis was done from the start to map vehicle limitations into motor requirements. The most evident requirement is compatibility with interfacing systems. However, the tire grip is a major limiting factor in all kinds of racing applications, as all forces the powertrain produces have to be transferred through the four small contact patches between the tires and the road. Because of this, thorough analysis was done in order to yield estimates of available grip, and this result was used to set the desired performance on the motor.

Revolve NTNU uses a small motor that connects to a planetary gearbox to make up the mechanical part of the powertrain. However, this choice is mainly based on the poor availability of high performance motors on the commercial market. An important part of the motor development process was to evaluate alternative implementations of an in-wheel electric motor. Based on desired performance from the vehicle analysis, the mostway to get sufficient power density into a 10-inch rim is to continue using the same concept.

One of the main design challenges for developing an in-wheel motor for 10-inch rims is the necessity for a very compact packed design to deliver required performance. By gaining knowledge on all included systems, external requirements and manufacturing limitations, a very compact design could be realized with extensive use of computer aided design. Besides pure performance, design

for manufacturing and assembly were in a high focus during the functional design stage in order to facilitate prototyping. This was regarded as an important success factor for the prototype project as Revolve has virtually no experience in motor manufacturing.

An initial magnetic design was set by the use of well known design layouts that exhibit high performance. The chosen layout was then optimized by the use of FE-simulations. Over 300 parametric sweeps were run to map the responses of the motor. In three different sweeps, the geometric parameters were determined to optimize the motor constant. However, by comparing the optimized design to the initial, the difference in magnetic output was found to be small. This indicates that once the outer diameter, layout and materials of the motor are set, there are only minor margins to be gained in modifications of the internal geometry, except adding more magnet volume. Because of this, the rotor diameter was pushed to be large as it could be hollow, saving significant amounts of weight. The final design had somewhat lower magnetic performance, but facilitated manufacturing of the end bell and saved 236g from the initial.

The optimization was based on maximization of the motor constant at a single operating temperature. This is a very simplified approach to the real problem. However, accounting for time and temperature variable effects and potentially external systems like inverter and cooling makes the optimization very complex due to the considerable increase of input and output parameters. Furthermore, the gains vs. effort of such an analysis can be questioned as there are inherent uncertainties and limitations to the modelling. One is the actual

copper fill factor and end turn length, another is the estimation of core losses. However, by calibrating a more complex computer model to real geometry and data from a prototype could yield further insight and possibly open for optimization for the next prototype iteration.

When the optimized performance was finished, a mechanical assessment was conducted to investigate potential vibration problems. As there are no large loads acting on the motor, the possible failure modes of a mechanical character are related to vibration. Especially resonance on the shaft in a torsional mode is dangerous, as shafts typically inhibit very little damping in torsion. A potential vibrational issue was discovered running at maximum speed over a larger time interval. The natural frequency in torsion can be increased by either increasing the shaft stiffness or decreasing its rotational inertia. However, as most of the compliance comes from the shaft segment at the bearing and spline, which is very limited in geometry, the shaft's torsional stiffness cannot be increased by any significant amount. The most considerable way to increase the natural frequency is therefore to reduce the rotational inertia, which can primarily be done in two ways: By making the shaft shorter, at the expense of decreased magnetic performance, or by reducing the radius of the rotor, compromising on the total motor weight and integration of the rotor temperature sensor.

Real motor performance is very dependent on the manufacturing quality. Geometrical and material tolerances of the magnetic and mechanical system are important to yield a smooth running motor with minor vibration and smooth torque output. The quality in core lamination and winding is important to

achieve high fill factor and minimal amounts of winding end turns, utilizing the available space to the fullest. Because of this, manufacturing of a prototype would be the next natural step in the development process. A general manufacturing procedure is already planned out, but it needs to be refined through physical experimentation. Furthermore, the first prototype will yield important real performance data that will yield further insight into operation and hopefully show the way towards future incremental optimization of the motor.

Bibliography

- [9] Dr. Duane Hanselman. *Brushless Motors: Magnetic Design, Performance, and Control*. 2012. ISBN: 978-0-9826926-1-5.
- [11] Dr. Dr. Harald Neudorfer. *Comparison of three different electric power-trains for the use in high performance Electric Go-Kart*. September 2007. ISBN: 978-1-4244-0890-0.
- [12] James R. Hendershot Jr. *AC, Brushless, Switched Reluctance Motor Comparisons*. URL: http://www.jimhendershot.com/Jim_Hendershot/Articles_files/acbrushlessssrmotorcomparison.pdf (visited on 07/20/2016).
- [16] ANSYS. *ANSYS Electromagnetics Suite 16.2, Documentation*.
- [17] Andre Alexander Laleng. *Early Stage Development of an Electric Motor, Project Thesis*. December 2015.
- [19] Hans B. Pacejka. *Tire and Vehicle Dynamics, Second Edition*. 2006. ISBN: 80-0-7506-6918-4.
- [22] Enstroy Motor Company. *Manual for EMRAX motors*. December 2014. URL: <http://www.enstroj.si/Electric-products/emrax-motorsgenerators.html> (visited on 07/20/2016).
- [26] Fridtjov Irgens. *Formelsamling mekanikk*. 1999. ISBN: 9788251915069.
- [27] SKF. *Rolling bearings and seals in electric motors and generators*. 2013.

-
- [28] SKF. *Rolling bearings - Product Catalogue*. 2013.
- [40] Gunnar Härkegård. *Dimensjonering av maskindeler*. 2004. ISBN: 82-519-1970-3.
- [41] Wei Tong. *Mechanical Design of Electric Motors*. 2014. ISBN: 978-1-4200-9143-4.
- [45] Jouni Ikäheimo Sami Ruoho Jere Kolehmainen. *Temperature Dependence of Resistivity of Sintered Rare-Earth Permanent-Magnet Materials*. 2010.
- [46] Lin Yoon Se Young. *Control of Surge in Centrifugal Compressors by Active Magnetic Bearings*. 2013. ISBN: 978-1-4471-4240-9.

Online Resources

- [1] Institution of Mechanical Engineers. *About Formula Student*. URL: <http://events.imeche.org/formula-student/about-us> (visited on 09/15/2015).
- [2] Society of Automotive Engineers. *About Formula SAE series*. URL: <http://students.sae.org/cds/formulaseries/about.htm> (visited on 09/15/2015).
- [3] Formula Student Germany. *Disciplines*. URL: <https://www.formulastudent.de/fsg/about/disciplines/> (visited on 09/15/2015).
- [18] SAE International. *2015 Formula SAE Rules*. URL: http://students.sae.org/cds/formulaseries/rules/2015-16_fsae_rules.pdf (visited on 07/20/2016).
- [20] FSUK. *FSUK 2015 Skid Pad Results*. URL: <http://formulastudent.imeche.org/docs/default-source/FS2015-Results/2015-skidpad-result-final.pdf?sfvrsn=0> (visited on 07/20/2016).
- [21] FSG. *FSG 2015 Acceleration Results*. URL: <https://www.formulastudent.de/fse/2015/results/> (visited on 07/20/2016).
- [31] Arnold Magnetics. *NdFeB Product List*. URL: <http://www.arnoldmagnetics.com/en-us/Products/Neodymium-Magnets> (visited on 07/20/2016).
- [32] Arnold Magnetics. *SmCo Product List*. URL: <http://www.arnoldmagnetics.com/en-us/Products/RECOMA-SmCo-Magnets-en> (visited on 07/20/2016).

- [33] Vacuumschmelze. *Soft Magnetic Cobalt-Iron-Alloys*. URL: http://www.vacuumschmelze.com/fileadmin/docroot/medialib/documents/broschueren/htbrosch/Pht-004_e.pdf (visited on 07/20/2016).
- [34] Arnold Magnetics. *Arnon Electrical Steel*. URL: <http://www.arnoldmagnetics.com/en-us/Products/Arnon-Electrical-Steel> (visited on 07/20/2016).
- [35] Engineering Toolbox. *Metals and Alloys - Densities*. URL: http://www.engineeringtoolbox.com/metal-alloys-densities-d_50.html (visited on 07/20/2016).
- [36] Engineering Toolbox. *Resistivity, Conductivity and Temperature Coefficients for common Materials*. URL: http://www.engineeringtoolbox.com/resistivity-conductivity-d_418.html (visited on 07/20/2016).
- [37] Engineering Toolbox. *Thermal Conductivity of Metals*. URL: http://www.engineeringtoolbox.com/thermal-conductivity-metals-d_858.html (visited on 07/20/2016).
- [38] Cooner Wire. *Product Catalogue, rev. 9.8*. URL: http://www.coonerwire.com/cooner_catalog_rev9-8.pdf (visited on 07/20/2016).
- [43] Interlloy. *1045 MEDIUM TENSILE CARBON STEEL BAR*. URL: <http://www.interlloy.com.au/our-products/carbon-steels/1045-medium-tensile-carbon-steel-bar/?output=pdf> (visited on 07/20/2016).
- [44] AZO Materials. *Titanium Alloys - Ti6Al4V Grade 5*. URL: <http://www.azom.com/article.aspx?ArticleID=1547> (visited on 07/20/2016).

Figure References

- [4] Electronics-micros. URL: <http://www.electronics-micros.com/electrical/b-h-curve/> (visited on 07/20/2016).
- [5] Northeastern. URL: <http://www.northeastern.edu/amml/mom/electromagnets.html> (visited on 07/20/2016).
- [6] Geek3. URL: https://en.wikipedia.org/wiki/Force_between_magnets#/media/File:VFpt_cylindrical_magnets_repelling.svg (visited on 07/20/2016).
- [7] Boundless. URL: <https://www.boundless.com/physics/textbooks/boundless-physics-textbook/induction-ac-circuits-and-electrical-technologies-22/magnetic-flux-induction-and-faraday-s-law-161/faraday-s-law-of-induction-and-lenz-law-569-6693/images/lenz-law/> (visited on 07/20/2016).
- [8] Electronics Tutorials. URL: <http://www.electronics-tutorials.ws/electromagnetism/magnetic-hysteresis.html> (visited on 07/20/2016).
- [10] HubPages. URL: <http://hubpages.com/technology/Hysteresis-loss-and-eddy-current-losses-Core-losses-types> (visited on 07/20/2016).

- [13] Yokogawa. URL: <http://www.dpaonthenet.net/article/62178/Optimising-new-motor-designs-for-electric-vehicle.aspx#> (visited on 07/20/2016).
- [14] Biezl. URL: https://en.wikipedia.org/wiki/Skin_effect#/media/File:Skin_depth.svg (visited on 07/20/2016).
- [15] Osco. URL: <http://www.osco.uk.com/products/cable-and-litz-wire/litz-wire-winding-wire> (visited on 07/20/2016).
- [23] Electricbike. URL: <https://www.electricbike.com/wp-content/uploads/2014/04/MotorAxialRadial.png> (visited on 07/20/2016).
- [24] Rclab. URL: <http://www.rclab.info/2014/01/the-basics-of-electric-power-brushless.html> (visited on 07/20/2016).
- [25] Industrialmaks. URL: <http://industrialmaks.com/> (visited on 07/20/2016).
- [29] Zureks. URL: https://upload.wikimedia.org/wikipedia/commons/4/44/Magnetic_energy.png (visited on 07/20/2016).
- [30] Arnold Magnetics. URL: <http://www.arnoldmagnetics.com/en-us/SmCo-vs-Neo> (visited on 07/20/2016).
- [39] K&J Magnetics. URL: <https://www.kjmagnetics.com/blog.asp?p=halbach-arrays> (visited on 07/20/2016).
- [42] Fagor Automation. URL: <http://www.fagorautomation.com/en/mecanizado-por-descarga-electrica-3/> (visited on 07/20/2016).

List of Figures

1.1	Endurance event at FSG 2014	12
1.2	Formula Student Germany 2013	12
1.3	Discipline scoring distribution in FSG	13
1.4	2012 car KA Borealis R [Sofie Brovold]	14
1.5	2013 car KA Aquilo R [Sofie Brovold]	15
1.6	2014 car KOG Arctos R [Torbjørn Buvarp]	15
1.7	2015 car Vilje [Martin Eie]	16
3.1	Main Motor Topologies	24
3.2	A general nonlinear BH curve [4]	25
3.3	Common Magnetic Field Sources	27
3.4	Electromagnetic Induction [7]	29
3.5	Magnetization curves of soft magnetic materials [8]	30
3.6	Electromagnetic Induction [8]	31
3.7	Eddy current loss in conductive materials [10]	33
3.8	Typical PMM in-runner cross section	37
3.9	Lap and concentrated windings, respectively [13]	38
3.10	Magnetic Circuit in motor ([9], fig. 4-1b)	41
3.11	Current Distribution in an AC conductor [14]	48
3.12	Litz Wire Construction [15]	48

3.13	Normalized Motor Constant vs Radius Ratio	55
3.14	Optimized Normalized Motor Constant vs Pole Count	56
4.1	Electric Powertrain Overview [17]	58
4.2	Revolve Accumulator 2015	59
4.3	Internal Resistance Relation [17]	60
4.4	Accumulator Voltage vs Energy Used [17]	60
4.5	Inverter and Motor Phase Connections	62
4.6	Δ -connection [17]	63
4.7	Simulink PWM Generator [17]	64
4.8	Fundamental Harmonic Fraction vs M-ratio [17]	64
4.9	Vector Control Block Diagram ([9], fig. 10-8)	65
4.10	Suspension and Rim Model [17]	66
4.11	Transmission and Motor	67
4.12	Tire Testing at Calspan [Calspan]	69
4.13	Least Square Fit of Tire Data	70
4.14	Fitted Normalized Curves for F_x [17]	71
4.15	Fitted Normalized Curves for F_y [17]	71
4.16	Skid Pad Layout ([18], p. 160)	73
4.17	Simulink Acceleration Model [17]	74
4.18	Finishing Time vs Grip and Efficiency [17]	75
4.19	Vehicle Acceleration Envelope [17]	76
4.20	Wheel Traction [17]	76
4.21	Proposed Motor Performance [17]	77
4.22	Desired Torque-Power Curve [17]	77
4.23	Optimum Lap [17]	78
4.24	Torque at Rear Wheel [17]	79
4.25	Simulation Verifications [17]	80

5.1	The Emrax Motor Family [22]	82
5.2	Peak Torque Density Relation [17]	83
5.3	Continuous Torque Density Relation [17]	83
5.4	Motor Weight Relation [17]	84
5.5	Rim Integrated Motor [17]	85
5.6	Upright Integrated Motor [17]	86
5.7	Modular Concentric Motor [17]	86
5.8	Modular Parallel Motor [17]	87
5.9	Radial vs Axial Motor [23]	89
5.10	Radial in-runner vs out-runner [24]	89
5.11	Cooling Concepts	90
5.12	Flow Lines through External Cooling System	91
6.1	Heidenhain ECI1100 Mock-up	96
6.2	The CT-CF02-C3 infrared sensor	97
6.3	Hylec Cable Gland	98
6.4	Deutsch ASDD006-09SKT-HE3	98
6.5	5-Axis Milling [25]	99
6.6	Mechanical Connection	101
6.7	Adapter Plate Connection	102
6.8	Hub and Transmission Interface	103
6.9	Adapter Plate	103
6.10	Cooling Sleeve	104
6.11	Encoder Integration	105
6.12	IR Sensor Mounting	106
6.13	Extended Sensor Compartment	107
6.14	Ground Cable Connection	108
6.15	Two Piece Design	109
6.16	Three Piece Design	110

6.17 Split Housing	112
6.18 Indeterminate Load Direction ([27], p. 67)	114
6.19 Bearing Temperature Gradients ([28], p.167)	115
6.20 Performance vs Preload ([28], p.212)	115
6.21 Hybrid Bearings ([27], p. 28)	117
6.22 Encoder Mounting Integration	119
6.23 Bearing Integration	120
6.24 Drive Side Bearing Assembly	121
6.25 Seal Integration and Bearing Retainment	122
6.26 Integration of wave washer at non-locating bearing	124
6.27 Max Energy Product [29]	126
6.28 Magnet Performance [30]	127
6.29 Magnetization Curves: SiFe vs CoFe	130
6.30 Core Losses: SiFe vs CoFe	131
6.31 Estimated Core Losses at 1.4T Peak Flux	134
6.32 Chosen slot and winding layout ([9], p. 376	137
6.33 Surface Mounted Magnets	138
6.34 Halbach Array [39]	139
6.35 Internal Spoke Magnets	140
6.36 Buried Magnets	141
6.37 Rotor Assembly	142
6.38 Free Body Diagram for One Magnet Segment	144
6.39 Required Sleeve Thickness for a 6mm Magnet Height	145
6.40 Shaft Assembly Cutout	146
6.41 Single Piece Core	148
6.42 Segmented Core	148
6.43 Wire EDM Machine [42]	150
6.44 Magnetic System Integration	152

6.45	O-ring installed in bearing seat	154
6.46	Interference Fit Between Core and Housing	155
6.47	Material Selection for Rotor Components	156
6.48	Calculator Input Parameters and Analytical Relations	160
6.49	Various Outputs for Single Fits	160
6.50	Contact Pressure Matrix for Double Fits	160
6.51	Bearing-Sleeve Contact Pressure Matrix	162
6.52	Shaft-Sleeve Contact Pressure Matrix	163
6.53	The bearing sleeve has different pressure sections	164
6.54	Technical Drawing of Stator Segment	165
7.1	Parametric Model	171
7.2	Simulation showing tooth field lines split at yoke intersection.	172
7.3	Thick lines are directional magnetic field probes	173
7.4	Visualization of the FE-mesh	175
7.5	Torque vs Mesh Variation	175
7.6	Minimum Directional Magnet Flux vs Mesh Variation	176
7.7	Magnetic Field Distribution	177
7.8	Motor Output Torque	177
7.9	Minimum Magnet Flux	178
7.10	Stator Core Losses	178
7.11	Motor Steel Flux Densities	179
7.12	Correlation between Magnet Height and Motor Constant	181
7.13	Goodness of Response Surface Fit	182
7.14	Response Surface for 0.5mm Rotor Yoke	183
7.15	Response Surface for 3mm Rotor Yoke	183
7.16	Correlation between Magnet Height and Motor Constant	186
7.17	Correlation between Magnet Height and Magnet Flux	186
7.18	Goodness of Response Surface Fit	187

7.19	Response Surface for $J_{rms} = 5$	188
7.20	Response Surface for $J_{rms} = 15$	188
7.21	Response Surface for $J_{rms} = 20$	189
7.22	Response Surface for $J_{rms} = 25$	189
7.23	Response Surface for $J_{rms} = 5$	190
7.24	Response Surface for $J_{rms} = 15$	190
7.25	Response Surface for $J_{rms} = 20$	191
7.26	Response Surface for $J_{rms} = 25$	191
7.27	Correlation between Magnet Height and Motor Constant	193
7.28	Correlation between Magnet Height and Magnet Flux	193
7.29	Motor Constant Response Surface	194
7.30	Magnet Flux Response Surface	195
7.31	Motor Constant Comparison	196
7.32	Minimum Magnet Flux Comparison	196
7.33	Back EMF at $J_{rms} = 0$	198
7.34	Back EMF at $J_{rms} = 25$	199
7.35	Back EMF vs Number of Turns	200
7.36	Motor Current vs Number of Turns	201
7.37	Motor Winding Layout	202
7.38	Permanent Magnet Skin Depth vs Frequency	203
7.39	Strong Air Gap Flux between Rotor and Stator	204
7.40	Jeffcott Rotor ([46], fig. 2.1a)	205
7.41	Stator Mesh	206
7.42	Hollow Hub Interface Cross Section	207
7.43	Hub Boundary Conditions	208
7.44	Adapter Bolt Connections	209
7.45	Deformations due to Load in Seat 1	210
7.46	Deformations due to Load in Seat 2	210

7.47 Rotor Mesh	212
7.48 Distributed Magnet Mass	213
7.49 Flexible Shaft Support	214
7.50 Campbell Diagram	215
7.51 Fundamental Conical Mode	216
7.52 Torsional Mode	216
7.53 Axial Mode	217
7.54 Secondary Conical Mode	217
7.55 Added Model Mass	218
7.56 Fundamental Cantilever Mode	218
7.57 Torsional Mode	219

List of Tables

3.1	Motor Comparison	36
5.1	Sample Motor Parameters	82
5.2	Concept Evaluation	88
5.3	Product Specification Form	93
6.1	Housing Design Comparison	111
6.2	Non-locating bearing selection	119
6.3	Locating bearing selection	123
6.4	Demagnetization Temperatures	128
6.5	Magnet Material Parameters	128
6.6	Coil Material [35] [36] [37]	132
6.7	Valid 10 pole layouts	136
6.8	Qualitative Winding Comparison	136
6.9	Qualitative Rotor Comparison	141
6.10	Stator Core Design Comparison	149
6.11	Stator Core Manufacturing	150
6.12	Ferromagnetic Engineering Materials, Quenched and Tempered	153
6.13	Non-Magnetic Engineering Materials	153
6.14	Recommended SKF 6005 Fits	161

6.15	Recommended SKF 6003 Fits	164
6.16	Stator Core Tolerances	166
6.17	Stator Core Fit	166
7.1	Rotor Inertia Comparison	185
7.2	Estimated Weight of Magnetic System	197
7.3	Terminal Back EMF Constants	199
7.4	Radial Bearing Stiffness	206
7.5	Bearing Seat Deformations	211
7.6	Rotor Support Stiffness	211
7.7	Motor Natural Frequencies	219

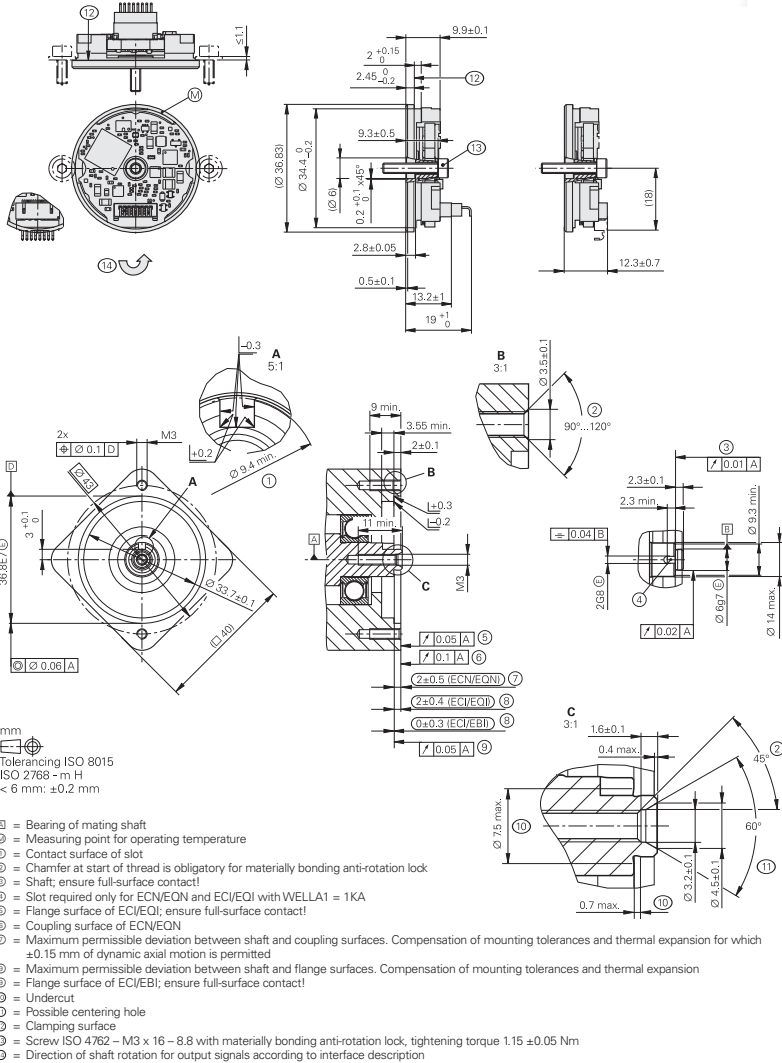
Appendix A

Data Sheets

A.1 Heidenhain ECI1100

ECI/EBI 1100 series

- Absolute rotary encoders
- Flange for axial mounting
- Blind hollow shaft
- Without integral bearing
- EBI 1135: Multiturn function via battery-buffered revolution counter



	Absolute	
	ECI 1118	EBI 1135
Interface	EnDat 2.2	
Ordering designation	EnDat22 ¹⁾	
Position values/revolution	262 144 (18 bits)	262 144 (18 bits; 19-bit data word length with LSB = 0)
Revolutions	–	65 536 (16 bits)
Calculation time t_{cal} Clock frequency	≤ 6 μs ≤ 8 MHz	
System accuracy	± 120"	
Electrical connection	Via 15-pin PCB connector	
Voltage supply	DC 3.6 V to 14 V	<i>Rotary encoder U_P</i> : DC 3.6 V to 14 V <i>Buffer battery U_{BAT}</i> : DC 3.6 V to 5.25 V
Power consumption (max.)	<i>Normal operation, 3.6 V:</i> 0.52 W <i>Normal operation, 14 V:</i> 0.6 W	
Current consumption (typical)	5 V: 80 mA (without load)	<i>Normal operation, 5 V:</i> 80 mA (without load) <i>Buffer battery²⁾:</i> 22 μA (with rotating shaft) 12 μA (at standstill)
Shaft	Blind hollow shaft Ø 6 mm, axial clamping	
Mech. perm. speed n	≤ 15 000 rpm	≤ 12 000 rpm
Mech. perm. acceleration	≤ 10 ⁵ rad/s ²	
Moment of inertia of rotor	0.2 · 10 ⁻⁶ kgm ²	
Permissible axial motion of measured shaft	± 0.3 mm	
Vibration 55 Hz to 2000 Hz Shock 6 ms	≤ 300 m/s ² (EN 60 068-2-6) ≤ 1000 m/s ² (EN 60 068-2-27)	
Max. operating temp.	115 °C	
Min. operating temp.	–20 °C	
Protection EN 60 529	IP00 ³⁾	
Mass	≈ 0.02 kg	
Valid for ID	728563-xx	820725-xx

¹⁾ External temperature sensor and online diagnostics are not supported. Compliance with the EnDat specification 297403 and the EnDat Application Notes 722024, Chapter 13, *Battery-buffered encoders*, is required for correct control of the encoder.

²⁾ At T = 25 °C; U_{BAT} = 3.6 V

³⁾ CE compliance of the complete system must be ensured by taking the correct measures during installation.

A.2 Micro-Epsilon CT-CF02-C3

Model		CT-SF02-C3	CT-SF15-C3	CT-SF22-C3
Optical resolution		2:1	15:1	22:1
Temperature range ¹		-50°C to 600°C	-50°C to 600°C	-50°C to 975°C
Spectral range		8 to 14µm		
System accuracy ²		±1% or ±1°C		
Repeatability ²		±0.5% or ±0.5°C		
Temperature resolution		±0.1°C		
Response time		150ms (95%)		
Emissivity/gain ¹		0.100 to 1.100		
Transmissivity/gain ¹		0.100 to 1.100		
Signal processing ¹		peak hold, valley hold, average, extended hold function with threshold and hysteresis		
Certificate of calibration		optional		
Outputs/analogue	channel 1 channel 2 optional	0/4 to 20mA, 0 to 5/10V, thermocouple J, K sensor temperature (-20 to 180°C as 0 to 5V or 0 to 10V), alarm output relay: 2 x 60VDC/ 42VACelf; 0.4A; optically isolated		
Outputs/digital	optional	USB, RS232, RS485, CAN, Profibus DP, Ethernet		
Output impedances	current output voltage output	mA max. 500Ω (with 8 to 36VDC) mV min. 100kΩ load impedance thermocouple 20Ω		
Inputs		programmable functional inputs for external emissivity adjustment, ambient temperature compensation, trigger (reset of hold functions)		
Cable length		1m, 3m (standard), 8m, 15m		
Power supply		8 to 36VDC; max. 100mA		
Environmental rating		IP 65 (NEMA-4)		
Ambient temperature	sensor controller	-20°C to 130°C	0 °C to 85°C	-20°C to 180°C
Storage temperature	sensor controller	-40°C to 130°C	-40°C to 85°C	-40°C to 180°C
Relative humidity		10 - 95%, non condensing		
Vibration	sensor	IEC 68-2-6: 3 G, 11 to 200Hz, any axis		
Shock	sensor	IEC 68-2-27: 50 G, 11ms, any axis		
Weight		sensor: 40g; controller: 420g		

¹ adjustable via controller or software
² ± ambient temperature 23 ±5°C; whichever is greater

Accessories page 42 - 45

<ul style="list-style-type: none"> ▶ CF lens ▶ Protective window ▶ Mounting bracket / Mounting bolt ▶ Air purge collar ▶ Right angle mirror 	<ul style="list-style-type: none"> ▶ Rail mount adapter for controller ▶ Massive housing ▶ Protective tube ▶ Laser sighting tool ▶ Digital-Interface kit 	<ul style="list-style-type: none"> ▶ Relay output module ▶ Accessory-Kit for use of the CT in hazardous locations ▶ Software CompactConnect ▶ Certificate of calibration
--	---	--

A.3 AMK DD5



Motor-Datenblatt motor data sheet

Formular Student Datum/date: 20.04.2015

Bezeichnung/name **DD5-14-10-POW** - 18600-B5

Teile-Nr./part number **A2370DD** Zeichn.-Nr./drawing no.:12703-01260

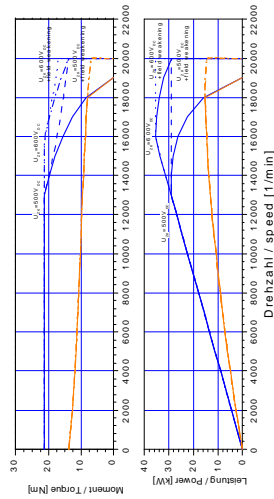
Motorbeschreibung motor description:

Motorprinzip/motor principle: synchron
 Kühlung/cooling type: Flüssigkeit
 Bauform/mounting type: IMB5
 Schutzart/degree of protection: IP 65
 Isolierklasse/insulation class: F

Leistungsdaten performance data:

Betriebsart/duty type: S1 $dT=80K$
 Dauerstillstandsmoment/continuous Stall Torque "M₀": 13,8 Nm
 Maximales Moment/maximum torque "M_{max}": 21 Nm
 Bemessungsmoment/rated torque "M_n" (ID32771): 9,8 Nm
 Bemessungsleistung/rated power "P_n": 12,3 kW
 Bemessungsdrehzahl/rated speed "n_n" (ID32772): 12000 rpm
 Theo. Leerlaufdrehzahl/theor. no-load-speed "n₀": 18617 rpm

Motorcharakteristiken performance - characteristics:



Kennlinie kann die maximal zulässige Drehzahl überschreiten! Characteristic may exceed technical speed limit of motor

Elektrische Daten electrical data:

Nennspannung/rated voltage "U_n" (ID32768): 350 V
 Nennstrom/rated current "I_n" (ID111): 41 Arms
 Dauerstillstandsstrom/cont. stall current "I₀" (ID34096): 53.1 Arms
 Maximalstrom/maximum current "I_{max}" (ID109): 100 Arms
 Maximale Dauer für/duration for "I_{max}" (ID34168): 1,24 s
 Drehmomentkonstante/torque constant "k_t": 0,26 Nm/Arms
 Spannungskonstante/voltage constant "k_e" (ID 34234): 18,8 V/kU/min
 Schaltung/connection type: D
 Polzahl/number of poles "2p" (ID32775): 10 Pole
 Klemmenwiderstand/terminal resistance "R_{kt}" (ID34164): 0,13 Ohm
 Klemmeninduktivität/terminal inductance "L_{kt}" (ID34167): 0,3 mH
 Querscheninduktivität/quadrature axis inductance "L_q" (ID34046): 0,54 mH
 Hauptachseninduktivität/direct axis inductance "L_d" (ID34045): 0,44 mH
 Magn.-Strom/magn. current "I_m" (ID32769): 70 Arms
 Magn.-Strom/magn. current "I_{m1}" (ID32770): 3,5 Arms
 Rotorzeitkonstante/rotor time constant "T_r" (ID32774): 0,01 s

Reglereinstellungen controller settings:

Stromregler current controller:

Verstärkung q-Achse/gain q-axis "K_{pd}" (ID34151): 1,62 V/A
 Verstärkung d-Achse/gain d-axis "K_{pd}" (ID34152): 1,72 V/A
 Nachstellzeitkonstante/time constant "T_{nd}" (ID34050): 1,2 ms
 Nachstellzeitkonstante/time constant "T_{nd}" (ID34052): 1,2 ms
 Adaption Verstärkung/adaption gain "K_{pa2}" (ID 34179): 20 %
 Adaption Nachstellzeit/adaption time constant "T_{nq2}" (ID 34180): 400 %
 Untere Anpaßschwelle/lower adaption limit "I_{ua}" (ID34177): 32 %
 Obere Anpaßschwelle/upper adaption limit "I_{oa}" (ID34178): 78 %

Drehzahlregler speed controller (default for plain motor):

Verstärkung/gain "K_{p_r}" (ID100): 40
 Nachstellzeitkonstante/time constant "T_{n_r}" (ID101): 10 ms

Spannungsregler voltage controller:

Spannungsregler/voltage controller "K_p" (ID34148): 0,08 A/V
 Spannungsregler/voltage controller "T_n" (ID34149): 6 ms
 Spannungsüberhöhung "G_u" (ID34235): 116 %
 Systemwiderstand "R_s" (ID34233): 0 Ohm

Für dieses Dokument und die darin enthaltenen Angaben behalten wir uns alle Rechte und technische Änderungen vor
 All rights reserved for this document and all information included. Technical modifications reserved
 (c) AMK Antriebs- und Steuerungstechnik GmbH Co. KG

Motor-Datenblatt motor data sheet



Bezeichnung/name **DD5-14-10-POW** - 18600-B5 - Formula Student Datum/date: 20.04.2015
 Teile-Nr./part numbe **A2370DD** Zeichn.-Nr./drawing no.: 12703-01260

Mechanische Daten mechanical data:

Gesamtmasse/motor mass "m": 3,55 kg
 Motorträgheitsmoment/inertia "J": 2,74 kgcm²
 Mech. zul. Drehzahl/mech. speed limit "Nmax": 20000 rpm
 Rundlauf/run out (DIN 42955): N
 Wuchtgüte/balancing quality: G2.5
 Schwingstärke/vibration level (DIN ISO 2373): N
 Passfedern/shaft key: -

Bremsendaten brake data:

Typ/type: -
 Bremsmoment/brake torque: Ntm
 Bremsstrom/brake current: A
 Bremsenspannung/brake voltage: V
 Spannungsart/voltage type: -
 Einfallzeit/engage time "Te": 0 ms
 max. Bremsenergie/max. braking energy: einmally/single engagement:
 Lebenslang/lifetime: J

Lüfterdaten fan data:

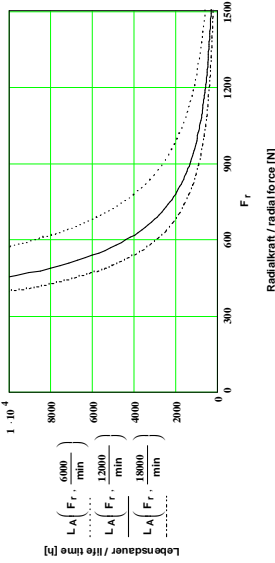
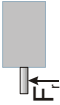
AMK-TNr./AMK part number: -
 Lüfterspannung/fan voltage: V
 Strom/current: A
 Frequenz/frequency: Hz

Wicklungsschutz thermistor:

Typ/type (ID34166): KTY84
 Ansprechtemp./operation temp: - °C
 Widerstand/resistance (25°C) <= : 629 Ω

Lagerbelastung bearing load:

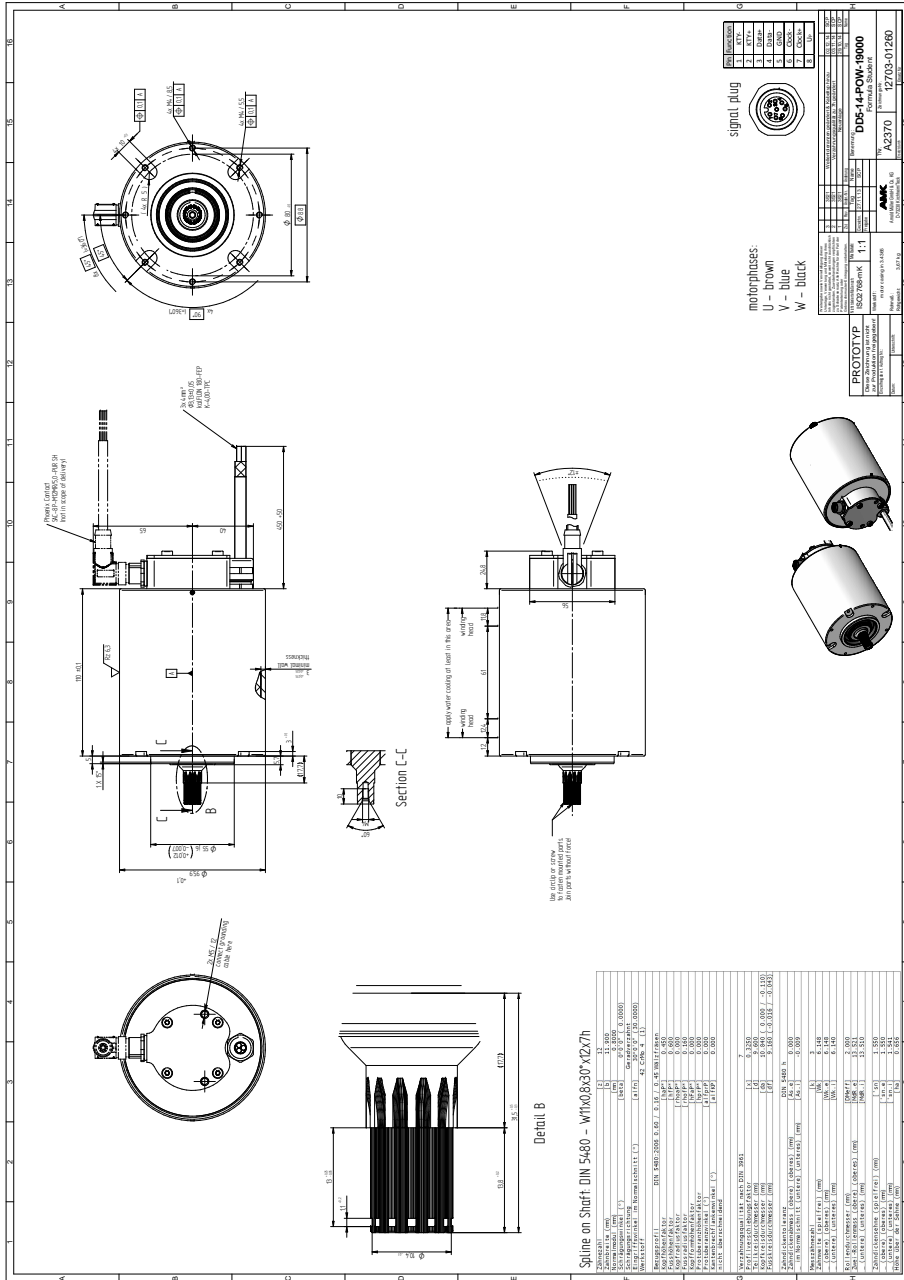
AMB - Lager/AB - side bearing:
 Lagerart/type of bearing: 6005 / 6003
 Fettsort/type of grease: GE2 / GE2
 theo. Fettgedauersdauer/grease life time: 13000 / 18000
 bei Nennrehzahl und 70°C Lagerlauf/runningtemp/rated speed and 158°F at outer bearing ring
 erforderliche Fettmenge/necessary grease quantity: 0 /
 Maximale Axialkraft bei Montage/max. axial force for assembly: 3275 N
A - Lager/A - side bearing:



Geberdaten position encoder data:

AMK-TNr./AMK part number: 108072 automatisch erstellt, Geber 18 Bit
 Typ/type: P
 Impulszahl/number of pulses: 262144
 Daten nur gültig mit entsprechender Wasserkühlung

Ersteller/created by: SMM Änderungsstatus Mechanik/revision motor-mechanics: 0.00 Änderungsdatum/motor revision motor date 30.03.2015
 Für dieses Dokument und die darin enthaltenen Angaben behalten wir uns alle Rechte und technische Änderungen vor.
 All rights reserved for this document and all information included. Technical modifications reserved (c) AMK Antriebs- und Steuerungstechnik GmbH Co. KG



A.4 N35EH



N35EH

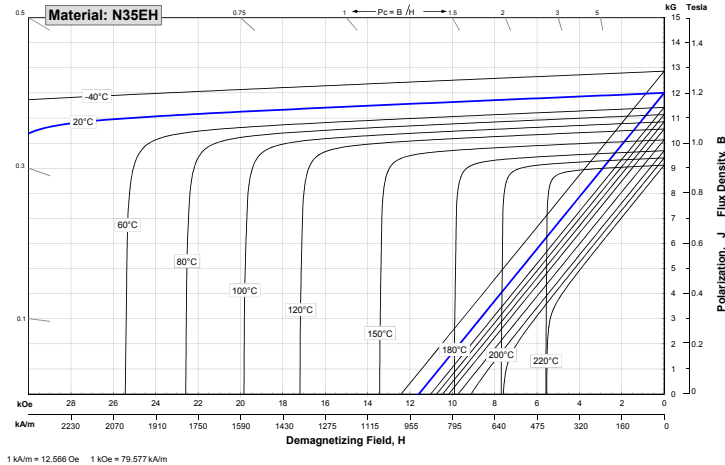
Sintered Neodymium-Iron-Boron Magnets

These are also referred to as "Neo" or NdFeB magnets. They offer a combination of high magnetic output at moderate cost. Please contact Arnold for additional grade information and recommendations for protective coating. Assemblies using these magnets can also be provided.

Characteristic	Units	Magnetic Properties		
		min.	nominal	max.
Br Residual Induction	Gauss	11,700	12,000	12,300
	mT	1170	1200	1230
H_B Coercivity	Oersteds	10,500	11,150	11,800
	kA/m	836	887	939
H_J Intrinsic Coercivity	Oersteds	30,000		
	kA/m	2,388		
BH_{max} Maximum Energy Product	MGOe	33	35	37
	kJ/m ³	263	279	295

Characteristic	Units	C //	C ⊥	
Thermal Properties	Reversible Temperature Coefficients ⁽¹⁾ of Induction, α(Br)	%/°C	-0.120	
	of Coercivity, α(Hc)	%/°C	-0.420	
	Coefficient of Thermal Expansion ⁽²⁾	ΔL/L per °C×10 ⁻⁶	7.5	-0.1
Thermal Conductivity	W / (m • K)		7.6	
Specific Heat ⁽³⁾	J / (kg • K)		460	
Curie Temperature, T _c	°C		310	
Other Properties	Flexural Strength	psi	41,300	
		MPa	285	
	Density	g/cm ³	7.5	
	Hardness, Vickers	Hv	620	
Electrical Resistivity, ρ	μΩ • cm		180	

Notes: (1) Coefficients measured between 20 and 200 °C
 (2) Between 20 and 200 °C (3) Between 20 and 140 °C



Notes The material data and demagnetization curves shown above represent typical properties that may vary due to product shape and size. Magnets can be supplied thermally stabilized or magnetically calibrated to customer specifications. Additional grades are available. Please contact the factory for information.

A.5 36CrNiMo6



Material No.: Code:

1.6582 34CrNiMo6

DE - Brand:

NCM**Chemical composition:**
(Typical analysis in %)

C	Cr	Mo	Ni				
0,34	1,50	0,25	1,50				

Steel properties:

CrNiMo-alloyed steel, supplied in quenched and tempered condition.

Applications:

Heavily loaded parts for mechanical engineering and motor construction.

Condition of delivery:

Quenched and tempered

Physical properties:

Thermal expansion coefficient $\left[\frac{10^{-6} \cdot \text{m}}{\text{m} \cdot \text{K}} \right]$ $\frac{20-100^\circ\text{C}}{12,1}$ $\frac{20-200^\circ\text{C}}{12,7}$ $\frac{20-300^\circ\text{C}}{13,2}$ $\frac{20-400^\circ\text{C}}{13,6}$

Thermal conductivity

$\left[\frac{\text{W}}{\text{m} \cdot \text{K}} \right]$ $\frac{20^\circ\text{C}}{33,7}$

Heat treatment:

Soft annealing

Temperature	Cooling	Hardness
650 - 680°C	furnace	max. 248 HB

Hardening

Temperature	Cooling	Tempering
830 - 860°C	oil	see tempering diagram

Mechanical properties in quenched and tempered condition (DIN EN 10083-1, 10/96)

Diameter d [mm]	< 16	>16 - 40	>40 - 100	>100 - 160	>160 - 250
Thickness t [mm]	< 8	8<t<20	20<t<60	60<t<100	100<t<160
Yield strength Re [N/mm ²]	min. 1000	min. 900	min. 800	min. 700	min. 600
Tensile strength Rm [N/mm ²]	1200 - 1400	1100 - 1300	1000 - 1200	900 - 1100	800 - 950
Elongation A [%]	min. 9	min. 10	min. 11	min. 12	min. 13
Reduction of area Z [%]	min. 40	min. 45	min. 50	min. 55	min. 55
Toughness CVN [J]	min. 35	min. 45	min. 45	min. 45	min. 45

0408

Dörrenberg Edelstahl GmbH · Hammerweg 7 · D-51766 Engelskirchen
Tel.: +49 22 63 / 79 1 · Fax: +49 22 63 / 79 20 5 · www.doerrenberg.deA company of the
GESCO group

A.6 42CrMo4



Material No.: Code:

1.7225 42CrMo4

DE - Brand:

M4S**Chemical composition:**
(Typical analysis in %)

C	Cr	Mo					
0,42	1,10	0,25					

Steel properties:

CrMo-alloyed steel, engineering steel supplied in quenched and tempered conditions. Good machinability.

Applications:

Components with high requirements on toughness, e.g. gear wheels, pinions, connecting rods, parts for mechanical engineering.

Condition of delivery:

Quenched and tempered

Physical properties:

Thermal expansion coefficient	$\frac{10^{-6} \cdot \text{m}}{\text{m} \cdot \text{K}}$	20-100°C	20-200°C	20-300°C	20-400°C
		12,1	12,7	13,2	13,6

Thermal conductivity

$\frac{\text{W}}{\text{m} \cdot \text{K}}$	20°C
	45,1

Heat treatment:

Soft annealing

Temperature	Cooling	Hardness
680 - 720°C	furnace	max. 241 HB

Normalizing

Temperature	Cooling	
850 - 880°C	air	

Hardening

Temperature	Cooling	Tempering
820 - 860°C	oil, water	see tempering diagram

Mechanical properties in quenched and tempered condition (DIN EN 10083-1, 10/96)

Diameter [mm]	< 16	>16 - 40	>40 - 100	>100 - 160	>160 - 250
Thickness t [mm]	< 8	8<t<20	20<t<60	60<t<100	100<t<160
Yield strength Re [N/mm ²]	min. 900	min. 750	min. 650	min. 550	min. 500
Tensile strength Rm [N/mm ²]	1100 - 1300	1000 - 1200	900 - 1100	800 - 950	750 - 900
Elongation A [%]	min. 10	min. 11	min. 12	min. 13	min. 14
Reduction of area Z [%]	min. 40	Min. 45	min. 50	min. 50	min. 55
Toughness CVN [J]	min. 30	min. 35	min. 35	min. 35	min. 35

0105

Dörrenberg Edelstahl GmbH · Hammerweg 7 · D-51766 Engelskirchen
Tel.: +49 22 63 / 79 1 · Fax: +49 22 63 / 79 20 5 · www.doerrenberg.deA company of the
GESCO group

A.7 AlumeC 89

ALUMEC 89

Properties

Physical data

Values at room temperature unless stated otherwise.

Density	kg/m ³ lbs/in ³	2 830 0.102
Modulus of elasticity	N/mm ² psi	71 500 10.3 x 10 ⁶
Coefficient of thermal expansion per °C from 20°C to 100°C per °F (68-212°F)		23 x 10 ⁻⁶ 12.8 x 10 ⁻⁶
Thermal conductivity	W/m °C Btu in/ft ² h °F	165 1 144
Specific heat capacity	J/kg °C Btu/lb °F	890 0.20

Tensile strength

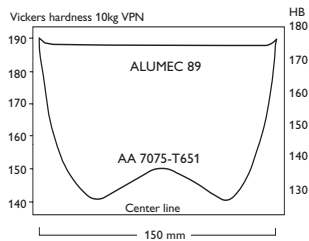
Tensile strength values, which for most practical purposes can be compared to compression strength values, should be regarded as typical.

Values at room temperature for different plate thicknesses.

	Tensile strength N/mm ²	Yield strength N/mm ²
Plate (thickness), mm		
> 10- 50	590	550
> 50-100	570	520
>100-150	550	500
>150-200	535	485
>200-300	430	365
Round bar Ø, mm		
40	680	630
100	680	620
200	670	610

Note that the plate is tested in the transverse direction and the round bar in the length direction.

HARDNESS DISTRIBUTION THROUGH THE PLATE CROSS SECTION



4

Machining

General

A major advantage when machining aluminium alloys is the possibility of using high cutting speeds. The reason is the low cutting force needed compared with steel and brass. Because of the excellent combination of mechanical and physical properties in AlumeC 89 the maximum cutting speed possible is very high, when suitable cutting tools are used. When using high speed milling machines, cutting speeds exceeding 3 500 m/min. (11 500 ft./min.) has been used with good results.

Cutting tool – design and material

Although aluminium alloys give low cutting forces, it is necessary to use high quality cutting tools. In order to achieve the highest possible cutting speed the use of cemented carbide tools, especially during turning and end milling, is ideal.

The same cutting tools normally used for steel can also be used for machining of AlumeC 89. However, for good production economy, tools with large positive angles should be used. The flute should have a large chip space and be polished to prevent chips clogging the cutter.

When sawing AlumeC 89, a coarse tooth saw blade is recommended.

Cooling/lubrication

The purpose of cutting fluid is to cool the work piece and to lubricate the cutting tool. Because of the high cutting speeds possible when machining AlumeC 89, cooling is important, although the heat conductivity of AlumeC 89 is very high. Good lubrication is of special importance during deep hole drilling, as there is a prolonged contact between chips and tool.

Cutting fluids recommended for steel may sometimes discolor the aluminium surface, if PH values are high. Most manufacturers of cutting fluid have universal fluids suitable for both steel and aluminium.

A.8 SS304



AK Steel Type 304 is a variation of the basic 18-8 grade, Type 302, with a higher chromium and lower carbon content. Lower carbon minimizes chromium carbide precipitation due to welding and its susceptibility to intergranular corrosion. In many instances, it can be used in the "as-welded" condition, while Type 302 must be annealed in order to retain adequate corrosion resistance.

Type 304L is an extra low-carbon variation of Type 304 with a 0.03% maximum carbon content that eliminates carbide precipitation due to welding. As a result, this alloy can be used in the "as-welded" condition, even in severe corrosive conditions. It often eliminates the necessity of annealing weldments except for applications specifying stress relief. It has slightly lower mechanical properties than Type 304.

Typical uses include architectural moldings and trim, kitchen equipment, welded components of chemical, textile, paper, pharmaceutical and chemical industry processing equipment.

AVAILABLE FORMS

AK Steel produces Type 304 Stainless Steel in thicknesses from 0.01" to 0.25" (0.025 to 6.35 mm) max. and widths up to 48" (1219 mm). For other thicknesses and widths, inquire.

COMPOSITION

	Type 304 %	Type 304L %
Carbon	0.08 max.	0.03 max.
Manganese	2.00 max.	2.00 max.
Phosphorus	0.045 max.	0.045 max.
Sulfur	0.030 max.	0.030 max.
Silicon	0.75 max.	0.75 max.
Chromium	18.00-20.00	18.0-20.0
Nickel	8.00-12.00	8.0-12.0
Nitrogen	0.10 max.	0.10 max.
Iron	Balance	Balance

SPECIFICATIONS

AK Steel Types 304 and 304L Stainless Steels are covered by the following specifications:

Type 304	Type 304L
AMS 5513	AMS 5511
ASTM A 240	ASTM A 240
ASTM A 666	ASTM A 666

MECHANICAL PROPERTIES

Typical Room Temperature Mechanical Properties

	UTS ksi (MPa)	0.2% YS ksi (MPa)	Elongation % in 2" (50.8 mm)	Hardness Rockwell
Type 304L	85 (586)	35 (241)	55	B80
Type 304	90 (621)	42 (290)	55	B82

304/304L-S-8-01-07

AK STEEL

304/304L STAINLESS STEEL DATA SHEET

PHYSICAL PROPERTIES

Density, 0.29 lbs/in³
8.03 g/cm³

Electrical Resistivity, microhm-in
(microhm-cm)

68°F (20°C) – 28.4 (72)
1200°F (659°C) – 45.8 (116)

Specific Heat, BTU/lb/°F (kJ/kg•K)
32 - 212°F (0 - 100°C) – 0.12 (0.50)

Thermal Conductivity, BTU/hr/ft²/ft/°F
(W/m•K)

at 212°F (100°C) – 9.4 (16.2)
at 932°F (500°C) – 12.4 (21.4)

Mean Coefficient of Thermal Expansion,
in/in/°F (µm/m•K)

32 - 212°F (0 - 100°C) – 9.4×10^{-6} (16.9)
32 - 600°F (0 - 315°C) – 9.6×10^{-6} (17.3)
32 - 1000°F (0 - 538°C) – 10.2×10^{-6} (18.4)
32 - 1200°F (0 - 649°C) – 10.4×10^{-6} (18.7)

Magnetic Permeability, H = 200
Oersteds, Annealed - 1.02 max.

Modulus of Elasticity, ksi (MPa)

28.0×10^3 (193 x 10³) in tension
 11.2×10^3 (78 x 10³) in torsion

Melting Range, °F (°C) – 2550 - 2650
(1399 - 1454)

CORROSION RESISTANCE

These steels exhibit excellent resistance to a wide range of atmospheric, chemical, textile, petroleum and food industry exposures.

OXIDATION RESISTANCE

The maximum temperature to which Types 304 and 304L can be exposed continuously without appreciable scaling is about 1650°F (899°C). For intermittent exposure, the maximum exposure temperature is about 1500°F (816°C).

HEAT TREATMENTS

Type 304 is non-hardenable by heat treatment. Annealing: Heat to 1900 - 2050°F (1038 - 1121°C), then cool rapidly. Thin strip sections may be air cooled, but heavy sections should be water quenched to minimize exposure in the carbide precipitation region.

Stress Relief Annealing: Cold worked parts should be stress relieved at 750°F (399°C) for 1/2 to 2 hours.

FORMABILITY

Types 304 and 304L have very good drawability. Their combination of low yield strength and high elongation permits successful forming of complex shapes. However, these grades work harden rapidly. To relieve stresses produced in severe forming or spinning, parts should be full annealed or stress-relief annealed as soon as possible after forming.

WELDABILITY

The austenitic class of stainless steels is generally considered to be weldable by the common fusion and resistance

techniques. Special consideration is required to avoid "hot cracking" by assuring formation of ferrite in the weld deposit. Types 304 and 304L are generally considered to be the most common alloys of this stainless class. When a weld filler is needed, AWS E/ER 308, 308L or 347 are most often specified. Types 304 and 304L Stainless Steels are well known in reference literature and more information can be obtained in this way.

METRIC CONVERSION

Data in this publication are presented in U.S. customary units. Approximate metric equivalents may be obtained by performing the following calculations:

Length (inches to millimeters) –
Multiply by 25.4

Strength (ksi to megapascals or
meganewtons per square meter) –
Multiply by 6.8948

Temperature (Fahrenheit to Celsius) –
(°Fahrenheit - 32) Multiply by 0.5556

Density (pounds per cubic inch to
kilograms per cubic meter) –
Multiply by 27,670

The information and data in this product data sheet are accurate to the best of our knowledge and belief, but are intended for general information only. Applications suggested for the materials are described only to help readers make their own evaluations and decisions, and are neither guarantees nor to be construed as express or implied warranties of suitability for these or other applications.

Data referring to mechanical properties and chemical analyses are the result of tests performed on specimens obtained from specific locations with prescribed sampling procedures; any warranty thereof is limited to the values obtained at such locations and by such procedures. There is no warranty with respect to values of the materials at other locations.

AK Steel and the AK Steel logo are registered trademarks of AK Steel Corporation.



Customer Service 800-331-5050

AK Steel Corporation
9227 Centre Pointe Drive
West Chester, OH 45069

www.aksteel.com

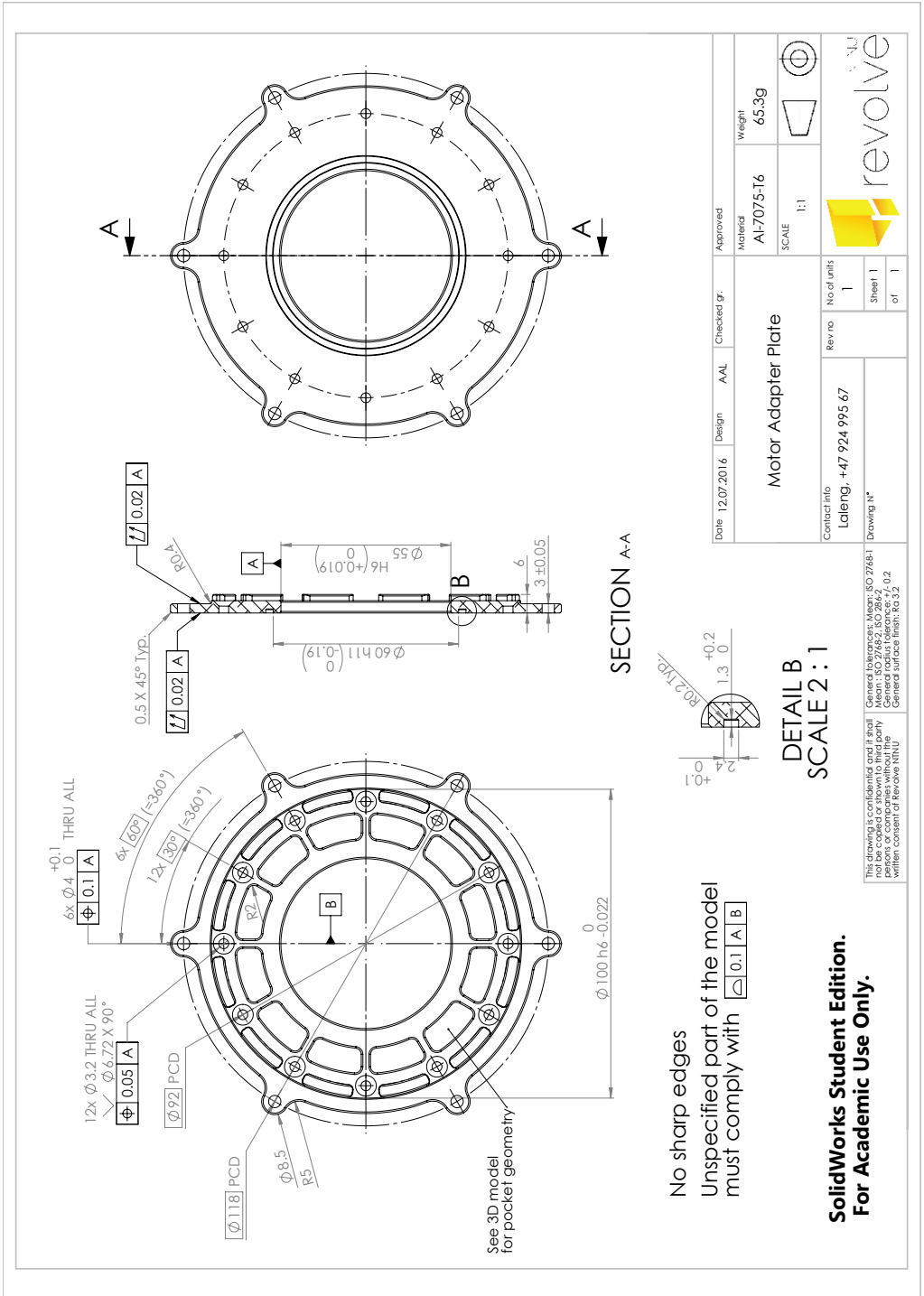
© 2007 AK Steel Corporation

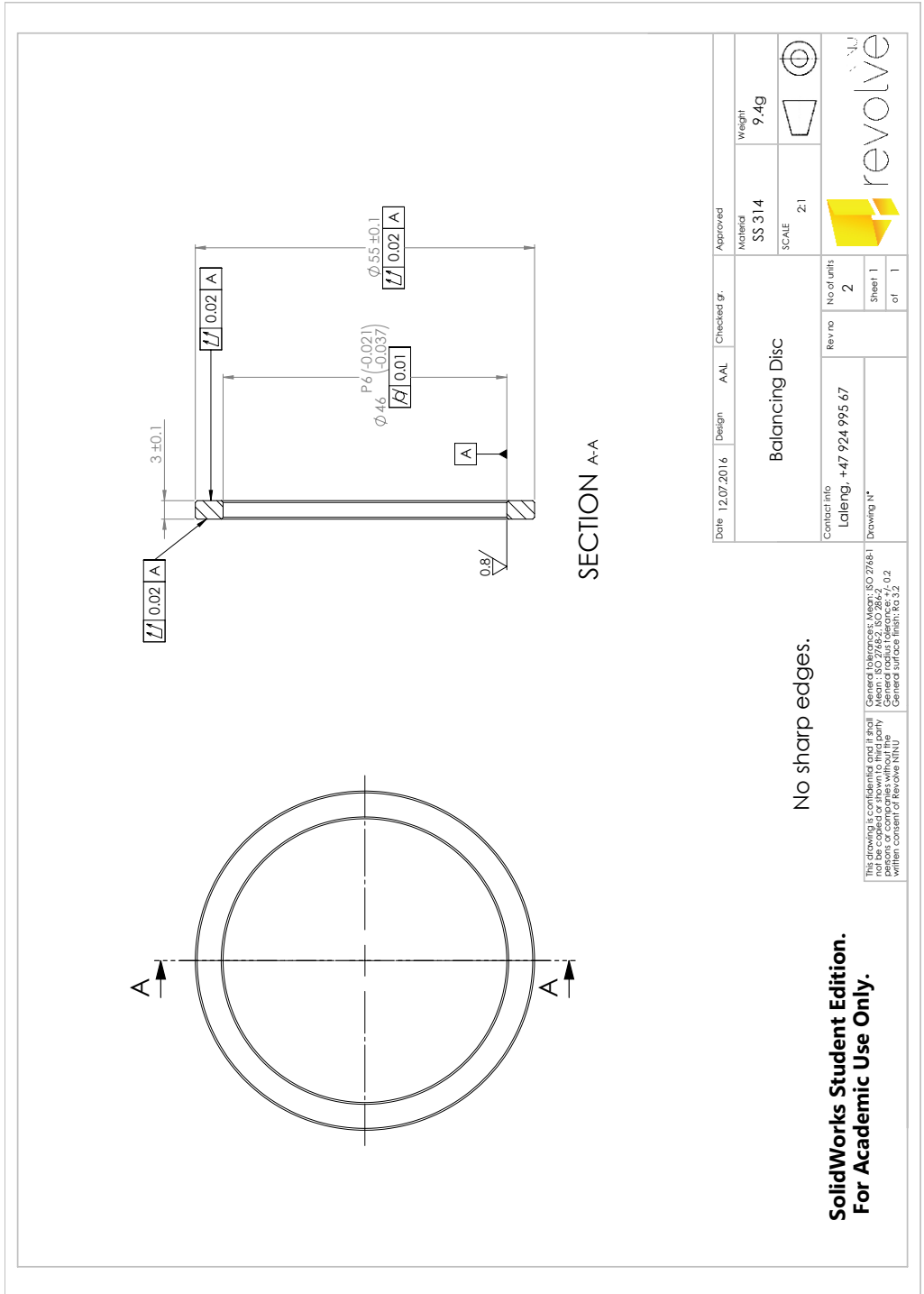


7100-0096 7/07

Appendix B

Technical Drawings



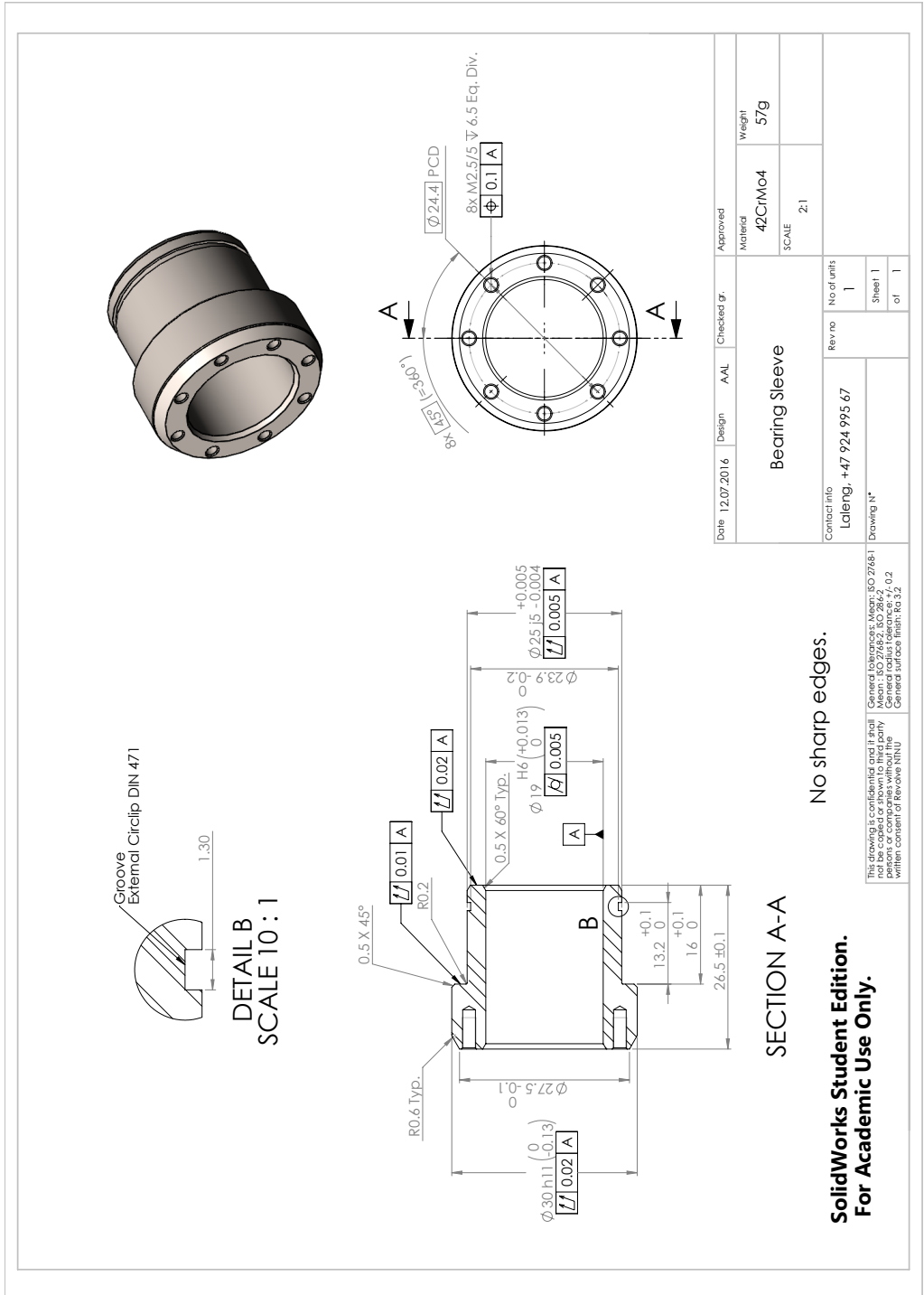


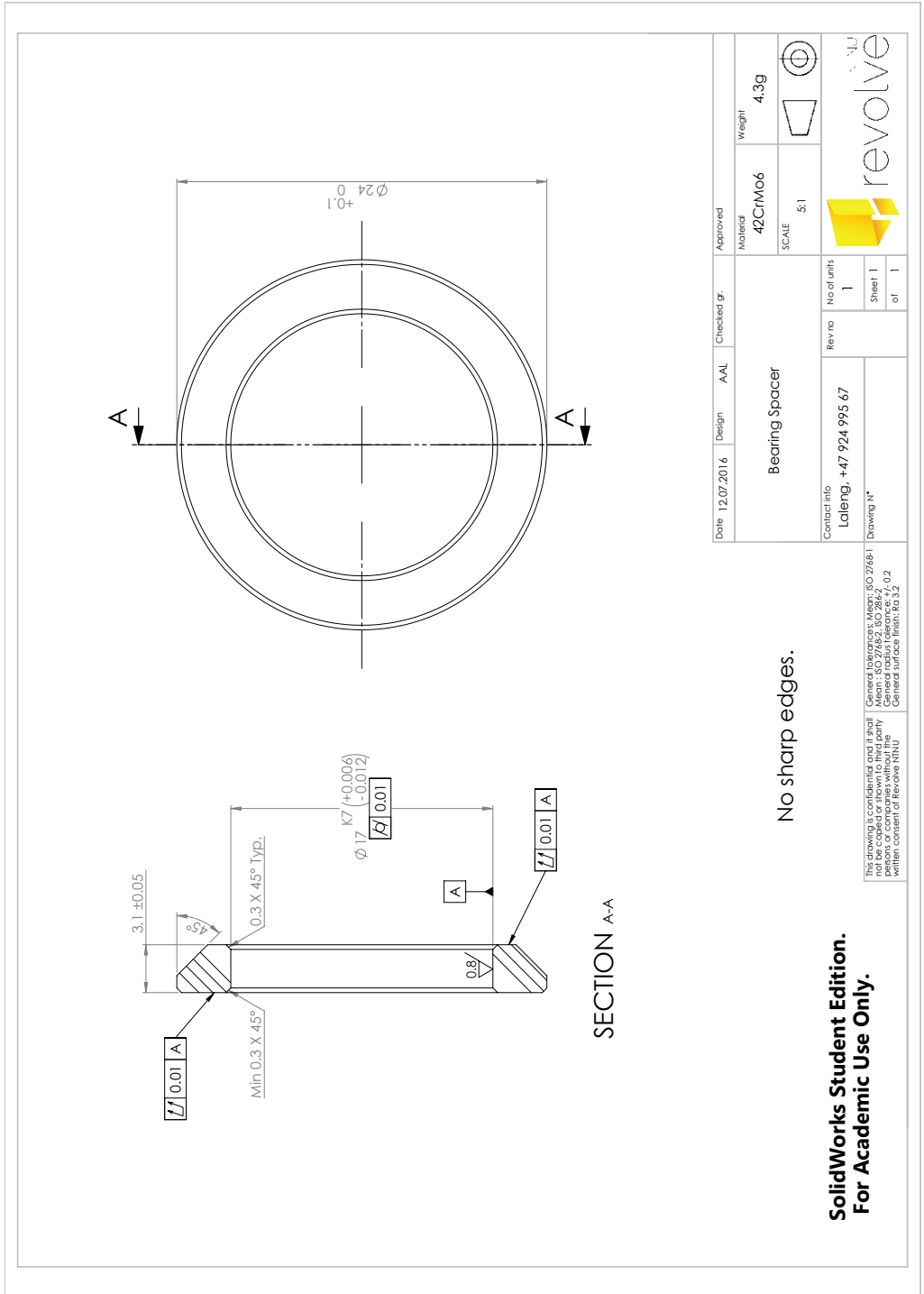
No sharp edges.

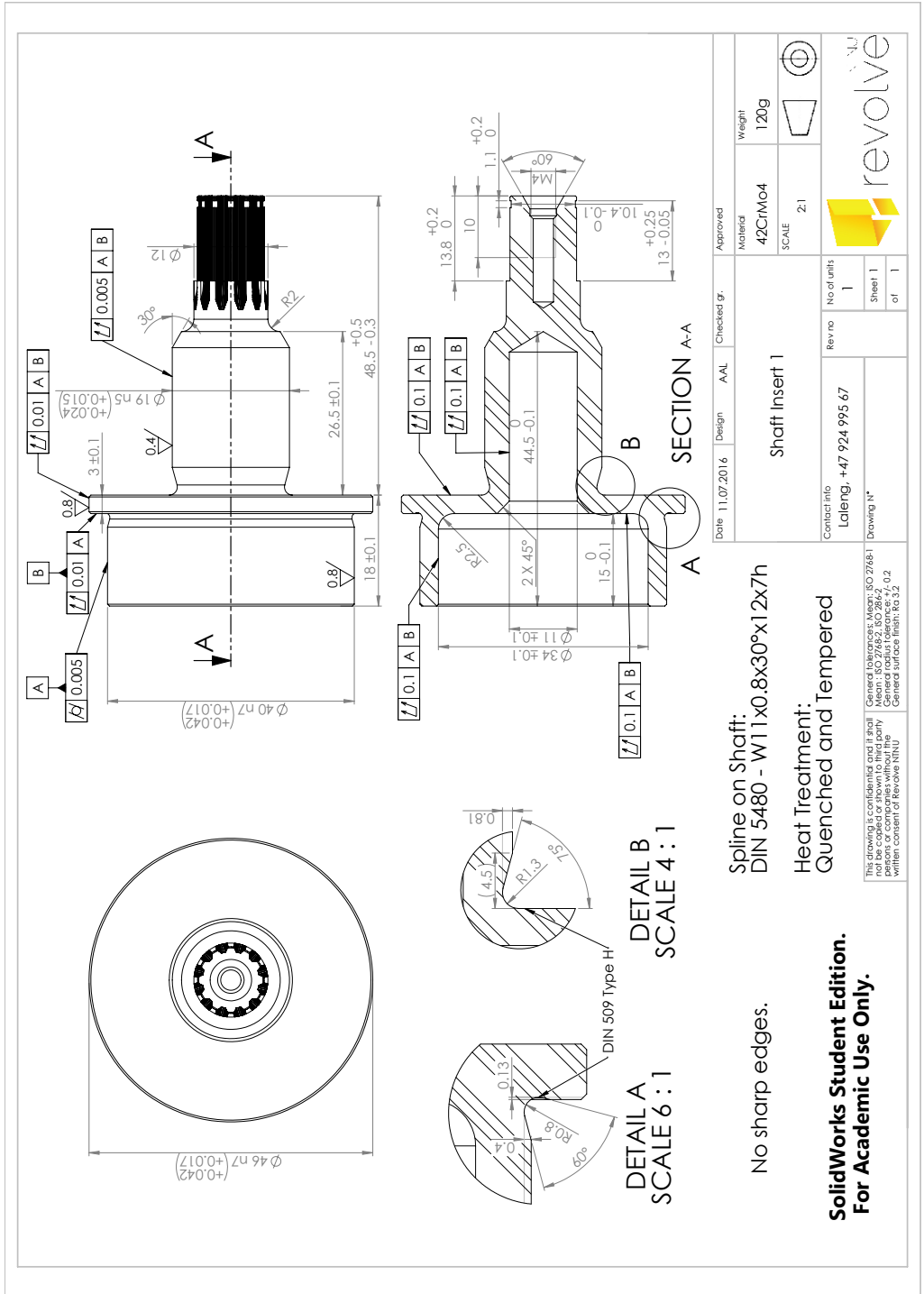
**SolidWorks Student Edition.
For Academic Use Only.**

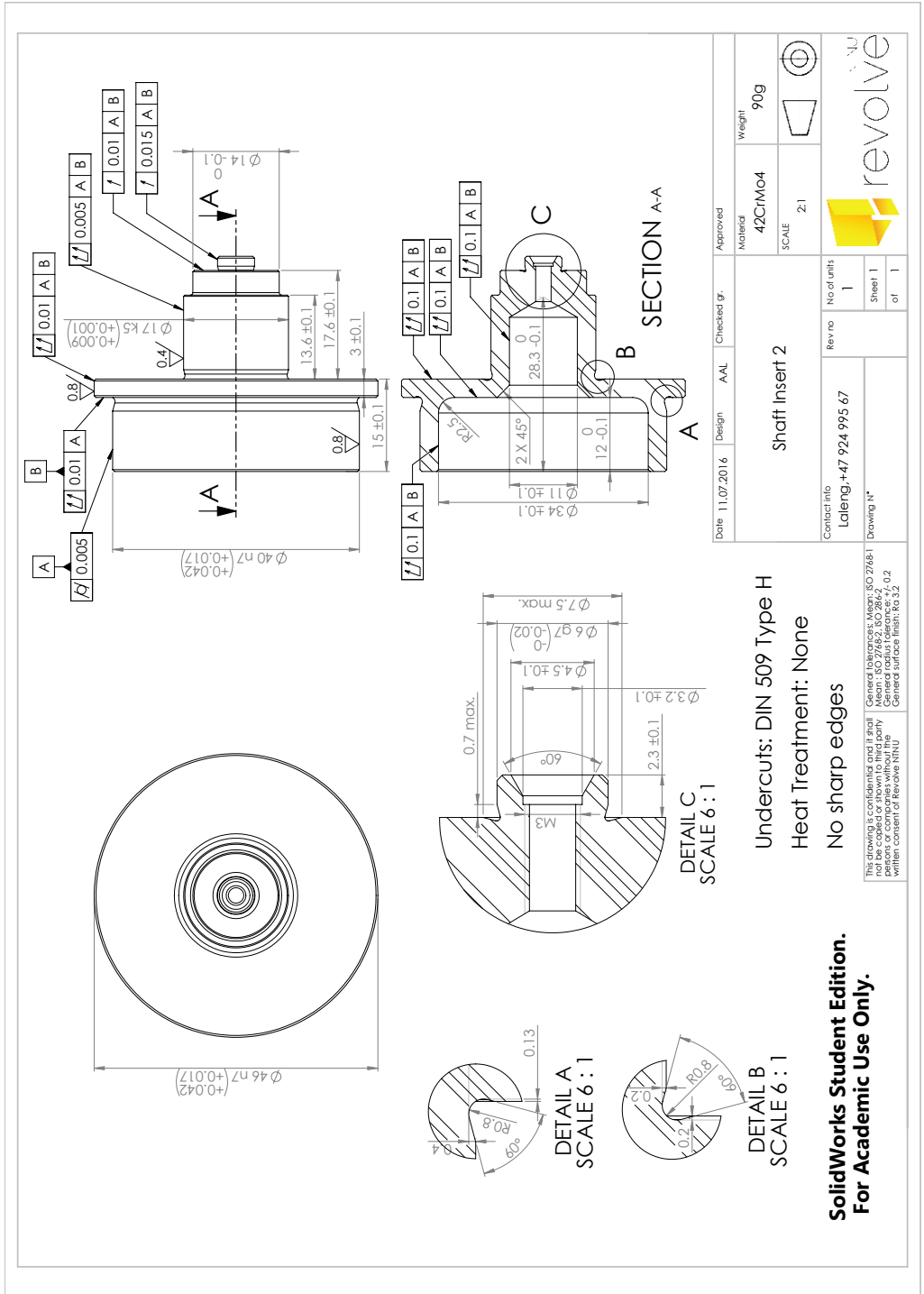
Date	12.07.2016	Design	AAL	Checked gr.	Approved
Balancing Disc			Material	SS 314	Weight
Contact info			SCALE	2:1	9.4g
Laleng, +47 924 995 67			Reviso	No of units	2
Drawing N°			Sheet	of	1
<p>This drawing is confidential and it shall not be copied or shown to third party without the written consent of Revolve NTNU.</p> <p>General tolerances: Mean: ISO 2768-1 Mean: ISO 2768-2, ISO 286-2 General surface finish: Ra 3.2</p>					

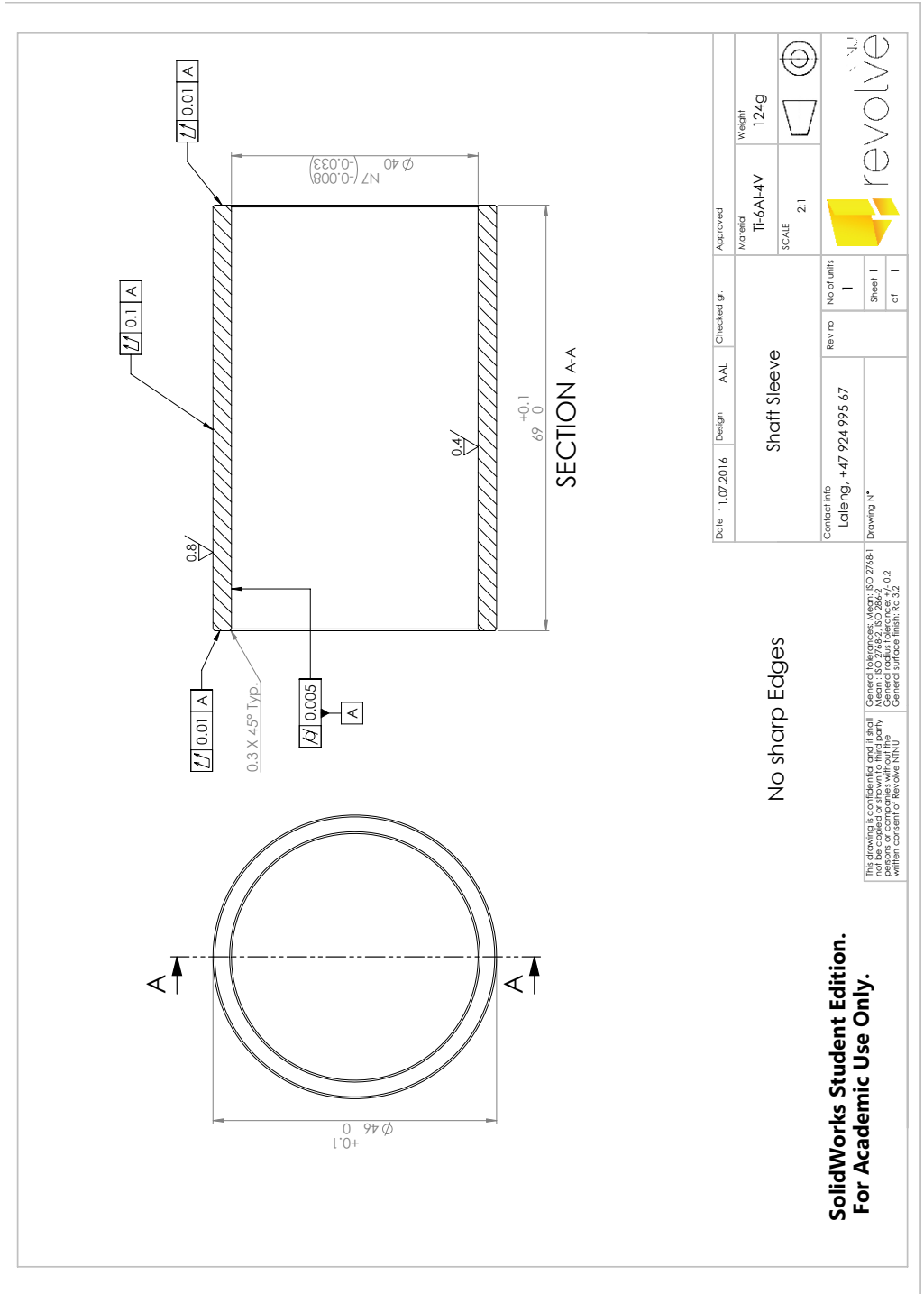


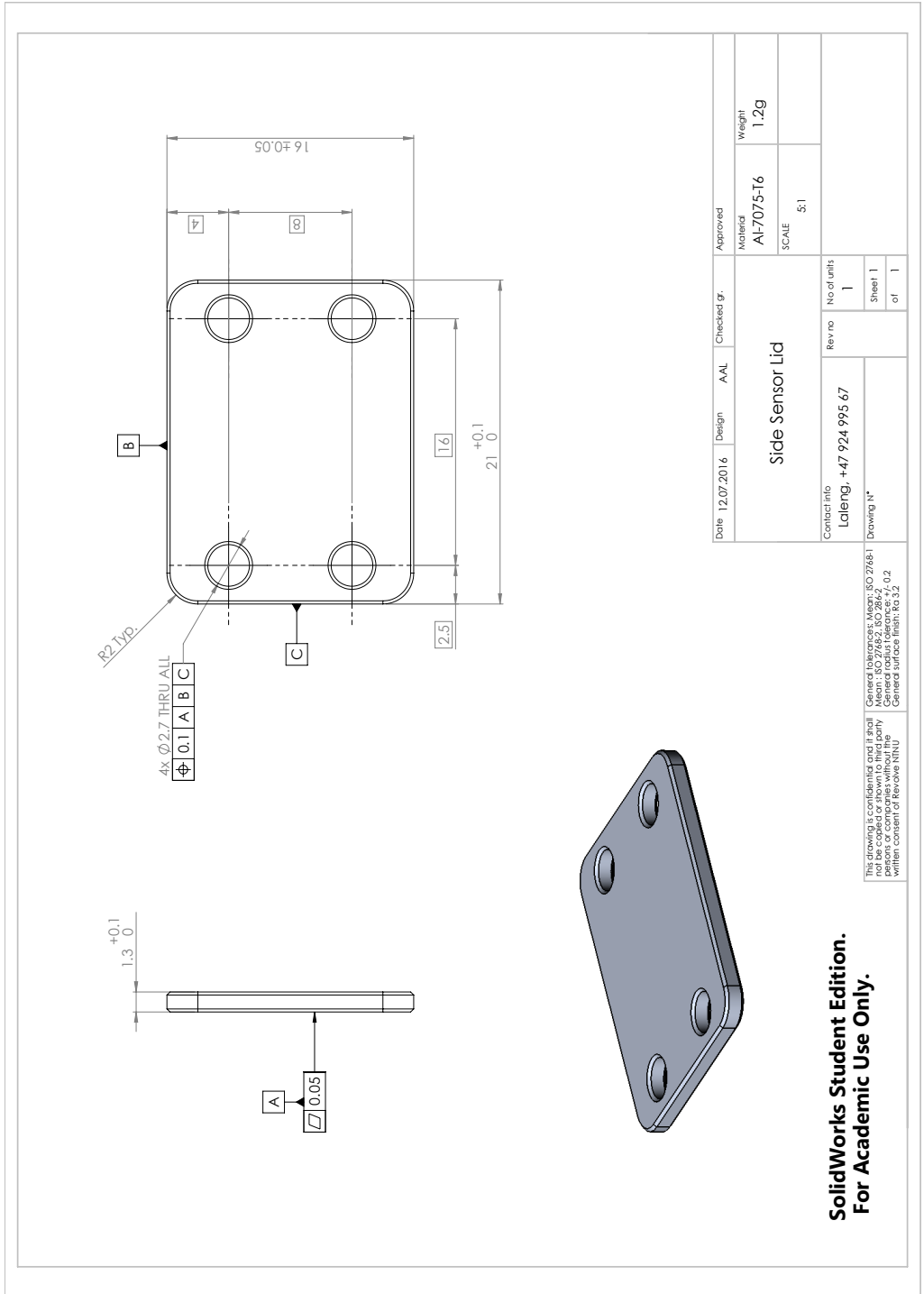


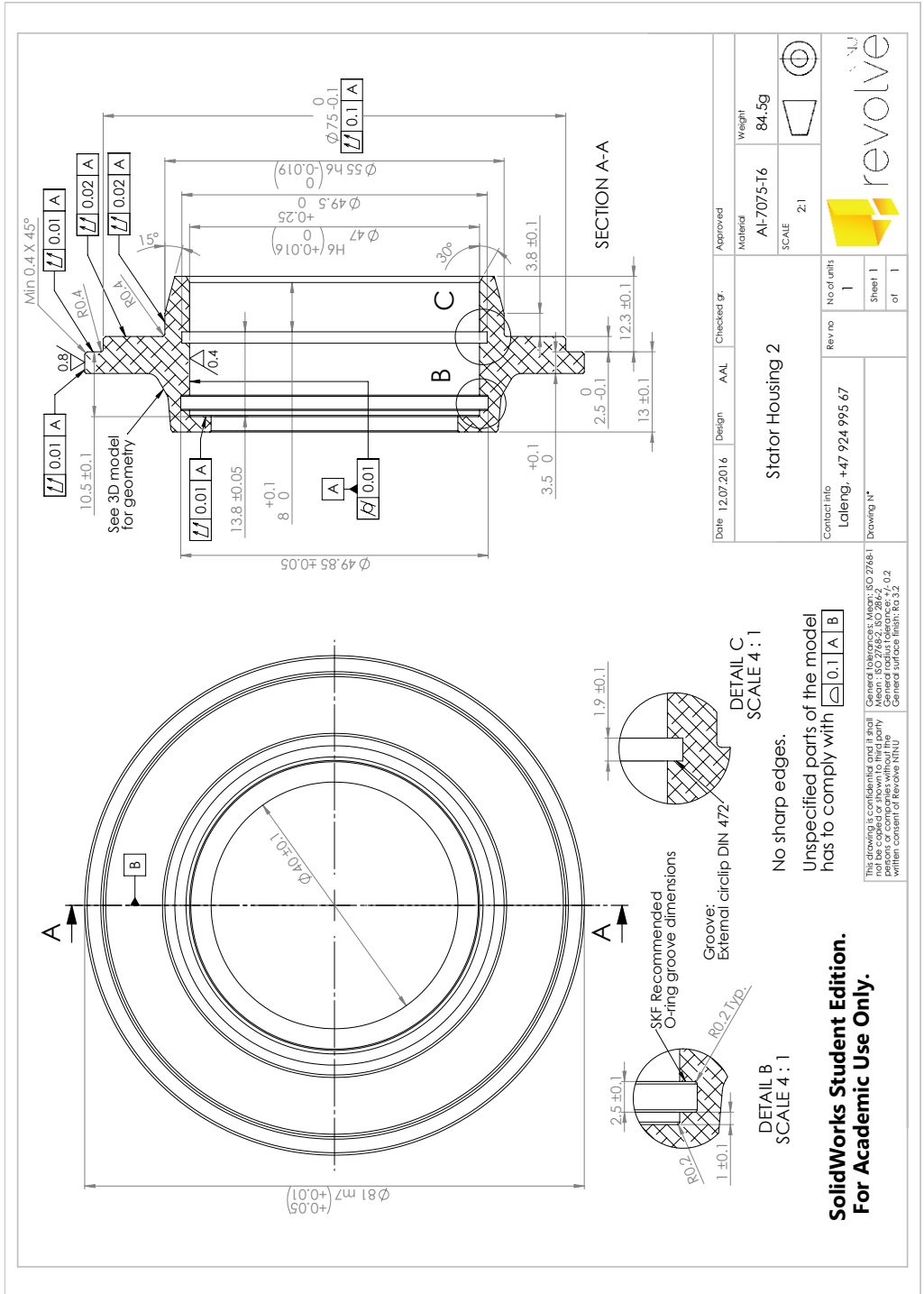


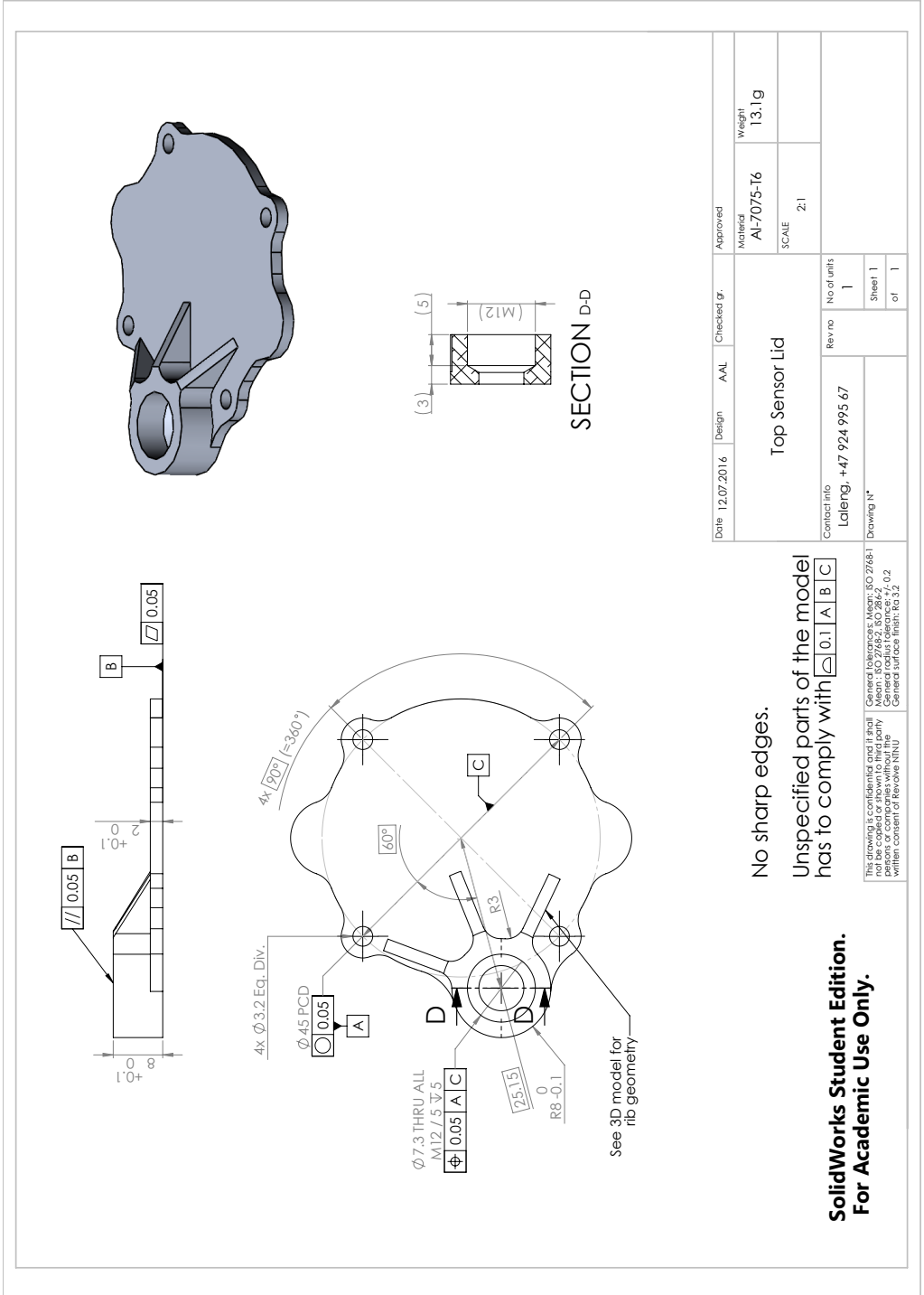


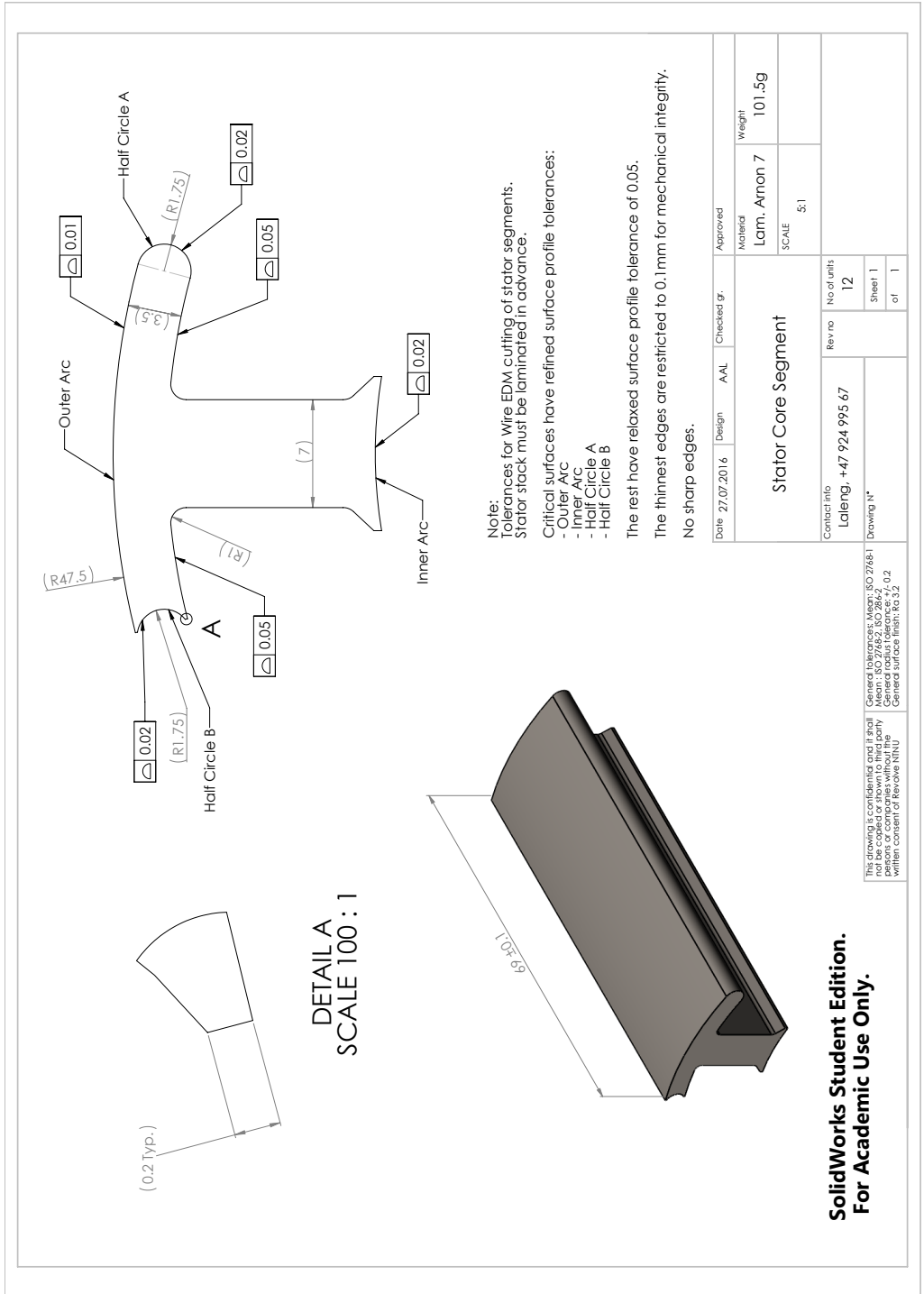












**SolidWorks Student Edition.
For Academic Use Only.**

Appendix C

Assembly Manual

Motor Assembly Manual

Introduction

This assembly manual has the purpose of documenting the planned assembly procedure for the first generation of Revolve's Electric Motors (REM01). Also, it is supposed to be actively used as a reference document during production to remember all the key steps during assembly.

The manual starts with an overview of all the required components for the motor itself, followed by an overview of production components (fixtures, etc.). This is to make sure all required components are available when the assembly starts. Note that tools are not included in this overview, but rather listed on the start of each assembly.

Using the name and part numbers, all custom components can be traced back to their respective production sheets (production drawing, etc.).

The assemblies are listed in a chronological order, starting with individual rotor and stator assemblies, then putting them together, and finally all the connections, seals, sensors, etc. It is advised to follow this order when assembling the motor, although some alternative orders are also possible.

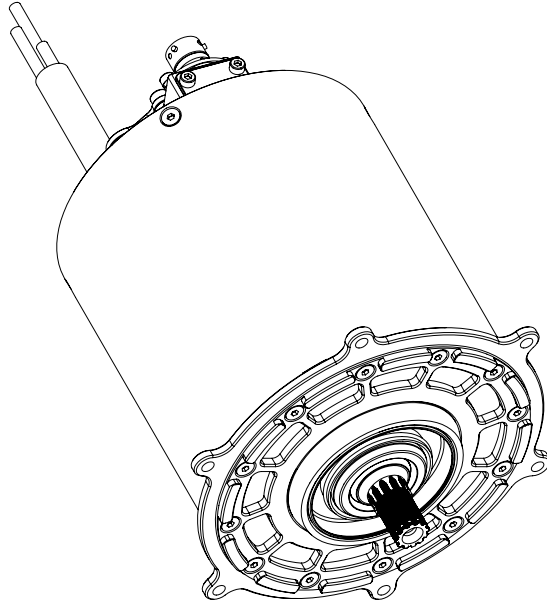
Furthermore, assemblies 8 to 12 are easy and relatively danger free to disassemble in case some parts need to be maintained or replaced.

It is also possible to disassemble the rotor from the stator, but it is not recommended. Only do this if it is strictly necessary - in this case contact the motor designer for instructions.

Table of Contents

Name	Assembly Number	Sheet(s)
Motor Component Overview	-	2
Production Component Overview	-	3
Magnetic Rotor Assembly	A1	4-11
Rotor Shaft Assembly	A2	12-17
Stator Assembly	A3	18-24
Stator Encapsulation	A4	25-29
Bearing Sleeve Assembly	A5	30
Stator to Rotor	A6	31-28
End Bell Connections	A7	39-40
Backside seal and Circlip	A8	41
Encoder and Connector	A9	42-44
Sensor Lids	A10	45
Motor Adapter Plate	A11	46
External Connections	A12	47

Isometrical View of Assembled Motor



Date	25.05.2016	Design	AAI	Checked gr.	Approved
Motor Assembly Instructions Introduction Table of Contents			Material	Weight	
			SCALE		
Contact info			Rev no		No of units
Laleng, +47 924 995 67					Sheet 1 of 47
Drawing N°			revolve		

This drawing is confidential and it shall not be copied or shown to third party without the written consent of Revolve NTNU. General tolerances: Mean: ISO 2768-1 Mean: ISO 2768-2, ISO 286-2. General surface finish: Ra 3.2.

**SolidWorks Student Edition.
For Academic Use Only.**

Motor Component Overview

Part names, numbers and quantity

Custom Manufactured Parts (P)

Part Name	Part Number	Quantity
Stator Segment	P01	12
Magnet Segment	P02	200
Rotor Core	P03	1
Shaft	P04	1
Stator Housing	P05	1
End Bell	P06	1
Bearing Sleeve	P07	1
Balancing Disc 1	P08	1
Balancing Disc 2	P09	1
Motor Adapter Plate	P10	1
Top Sensor Lid	P11	1
Side Sensor Lid	P12	1

Fasteners (F)

Part Name	Part Number	Quantity
Countersunk Socket Head Screw: [DIN991] M3 x 10 - 10N	F01	16
Socket Head Screw: [DIN912 / ISO 4762] M3 x 16 - 16N	F02	1
Socket Head Screw: [DIN912 / ISO 4762] M3 x 8 - 8N	F03	6
Socket Head Screw: [DIN912 / ISO 4762] M3 x 6 - 6N	F04	1
Socket Head Screw: [DIN912 / ISO 4762] M2.5 x 12 - 12N	F05	1
Socket Head Screw: [DIN912 / ISO 4762] M2.5 x 6 - 6N	F06	2
Socket Head Screw: [DIN912 / ISO 4762] M2.5 x 5 - 5N	F07	4
Washer: [DIN6902] A3.2	F08	2
Washer: [DIN6902] C2.75	F09	1

**SolidWorks Student Edition.
For Academic Use Only.**

This drawing is confidential and it shall not be copied or shown to third party without the written consent of Revolve NTNU.

General tolerances: Mean: ISO 2768-1
Mean: ISO 2768-2, ISO 286-2
Holes: ISO 2768-1, ISO 2768-2
General surface finish: Ra 3.2

Standard Components (S)

Part Name	Part Number	Quantity
Deep Groove Ball Bearing: SKF 6005	S01	1
Deep Groove Ball Bearing: SKF E2.6003-2Z	S02	1
Shaft Seal: SKF 30x47x8 CRW1 V	S03	1
O-ring: James Walker 50-043	S04	1
O-ring: James Walker 50-036	S05	1
O-ring: James Walker 50-032	S06	1
O-ring: James Walker 50-028	S07	1
Shaft Circlip: DIN471 25x1.2	S08	1
Bore Circlip: DIN472 47x1.75	S09	1

Electric Components (E)

Part Name	Part Number	Quantity
Deutsch Connector ASDD006-09SKT-HE 3	E01	1
Heidenhein ECI 1100 Encoder	E02	1
Thermistor	E03	1
Connector Gasket	E04	1
Cable Gland: 18110710 Hylec	E05	1
Cable Gland: 1111006 Hylec	E06	1
Ring Connector: RS613-9334	E07	1
Three Phase Cable: Radox 3x4 AWG-28	E08	-
Grounding Wire (AWG12)	E09	-

Date	Design	AAL	Checked gr.	Approved
Motor Component Overview Part names, numbers and quantity				
Material			Weight	
SCALE				
Contact info		Rev no	No of units	
Laleng, +47 924 995 67		Sheet 2	of 47	

Production Component Overview

Part names, numbers and quantity

Assembly Fixtures (AF)

Part Name	Part Number	Quantity
Housing Lower Fixture	AF01	12
Housing Upper Fixture	AF02	200
Housing Fixture Bottom	AF03	1
VPI Motor Plug	AF04	1
VPI Motor Plug Backplate	AF05	1
VPI Motor Leg	AF06	1
Stator Bottom Fixture	AF07	1
Stator Yoke Fixture	AF08	1
Stator Center Fixture	AF09	1
Rotor Shaft Fixture	AF10	1
Rotor Magnet Top Fixture	AF11	1
Rotor Magnet Bottom Fixture	AF12	1
Rotor Magnet Fixture Washer	AF13	1
Threaded Rod (M6 x 1.0 - 100)	AF14	2
Press Block	AF15	1
Aligning Block	AF16	1
Block Backplate	AF17	2
Bottom Oven Fixture	AF18	1
Top Oven Fixture	AF19	1

Fixture Fasteners (FF)

Part Name	Part Number	Quantity
Socket Head Screw: (DIN912 / ISO 4762) M3 x 16 - 16N	FF01	6
Socket Head Screw: (DIN912 / ISO 4762) M4 x 25 - 25N	FF02	1
Socket Head Screw: (DIN912 / ISO 4762) M4 x 20 - 20N	FF03	4
Socket Head Screw: (DIN912 / ISO 4762) M6 x 20 - 20N	FF04	1
Socket Head Screw: (DIN912 / ISO 4762) M2.5 x 8 - 8N	FF05	4
Hexagon Nut: (ISO 4034) M6	FF06	2

SolidWorks Student Edition.
For Academic Use Only.

This drawing is confidential and it shall not be copied or shown to third party without the written consent of Revolve NTHU.

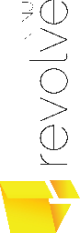
General tolerances: Mean: ISO 2768-1
Mean: ISO 2768-2, ISO 286-2
General surface finish: Ra 3.2

Vacuum Infusion (V)

Part Name	Part Number	Quantity
Vacuum Tank	V01	1
Vacuum Tank Lid	V02	1
O-ring: James Walker 50-031	V03	1
O-ring: James Walker 50-050	V04	1

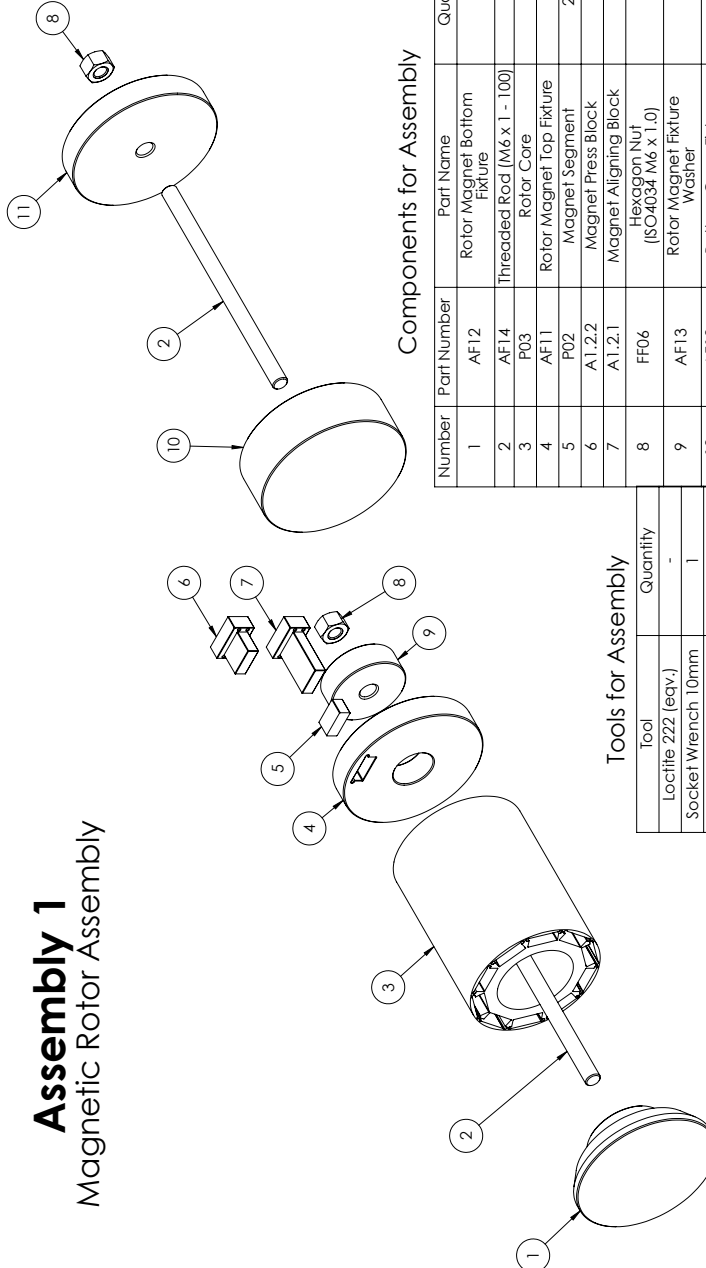
Referred Assemblies (A)

Assembly Name	Part Number	Quantity
Magnetic Rotor Assembly	A1	1
Magnet Aligning Block	A1.2.1	1
Magnet Press Block	A1.2.2	1
Rotor Shaft Assembly	A2	1
Stator Assembly	A3	1
Stator Encapsulation	A4	1
Bearing Sleeve Assembly	A5	1

Date	Design	AAL	Checked gr.	Approved	Material	Weight
Production Component Overview Part names, numbers and quantity						
Contact info			Rev no	No of units		
Laleng, +47 924 995 67						
Drawing N°			Sheet 3	of 47		
						

Assembly 1

Magnetic Rotor Assembly



Components for Assembly

Number	Part Number	Part Name	Quantity
1	AF12	Rotor Magnet Bottom Fixture	1
2	AF14	Threaded Rod (M6 x 1 - 100)	2
3	P03	Rotor Core	1
4	AF11	Rotor Magnet Top Fixture	1
5	P02	Magnet Segment	200
6	A1.2.2	Magnet Press Block	1
7	A1.2.1	Magnet Aligning Block	1
8	FF06	Hexagon Nut (ISO4034 M6 x 1.0)	2
9	AF13	Rotor Magnet Fixture Washer	1
10	AF18	Bottom Oven Fixture	1
11	AF19	Top Oven Fixture	1

Tools for Assembly

Tool	Quantity
Loctite 222 (equiv.)	-
Socket Wrench 10mm	1
Epoxy Glue Araldite 4859	-
Epoxy Release Agent Frekote NC44	-
Spatula (Plastic/Wood)	Several
Plastic Syringe	Several
Plastic Gloves	Several
Wiping Paper	-
Lint Free Cloth	-
Oven	1

NOTE: This assembly contains permanent magnets which will attract all ferromagnetic materials. In order to protect the parts from dust and impact damage, the assembly should be done in a clean environment and caution must be taken when magnetic parts are close to ferromagnetic materials.

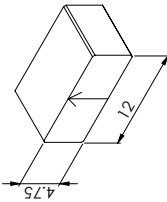
**SolidWorks Student Edition.
For Academic Use Only.**

Date: 25.05.2016	Design: AAL	Checked: gr.	Approved:
Assembly 1 Magnetic Rotor Assembly			
Material:		Weight:	
SCALE:			
Contact info:	Rev no:	No of units:	
Laleng, +47 924 995 67			
Sheet 4 of 47			

This drawing is confidential and it shall not be copied or shown to third party without the written consent of Revolve NTNU. General tolerances: Mean: ISO 2768-1 Mean: ISO 2768-2, ISO 286-2, ISO 2875. General surface finish: Ra 3.2.

Assembly 1.1 Magnetization Orientation Marking

Marking Magnets

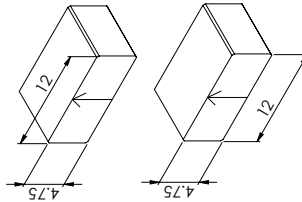


- Step 1: Take out one magnet for reference
- Step 2: Identify the direction parallel to the magnetization by measuring its dimensions
- Step 3: Draw an arrow on the magnet's side with a marker (It does not matter if it points north or south)

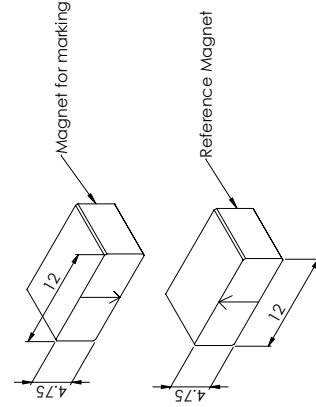
- Step 4: Take a new magnet
- Step 5: Identify the direction parallel to the magnetization by repeating step 2
- Step 6: Determine it's direction of magnetization by comparing it to the reference
- Step 7: Mark it with an arrow in the direction of magnetization (so it complies with the figure below)
- Step 8: Repeat step 4-7 to mark all magnets

NOTE: Magnets are very brittle and sensitive to shocks, so the magnets should be packed in a soft material and clamped during comparison to avoid them crashing into each other. Also note the danger of clamping fingers during comparison.

Attraction
(Same direction of polarity)



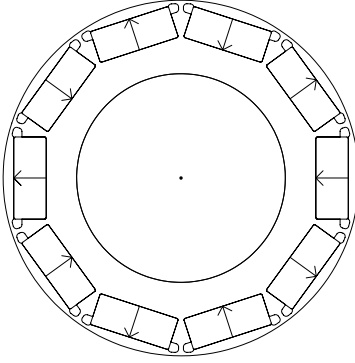
Repulsion
(Opposite direction of polarity)



**SolidWorks Student Edition.
For Academic Use Only.**

NOTE:
Take caution when handling magnets as they will attract all ferromagnetic materials. In order to protect them from being damaged from metal dust/chips and impacts, it's very important to handle them in a clean room and keep ferromagnetic materials away.

Magnetization Orientation



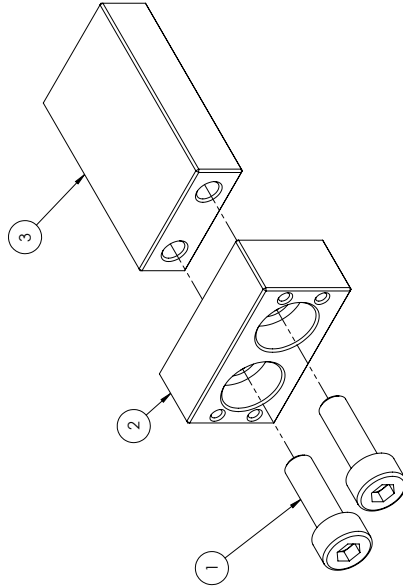
In order to make the rotor function properly, it is of paramount importance that the magnets are inserted into the core with the correct polarity. As shown in the figure above, all the magnets in one slot should have the same direction of magnetization. In the adjacent slots, the magnets should have opposite polarity with respect to the radial direction. Failure to comply with this pattern will cause spurious cogging torque and diminish motor performance.

Date	25.05.2016	Design	AAI	Checked gr.	Approved
Material			Weight		
SCALE					
Assembly 1.1 Magnetization Orientation Marking					
Contact info		Rev no		No of units	
Laleng, +47 924 995 67				Sheet 5 of 47	
Drawing N°					

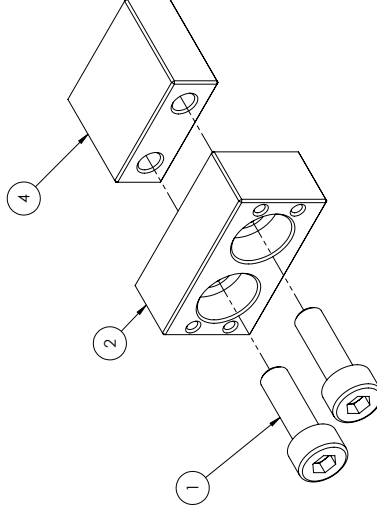
This drawing is confidential and it shall not be copied or shown to third party without the written consent of Revolve NTNU.
 General tolerances: Mean: ISO 2768-1
 Mean: ISO 2768-2, ISO 286-2
 General surface finish: Ra 3.2

Assembly 1.2 Magnet Block Assemblies

Magnet Aligning Block (A1.2.1)



Magnet Press Block (A1.2.2)



Assembly Procedure

Step 1: Assemble the aligning block and press block to the backplate as shown above

Components for Assembly

Number	Part Number	Part Name	Quantity
1	FF05	Socket Head Screw (ISO 4762) M2.5 x 8 - 8N	1
2	AF17	Block Backplate	2
3	AF16	Aligning Block	1
4	AF15	Press Block	1

Date: 25.05.2016 Design: AAL Checked gr.: Approved

Assembly 1.2 Magnet Block Assemblies		Material	Weight
Contact info		SCALE	
Laleng, +47 924 995 67			
Rev no		No of units	
Drawing n°		Sheet 6 of 47	

Tools for Assembly

Tool	Quantity
Unbrako Key 2.0mm	1

This drawing is confidential and it shall not be copied or shown to third party without the written consent of Revolve NTNU. General tolerances: Mean: ISO 2768-1 Mean: ISO 2768-2, ISO 286-2. General surface finish: Ra 3.2.

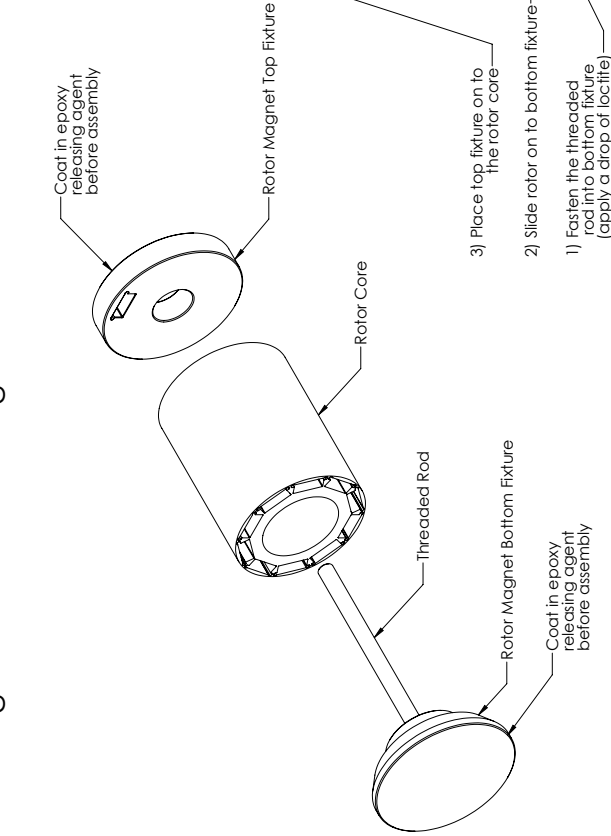
**SolidWorks Student Edition.
For Academic Use Only.**



Assembly 1.3

Rotor Magnet Fixture Mounting

Cross section of fixture assembly



Assembly Procedure

- Step 1: Coat the fixtures in a epoxy releasing agent
- Step 2: Apply a drop of locitite into the bottom fixture
- Step 3: Fasten the threaded rod into the bottom fixture
- Step 4: Slide the rotor core and top fixture on to the bottom fixture

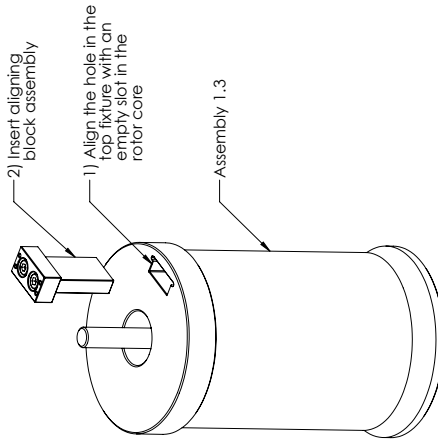
NOTE: The oven fixture also needs to be coated in a epoxy releasing agent. Do this at the same time as coating the rotor fixture. It needs to be done BEFORE Assembly 1.5 is started.

**SolidWorks Student Edition.
For Academic Use Only.**

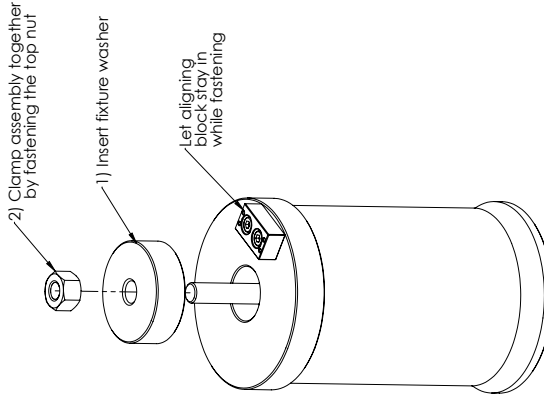
Date	25.05.2016	Design	AAL	Checked gr.	Approved	Material	Weight
Assembly 1.3 Rotor Magnet Fixture Mounting				SCALE			
Contact info	Rev no		No of units				
Laleng, +47 924 995 67							
Drawing N°	Sheet 7		of 47				

This drawing is confidential and it shall not be copied or shown to third party without the written consent of Revolve NTNU.
 General tolerances: Mean: ISO 2768-1
 Mean: ISO 2768-2, ISO 286-2
 General surface finish: Ra 3.2

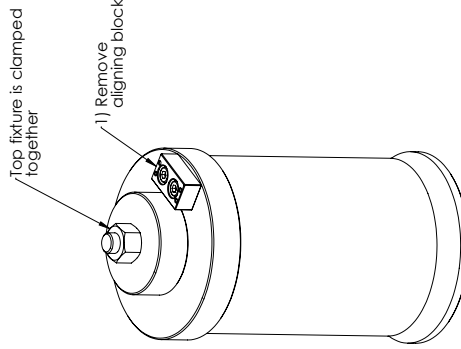
Assembly 1.4 Rotor Magnet Fixture Aligning



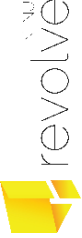
Step 1: Align the fixture



Step 2: Clamp fixture in alignment



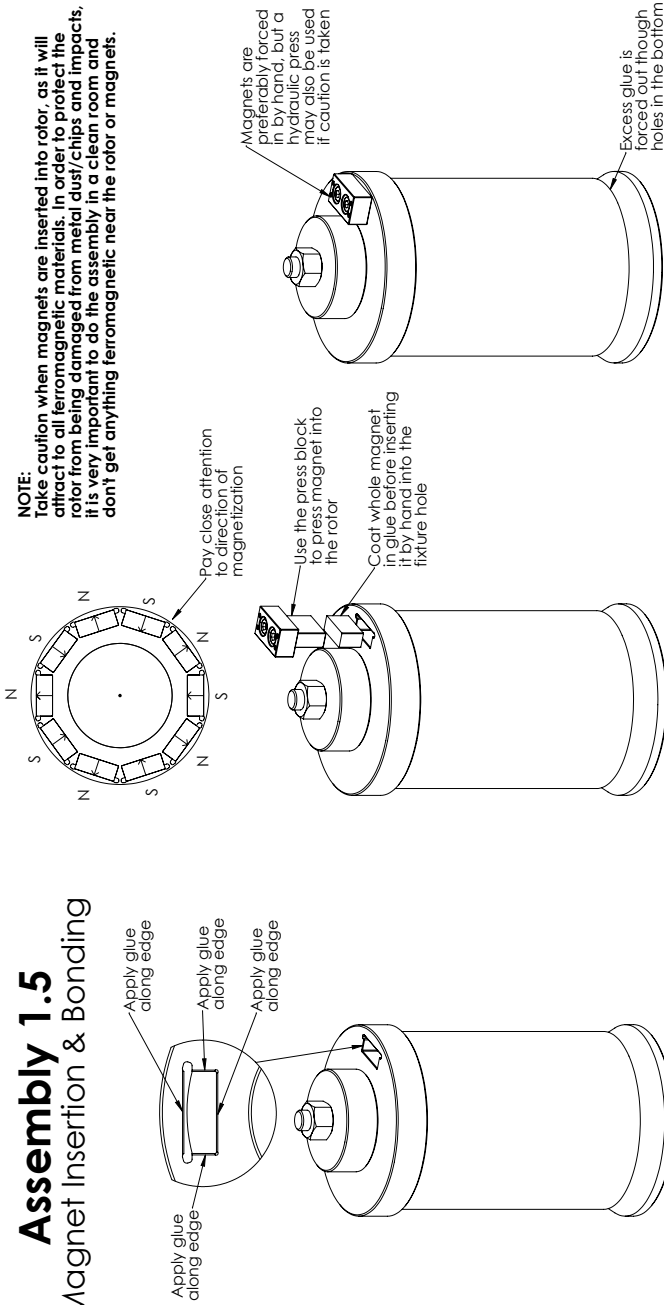
Step 3: Remove alignment block

Date	25.05.2016	Design	AAL	Checked gr.	Approved	Material	Weight
Assembly 1.4 Rotor Magnet Fixture Aligning				SCALE			
Contact info		Rev no		No of units			
Laleng, +47 924 995 67				Sheet 8 of 47			

**SolidWorks Student Edition.
For Academic Use Only.**

This drawing is confidential and it shall not be copied or shown to third party without the written consent of Revolve NTNU.
 General tolerances: Mean: ISO 2768-1
 Mean: ISO 2768-2, ISO 286-2
 General surface finish: Ra 3.2

Assembly 1.5 Magnet Insertion & Bonding



Step 2 & 3

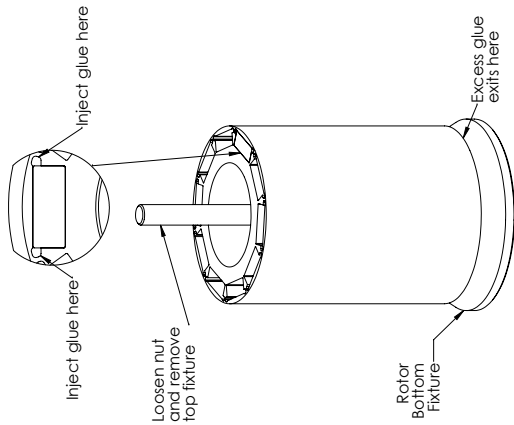
Assembly Procedure

- Step 1: Use a spatula to apply glue to all the straight edges of the magnet hole, through the whole rotor length.
- Step 2: Coat a magnet segment in glue and insert it into the fixture hole by hand while paying close attention to the direction of magnetization (see Assembly 1.1).
- Step 3: Use the press block to push the magnet segment into the rotor. Wipe away excess glue that comes out of the bottom of the rotor and through the press block.
- Step 4: Repeat step 2 and 3 until the whole rotor length is filled with magnet segments.

**SolidWorks Student Edition.
For Academic Use Only.**

Date	25.05.2016	Design	AAI	Checked gr.	Approved
Assembly 1.5 Magnet Insertion & Bonding				Material	Weight
Contact info				SCALE	
Laleng, +47 924 995 67				No. of units	
Drawing N°				Sheet 9	of 47
<small>This drawing is confidential and it shall not be copied or shown to third party without the written consent of Revolve NTNU.</small>				<small>General tolerances: Mean: ISO 2768-1 Mean: ISO 2768-2, ISO 286-2 General surface finish: Ra 3.2</small>	

Assembly 1.6 Slot finishing & Curing



Step 1 to Step 3

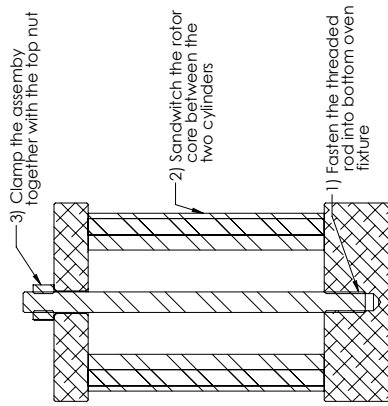
Assembly Procedure

- Step 1: Unfasten the top nut and remove the top fixture and the fixture washer
- Step 2: Use a plastic syringe to inject glue into the air holes on either side of the magnet.
- Step 3: Wipe excess glue that comes out of the bottom of the fixture
- Step 4: If there is sufficient pot life left for the applied glue to fill another rotor slot with magnets, wipe the fixture clean and go back to Assembly 1.4
- Step 5: If the pot life is running out, disassemble the rotor from its fixture and wipe all surfaces clean using a lint free cloth. Don't wipe inside the magnet slots. Wipe the rotor fixture with paper.
- Step 6: Assemble the oven fixture to the rotor. The fixture must have a releasing agent coating at this step. See the figure to the right.
- Step 7: Cure the rotor in the oven to bond the magnets in place.
- Step 8: Go back to Assembly 1.4 if there are any empty magnet slots

**SolidWorks Student Edition.
For Academic Use Only.**

NOTE:
Take caution when magnets are inserted into rotor, as it will attract to all ferromagnetic materials. In order to protect the rotor from being damaged from metal dust and impacts, it is very important to do the assembly in a clean room and don't get anything ferromagnetic near the rotor.

Oven Assembly Cross Section



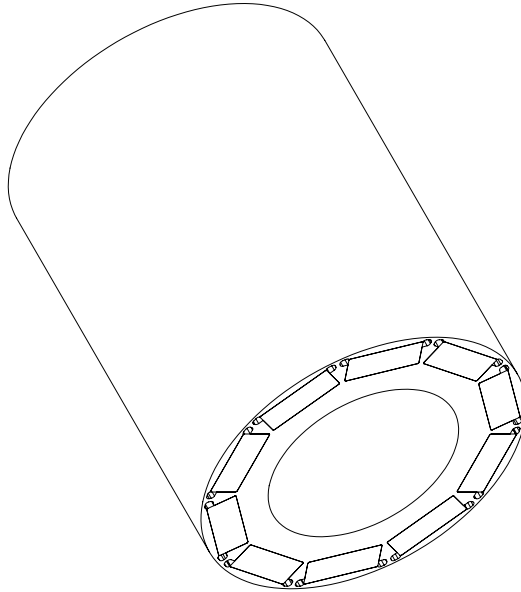
Step 6 & 7

Date	25.05.2016	Design	AAL	Checked gr.	Approved	Material	Weight
Assembly 1.6 Slot finishing & Curing				SCALE			
Contact info		Rev no		No of units			
Laleng, +47 924 995 67				Sheet 10 of 47			

This drawing is confidential and it shall not be copied or shown to third party without the written consent of Revolve NTNU
 General tolerances: Mean: ISO 2768-1
 Mean: ISO 2768-2, ISO 286-2, 0.2
 General surface finish: Ra 3.2

Assembly 1

Finished Magnetic Rotor Assembly



NOTE: As the rotor are now magnetic, it should always be handled with care when there's ferromagnetic material around. When not handled, it should be packed in plastic to protect it from dust and metal chips.

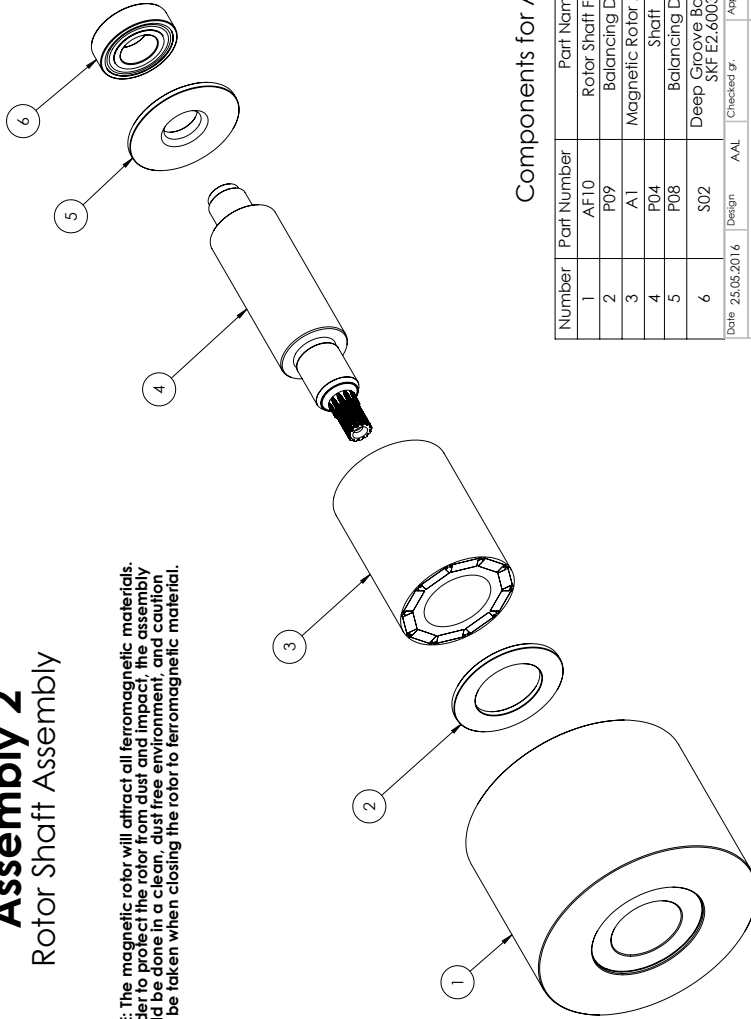
**SolidWorks Student Edition.
For Academic Use Only.**

Date: 25.05.2016	Design: AAL	Checked gr.	Approved
Assembly 1 Finished Magnetic Rotor Assembly		Material	Weight
Contact info: Laleng, +47 924 995 67		SCALE	
Rev no		No of units	
Drawing N°		Sheet 11 of 47	

This drawing is confidential and it shall not be copied or shown to third party without the written consent of Revolve NTNU.
General tolerances: Mean: ISO 2768-1
Mean: ISO 2768-2, ISO 286-2
General surface finish: Ra 3.2

Assembly 2 Rotor Shaft Assembly

NOTE: The magnetic rotor will attract all ferromagnetic materials. In order to protect the rotor from dust and impact, the assembly should be done in a clean, dust free environment, and caution must be taken when closing the rotor to ferromagnetic material.



Components for Assembly

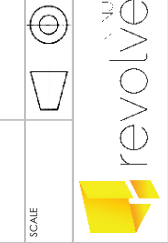
Number	Part Number	Part Name	Quantity
1	AF10	Rotor Shaft Fixture	1
2	P09	Balancing Disc 2	1
3	A1	Magnetic Rotor Assembly	1
4	P04	Shaft	1
5	P08	Balancing Disc 1	1
6	S02	Deep Groove Ball Bearing SKF E2.6003-Z1	1

Tools for Assembly

Tool	Quantity
Oven	-
Gloves (120degC)	2

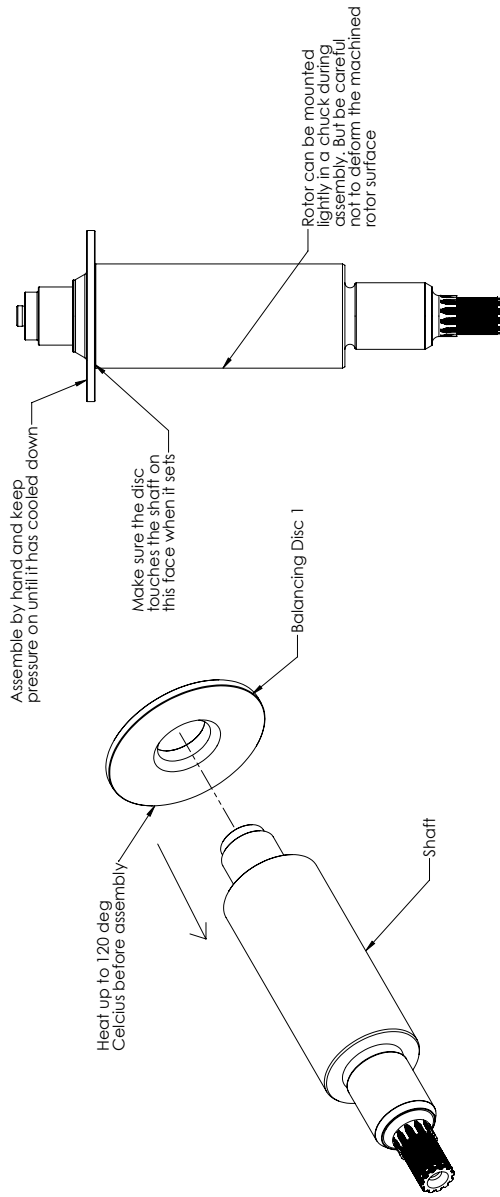
General tolerances: Mean: ISO 2768-1
Mean: ISO 2768-2, ISO 286-2
General surface finish: Ra 3.2
General surface finish: Ra 3.2

**SolidWorks Student Edition.
For Academic Use Only.**



Revolve
Sheet 12
of 47

Assembly 2.1 Shrink Fitting Balancing Disc 1



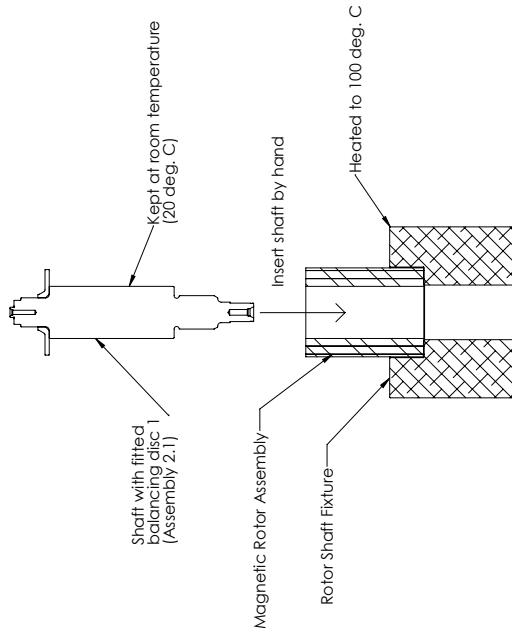
Assembly Procedure

- Step 1: Mount the shaft in a chuck, holding it up as shown on the figure to the right
- Step 2: Heat the balancing disc up to 120 degrees in an oven
- Step 3: Use gloves and slide the balancing disc on to the shaft as shown
- Step 4: Keep hand pressure on the disc while cooling to ensure it sets all the way in

**SolidWorks Student Edition.
For Academic Use Only.**

Date	25.05.2016	Design	AAL	Checked gr.	Approved
Assembly 2.1 Shrink Fitting Balancing Disc 1				Material	Weight
Contact info				SCALE	
Laleng, +47 924 995 67				No. of units	
Drawing N°				Sheet 13	revolve
General tolerances: Mean: ISO 2768-1 Mean: ISO 2768-2, ISO 286-2 Surface texture: Rmax: 3.2 General surface finish: Ra: 3.2				of 47	

Assembly 2.2 Shrink fit magnetic rotor to shaft

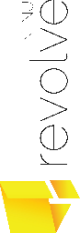


Keep a downwards pressure by hand on the balancing disc while the rotor core cools down

Assembly Procedure

- Step 1: Place rotor core within the rotor assembly fixture as shown
- Step 2: Heat the rotor core and assembly fixture up to 100 degrees C. in the oven
- Step 3: Insert the shaft into the rotor core by hand
- Step 4: Keep a downwards hand pressure on shaft until the rotor core has cooled down

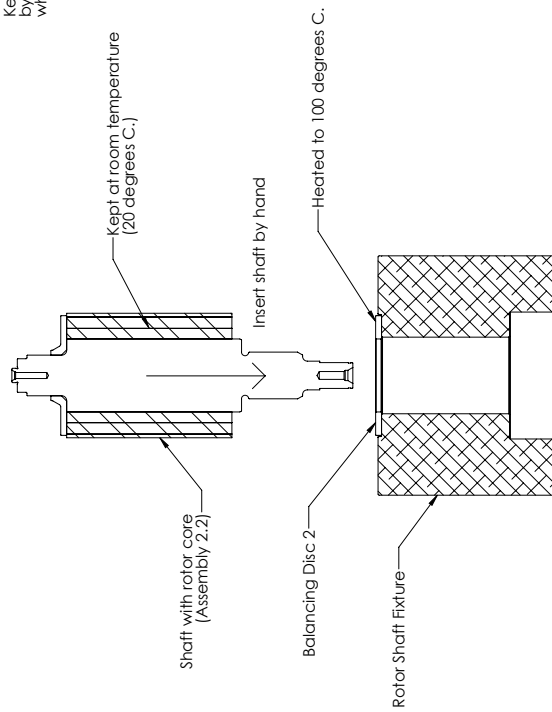
**SolidWorks Student Edition.
For Academic Use Only.**

Date	25.05.2016	Design	AAL	Checked gr.	Approved	Material	Weight
Assembly 2.2 Shrink fit magnetic rotor toshaft				SCALE			
Contact info		Rev no		No of units			
Laleng, +47 924 995 67				Sheet 14 of 47			
Drawing 1*							

This drawing is confidential and it shall not be copied or shown to third party without the written consent of Revolve NTHU.
General tolerances: Mean: ISO 2768-1
Mean: ISO 2768-2, ISO 286-2
General surface finish: Ra 3.2

Assembly 2.3

Shrink fit balancing disc 2 to shaft



Assembled Cross Section View

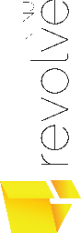
Keep a downwards pressure by hand on the balancing disc while the rotor core cools down

Balancing Disc 2

Assembly Procedure

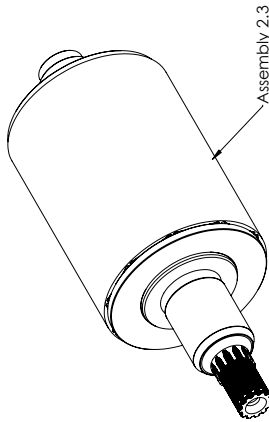
- Step 1: Turn the rotor assembly fixture up-side-down compared to assembly 2.2 and place balancing disc 2 into the slot
- Step 2: Heat the balancing disc and assembly fixture up to 100 degrees C. in the oven
- Step 3: Insert the shaft into the balancing disc
- Step 4: Keep a downwards hand pressure on shaft until the balancing disc has cooled down

**SolidWorks Student Edition.
For Academic Use Only.**

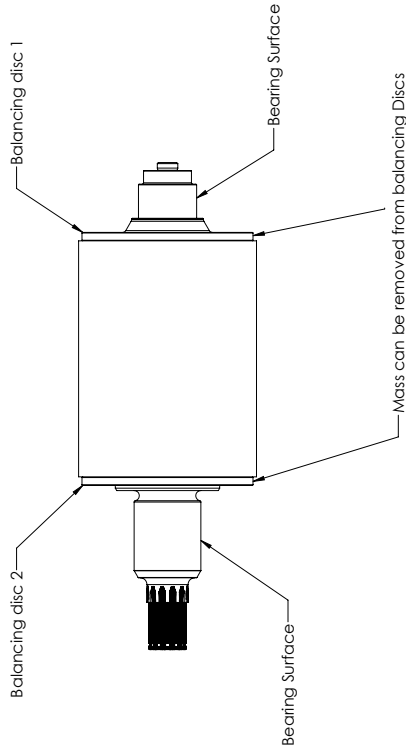
Date: 25.05.2016	Design: AAL	Checked gr.	Approved
Assembly 2.3 Shrink fit balancing disc 2 to shaft		Material	Weight
Contact info Laleng, +47 924 995 67		SCALE	
Rev no		No of units	
Drawing N°		Sheet 15 of 47	
<small>This drawing is confidential and it shall not be copied or shown to third party without the written consent of Revolve NTNU. General tolerances: Mean: ISO 2768-1 Mean: ISO 2768-2, ISO 286-2, ISO 2875. General surface finish: Ra 3.2.</small>			

Assembly 2.4 Rotor Balancing

Assembly ready for balancing



NOTE: The magnetic rotor will attract all ferromagnetic materials. In order to protect the rotor from dust and impact, the assembly should be done in a clean, dust free environment, and caution must be taken when closing the rotor to ferromagnetic material.



Assembly Procedure

Step 1: Send the rotor to a balancing machine

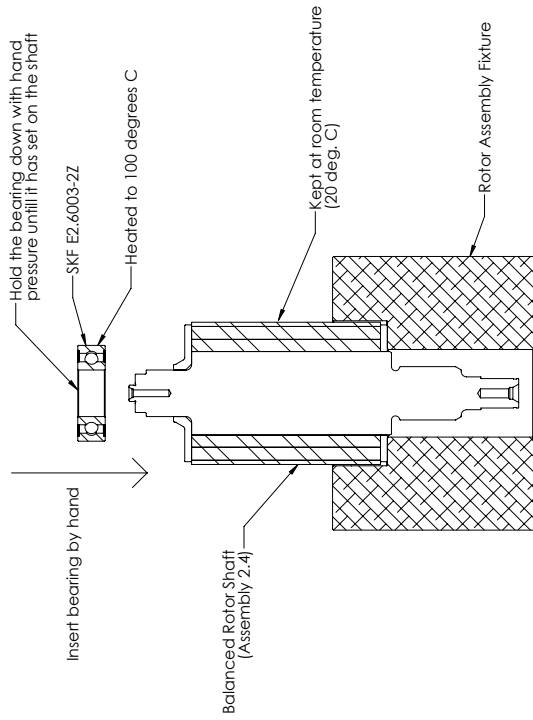
Step 2: Balance the rotor statically and dynamically by removing mass from the balancing discs

Max rotor speed: 20 KRPM

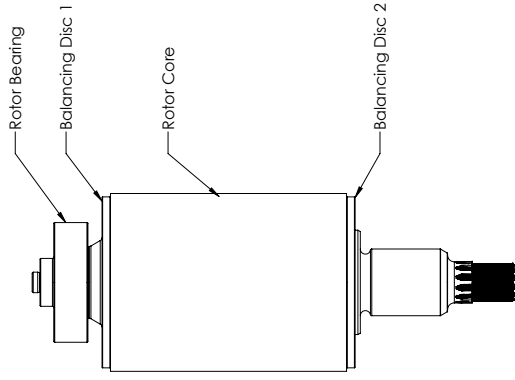
**SolidWorks Student Edition.
For Academic Use Only.**

Date: 25.05.2016		Design: AAL	Checked gr.	Approved Material	Weight
Contact info: Laleng, +47 924 995 67		Rev no		No of units	
Drawing N°		Sheet 16		of 47	
General tolerances: Mean: ISO 2768-1 Mean: ISO 2768-2, ISO 286-2 General surface finish: Ra 3.2					
This drawing is confidential and it shall not be copied or shown to third party without the written consent of Revolve NTNU					

Assembly 2.5 Rotor Bearing Mounting



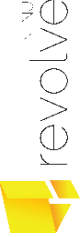
Finished Rotor Assembly



Assembly Procedure

- Step 1: Put the balanced rotor assembly back in the fixture as shown on the figure to the left
- Step 2: Heat the ball bearing up to 100deg.C
- Step 3: Insert the bearing on to its seat on the shaft
- Step 4: Keep a downwards hand pressure on the bearing until it has set on the shaft

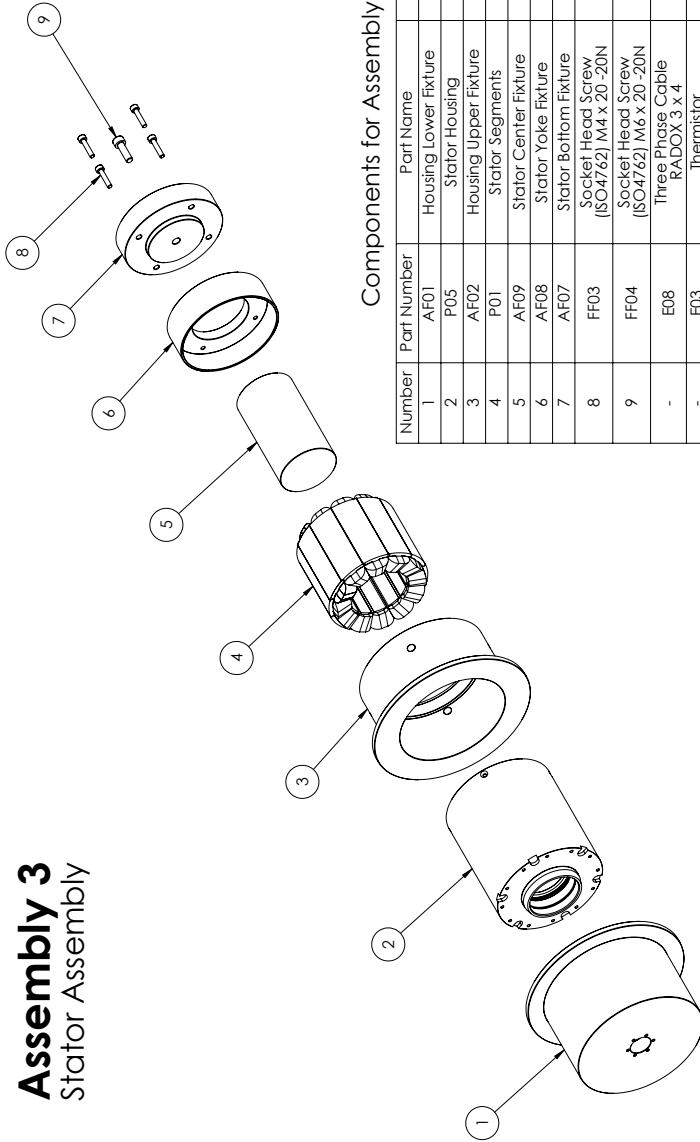
**SolidWorks Student Edition.
For Academic Use Only.**

Date: 25.05.2016	Design: AAL	Checked gr.	Approved Material	Weight
Assembly 2.5 Rotor Bearing Mounting			SCALE	
Contact info: Laleng, +47 924 995 67	Rev no	No of units		
Drawing N°	Sheet 17	of 47		

This drawing is confidential and it shall not be copied or shown to third party without the written consent of Revolve NTNU.
General tolerances: Mean: ISO 2768-1
Mean: ISO 2768-2, ISO 286-2
General surface finish: Ra 3.2

Assembly 3

Stator Assembly



Components for Assembly

Number	Part Number	Part Name	Quantity
1	AF01	Housing Lower Fixture	1
2	P05	Stator Housing	1
3	AF02	Housing Upper Fixture	1
4	P01	Stator Segments	12
5	AF09	Stator Center Fixture	1
6	AF08	Stator Yoke Fixture	1
7	AF07	Stator Bottom Fixture	1
8	FF03	Socket Head Screw (ISO 4762) M4 x 20-20N	4
9	FF04	Socket Head Screw (ISO 4762) M6 x 20-20N	1
-	E08	Three Phase Cable RADOX 3 x 4	-
-	E03	Thermistor	1
-	E09	Grounding Wire (12AWG)	-

Tools for Assembly

Tool	Quantity
Unbrako Key 3.0mm	1
Unbrako Key 5.0mm	1
Oven	-
Soldering Equipment	2
Kapton Tape	-

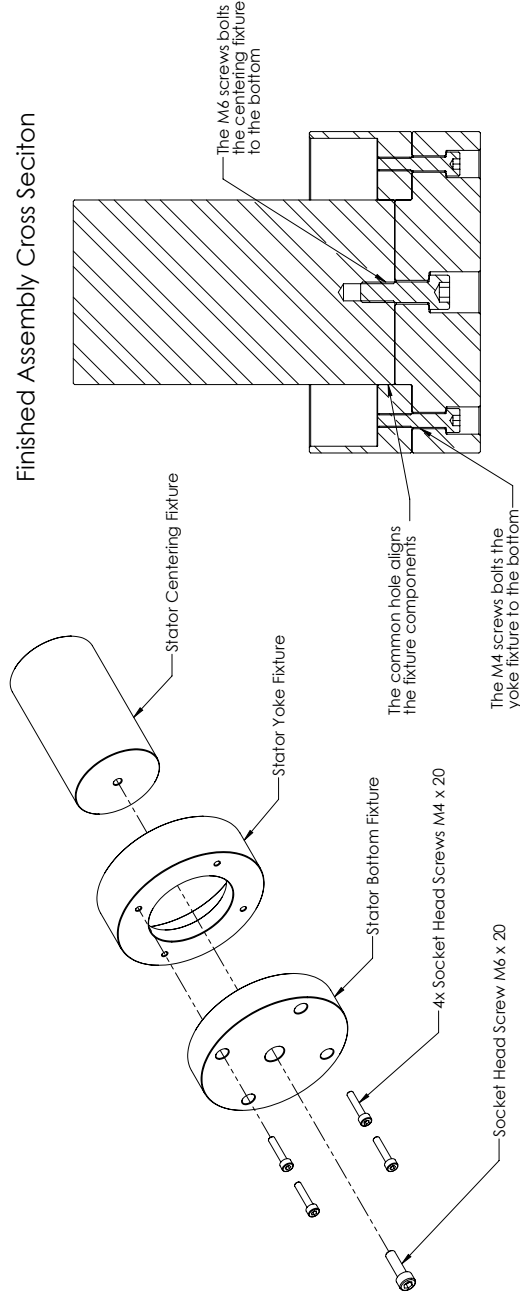
This drawing is confidential and if it is not be copied or shown to third party without the written consent of Revolve NTNU.
 General tolerances: Mean: ISO 2768-1
 Mean: ISO 2768-2, ISO 286-2
 General surface finish: Ra 3.2

**SolidWorks Student Edition.
 For Academic Use Only.**

Material: _____
 SCALE: _____
 Weight: _____

Rev no: Lateng, +47 924 995 67
 No of units: 18
 Sheet 18 of 47

Assembly 3.1 Stator Fixture



Assembly Procedure

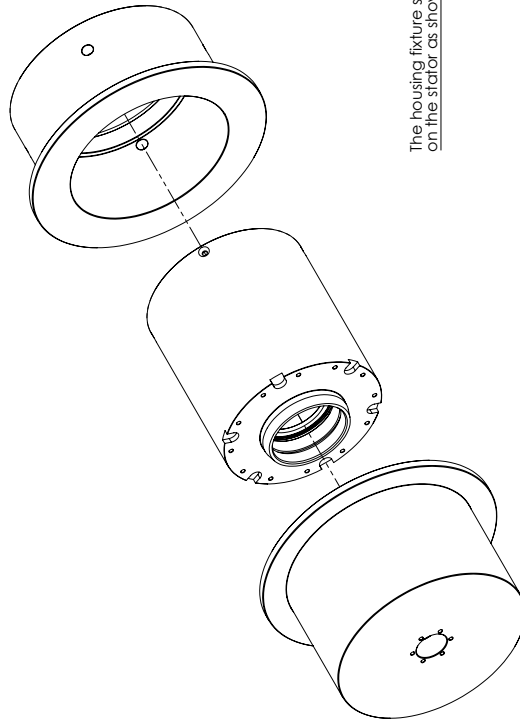
- Step 1: Mount the yoke fixture to the bottom fixture
- Step 2: Mount the centering fixture to the bottom fixture

NOTE: Bolt Pretension is not important in this assembly. Just pretension so things are held firmly together.

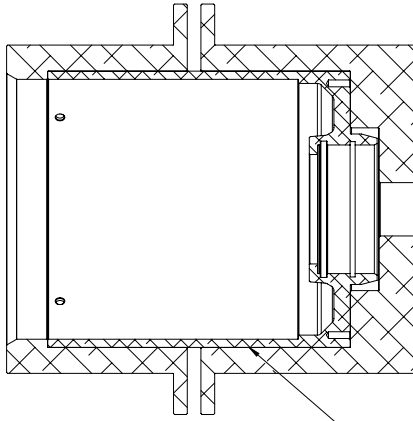
**SolidWorks Student Edition.
For Academic Use Only.**

Date	25.05.2016	Design	AAL	Checked gr.	Approved	Material	Weight
Assembly 3.1 Stator Fixture				SCALE			
Contact info		Rev no		No of units			
Laleng, +47 924 995 67				Sheet 19 of 47			
Drawing N°		General tolerances: Mean: ISO 2768-1 Mean: ISO 2768-2, ISO 286-2 Surface texture: Rmax: 0.2 General surface finish: Ra 3.2					

Assembly 3.2 Stator Housing Fixture



Finished Assembly Cross Section

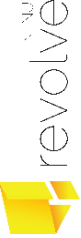


The housing fixture slides on the stator as shown

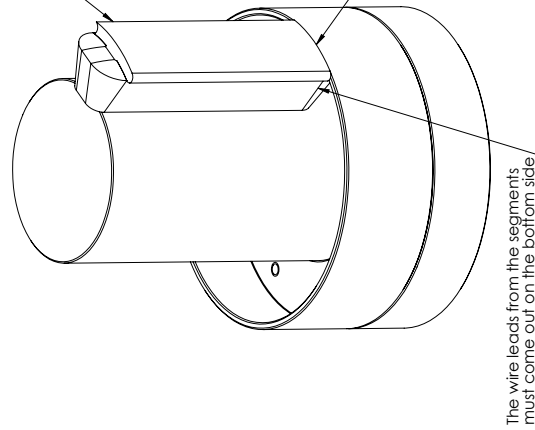
Assembly Procedure

Step 1: Slide the housing fixture on to the stator housing as shown

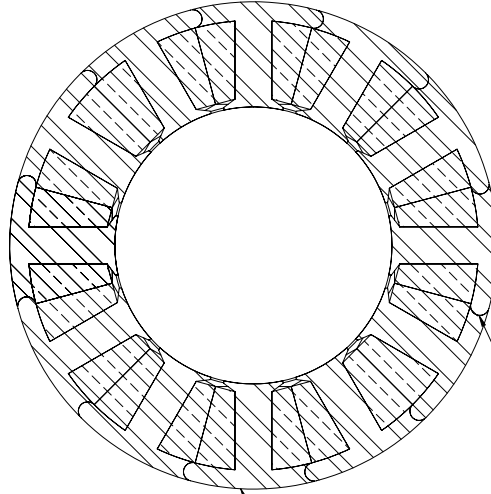
**SolidWorks Student Edition.
For Academic Use Only.**

Date: 25.05.2016	Design: AAL	Checked gr.	Approved	Material	Weight
Assembly 3.2 Stator Housing Fixture			SCALE		
Contact info: Laleng, +47 924 995 67	Rev no	No of units			
Drawing N°	Sheet 20	of 47			
<small>This drawing is confidential and it shall not be copied or shown to third party without the written consent of Revolve NTNU.</small> <small>General tolerances: Mean: ISO 2768-1 Mean: ISO 2768-2, ISO 286-2 General surface finish: Ra 3.2</small>					

Assembly 3.3 Stator Assembly (1/2)



Complete Stator Cross Section



Note how the stator segments locks into each other

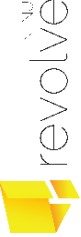
Assembly Procedure

- Step 1: Start stacking the stator segments as shown above
- Step 2: Continue until all segments are locked into each other like shown on the figure to the right

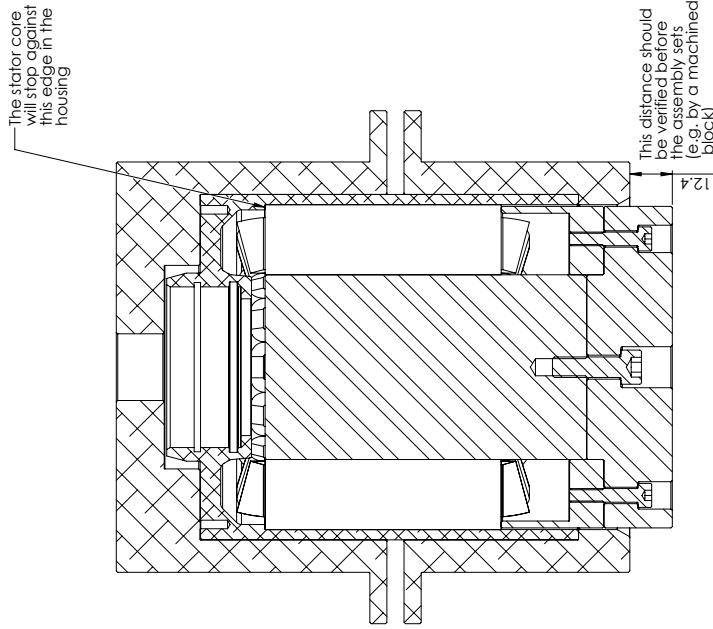
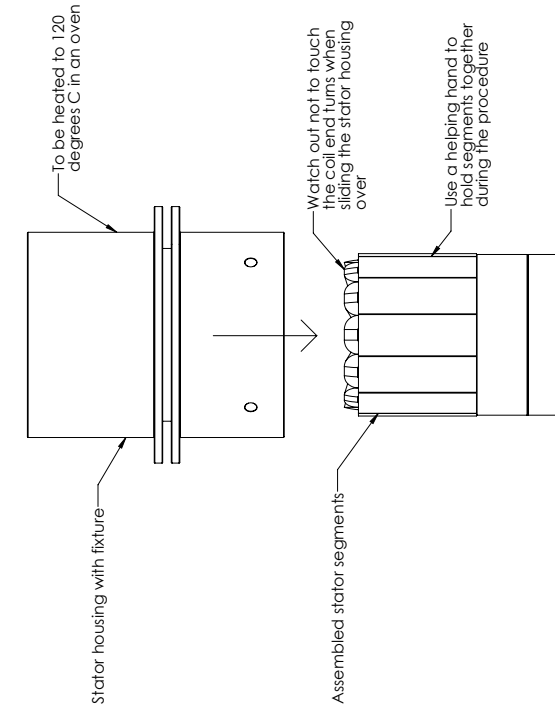
NOTE:

Make sure all the wire leads hangs downwards, i.e. no wire leads should leave the stator from the top

**SolidWorks Student Edition.
For Academic Use Only.**

Date	25.05.2016	Design	AAL	Checked gr.	Approved	Material	Weight
Assembly 3.3 Stator Assembly (1/2) Stator Core Assembly				SCALE			
Contact info	Laleng, +47 924 995 67			Rev no	No of units		
				Drawing n°	Sheet 21	of 47	
<small>General tolerances: Mean: ISO 2768-1 Mean: ISO 2768-2, ISO 286-2, 0.2 General surface finish: Ra 3.2</small>							
<small>This drawing is confidential and it shall not be copied or shown to third party without the written consent of Revolve NTNU</small>							

Assembly 3.3 Stator Assembly (2/2)

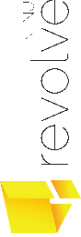


Assembly Procedure

- Step 1: Preheat the stator housing with fixture to 120 degrees
- Step 2: Grab it by the flanges and insert it by hand over the stacked stator segments
- Step 3: Hold a light push on the housing until the assembly has cooled down
- Step 4: Remove the fixtures from the assembly

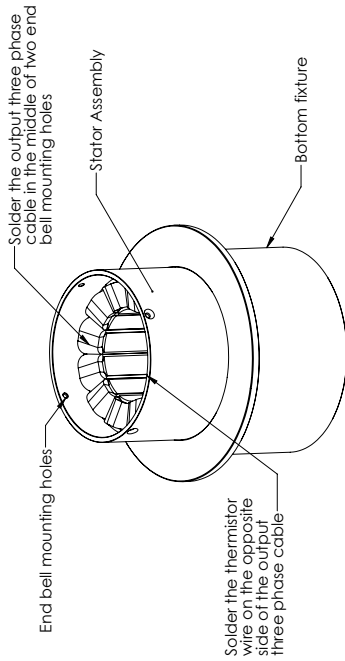
NOTE:
If the flanges are a bit small to hold, a bigger flange may be machined on and bolted on

**SolidWorks Student Edition.
For Academic Use Only.**

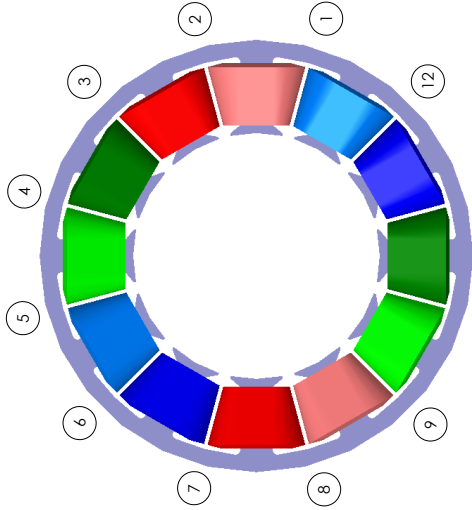
Date: 25.05.2016	Design: AAL	Checked gr.	Approved
Assembly 3.3 Stator Assembly (2/2) Stator Shrink Fitting		Material	Weight
Contact info: Laleng, +47 924 995 67	Rev no	SCALE	No of units
Drawing N°	Sheet 22	of 47	
			

This drawing is confidential and it shall not be copied or shown to third party without the written consent of Revolve NTNU.
General tolerances: Mean: ISO 2768-1
Mean: ISO 2768-2, ISO 286-2
General surface finish: Ra 3.2

Assembly 3.4 Soldering Coil Connections



Coil Connections (All coils in a phase are connected in series)



Assembly Procedure

- Step 1: Put stator inside the lower fixture for stability during soldering.
- Step 2: Solder the coil connections in series into phase A, B, and C. (See table)
- Step 3: Solder extensions to each phase input and output
- Step 4: Isolate the phase extensions, e.g. using Kapton tape
- Step 5: Create a Y-connection by soldering the outputs of each phase together into one center node
- Step 6: Isolate the center node, e.g. wrapping it in Kapton tape
- Step 7: Solder the inputs of all phases to a three-phase cable extension in the middle between two end bell mounting holes
- Step 8: Solder a grounding wire to the shielding of the three phase cable
- Step 8: Fasten all the wiring to the end turns to make it as compact as possible
(End turns cannot stick further out than 7mm from the stator housing edge - check mechanical compatibility by trying to mount end bell)
- Step 9: Fasten thermistor to the end turns at the opposite side of the output three phase cable, e.g. using Kapton tape

NOTE: Make sure all isolations between the phases are able to withstand a potential of 600V SolidWorks Student Edition. For Academic Use Only.

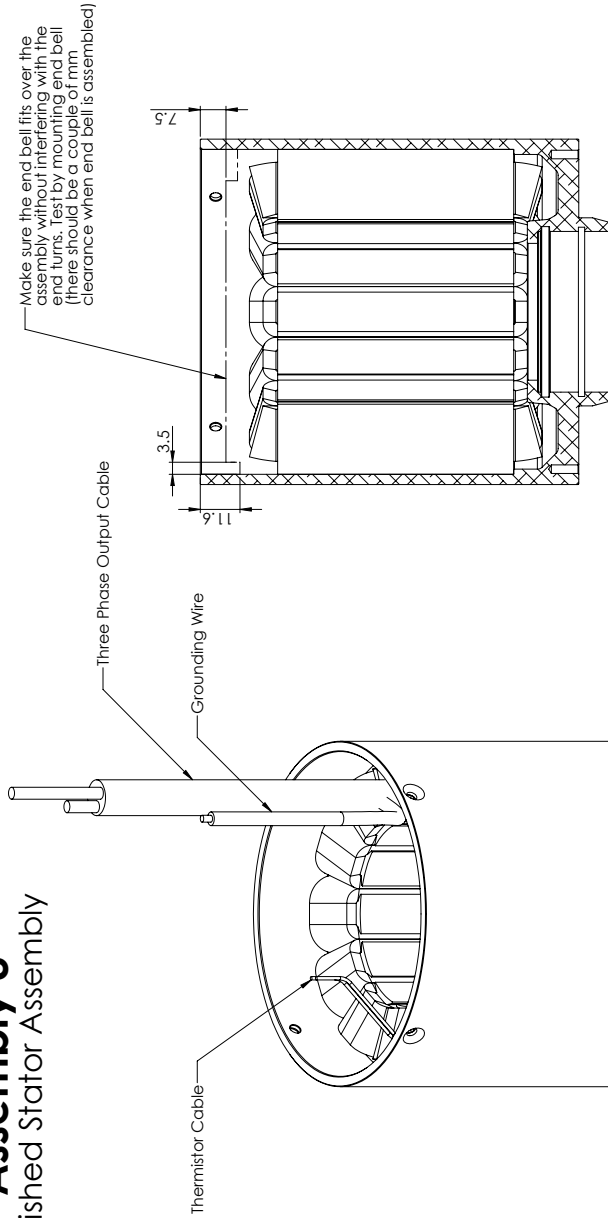
Coil	Phase A		Phase B		Phase C	
	In	Out	In	Out	In	Out
1	1	2	5	6	9	10
2	3	2	7	6	11	10
3	8	7	12	11	4	3
4	8	9	12	1	4	5

Date	25.05.2016	Design	AAI	Checked gr.	Approved
Assembly 3.4 Soldering Coil Connections			Material	SCALE	Weight
Contact info	Laleng, +47 924 995 67		Rev no	No of units	
Drawing N°			Sheet 23	of 47	

This drawing is confidential and it shall not be copied or shown to third party without the written consent of Revolve NTNU. General tolerances: Mean: ISO 2768-1, Mean: ISO 2768-2, ISO 286-2, General surface finish: Ra 3.2.

Assembly 3

Finished Stator Assembly



This drawing is confidential and it shall not be copied or shown to third party without the written consent of Revolve NTNU.

General tolerances: Mean: ISO 2768-1
 Mean: ISO 2768-2, ISO 2864-2
 General surface finish: Ra 3.2

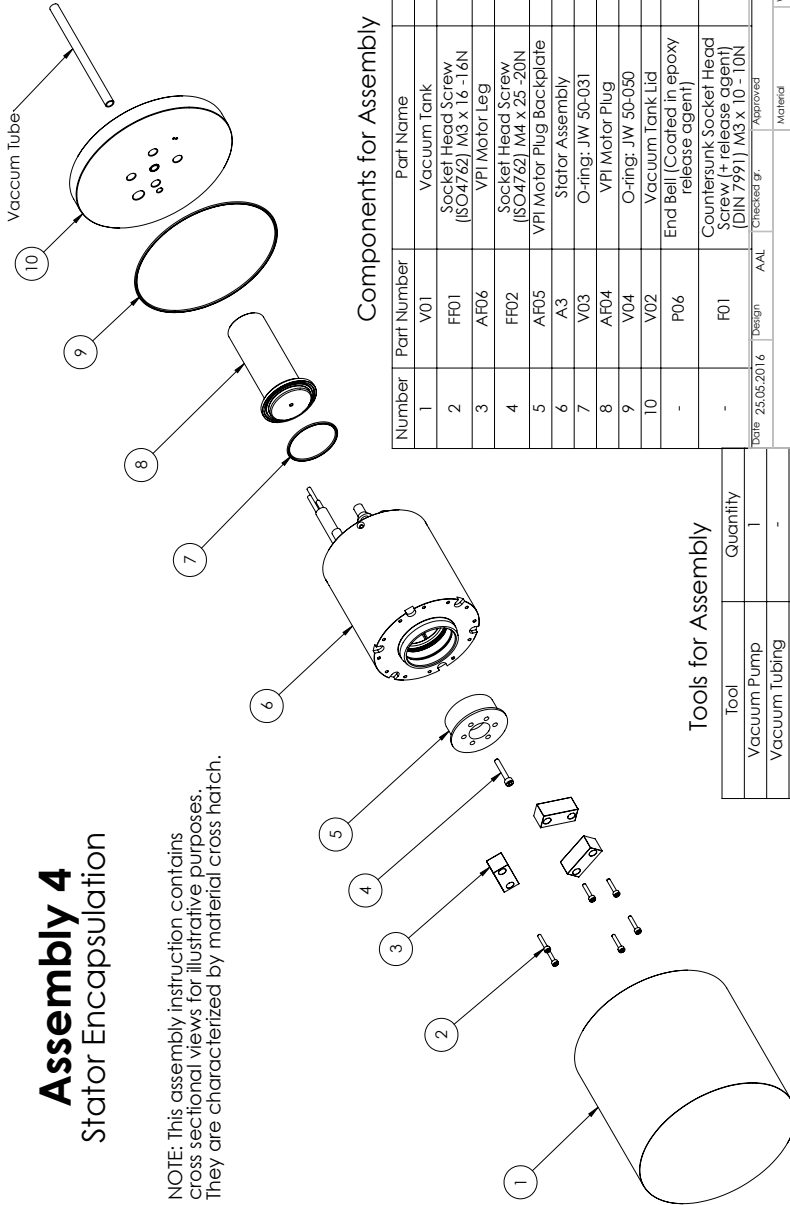
**SolidWorks Student Edition.
 For Academic Use Only.**

Date: 25.05.2016	Design: AAL	Checked gr.	Approved
Assembly 3 Finished Stator Assembly			Material
Contact info			Weight
Laleng, +47 924 995 67			SCALE
Rev no			
No of units			
Drawing n°			
Sheet 24			
of 47			

Assembly 4

Stator Encapsulation

NOTE: This assembly instruction contains cross sectional views for illustrative purposes. They are characterized by material cross hatch.



Components for Assembly

Number	Part Number	Part Name	Quantity
1	V01	Vacuum Tank	1
2	FF01	Socket Head Screw (ISO4762) M3 x 16-16N	6
3	AF06	VPI Motor Leg	3
4	FF02	Socket Head Screw (ISO4762) M4 x 25-20N	1
5	AF05	VPI Motor Plug Backplate	1
6	A3	Stator Assembly	1
7	V03	O-ring: JW 50-031	1
8	AF04	VPI Motor Plug	1
9	V04	O-ring: JW 50-050	1
10	V02	Vacuum Tank Lid	1
-	P06	End Bell (Coated in epoxy release agent)	1
-	F01	Countersunk Socket Head Screw (+ release agent) (DIN 7991) M3 x 10-10N	4

Tools for Assembly

Tool	Quantity
Vacuum Pump	1
Vacuum Tubing	-
T-joints and switches	-
Epoxy Lock	1
Oven	1
Epoxy Encapsulant	-
Epoxy Release Agent (e.g. Frekote NC44)	-

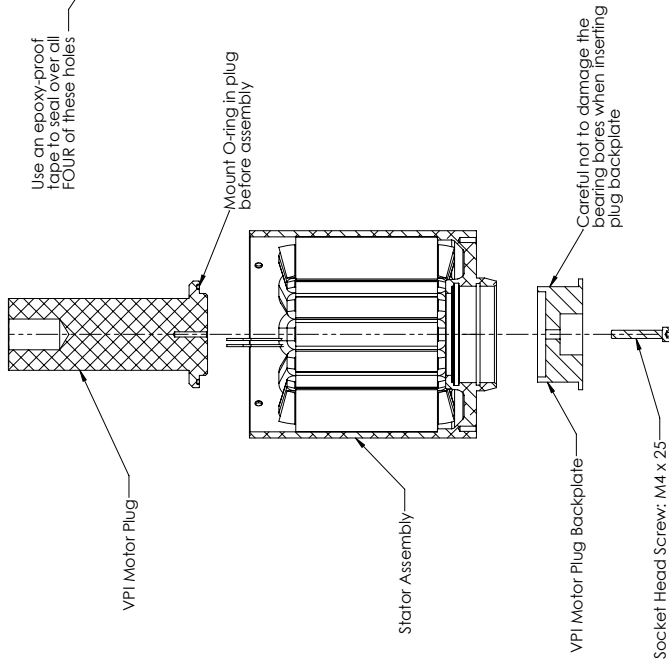
NOTE: Vacuum tank may be omitted from assembly if one of sufficient size or a real VPI tank during production

SolidWorks Student Edition.
For Academic Use Only.

This drawing is confidential and it shall not be copied or shown to third party without the written consent of Revolve NTNU.
General tolerances: Mean: ISO 2768-1
Mean: ISO 2768-2, ISO 286-2, 0.2
General surface finish: Ra 3.2

Date: 25.05.2016	Design: AAL	Approved:	Material:	Weight:
Assembly 4 Stator Encapsulation			SCALE:	
Contact info:	Rev no:	No. of units:		
Laleng, +47 924 995 67	Sheet 25	of 47		

Assembly 4.1 VPI Plug Mounting



Assembly Procedure

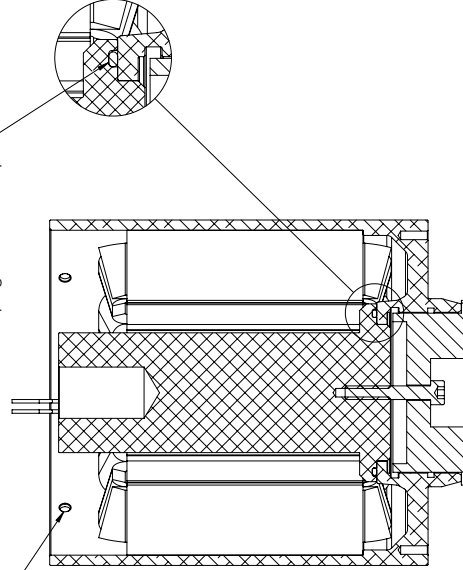
- Step 1: Assemble plug to stator housing as shown
- Step 2: Tighten the ball tightly. It is just to seal the plug
- Step 3: Use an epoxy proof tape to seal the FOUR ball holes in the stator

NOTE:

Make sure the O-ring is fitted within the groove after assembly. It might be easier to mount the plug up-side-down compared to the drawing

Use an epoxy-proof tape to seal over all FOUR of these holes

Make sure the O-ring seals the gap between the stator and plug after assembly



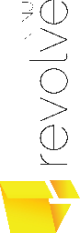
VPI Motor Plug

Stator Assembly

VPI Motor Plug Backplate

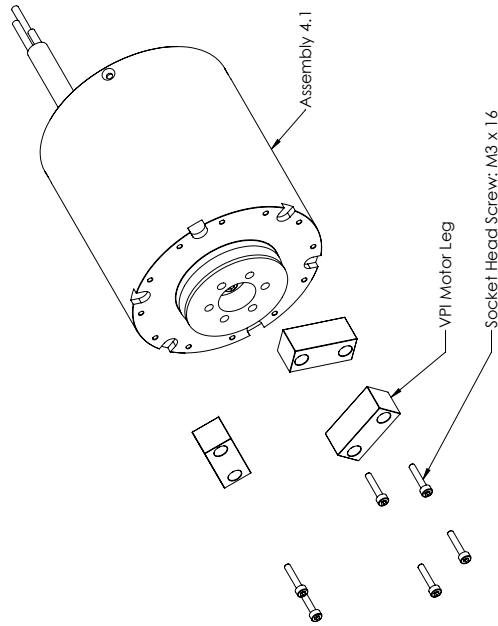
Socket Head Screw: M4 x 25

Careful not to damage the bearing bores when inserting plug backplate

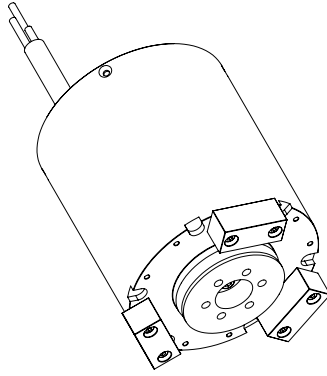
Date	25.05.2016	Design	AAJ	Checked gr.	Approved	Material	Weight
Assembly 4.1 VPI Plug Mounting				SCALE			
Contact info		Rev no		No of units			
Laleng, +47 924 995 67				Sheet 26		of 47	
Drawing 1*		General tolerances: Mean: ISO 2768-1 Mean: ISO 2768-2, ISO 286-2 General surface finish: Ra 3.2		This drawing is confidential and it shall not be copied or shown to third party without the written consent of Revolve NTNU			

**SolidWorks Student Edition.
For Academic Use Only.**

Assembly 4.2 VPI Leg Mounting



Finished Assembly



Assembly Procedure

Step 1: Mount the THREE legs to the stator casing as shown by the illustration

NOTE: Just snug the bolts sufficiently to hold the legs in place

**SolidWorks Student Edition.
For Academic Use Only.**

Date: 25.05.2016	Design: AAL	Checked gr.	Approved
Assembly 4.2 VPI Leg Mounting		Material	Weight
Contact info: Laleng, +47 924 995 67		SCALE	
Rev: 0		No. of units	
Drawing N°		Sheet 27	revolve
General tolerances: Mean: ISO 2768-1 Mean: ISO 2768-2, ISO 286-2 Surface texture: Rmax: 3.2 General surface finish: Ra: 3.2		of 47	

Assembly 4.3 Stator Impregnation

The vacuum hose must be kept out of the epoxy during VPI to make sure it only draws air

These end bell mounting holes are sealed by tape during the VPI process

The stator should be filled up to this level by the epoxy during VPI

There will be residual epoxy around the lower end turns after draining. This is removed by turning the assembly on its head and let it flow out by gravity (Step 13)

Procedure

Preparation:

- Step 1: Put the stator assembly into the vacuum tank
- Step 2: Insert FOUR epoxy hoses between the stator and motor plug
- Step 3: Guide the Three phase cable, grounding cable, thermistor cables and vacuum hoses through the tank lid
- Step 4: Insert a vacuum connection (hose) to the lid for vacuum
- Step 5: Seal all the lid connections by sealant tape

Impregnation:

- Step 6: Depressure the chamber
- Step 7: Let epoxy into the hoses that goes down the stator while vacuum is held
- Step 8: Fill the whole stator with epoxy until it reaches the top of the plug
- Step 9: Shut off the epoxy flow, but keep the vacuum on
- Step 10: Bubbles will flow from the coils while the epoxy pots all the voids
- Step 11: After 60% of the gel time of the epoxy and all bubbles are gone, switch off the vacuum and let air in through the vacuum hose
- Step 12: Put vacuum on the epoxy hoses to drain the stator for epoxy

Cleaning Residual Epoxy:

- Step 13: Remove the stator from the chamber and clean the residual epoxy by turning the stator assembly up-side-down and wiping with a lint-free cloth
- Step 14: Put the stator back on its feet and make sure there is a thin layer of epoxy all around the stator coils and core, but no epoxy around the stator opening where the end bell is to be inserted
- Step 15: Remove the sealing tape from the end bell holes
- Step 16: Remove the motor plug from the assembly by reversing Assembly 9.1
- Step 17: Wipe once again around the areas where the plug was mounted
- Step 18: Make sure no epoxy is left on the bearing bore in the stator housing

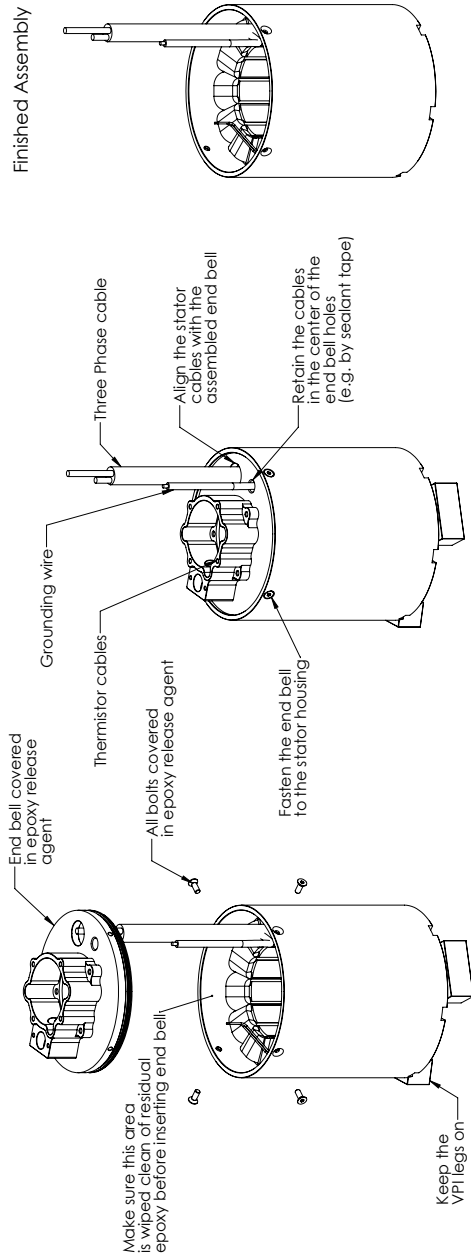
Date	25.05.2016	Design	AAL	Checked gr.	Approved
Assembly 4.3 Stator Impregnation			Material	Weight	
Contact info			SCALE		
Laleng, +47 924 995 67			Rev no	No of units	
				Sheet 28	of 47

General tolerances: Mean: ISO 2768-1
 Mean: ISO 2768-2, ISO 286-2
 General surface finish: Ra 3.2

This drawing is confidential and it shall not be copied or shown to third party without the written consent of Revolve NTNU

**SolidWorks Student Edition.
For Academic Use Only.**

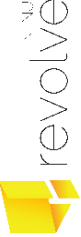
Assembly 4.4 Encapsulant Curing



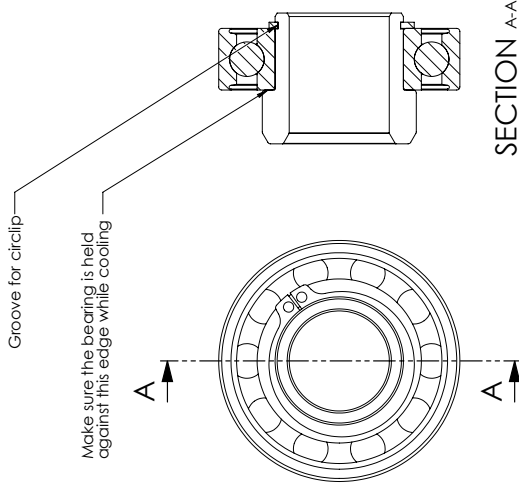
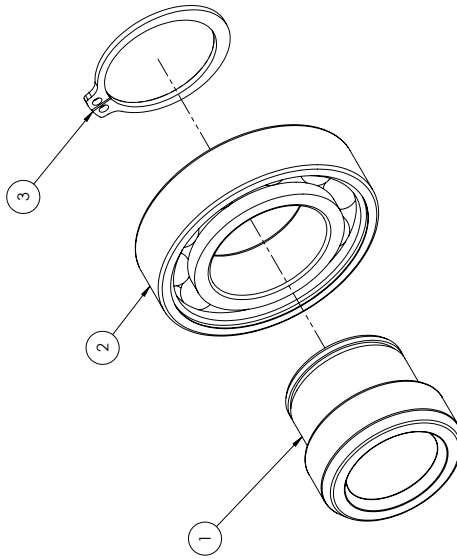
Assembly Procedure

- Step 1: Make sure the end bell with fasteners are coated with an epoxy release agent and the stator housing is wiped clean of residual epoxy in the opening.
- Step 2: Slide the end bell into the stator while inserting the stator cables into their respective holes in the end bell. This includes the three phase cable, grounding wire and thermistor cables.
- Step 3: Fasten the end bell and retain the cables centered with respect to the end bell holes.
- Step 4: Put the stator on its legs into the oven for curing.
- Step 5: Remove end bell and VPI legs after curing.

**SolidWorks Student Edition.
For Academic Use Only.**

Date	25.05.2016	Design	AAL	Checked gr.	Approved	Material	Weight
Assembly 4.4 Encapsulant Curing				SCALE			
Contact info	Rev no		No of units				
Laleng, +47 924 995 67		Sheet 29 of 47					
<small>This drawing is confidential and it shall not be copied or shown to third party without the written consent of Revolve NTNU. General tolerances: Mean: ISO 2768-1 Mean: ISO 2768-2, ISO 286-2, 0.2 General surface finish: Ra 3.2</small>							

Assembly 5 Bearing Sleeve Assembly



Assembly Procedure

- Step 1: Heat the bearing (2) up to 100 degrees C
- Step 2: Slide the hot bearing on to bearing sleeve (2) and hold it against the edge while it cools down
- Step 3: Fasten the external circlip in its designated groove on the bearing sleeve

Tools for Assembly

Tool	Quantity
External Circlip Tool	1
Oven	1
Gloves (100degC)	2

This drawing is confidential and it shall not be copied or shown to third party without the written consent of Revolve NTHU.
 General tolerances: Mean: ISO 2768-1
 Mean: ISO 2768-2, ISO 286-2
 General surface finish: Ra 3.2

**SolidWorks Student Edition.
For Academic Use Only.**

Components for Assembly

Number	Part Number	Part Name	Quantity
1	P07	Bearing Sleeve	1
2	S01	Deep Groove Ball Bearing SKF Explorer 6005	1
3	S08	Shaft Circlip (DIN471) 25 X 1.2	1

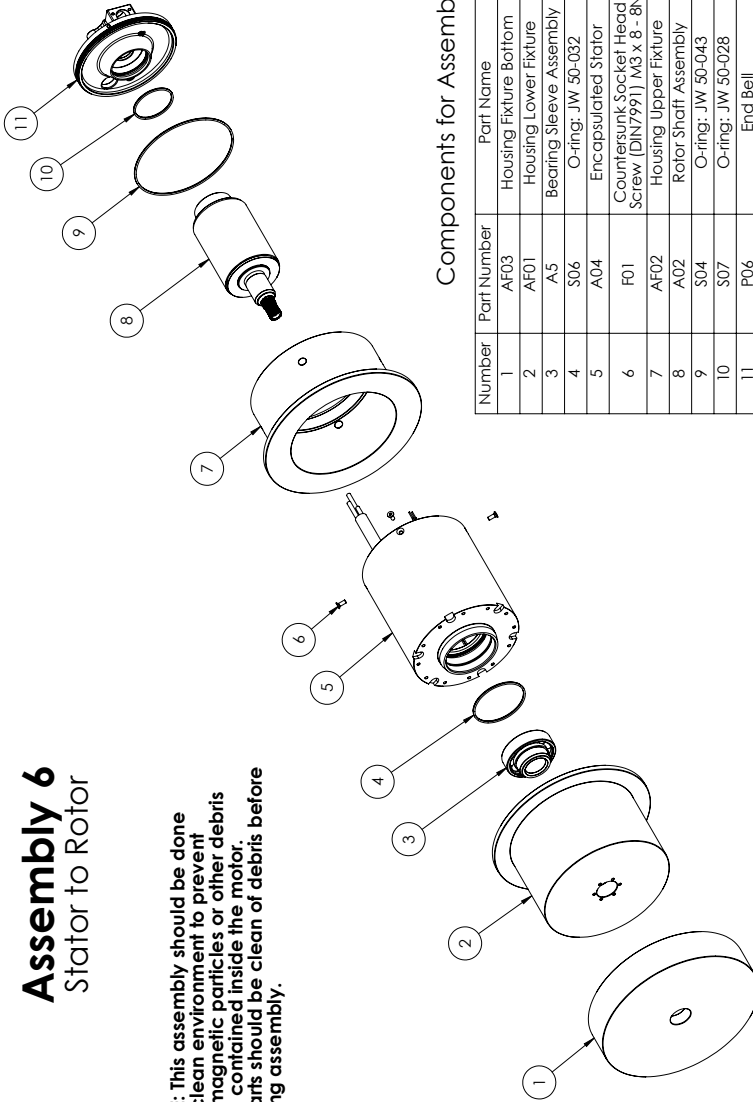
Date: 25.05.2016	Design: AAL	Checked: gr.	Approved:	Material:	Weight:
Assembly 5 Bearing Sleeve Assembly					
Contact info			Rev. No		
Lateng, +47 924 995 67			No. of units		
Drawing 1*			Sheet 30		
			of 47		



Assembly 6

Stator to Rotor

NOTE: This assembly should be done in a clean environment to prevent ferromagnetic particles or other debris to be contained inside the motor. All parts should be clean of debris before starting assembly.



Components for Assembly

Number	Part Number	Part Name	Quantity
1	AF03	Housing Fixture Bottom	1
2	AF01	Housing Lower Fixture	1
3	A5	Bearing Sleeve Assembly	1
4	S06	O-ring: JW 50-032	1
5	A04	Encapsulated Stator	1
6	F01	Countersunk Socket Head Screw (DIN/991) M3 x 8 - 8N	4
7	AF02	Housing Upper Fixture	1
8	A02	Rotor Shaft Assembly	1
9	S04	O-ring: JW 50-043	1
10	S07	O-ring: JW 50-028	1
11	P06	End Bell	1

Tools for Assembly

Tool	Quantity
Oven	-
Unbrako 2.0mm	1
Locifite 222 (eqv.)	-
Gloves (100degC)	2

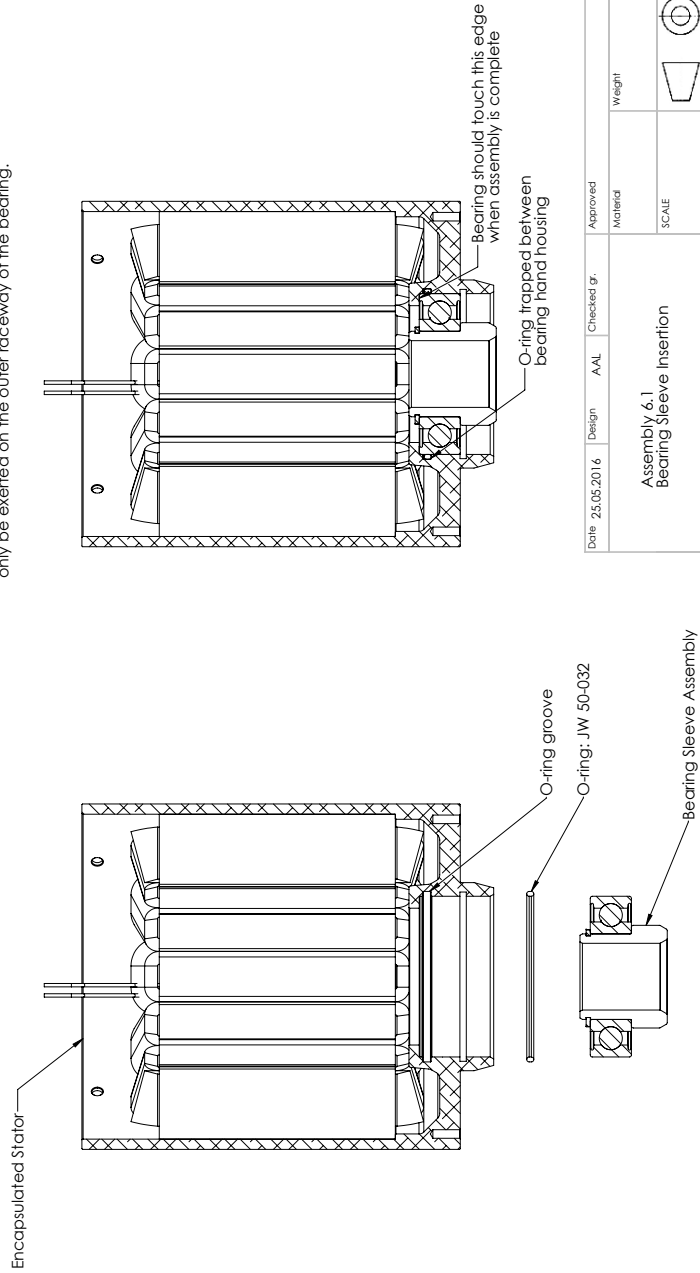
This drawing is confidential and it may not be copied or shown to third party without the written consent of Revolve NTNU. General tolerances: Mean: ISO 2768-1 Mean: ISO 2768-2, ISO 286-2. General surface finish: Ra 3.2.

NOTE: This assembly instruction contains a lot of cross sectional views. Unless otherwise is stated, the views should be considered as cross sectional.

**SolidWorks Student Edition.
For Academic Use Only.**

Date: 25.05.2016		Design: AAL	Checked: gr.	Approved:
Material:		Weight:		
SCALE:				
Contact info:		Rev no:	No of units:	
Laleng, +47 924 995 67		Sheet 31	of 47	

Assembly 6.1 Bearing Sleeve Insertion



Assembly Procedure:

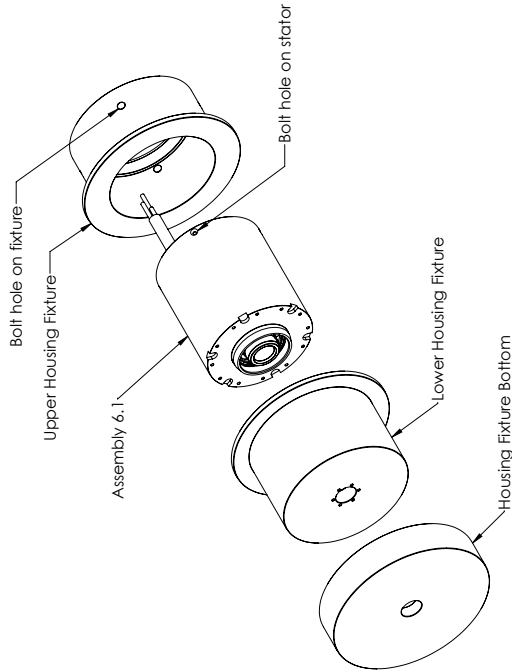
- Step 1: Insert the O-ring into its groove in the stator
 - Step 2: Heat stator to 100 degrees
 - Step 3: Insert Bearing Assembly all the way into the bore
 - Step 4: Hold hand pressure on the bearing until the stator has cooled
- NOTE: If the bearing is not pushed all the way, a hydraulic press must be used to force the bearing all the way in. In this case, the pressure must only be exerted on the outer raceway of the bearing.

Date: 25.05.2016	Design: AAL	Checked gr.	Approved
Assembly 6.1 Bearing Sleeve Insertion		Material	Weight
Contact info: Laleng, +47 924 995 67		SCALE	
Rev no		No of units	
Drawing N°		Sheet 32 of 47	

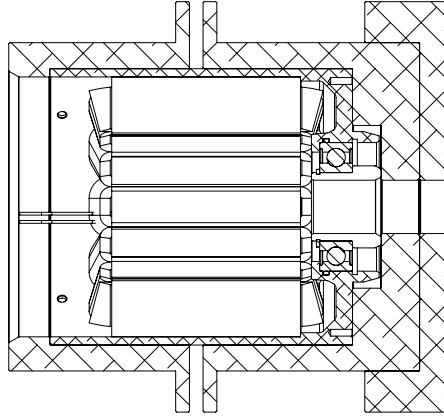
This drawing is confidential and it shall not be copied or shown to third party without the written consent of Revolve NTNU.
 General tolerances: Mean: ISO 2768-1
 Mean: ISO 2768-2, ISO 286-2
 General surface finish: Ra 3.2

**SolidWorks Student Edition.
For Academic Use Only.**

Assembly 6.2 Fixture Mounting



Finished Assembly Cross Section



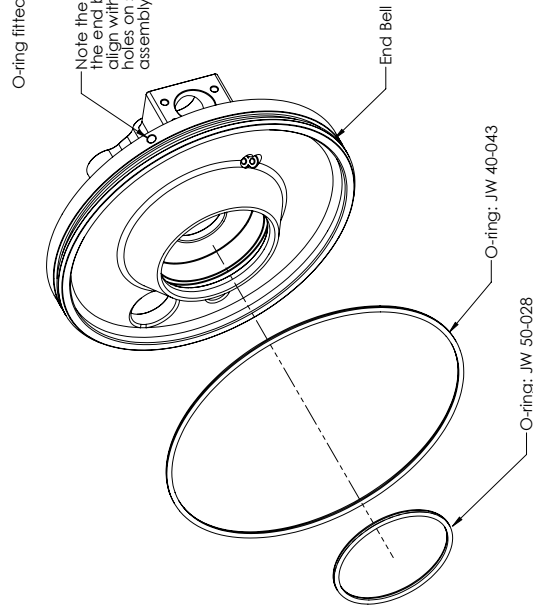
Assembly Procedure:

- Step 1: Slide the fixture over the stator as shown
- Step 2: Make sure the FOUR holes on the stator housing aligns with the corresponding holes on the fixture

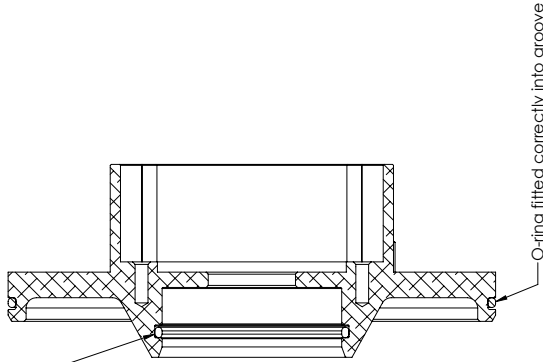
**SolidWorks Student Edition.
For Academic Use Only.**

Date: 25.05.2016	Design: AAL	Checked gr.	Approved Material	Weight
Assembly 6.2 Fixture mounting			SCALE	
Contact info: Laleng, +47 924 995 67		Rev no	No of units	
Drawing n°		Sheet 33	of 47	
<small> General tolerances: Mean: ISO 2768-1 Mean: ISO 2768-2, ISO 286-2 General surface finish: Ra 3.2 This drawing is confidential and it shall not be copied or shown to third party without the written consent of Revolve NTNU </small>				

Assembly 6.3 End Bell Preparation



Finished Assembly Cross Section



Assembly Procedure:

Step 1: Place both O-rings within their designated grooves on the end bell as shown
 NOTE: Be careful not to stretch the outer O-ring too much while assembling.

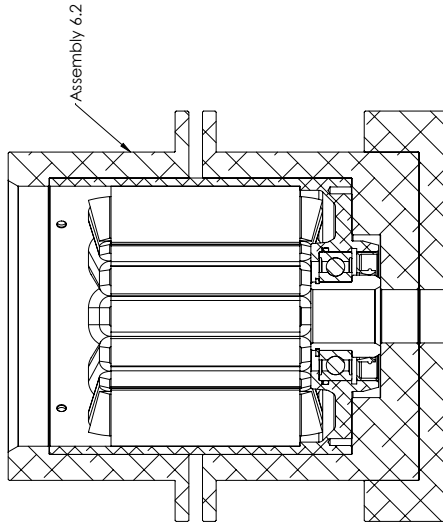
**SolidWorks Student Edition.
 For Academic Use Only.**

Date: 25.05.2016	Design: AAL	Checked gr.	Approved
Assembly 6.3 End Bell Preparation		Material	Weight
Contact info: Laleng, +47 924 995 67		SCALE	
Rev no		No of units	
Drawing N°		Sheet 34 of 47	

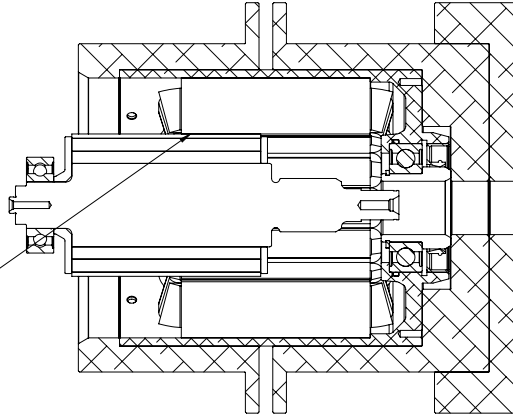
This drawing is confidential and it shall not be copied or shown to third party without the written consent of Revolve NTNU.
 General tolerances: Mean: ISO 2768-1
 Mean: ISO 2768-2, ISO 286-2, 0.2
 General surface finish: Ra 3.2

Assembly 6.4 Stator-Rotor Assembly (1/3)

Due to the permanent magnets within the rotor, the rotor will attract to the stator teeth and stick to the inner stator wall. The friction should be large enough to hold the rotor in place.



Step 1: Preheat Stator to 100 degC in an oven
(Use IR-thermometer to verify temperature)



Step 2: Carefully slide rotor into stator by hand
approximately 30mm (half the core length)

NOTE:

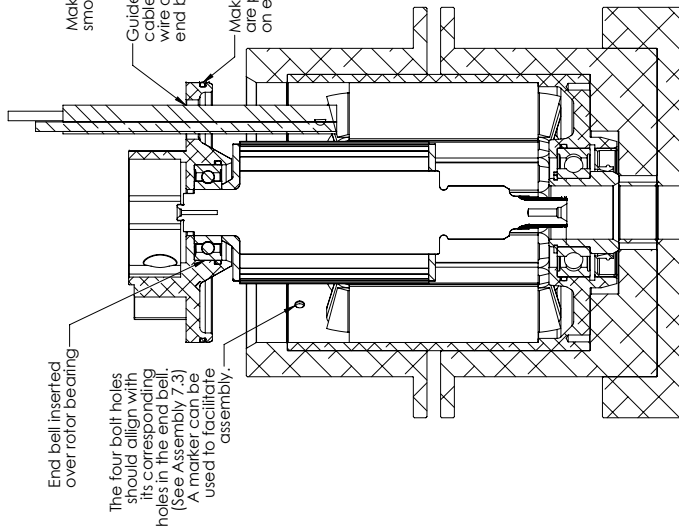
The Stator-Rotor assembly is done by shrink fitting. When the stator is removed from the oven, the assembly procedure from step 2 through 4 should happen as fast as possible before the stator cools. Thus, the assembly steps should be read beforehand. Also both rotor and prepared end bell with O-rings should be easily accessible during the assembly procedure.

**SolidWorks Student Edition.
For Academic Use Only.**

Date: 25.05.2016	Design: AAL	Checked gr.	Approved
Assembly 6.4 Stator-Rotor Assembly, step 1 & 2		Material	Weight
Contact info: Laleng, +47 924 995 67		SCALE	
Rev no		No of units	
Drawing N°		Sheet 35	of 47
General tolerances: Mean: ISO 2768-1 Mean: ISO 2768-2, ISO 286-2 General surface finish: Ra 3.2		This drawing is confidential and it shall not be copied or shown to third party without the written consent of Revolve NTNU	

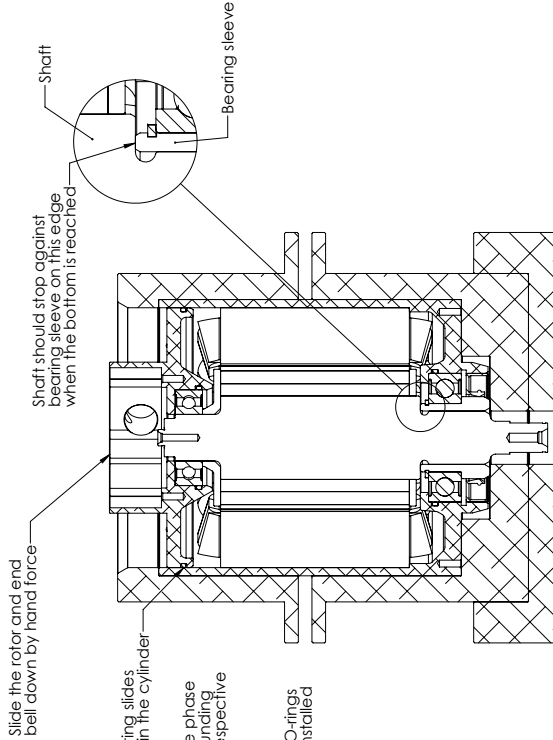


Assembly 6.4 Stator-Rotor Assembly (2/3)



Step 3: Insert the end bell over the rotor bearing and make sure the radial threaded bolt holes on the end bell align with its corresponding holes in the stator casing and fixture.

**SolidWorks Student Edition.
For Academic Use Only.**



Step 4: Push the axle all the way into the bearing sleeve by pushing on the top of the end bell with hand force in a straight, downward manner. Watch out that the outer O-ring on the end bell glides smoothly into the cylinder. When the shaft stops, keep hand pressure until the stator has cooled.

Date	25.05.2016	Design	AAJ	Checked gr.	Approved
Assembly 6.4 Stator-Rotor Assembly, step 3 & 4				Material	Weight
Contact info Laleng, +47 924 995 67				SCALE	
Rev no				No of units	
Drawing 1*				Sheet 36 of 47	

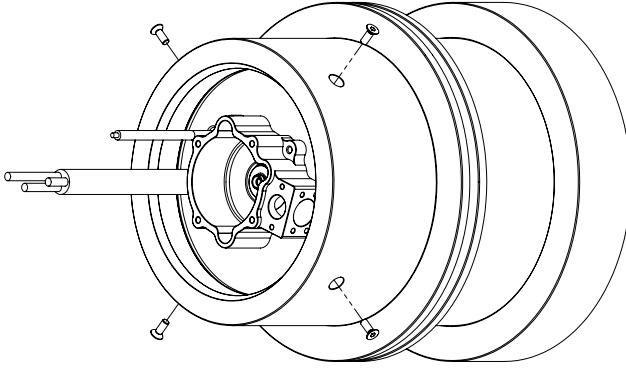
This drawing is confidential and it shall not be copied or shown to third party without the written consent of Revolve NTHU.
General tolerances: Mean: ISO 2768-1
Mean: ISO 2768-2, ISO 286-2, 0.2
General surface finish: Ra 3.2

Assembly 6.4 Stator-Rotor Assembly (3/3)

Encoder mounting holes may be used for a withdrawal tool.

Pull carefully on end bell to lift it 1mm out.

The bolt holes on the stator should align up with the tapped holes on the end bell circumference.



Step 6: Fasten the four bolts to the end bell, locking it to the stator. Put Loctite 222 on the bolts before inserting. ONE of the FOUR bolts should be pretensioned to 1.2Nm, while the remaining THREE should be barely tightened. Let the Loctite set when finished. Afterwards the fixture can be removed

Step 5: When the stator has cooled, carefully use hand force to pull the end bell back (1mm) to align the mounting holes with the stator and fixture.

NOTE:

If the end bell is too hard to pull up by hand, a withdrawal tool can simply be made, using the two threaded holes for the encoder and pushing on the shaft. If this is done, one should be careful not to damage the shaft's end, as it will be connected to an encoder.

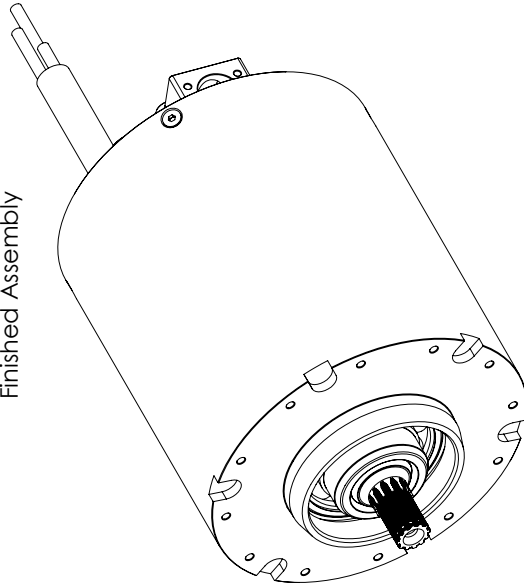
**SolidWorks Student Edition.
For Academic Use Only.**

Date: 25.05.2016	Design: AAL	Checked gr.	Approved
Assembly 6.4 Stator-Rotor Assembly, step 5 & 6		Material	Weight
Contact info Laleng, +47 924 995 67		SCALE	
Rev no		No of units	
Drawing N°		Sheet 37 of 47	
<small>This drawing is confidential and it shall not be copied or shown to third party without the written consent of Revolve NTNU.</small> <small>General tolerances: Mean: ISO 2768-1 Mean: ISO 2768-2, ISO 286-2 General surface finish: Ra 3.2</small>			

Assembly 6

Stator-Rotor Assembly

Finished Assembly



NOTE: As the end bell holes are still open for debris, the finished assembly should always be packed in plastic when not handled until the motor housing is completely sealed (Assembly 7 and 8)

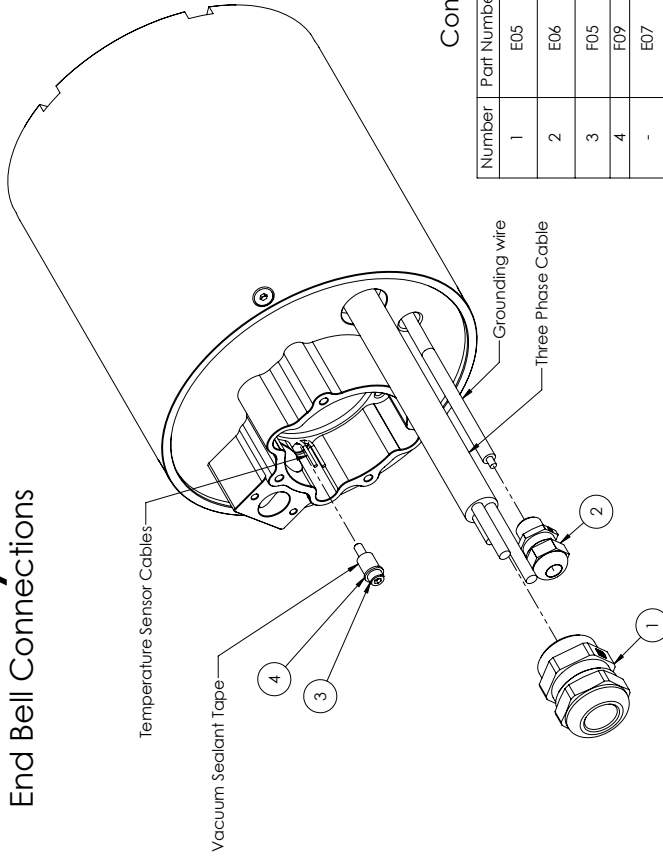
**SolidWorks Student Edition.
For Academic Use Only.**

Date: 25.05.2016	Design: AAL	Checked gr.	Approved
Assembly 6 Finished Stator-Rotor Assembly		Material	Weight
Contact info: Laleng, +47 924 995 67		SCALE	
Rev: 0		No. of units	
Drawing N°		Sheet 38	
General tolerances: Mean: ISO 2768-1 Mean: ISO 2768-2, ISO 286-2 Surface texture: Rmax: 3.2 General surface finish: Ra: 3.2		of 47	

This drawing is confidential and it shall not be copied or shown to third party without the written consent of Revolve NTNU

Assembly 7

End Bell Connections



Components for Assembly

Number	Part Number	Part Name	Quantity
1	E05	Cable Gland Hylec 18110710	1
2	E06	Cable Gland Hylec 111006	1
3	F05	Socket Head Screw (ISO4762) M2.5 x 12 - 12N	1
4	F09	Washer DIN6902 - C2.75	1
-	E07	Ring Connector RS613-9384	1
-	F04	Socket Head Screw (ISO4762) M3 x 6 - 6N	1

Tools for Assembly

Tool	Quantity
Wrench 20mm	2
Wrench 11mm	2
Unbrako 2.0mm	1
Unbrako 2.5mm	1
Locitite 222 (equiv.)	-
Vacuum Sealant Tape	-

**SolidWorks Student Edition.
For Academic Use Only.**

This drawing is confidential and it shall not be copied or shown to third party without the written consent of Revolve NTNU.

General tolerances: Mean: ISO 2768-1
Mean: ISO 2768-2, ISO 286-2
General surface finish: Ra 3.2



Rev no
Laleng, +47 924 995 67

No of units

Sheet 39 of 47

Assembly 7
End Bell Connections

Date 25.05.2016 Design AAL Checked gr. Approved

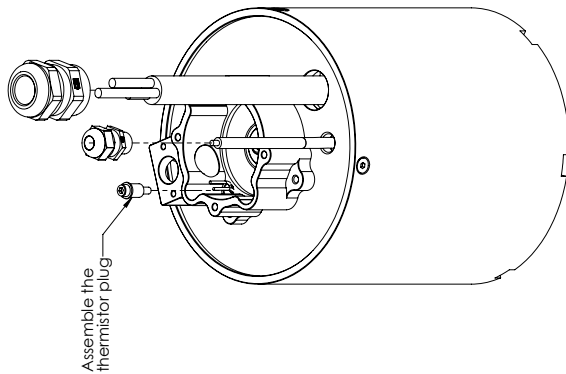
Material

SCALE

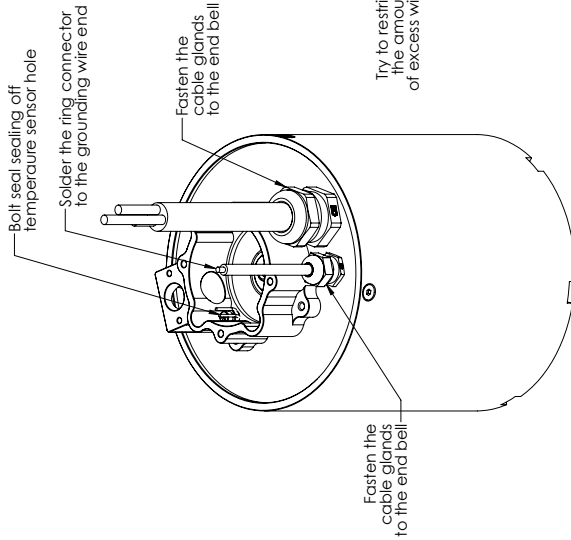
Weight



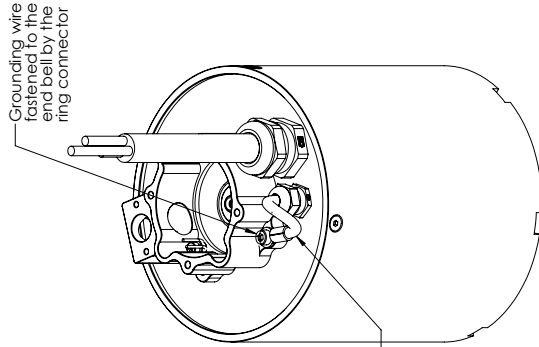
Assembly 7.1 End Bell Connections



Step 1



Step 2 to Step 4

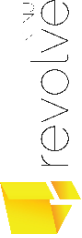


Step 5

Assembly Procedure

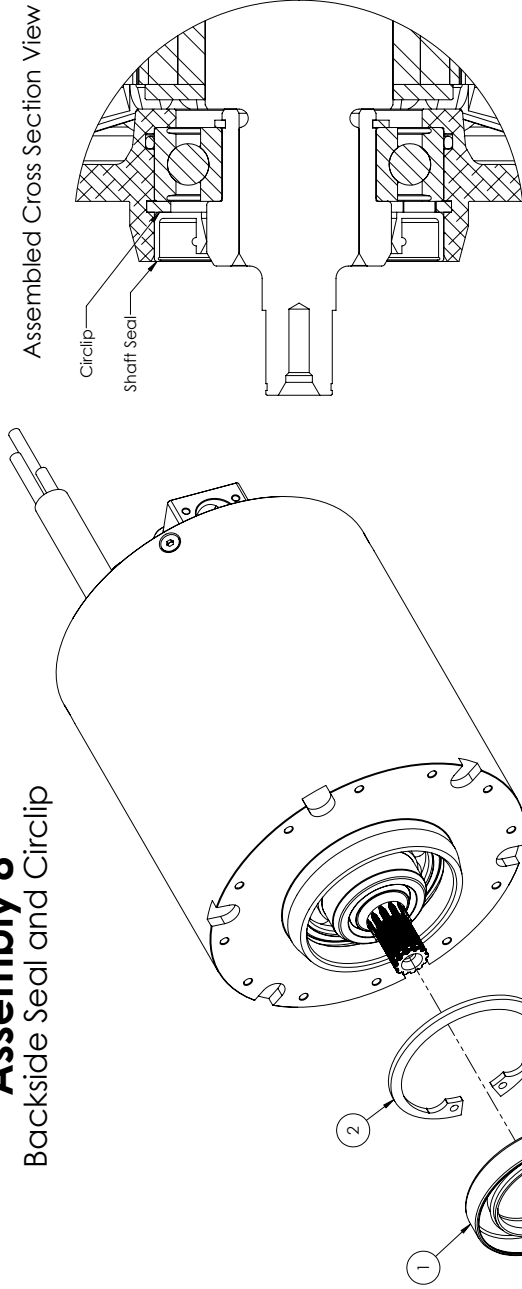
- Step 1: Prepare the thermistor plug by wrapping sealant tape around the screw/washer as shown
- Step 2: Fasten the thermistor plug into its hole
- Step 3: Slide the cable glands over the three phase and ground cables from the stator windings and fasten them to the end bell
- Step 4: Solder the ring connector to the grounding wire
- Step 5: Fasten the ring connector to the motor end bell using the M3 bolt. Use a drop of loctite to secure it in place

**SolidWorks Student Edition.
For Academic Use Only.**

Date	25.05.2016	Design	AAL	Checked gr.	Approved	Material	Weight
Assembly 7.1 End Bell Connections				SCALE			
Contact info		Rev no		No of units			
Laleng, +47 924 995 67				Sheet 40		of 47	
Drawing N°				<small> This drawing is confidential and it shall not be copied or shown to third party without the written consent of Revolve NTNU General tolerances: Mean: ISO 2768-1 Mean: ISO 2768-2, ISO 286-2 General surface finish: Ra 3.2 </small>			

Assembly 8

Backside Seal and Circlip



Assembly Procedure

- Step 1: Lock the circlip (2) in its groove in the motor casing
- Step 2: Insert the shaft seal (1) into the motor casing by hand
- Step 3: Put three drops of Loctite 222 with even spacing around the seal circumference
- Step 4: Make sure the loctite hardens sufficiently to retain the seal

Tools for Assembly

Tool	Quantity
Circlip Tool	1
Loctite 222 (eqv.)	-

This drawing is confidential and it shall not be copied or shown to third party without the written consent of Revolve NTNU. General tolerances: Mean: ISO 2768-1 Mean: ISO 2768-2, ISO 286-2 General surface finish: Ra 3.2

Components for Assembly

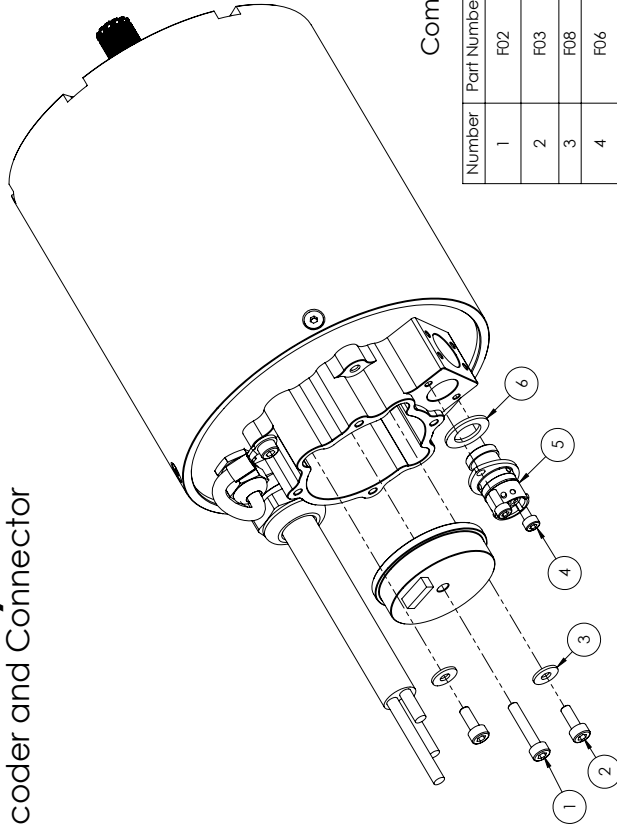
Number	Part Number	Part Name	Quantity
1	S03	Shaft Seal SKF 30x47x8 CRW1 V	1
2	S09	Bores Circlip (DIN472) 47 - 1,75	1

Date: 25.05.2016	Design: AAL	Checked gr.:	Approved:	Material:	Weight:
Assembly 8 Backside Seal and Circlip					
Contact info:			Rev no:	No of units:	
Laleng, +47 924 995 67				Sheet 41 of 47	

**SolidWorks Student Edition.
For Academic Use Only.**

Assembly 9

Encoder and Connector



Components for Assembly

Number	Part Number	Part Name	Quantity
1	F02	Socket Head Screw (ISO 4762) M3 x 1.6 - 6N	1
2	F03	Socket Head Screw (ISO 4762) M3 x 8 - 8N	2
3	F08	Washer (DIN6902 - A3.2)	2
4	F06	Socket Head Screw (ISO 4762) M2.5 x 6 - 6N	2
5	E01	Deutsch Connector ASDD0006-09SKT-HE3	1
6	E04	Connector Gasket	1

Tools for Assembly

Tool	Quantity
Unbrako Key 2.0mm	1
Unbrako Key 2.5mm	1

This drawing is confidential and its use not be copied or shown to third party without the written consent of Revolve NTHU.

General tolerances: Mean: ISO 2768-T
Max: ISO 2768-2, ISO 2864-2
Min: ISO 2768-1, ISO 2864-1
General surface finish: Ra 3.2

**SolidWorks Student Edition.
For Academic Use Only.**

Assembly 9

Encoder and Connector

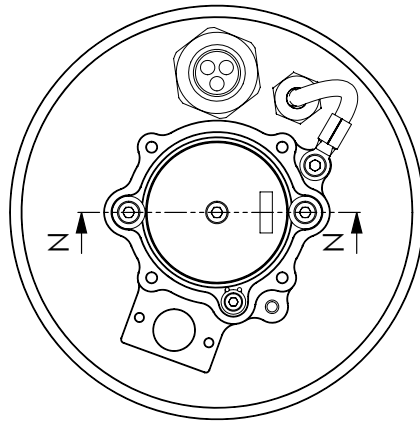
Contact info	Rev no	No of units
Laleng, +47 924 995 67		
Drawing n°	Sheet 42	of 47

Material

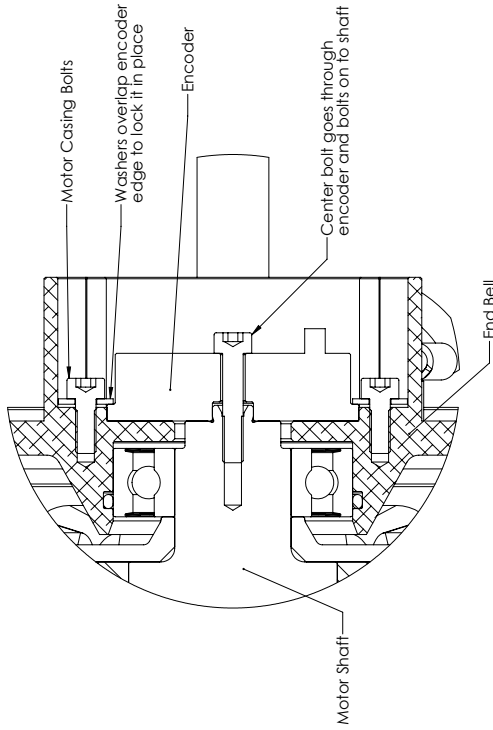
Weight

SCALE

Assembly 9.1 Encoder Mounting



Assembled Cross Section A-A



Assembly Procedure

- Step 1: Place encoder within its groove in the casing
- Step 2: Fasten encoder to motor shaft by the center bolt. Pre-tension to 1.15Nm (+/- 0.05).
- Step 3: Fasten the two motor casing bolts with washers to lock the encoder to end bell. Pre-tension to 0.7Nm

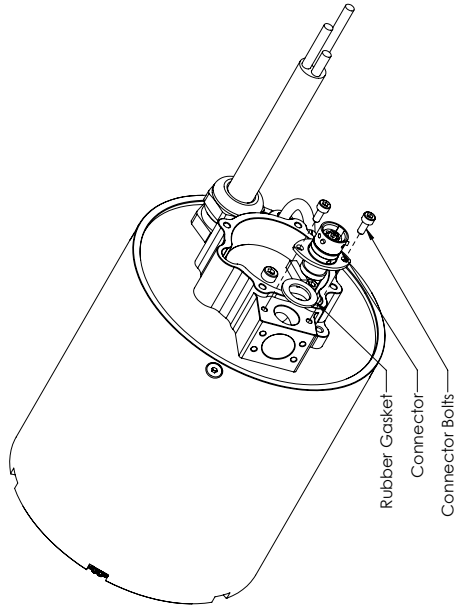
**SolidWorks Student Edition.
For Academic Use Only.**

Date	25.05.2016	Design	AAI	Checked gr.	Approved	Material	Weight
Assembly 9.1 Encoder Mounting				SCALE			
Contact info		Rev no		No of units			
Laleng, +47 924 995 67				Sheet 43		of 47	
Drawing N°							

This drawing is confidential and it shall not be copied or shown to third party without the written consent of Revolve NTNU.
 General tolerances: Mean: ISO 2768-1
 Mean: ISO 2768-2, ISO 286-2, 0.2
 General surface finish: Ra 3.2

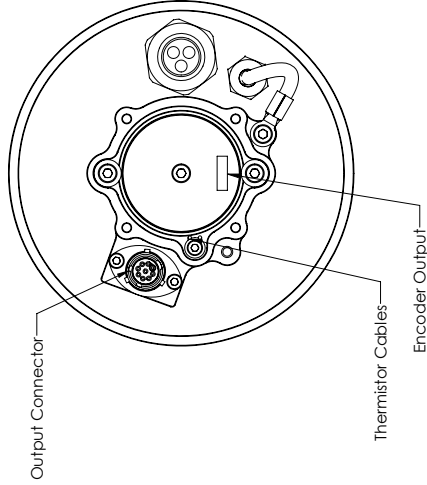
Assembly 9.2 Connector Mounting & Wiring

Fasten connector to motor



Step 2 & 3

Connect all sensors to output connector



Step 4 & 5

Assembly Procedure

- Step 1: Solder a connection to the back side of the connector
- Step 2: Insert the connection through the hole and into the encoder compartment
- Step 3: Fasten the connector with two bolts, having a rubber gasket in between for sealing
- Step 4: Connect the encoder and thermistor cables to the connector
- Step 5: Fasten all wiring so there is no significant slack in the cables

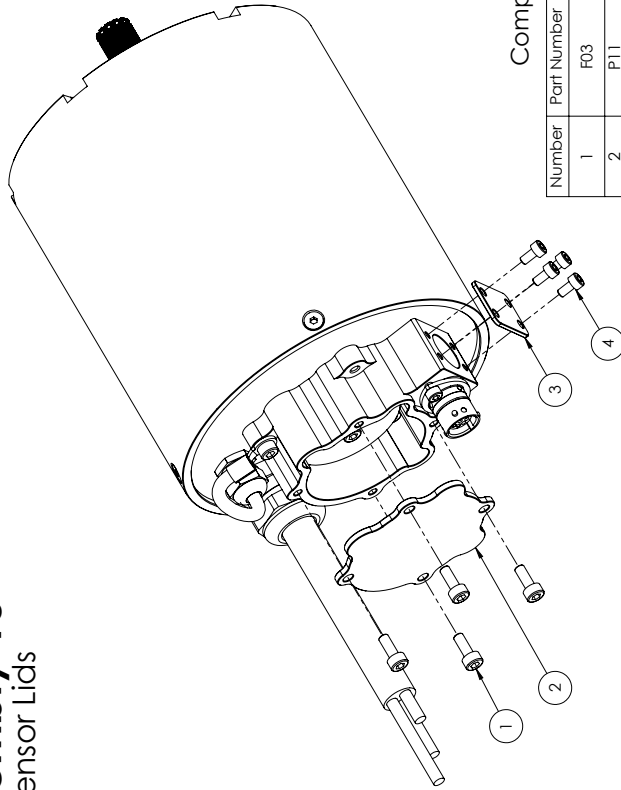
**SolidWorks Student Edition.
For Academic Use Only.**

Date: 25.05.2016	Design: AAL	Checked gr.	Approved Material	Weight
Assembly 9.2 Connector Mounting & Wiring			SCALE	
Contact info Laleng, +47 924 995 67		Rev no	No of units	
Drawing N°		Sheet 44	of 47	

This drawing is confidential and it shall not be copied or shown to third party without the written consent of Revolve NTNU.
General tolerances: Mean: ISO 2768-1
Mean: ISO 2768-2, ISO 2864-2
General surface finish: Ra 3.2

Assembly 10

Sensor Lids



Assembly Procedure

- Step 1: Apply liquid silicone gasket on the top and side flange
- Step 2: Evenly apply gasket and wipe off the excess
- Step 3: Insert the gasket into the corresponding slots
- Step 4: Tighten the M3 bolts to 1.2 Nm and the M2.5 to 0.5Nm
- Step 5: Wipe off the excess silicone

Tools for Assembly

Tool	Quantity
Unbrako Key 2.0mm	1
Unbrako Key 2.5mm	1
Silicone Gasket on Tube	-

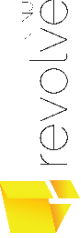
This drawing is confidential and it may not be copied or shown to third party without the written consent of Revolve NTU.

General tolerances: Mean: ISO 2768-1
Mean: ISO 2768-2, ISO 286-2
Surface texture: Ra 3.2
General surface finish: Ra 3.2

**SolidWorks Student Edition.
For Academic Use Only.**

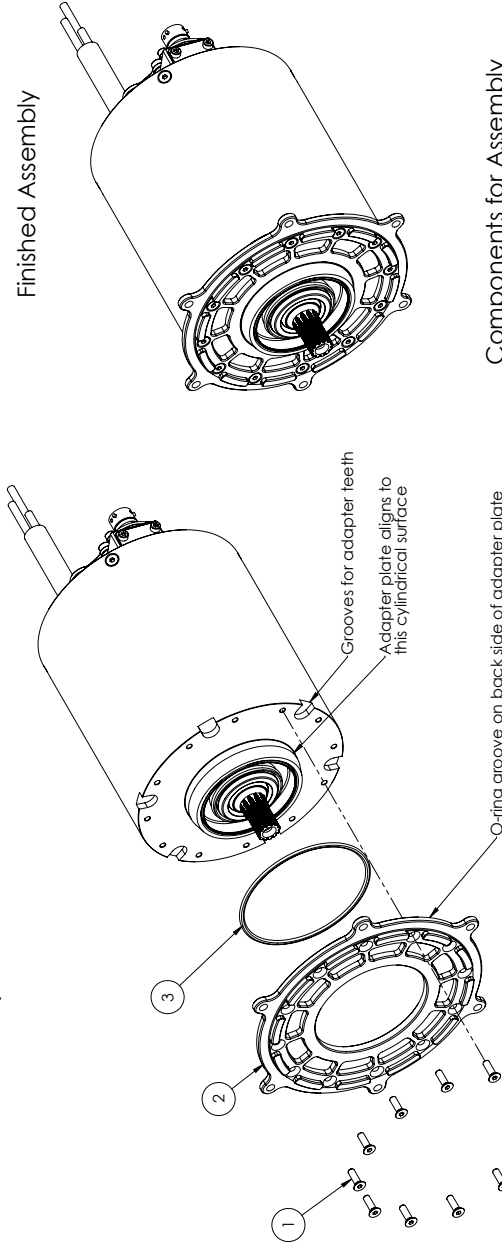
Components for Assembly

Number	Part Number	Part Name	Quantity
1	F03	Socket Head Screw (ISO 4762) M3 x 8 -8N	4
2	P11	Top Sensor Lid	1
3	P12	Side Sensor Lid	1
4	F07	Socket Head Screw (ISO 4762) M2.5 x 5 -5N	4

Date: 25.05.2016	Design: AAL	Checked gr.:	Approved:	Material:	Weight:
Assembly 10					
Sensor Lids					
Contact info:	Rev no:	No. of units:			
Laleng, +47 924 995 67					
Drawing n°:		Sheet 45			
		of 47			

Assembly 11

Motor Adapter Plate



Assembly Procedure:

- Step 1: Fit O-ring (3) into the groove on the back side of the adapter plate
- Step 2: Align the teeth of the adapter plate (2) with the grooves on the motor
- Step 3: Fasten all the screws (1) lightly to the motor, through the adapter plate
- Step 4: Tighten all bolts to 1.2Nm in a star pattern, use loctite if necessary

Tools for Assembly

Tool	Quantity
Unbrako Key 2.0mm	1
Loctite 222 (eav.)	-

This drawing is confidential and it shall not be copied or shown to third party without the written consent of Revolve NTNU. General tolerances: Mean: ISO 2768-1 Mean: ISO 2768-2, ISO 286-2. General surface finish: Ra 3.2.

**SolidWorks Student Edition.
For Academic Use Only.**

Components for Assembly

Number	Part Number	Part Name	Quantity
1	F01	Countersunk Socket Head Screw (DIN7991) M3 x 10 - 10N	12
2	P10	Motor Adapter Plate	1
3	S05	O-ring: JW 050-036	1

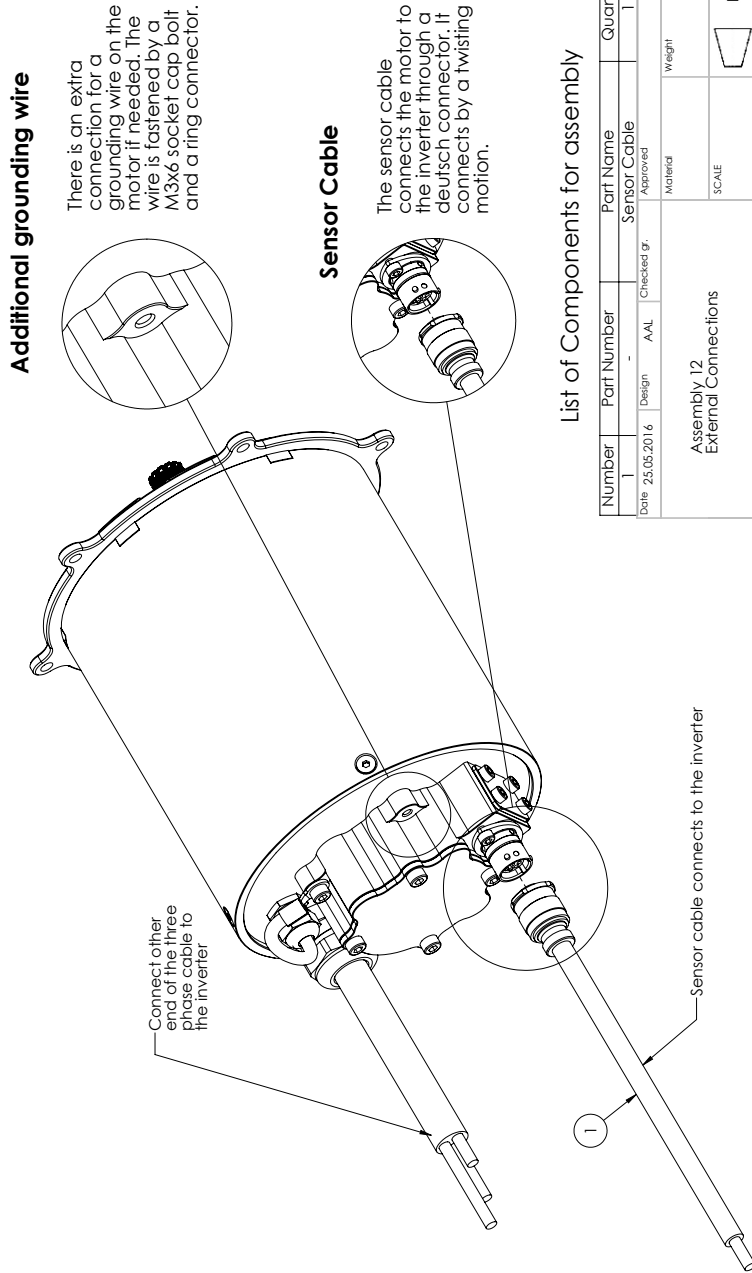
Date	Design	Checked	gr.	Approved	Material	Weight
25.05.2016	AAL					

Assembly 11		Motor Adapter Plate	
Contact info	Lateng, +47 924 995 67	Rev no	No of units
Drawing N°		Sheet 46	of 47



Assembly 12

External Connections



List of Components for assembly

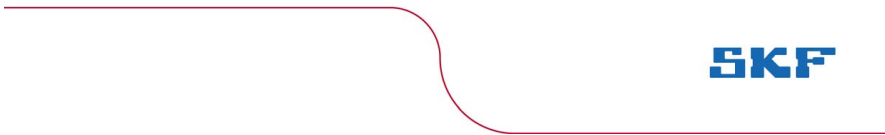
Number	Part Number	Part Name	Quantity
1	-	Sensor Cable	1
Date: 25.05.2016		Design: AAL	Checked gr.:
Approved		Material	Weight
SCALE		SCALE	
Contact info		Rev. no.	No. of units
Laleng, +47 924 995 67			Sheet 47 of 47
Drawing 1*			

This drawing is confidential and it shall not be copied or shown to third party without the written consent of Revolve NTNU.
 General tolerances: Mean: ISO 2768-1
 Mean: ISO 2768-2, ISO 286-2, 0.2
 General surface finish: Ra 3.2

**SolidWorks Student Edition.
For Academic Use Only.**

Appendix D

SKF Bearing Stiffness Calculation



SKF

Harry Opdal



Table of contents

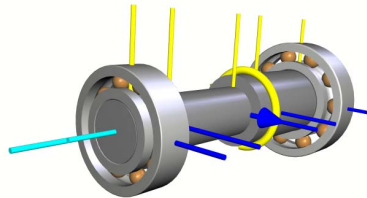
1. Bearings	4
1.1. Bearing geometry	4
1.2. Bearing loads	5
1.2.1. Bearing loads, local	5
1.2.2. Bearing loads, axial and radial	5
1.2.3. Bearing row loads	5
1.3. Bearing contact data	6
2. Contact pressure	7
2.1. Bearing max. contact pressure	7
2.2. Bearing max. pressure with/except edge	7
3. Lubricant	8
3.1. Lubricant data	8
3.2. Bearing lubrication conditions	8
4. Speed	8
4.1. Bearing speed	8
4.2. Shaft speed	8



SKF SimPro Expert - Calculation Report

Project:
Customer:
Date:
Report id:

SKF Norge AS
Application Engineering
Name





1. Bearings

1.1. Bearing geometry

Analyses	Bearing	Type	Version	LC state	Quality class
Static_1	MotorShaft->6003 C3	DGBB	2.18	RELEASED	Explorer
	MotorShaft->6005 C3	DGBB	2.19	RELEASED	Explorer

Begge lager har keramiske kuler slik at lager tilsvarer

6005 2RSLTN9/HC5C3WT og

6003 2RSLTN9/HC5C3WT

Lager i beregningen har ikke tetninger men det har ingen virkning på stivheten

Analyses	Bearing	Type	Designation	d [mm]	D [mm]	Be [mm]	C0 [kN]	C [kN]	Pu [kN]	Quality	Version
Static_1	MotorShaft->6003 C3	DGBB	6003	17	35	10.0	3.25	6.37	0.14	Explorer	2.18
	MotorShaft->6005 C3	DGBB	6005	25	47	12.0	6.55	11.90	0.28	Explorer	2.19



1.2. Bearing loads

1.2.1. Bearing loads, local

Analyses	Bearing	Type	Forces [N]			Moments [Nm]		
			X	Y	Z	YZ	ZX	XY
Static_1	MotorShaft->6003 C3	DGBB	987	0	33	0	0	0
	MotorShaft->6005 C3	DGBB	1013	0	-33	0	1	0

Forces and moments acting on the IR
Forces and moments are displayed in the local coordinate system

1.2.2. Bearing loads, axial and radial

Analyses	Bearing	Type	Radial load [N]	Axial load [N]	Moments [Nm]		
					YZ	ZX	XY
Static_1	MotorShaft->6003 C3	DGBB	987.06	33.02	0	0	0
	MotorShaft->6005 C3	DGBB	1012.99	-33.26	0	1	0

Forces acting on the IR
Forces are displayed in the local coordinate system

1.2.3. Bearing row loads

Analyses	Bearing row	Forces [N]			Moments [Nm]		
		X	Y	Z	YZ	ZX	XY
Static_1	MotorShaft->6003 C3->ReDGBB_1	987	0	33	0	0	0
	MotorShaft->6005 C3->ReDGBB_1	1013	0	-33	0	1	0

Forces and moments in the local coordinate system



1.3. Bearing contact data

Analyses	Bearing	RE	RE position [deg]	Load IR [N]		Angle IR [min]	Def. IR [um]	Load OR [N]		Angle OR [min]	Def. OR [um]
Static_1	MotorShaft->6003 C3->ReDGBB_1	1	0	508	116.3	7	508	119.1	9		
		2	36	296	91.9	5	296	94.2	6		
		3	72	0	68.6	0	0	10.9	0		
		4	108	0	-262.9	0	0	-28.5	0		
		5	144	0	-756.4	0	0	-61.7	0		
		6	180	0	-1053.9	0	0	-74.8	0		
		7	216	0	-756.4	0	0	-61.7	0		
		8	252	0	-262.9	0	0	-28.5	0		
		9	288	0	68.6	0	0	10.9	0		
		10	324	296	91.9	5	296	94.2	6		
	MotorShaft->6005 C3->ReDGBB_1	1	0	536	-110.5	6	536	-112.4	8		
		2	36	295	-93.4	4	295	-95.0	5		
		3	72	0	-182.2	0	0	-9.3	0		
		4	108	0	77.8	0	0	4.0	0		
		5	144	0	409.7	0	0	14.9	0		
		6	180	0	584.9	0	0	19.1	0		
		7	216	0	409.7	0	0	14.9	0		
		8	252	0	77.8	0	0	4.0	0		
		9	288	0	-182.2	0	0	-9.3	0		
		10	324	295	-93.4	4	295	-95.0	5		

- Position: angular position of rolling elements, counterclockwise from X-axis towards Y-axis
- Load: contact loads
- Angle: change in contact angle
- Def: deformation of contacts

Bearing stiffness

Analyses	Objects	Elements	Bearing stiffness				
			X [1/m]	Y [1/m]	Z [1/m]	YZ [1/rad]	XZ [1/rad]
Static_1	MotorShaft->6003 C3	Fx [N]	1.01E08	0	3.27E06	0	-3.85E04
		Fy [N]	0	2.79E07	0	9.45E03	0
		Fz [N]	3.27E06	0	4.32E06	0	-5.06E04
		Myz [Nm]	0	9.46E03	0	1.35E02	0
		Mxz [Nm]	-3.85E04	0	-5.06E04	0	5.87E02
	MotorShaft->6005 C3	Fx [N]	1.16E08	0	-3.73E06	0	6.05E04
		Fy [N]	0	3.16E07	0	-1.52E04	0
		Fz [N]	-3.73E06	0	3.30E06	0	-5.36E04
		Myz [Nm]	0	-1.52E04	0	1.93E02	0
		Mxz [Nm]	6.05E04	0	-5.36E04	0	8.63E02



Bearing stiffness is defined as the contact stiffness of the IR in relation to the OR, in the actual IR coordinate system. Please note that the stiffness is derived for constant displacement and not for constant load. Be aware that ring stiffness is not included in the bearing stiffness matrix (only contact stiffness is considered). Be careful with using the bearing stiffness matrix when the bearing rings are made flexible. Using then the bearing stiffness in e.g. an external FEM package, leads to inconsistency because the flexible terms (Fourier and Chebyshev deformation shapes) in the flexible bearing ring can not be directly coupled to FEM nodes in the external package.

2. Contact pressure

2.1. Bearing max. contact pressure

Analyses	Bearing	Slice	RE	Contact pressure IR [N/mm ²]	Contact pressure OR [N/mm ²]
				1	1
Static_1	MotorShaft->6003 C3->ReDGBB_1	1	1		
		21		2881	3104
	MotorShaft->6005 C3->ReDGBB_1	1	1		
		21		2290	2498

2.2. Bearing max. pressure with/except edge

Analyses	Bearing	Max pressure IR [N/mm ²]	Max pressure OR [N/mm ²]	Max pressure except edge IR [N/mm ²]	Max pressure except edge OR [N/mm ²]
Static_1	MotorShaft->6003 C3	2881	3104	2881	3104
	MotorShaft->6005 C3	2290	2498	2290	2498



3. Lubricant

3.1. Lubricant data

Analyses	Lubricant	Type	Method etaC	Viscosity at 40 C [mm2/s]	Viscosity at 100 C [mm2/s]
Static_1	WT	Grease	ISO 281 2007	70.00	9.40

3.2. Bearing lubrication conditions



No data found for this table

4. Speed

4.1. Bearing speed

Analyses	Bearing	Bearing type	Speed [rpm]	A [mm/min]
Static_1	MotorShaft->6003 C3	DGGB	100	2600
	MotorShaft->6005 C3	DGGB	100	3600

Rotation speed of the IR relative to the OR
 Speed factor A is the rotational speed times bearing mean diameter

4.2. Shaft speed

Analyses	Objects	Rotation speed [rpm]
Static_1	MotorShaft->Rotation speed_1	100